IMPACT OF CLIMATE CHANGE ON HYDROMETEOROLOGICAL VARIABLES IN BHIMA BASIN (INDIA)

Ph.D. THESIS

By

MURUMKAR ASMITA RAMKRISHNA

DEPARTMENT OF HYDROLOGY

INDIAN INSTITUTE OF TECHNOLOGY ROORKEE

ROORKEE-247 667 (INDIA)
DECEMBER 2014

IMPACT OF CLIMATE CHANGE ON HYDROMETEOROLOGICAL VARIABLES IN BHIMA BASIN (INDIA)

A THESIS

Submitted in partial fulfilment of the
requirements for the award of the degree
of
DOCTOR OF PHILOSOPHY
in
HYDROLOGY

by
MURUMKAR ASMITA RAMKRISHNA

DEPARTMENT OF HYDROLOGY

INDIAN INSTITUTE OF TECHNOLOGY ROORKEE
ROORKEE-247 667 (INDIA)
DECEMBER 2014

INDIAN INSTITUTE OF TECHNOLOGY ROORKEE

ROORKEE

CANDIDATE'S DECLARATION

I hereby certify that the work which is being presented in the thesis entitled **"IMPACT OF CLIMATE CHANGE ON HYDROMETEOROLOGICAL VARIABLES IN BHIMA BASIN (INDIA)"** in partial fulfilment of the requirements for the award of the Degree of **Doctor of Philosophy** and submitted in the Department of Hydrology of the Indian Institute of Technology Roorkee, Roorkee is an authentic record of my own work carried out during a period from July, 2009 to December, 2014 under the supervision of Dr. D.S. Arya, Associate Professor, Department of Hydrology, Indian Institute of Technology Roorkee, Roorkee.

The matter presented in this thesis has not been submitted by me for the award of any other degree of this or any other institute.

(MURUMKAR ASMITA RAMKRISHNA)

This is to certify that the above statement made by the candidate is correct to the best of my knowledge.

Dated: **(D.S. Arya)**

Supervisor

ACKNOWLEDGEMENTS

Place: Roorkee   Murumkar Asmita Ramkrishna

ABSTRACT

The impacts of future climate change on water resources and agriculture have become a world-wide concern these days. India and many other developing countries are expected to be seriously affected by the consequences of climate change (IPCC, 2001). Consequently, assessment of climate change impacts on hydrology and water resources are becoming an integral part of the water resources management and planning studies. In this context, assessment of the climate change impacts at basin-scale in the Bhima River basin was undertaken.

Data of two basin's namely the Bhima River basin and the Nira River basin were analysed in this study. The Bhima River, tributary of the Krishna River (India), is a major river in the central India. It flows for about 861 km through Maharashtra, Karnataka, and Telangna before joining the Krishna River near Kudlu in Raichur districts in Karnataka state covering an area of about 70,614 km2. The river originates in the Sahyadri Range (popularly known as the "Western Ghats") in Maharashtra. The Nira River basin is a nested sub-basin of the Bhima River basin which is located in the state of Maharashtra having an area of 6900 km2 and a total length of about 180 km.

Following were the major objectives of the study:

i. To study the spatio-temporal variability of meteorological variables (i.e. temperature and rainfall) in the Bhima River basin.

ii. To analyse the association and impact of ENSO on monsoon rainfall in the Bhima River basin.

iii. To evaluate changes in meteorological variables (i.e. temperature and rainfall) under various emission scenarios in the Bhima basin using statistical downscaling approach.

iv. To assess the impact of projected climate change on streamflows of the Bhima River using Variable Infiltration Capacity model.

v. To analyse the suitability of gridded rainfall datasets in studying the impact of climate change using a case study of the Nira River basin.

Assessing the impacts of climate change on water resources is a multi-step evaluation process as described by Frederick and Gleick (1999). The present study also follows the proposed methodology and the steps are enumerated below:

(i)   analysis of spatio-temporal changes in hydrometeorological variables (temperature, rainfall and streamflow) using Mann-Kendall/Modified Mann-Kendall test, Theil and Sen's Median Slope test and Van Belle and Hughes' Homogeneity of Trend test in the Bhima basin;

(ii) assessment of the association of monsoon rainfall with El Niño Southern Oscillations (ENSO) using correlation analysis;

(iii) projection of meteorological variables using LARS-WG under three emission scenarios (A1B, A2 and B1) during three time spans (i.e 2011-2030, 2046-2065 and 2080-2099) and their analysis using change factor approach; and,

(iv) assessment of climate change impacts on streamflows using a macro-scale hydrological model Variable Infiltration Capacity (VIC) .

An attempt was also made to compare the results of the climate change analysis on rainfall in the Nira basin using two rainfall datasets; observed dataset obtained from IMD and gridded dataset obtained from IMD.

Analysis of Spatio-temporal Variability of Meteorological Variables

The analysis of past temperature records showed decreasing trend in minimum temperatures during summer and winter seasons whereas an increasing trend during monsoon and post-monsoon seasons. However, the seasonal maximum and seasonal mean temperatures showed increasing and decreasing trends respectively. On an annual scale, minimum, maximum, and mean temperatures showed an increasing trend.

The rainfall data was analysed in two time periods i.e. 1901-2004 and 1961-2004 in order to assess the effects of increased anthropogenic activities in the latter period. Analysis of the seasonal rainfall data indicated a decrease in the summer and winter rainfall during the 1901-2004 timescale whereas an increase in the monsoon and post monsoon rainfall during the same period. For the second time scale (1961-2004), the summer and monsoon rainfall showed a decreasing trend while an increasing trend was found in the rainfall in the other two seasons.

The analysis of the data on annual scale shows that the rainfall increased over the last century (15% increase), however there is a decrease in the annual rainfall during 1961-2004 (11% decrease). This disparity is indicative of the effects of anthropogenic climate change. There is considerable spatial variation in the rainfall data over the basin. While the central parts of the basin showed an increase in rainfall (1901-2004) the upper and lower parts showed decreasing trends of rainfall (1961-2004).

Analysis of Relationship of Monsoon rainfall and ENSO

The monsoon rainfall showed significant correlation with the monsoon ENSO indices at majority of grid points in the basin. A significant positive correlation with the monsoon SOI and a negative correlation with monsoon MEI and N3.4 was found. On an average 15% more rainfall was received during monsoon season in La Niña phase and 9% less during El Niño phase in the basin.

Impact of Climate Change on Meteorological Variables

The minimum and maximum temperatures of all seasons are projected to increase with a maximum increase in the A2 scenario and a minimum increase in the B1 scenario. The highest/lowest increase in minimum and maximum temperatures were observed in winter/monsoon season. Spatial pattern of change factors of annual minimum and maximum temperatures over the basin indicated a greater rise in the middle part than other parts.

There is considerable variation in the rainfall projections of the GCMs. However the seasonal rainfall was projected to increase at most of the grids. The annual rainfall projections indicated 3.2 to 18.4% increase with respect to the baseline period (i.e 1961-90). Overall, an increase in annual rainfall is projected across the entire basin, except for a small portion of the upper part of the basin.

Impact of Climate Change on Future Streamflow

The analyses of the results show that the flows are likely to increase across all time spans and scenarios. This is in consonance with the overall trend of future rainfall. Apart from post-monsoon, the flows are likely to increase in the other seasons.

The comparison of observed and gridded rainfall data suggested that the observed data give better representation of changes than the gridded data. Thus, it was concluded that the observed data should be preferred over the gridded data whenever both are available for a basin. However, in case of limited data availability, gridded data can also prove to be reliable in terms of identifying the general trends in the hydrometeorological series, and comparing the relative differences between various scenarios. Overall, it was concluded that results of the analysis carried out using observed rainfall data are in agreement with the findings of the gridded data.

Table of Contents

List of Tables

List of Figures

ABBREVIATIONS

%: percentage

AOGCMs: Atmosphere-Ocean General Circulation Models

CDFs: Cumulative Distribution Functions

CF: change factor

CMIP3: Climate Model Inter-comparison Project Phase 3

CMs: Climate Models

CO_2: carbon dioxide

cumec: cubic meter per second

cusec: cubic feet per second

CV: Coefficient of Variation

CWC: Central Water Commission

DEM: Digital Elevation Model

e.g.: for example (from the Latin exempli gratia)

eq: equivalent

ENSO: El Niño Southern Oscillations

ESA: European Space Agency

et al.: and others (from the Latin et alii)

etc.: and so forth (from the Latin et cetera)

FAO: Food and Agriculture Organization

GCM: General Circulation Model/Global Climate Model

GIS: Geographical Information System

HEC-HMS: Hydrological Engineering Centre's Hydrological Modeling System

i.e.: that is (from the Latin id est)

IAM: Integrated Assessment Models

IDW: Inverse Distance Weighted

IMD: India Meteorological Department

IPCC: Intergovernmental Panel on Climate Change

ISRO: Indian Space Research Organization

Km: kilometer

km^2: square kilometer

KS: Kolmogorov-Smirnov

LAI: Leaf Area Index

LARS-WG: Long Ashton Research Station Weather Generator

m: meter

m²: square meter

m³: cubic meter

MEI: Multivariate ENSO Index

MHMs: Macro-scale Hydrological Models

MK: Mann-Kendall

mm: millimeter

MMK: Modified Mann-Kendall

MODIS: Moderate Resolution Imaging Spectroradiometer

msl: mean sea level

MSLP: Mean Sea Level Pressure

N3.4: Nino 3.4

NASA: National Aeronautics and Space Administration

NCAR: National Centre for Atmospheric Research

NOAA: National Oceanic and Atmospheric Administration

NSE: Nash-Sutcliffe efficiency

ºC: degree centigrade

PBIAS: Percent bias

PMW: Pettit-Mann-Whitney

ppm: parts per milion

r: Correlation Coefficient

R²: Coefficient of Determination

RCM: Regional Climate Model

RCPs: Representative Concentration Pathways

RSR: Ratio of the root mean square error to the standard deviation of measured data

s: second

SCENGEN: A Regional Climate SCENario GENerator

SD: Standard Deviation

SDSM: Statistical DownScaling Model

SOI: Southern Oscillation Index

SRES: Special Report on Emissions Scenarios

SRTM: Shuttle Radar Topography Mission

SWAT: Soil and Water Assessment Tool

UH: Unit Hydrograph

UNESCO: United Nations Educational, Scientific and Cultural Organization

VIC: Variable Infiltration Capacity

WMO: World Meteorological Organisation

WRIS: Water Resources Information System

APHRODITE: Asian Precipitation Highly Resolved Observational Data Integration Towards Evaluation

India-WRIS: Water Resources Information System of India

UNFCC: United Nations Framework on Climate Change

CHAPTER 1: INTRODUCTION

Climate change, as defined by Inter-governmental Panel on Climate Change, refers to a change in the state of climate that can be identified by changes in the mean and/or the variability of its properties, and that persist for an extended period, typically decades or longer. Climate change and related issues have now become an urgent and pervasive preoccupation across the world because dealing with it is a global challenge requiring an ambitious global response.

Inter-governmental Panel on Climate Change (IPCC) assesses the scientific, technical and socio-economic information for understanding the risk of climate change. IPCC assessment indicates that the availability and distribution of freshwater resources will be greatly affected by climate change and the vulnerability of global population to water scarcity could increase in future (Parry, 2007). Thus, impacts of future climate change on water resources and agriculture have become a world-wide concern. India and many other developing countries would be seriously affected by the consequences of climate change (IPCC, 2001). Consequently, studies focused on assessing climate change impacts on hydrology and water resources are becoming prevalent (Leavesley 1994; Xu 1999). Most of these studies use hydrologic models and data derived from climate-change scenarios simulated using General Circulation Models (GCMs) for conducting studies at river basin, national, continental and global scales. The intricate link of water with both society and nature underlines the need of analysing how a change in global climate could affect regional water availability and supplies.

Assessing effects of climate change on water resources is a multi-step evaluation process, which involves extensive modelling and simulation of various components of the global climate as well as global hydrological cycle. In a report prepared for the Pew Center on Global Climate Change, Frederick and Gleick (1999) proposed a five-step methodology to study the impact of climate change on water resources. These steps are enumerated below:

i. GCMs simulation to model future climate conditions on a global scale;
ii. Downscaling of GCM data to river basin scale;
iii. Hydrologic modelling of streamflow using downscaled data;
iv. Assessment of the impacts of altered streamflow on water resources; and

1

v.   Evaluation of impacts on the users of water resources systems.

While the present work adopts broadly the above approach, the primary goal is to assess the impact of climate change on meteorological parameters like temperature and rainfall using gridded datasets in the Bhima River basin in India. The association of El Niño Southern Oscillation (ENSO) with monsoon rainfall is also investigated. A comparative analysis of the impact of climate change on rainfall and relationship of ENSO with monsoon rainfall using observed and gridded rainfall datasets are also investigated for a nested basin namely the Nira River basin which is one of the sub-basin of the Bhima River basin. It aimed at finding the suitability of the gridded data in place of the observed data.

1.1 OBJECTIVES

Following are the major objectives of the study:

i.   To study the spatio-temporal variability of meteorological variables (i.e. temperature and rainfall) in the Bhima basin.

ii.   To analyse the association and impact of ENSO on monsoon rainfall in the Bhima basin.

iii.   To obtain meteorological variables (i.e. temperature and rainfall) for projected climate scenarios in the Bhima basin using statistical downscaling approach.

iv.   To assess the impact of projected climate change on streamflow of the Bhima using Variable Infiltration Capacity model.

v.   To find suitability of gridded rainfall dataset in studying the impact of climate change using the Nira basin observed data.

1.2 OUTLINE OF THESIS

The thesis is organized in eight chapters. The analysis of the data is presented in Chapters 3 to 7. These Chapters includes sub-sections on review of literature, specific objectives, data used, methodology, results, and summary and discussion. A brief description of the contents of the Chapters is given below:

Chapter 1 is an introductory chapter stating the objectives of the study and detailing the layout of the thesis.

Chapter 2 consist a general review on climate change and climate change studies relevant to the objectives of the study.

Chapter 3 analyses the presence of trends in meteorological variables in the Bhima River basin addressing the first objective of the thesis. The analysis of meteorological variables was carried out using gridded data obtained from India Meteorological Department (IMD).

Chapter 4 presents the relationship between ENSO and monsoon rainfall. Correlation analysis was performed using various ENSO indices and monsoon rainfall data. The impact of ENSO phases (El Niño and La Niña) on occurrence of monsoon rainfall of the basin was analysed.

Chapter 5 describes the statistical downscaling of meteorological variables using 15 GCMs outputs for three emission scenarios (A1B, A2 and B1) over three time spans. Furthermore, this chapter presents the impact of climate change on meteorological variables of the basin.

Chapter 6 presents hydrological modelling of streamflow of the Bhima River and impact of climate change on streamflow using Variable Infiltration Capacity model. Projected streamflow were generated using the downscaled dataset prepared in Chapter 5.

Chapter 7 presents a comparative analysis of trends in the Nira basin using gridded and observed data. Relationship analysis between ENSO events and observed and gridded rainfall data are also presented in this chapter.

Chapter 8 describes conclusions, limitations and future scope of the present work.

CHAPTER 2: CLIMATE CHANGE: AN OVERVIEW

2.1 GENERAL

Weather and climate are an integral part of life on Earth influencing the food production and prosperity of the human race (IPCC, 2001c). Weather, characterized by the temperature, precipitation, wind, solar radiation, clouds, air pressure and humidity, is the fluctuating state of the atmosphere (IPCC, 2001c, Oliver and Hidore, 2003). Climate is defined as the average of meteorological conditions (Graedel and Crutzen, 1993). It refers to the average weather in terms of its mean and variability spanning a period of time ranging from months to thousands or millions of years. The globally accepted period used in modern scientific measures of climate is 30 years (IPCC, 2001c). Variation of climate in space and time can be traced back to natural as well as anthropogenic factors (IPCC, 2001c).

The IPCC fourth assessment report (AR4) concluded that the changes in temperature, sea level, and snow cover in northern hemisphere during 1850 to the present based on direct observations, establishes beyond doubt the fact of global warming. The concentration of CO_2 in the atmosphere has increased by 31% since 1750 and the present CO_2 concentration has not been exceeded during the past 4,20,000 years (Prentice *et al*., 2001). This increase in greenhouse gas concentrations is likely to have induced most of the observed warming over the last 50 years (Mitchell *et al*., 2001).Warming over land will be more in comparison to the global annual mean because of less water availability for evaporative cooling and the smaller thermal inertia of the atmosphere as compared to the oceans (Meehl *et al*. 2007). Climate change induced frequency of extreme events can potentially harm the society in multitude of ways and thus lead to civic and political instability.

2.2 CAUSES OF CLIMATE CHANGE

Changes in radiation balance of the earth can be brought about by

- changing incoming solar radiation (e.g., by changes in solar activity or earth's orbit),

- changing fraction of reflected solar radiation (i.e., albedo, e.g., by changes in land surface characteristics, cloud cover or atmospheric particles), and

- changing outgoing long wave radiation from earth (e.g., varying greenhouse gas concentrations, and to some extent, cloud cover).

The two categories *viz.* natural and human (anthropogenic) are the causes of climate change. The natural variability and fluctuations of the climate system have always been part of the Earth's history.

2.2.1 Natural Causes

Volcanic eruptions, ocean currents, the earth's orbital changes and solar variations are the natural causes which influence the earth's climate. The eruption of a volcano emits huge amounts of water vapour, SO_2, dust and ash into the atmosphere. Large volumes of gases, dust and ash can affect the climatic pattern for years by increasing planetary reflectivity thereby causing atmospheric cooling.

During the last few decades El Niño-southern Oscillation (ENSO) has been regarded as the dominant climate mode in the equatorial Pacific with worldwide linked-effects on climate (Ropelewski and Halpert, 1987; Kiladis and Diaz, 1989). Webster and Palmer (1997) explained that Indian monsoon rainfall negatively correlated with ENSO in which a weak (strong) monsoon is related to a warm (cold) event.

2.2.2 Anthropogenic Causes

The incoming solar radiation comes in as short wave insolation and on reflection from the Earth transforms into long wave terrestrial radiation which gets trapped in the atmosphere by certain gases. These gases are transparent to short waves but opaque to long wave radiations and hence cause warming of the Earth. These gases are collectively known as greenhouse gases. These gases are instrumental in keeping the average surface temperature of Earth around 15°C. The Earth's average surface temperature would be around -23°C without the natural greenhouse effect.

Major causes of human induced climate changes are industrialisation driven fossil fuel burning and land use changes. Human activity has increased the concentration of greenhouse gases in the atmosphere since the industrial revolution (http://climate.nasa.gov/causes/). This increase, has led to more heat being retained by the atmosphere thereby increasing the global average surface temperatures. This rise in temperature is termed global warming. Global

warming affects other components of the climate and these changes are together known as anthropogenic (human induced) climate change.

Carbon dioxide (CO_2), methane (CH_4), nitrous oxide (N_2O) and the halocarbons (a group of gases containing fluorine, chlorine and bromine) are the four principal greenhouse gases resulted from human activities (IPCC, 2007).

2.3 GLOBAL CONSEQUENCES OF CLIMATE CHANGE

Global climate change has already had observable effects on the environment. Increasing the variability in precipitation and streamflow due to changing climate and rise of sea level posing a threat to the coastal cities are the two most prominent challenges presented by the changing climate.

2.3.1 Global Warming

The global average combined land and ocean surface temperature data as calculated by a linear trend, show a warming of 0.85 [0.65 to 1.06] °C, over the period of 1880–2012 (Hartman *et al.,* 2013). Warming and precipitation are expected to show considerable spatial variability. Changing frequency and intensity of extreme weather events are likely to have major impact on natural and human ecosystems (Aerts and Droogers, 2004).

The observed temperature data from 1861 to 2000 indicates that the global temperature is increasing; and most of the warming has occurred during the second half of the twentieth century (IPCC, 2001a). The equivalent linear rate of global temperature trend for the period of 1861 to 2000 was 0.044°C/decade, but that for the period of 1901 to 2000 was 0.058°C/decade. The warming rate over the period of 1976-2000 was nearly twice of the rate in between the years 1910-1945. Analysis of daily minimum and maximum temperature data reveals that the rate of increase of minimum temperature is double that of maximum temperature (IPCC, 2001c).

2.3.2 Sea Level Rise

There is strong evidence that the global sea level rise occurred gradually over the 20th century. The IPCC AR4 (IPCC, 2007) reported that between the years 1961 and 2003, the rate of rise of global average was at an average rate of 1.8mm/year, with a range of 1.3–2.3 mm/year. There

are two main factors that have contributed to observed sea level rise (Bindoff *et al*., 2007). The first is thermal expansion: as ocean water warms, it expands (Albritton *et al*., 2007). The second is from the increased melting of land based glaciers and ice sheets which comprise the major fresh water reserves. Based on expert judgment, it can be concluded with greater than 90% probability that human induced causes have contributed to sea level rise in the second half of the 20th century (Solomon *et al*., 2007).

2.4 HOW TO STUDY CLIMATE CHANGE

Depending on the approach, climate change studies may be classified into two broad groups: (i) analysis of observed records of climatological parameters and proxies (like tree rings and ice cores), and (ii) modeling using GCM and Regional Circulation Model (RCM).

2.4.1 Past Climate

Climate proxies, which are preserved physical characteristics of the past are used to reconstruct the climatic records of the respective periods. Tree rings, ice cores, sub-fossil pollen, borehole drilling, coral deposits, lake and oceanic sediments analysis, and carbonate speleothems are some of the climate proxies.

2.4.2 Future Climate

GCMs are used to simulate the future climate of the globe. A reference baseline period has been considered in climate scenario to calculate changes in climate. This baseline data set serves to characterize the sensitivity of the exposure unit to present-day climate. It usually serves as the base on which data sets that represent climate change are constructed. WMO defined a 30 year 'normal' for climatological baseline period. A time period during 1961-1990 is popular baseline period which provides a standard reference for many impact studies.

2.5 GENERAL CIRCULATIONS MODELS

A GCM is a mathematical representation of the Earth's climate system, used in the study of climate, and the impacts of climate change on both natural and human systems. In general, a GCM represents physical processes in the atmosphere, ocean, cryosphere (glaciers and ice sheets), and land surface. A GCM illustrates the climate using a three dimensional grid over the globe of having horizontal resolution of 250 to 600 km, 10 to 20 vertical layers in the

atmosphere and as many as 30 layers in the oceans (IPCC, 2009) (Figure 2.1). The effectiveness of GCMs in studying climate change depends on the level of complexity and ability to simulate the main physical processes that effect climate. A number of research centers around the world have developed their own GCMs, but all these predictions contain uncertainties. More than 30 GCMs have been used in the climate change study by IPCC (2001a). The A1B, B1 and A2 emissions scenarios are most widely IPCC projections (Meehl *et al*., 2007; Randall *et al*., 2007).

To capture the different probable conditions of future emissions, different emission scenarios have been developed. These emission scenarios are explained in detail in next section. A GCM will produce different results for different scenarios. Even if each of the different GCMs uses the same emissions scenario, the largest uncertainty arises from the models themselves. They will result in reasonably different predictions due to the different ways have been used to represent aspects of the climate system (Robert and Colin, 2007).
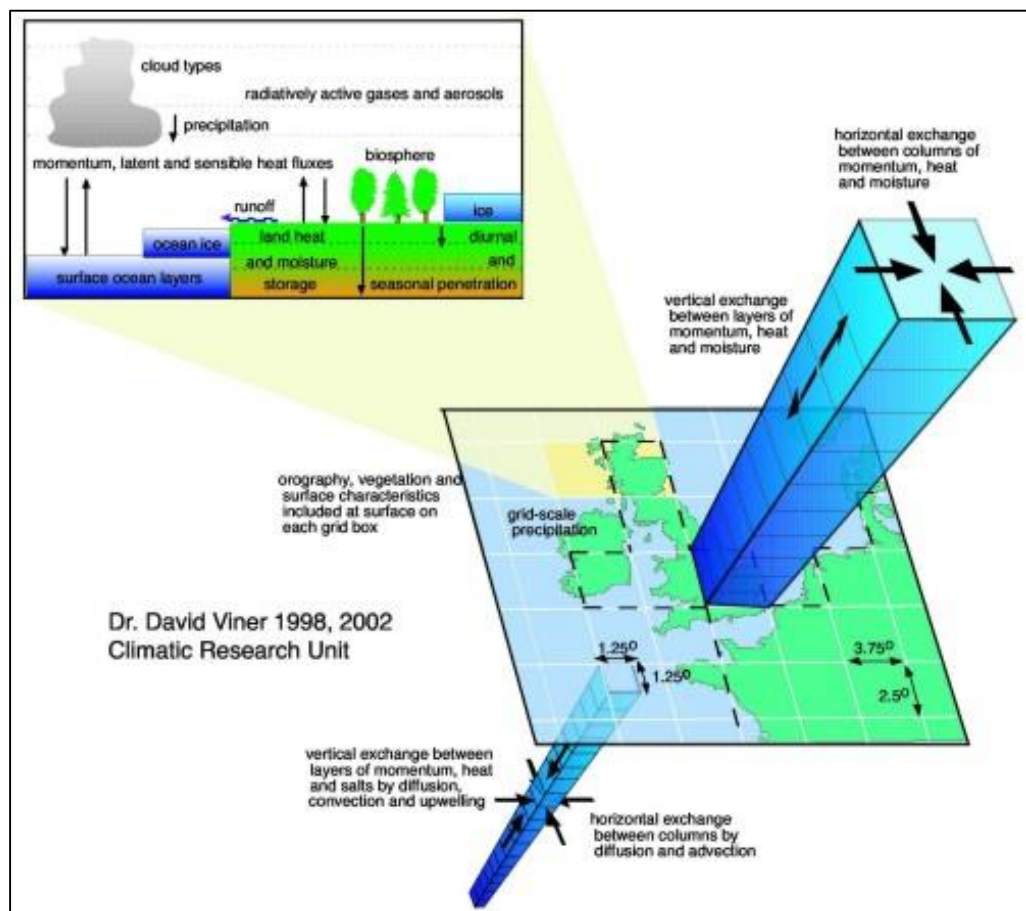
Figure 2.1 Schematics of grids and layers of a typical GCM
(Source: http://www.ipcc-data.org/guidelines/pages/gcm_guide.html)

2.5.1 The SRES Emission Scenario

A scenario is a coherent, internally consistent and plausible description of a possible future state of the world According to the IPCC. The IPCC has developed a range of scenarios in the Fourth Assessment Report (known as the SRES -Special Report on Emission scenarios) to understand potential climate change impacts of future developments on the global environment with special reference to the production of greenhouse gases and aerosol emissions. There are four main families of SRES as A1, A2, B1 and B2 (TGICA, 2007; Bates *et al*., 2008; Nakicenovic *et al*., 2000) representing different demographic, social, economic, technological and environmental developments (Table 2.1).

Table 2.1 Key differences between the potential pathways of global socio-economic development

Economic emphasis →		Regional Emphasis
A1 scenario **World:** market-oriented **Economy:** fastest per capita growth **Population:** 2050 peak, then decline **Governance:** strong regional interactions; income convergence **Technology:** three scenario groups: • A1FI: fossil intensive • A1T: non-fossil energy sources • A1B: balanced across all sources	**A2 scenario** **World:** differentiated **Economy:** regionally oriented; lowest per capita growth **Population:** continuously increasing **Governance:** self-reliance with preservation of local identities **Technology:** slowest and most fragmented development	
B1 scenario **World:** convergent **Economy:** service and information based; lower growth than A1 **Population:** same as A1 **Governance:** global solutions to economic, social and environmental sustainability **Technology:** clean and resource-efficient	**B2 scenario** **World:** local solutions **Economy:** intermediate growth **Population:** continuously increasing at lower rate than A2 **Governance:** local and regional solutions to environment protection and social equity **Technology:** more rapid than A2; less rapid, more diverse than A1/B1	
Global integration ↑	← Environmental emphasis	

(Source: Nakicenovic *et al.* 2000)

The storylines can be summarized as follows:

- **A1 scenario family:** - the world sees very rapid economic growth, global population peaks in the mid-century and decline thereafter, and rapid introduction of new and more efficient technologies.

- **B1 scenario family:** - the world as a convergent world with the same global population as in the A1 storyline but with rapid changes in economic structures toward a service and information economy, with reductions in materials intensity, and the introduction of clean an resource efficient technologies.

- **A2 scenario family:** - the world as continuously increasing global population and regionally oriented economic growth that is more fragmented and slower than in other storylines.

- **B2 scenario family:** - the world emphasis goes to local solutions to economic, social, and environmental sustainability, with continuously increasing population (lower than A2) and intermediate economic development.

2.5.2 Representative Concentration Pathways

The need for new scenarios prompted the IPCC to request the scientific communities to develop a new set of scenarios to facilitate future assessment of climate change (IPCC, 2007) Development of such scenarios are not a part of the IPCC process, leaving new scenario development to the research community (Moss *et al*., 2010). Development of a scenario set containing emission, concentration and land-use trajectories are referred to as "*representative concentration pathways*" (RCPs).

The IPCC has adopted four greenhouse gas concentration trajectories (RCPs) for its fifth Assessment Report. The main purpose of the development of the RCPs is to provide information on possible development trajectories for the main forcing agents of climate change, consistent with current scenario literature. Climate models and Integrated Assessment Models will be used subsequently for the development of RCPs. The overview of RCPs with similarities with SRES is given in table 2.2.

Table 2.2 Overview of RCPs and similarities with SRES

RCPs	Description	SRES	Particular difference
RCP8.5	Rising radiative forcing pathway leading to 8.5 W/m^2 (~1370 ppm CO_2 eq) by 2100	A1FI	Median temperature in RCP8.5 rise slower than in SRES during the period between 2035 and 2080, and faster during other periods of the twenty-first century
RCP6	Stabilization without overshoot pathway to 6 W/m^2(~850 ppm CO_2 eq) at stabilization after 2100	B2	Median temperatures in RCP6 rise faster than in SRES B2 during the three decades between 2060 and 2090, and slower during other periods of the twenty-first century
RCP4.5	Stabilization without overshoot pathway to 4.5 W/m^2(~650 ppm CO_2 eq) at stabilization after 2100	B1	Median temperatures in RCP4.5 rise faster than in SRES B1 until mid-century, and slower afterwards
RCP2.6	Peak in radiative forcing at ~3 W/m^2 (~490 ppm CO_2 eq) before 2100 and then decline (the selected pathway declines to 2.6 W/m^2 by 2100)	None	

(Source: Rogelj, 2012)

2.6 DOWNSCALING

The process of deriving finer resolution data (e.g., for a particular site) from a coarser resolution GCM data is known as downscaling. The relationship, or set of relationships can be defined between the climate of the site and large-scale (i.e., GCM grid) climate for derivation of more realistic values of the future climate at the site scale. GCMs generally operate at coarse resolutions across the continents, but finer resolutions data are required for modelling of catchment hydrology (Bergkamp *et al*. 2003). Furthermore, the GCM predicted data typically do not account for the spatial and temporal variability of climate data observed at catchment scales.

The weakness of linking GCMs with hydrological processes is the exclusion of daily and inter-annual climatic variability within GCMs, and the mismatching of spatial scales between GCMs (typically a few hundred km) and hydrological processes. Downscaling techniques are used to help include daily variability within GCMs and to help quantify the relative significance of different sources of uncertainty affecting water resource projections (Meehl *et al*. 2007). Using multi-model ensemble means for regional studies has proven

superior to using a single climate model because averaging the model projections reduces both mean errors and variance in the models (Pierce *et al.* 2009).

Therefore number of techniques has been developed for impacts studies by obtaining more detailed regional and site scenarios of climate change. These downscaling techniques have been designed to bridge the gap between the information that the climate modelling community can currently provide and that required by the impacts research community (Wilby and Wigley, 1997). Mainly, there are two types of downscaling techniques - dynamic downscaling and statistical downscaling - that are used for climate change studies.

2.6.1 Dynamic Downscaling

Dynamic downscaling involves driving a Regional Climate model (RCM) at high resolution using the output of a GCM as the boundary condition for the region of interest. RCM simulates explicitly the atmospheric dynamics, thermodynamics, and related physical processes that, together, create what we describe as weather. Regional climate can be generated by running the RCM over an extended period, and calculating the means and probability distributions of the atmospheric states.

2.6.2 Statistical Downscaling

A mathematical relationship between a large-scale climate field or variable and a local-scale observation is known as statistical downscaling. The outcome of statistical downscaling is almost invariably a point estimate of the climate in terms of observed quantities, usually temperature and precipitation. The relationships between observed large-scale predictor and observed local-scale predictors and observed local scale predictands can develop in this technique. Then these relationships are applied to the large scale fields which are then simulated realistically.

The large scale climatic state and regional/local physiographic features are two necessary factors required in statistical technique. Firstly, a statistical model is developed which relates large scale climate variables (predictors) to regional/local variables (predictands) for derivation of regional or local climate information. Then the large scale output of a GCM simulation is fed into this statistical model to estimate the corresponding local and regional climate characteristics.

The advantages of statistical downscaling methodologies over dynamical downscaling approaches are given in table 2.3. Statistical downscaling is seen as a highly adopted technique from the aspects of low-cost and rapid assessments of localized climate change impacts.

Table 2.3 Advantages and disadvantages of dynamic and statistical downscaling

Statistical Downscaling	Dynamical Downscaling
Advantages	
•Station-scale climate information from GCM-scale output	•10–50 km resolution climate information from GCM–scale output
•Cheap, computationally undemanding and readily transferable	•Respond in physically consistent ways to different external forcings
•Ensembles of climate scenarios permit risk/ uncertainty analyses	•Resolve atmospheric processes such as orographic precipitation
•Applicable to 'exotic' predictands (air quality and wave heights)	• Consistency with GCM
Disadvantages	
•Dependent on the realism of GCM boundary forcing	• Dependent on the realism of GCM boundary forcing
•Choice of domain size and location affects results	• Choice of domain size and location affects results
• Requires high quality data for model calibration	•Requires significant computing resources
•Predictor–predictand relationships are often non–stationary	•Ensembles of climate scenarios seldom produced
• Choice of predictor variables affects results	•Initial boundary conditions affect results
• Choice of empirical transfer scheme affects results	•Choice of cloud/ convection scheme affects (precipitation) results
•Low–frequency climate variability problematic	•Not readily transferred to new regions or domains
•Always applied off-line, therefore, results do not feedback into the host GCM	•Typically applied off-line, therefore results do not always feedback into the host GCM

(Source: Wilby and Dawson, 2004)

2.7 ROLE OF HYDROLOGICAL MODELS IN CLIMATE CHANGE STUDY

Xu (1999) identified four main gaps between the current abilities of GCMs and the needs of hydrologic models. These gaps can be summarized below:

i. **Spatial scale mismatch:** On one hand, GCMs deal most efficiently with fluid dynamics on the continental scale with horizontal grid resolution of several hundred kilometres, on the other hand hydrological models often work on the catchment scale which is covered by a few GCM grid cells if not contained within one cell.

ii. **Temporal scale mismatch:** Although GCMs use short time steps of 10-30 minutes, their output is archived on longer time steps of several hours to a day and most verifications are based on long-term means (monthly or seasonal) which is their most reliable temporal scale. Hydrologic impact models generally require a daily time step or shorter.

iii. **Vertical level mismatch:** GCMs simulate the free atmosphere more satisfactorily because of its spatial and temporal homogeneity. However, hydrologic models require surface variables (e.g. surface temperature, precipitation).

iv. **Variable accuracy mismatch:** GCMs were conceptually designed to simulate average large-scale circulation, therefore they predict air pressure, temperature, and wind quite well especially in the upper atmosphere. Precipitation, cloud cover, and soil moisture, which are the important variables needed for hydrological studies are less well modelled.

The gaps between the relationship between hydrologic modelling and climate modelling are represented in table 2.4. It reveals that GCMs ability to predict spatial and temporal distributions of climatic variables decline from global to regional to local catchment scales, and from annual to monthly to daily amounts. However, the hydrological importance of climate predictions increases from global to local scales and from annual to daily amounts.

Table 2.4 Some exiting gaps between GCM's simulation ability and hydrological requirements

	Better simulated	Less-well simulated	Not well simulated
Spatial scales mismatch	Global 500x500 km	Regional 50x50 km	Local 0-50 km
Temporal scales mismatch	Mean annual and seasonal	Mean monthly	Mean daily
Vertical scales mismatch	500 hPa	800 hPa	Earth Surface
Working variables mismatch	Wind Temperature Air pressure	Cloudiness Precipitation Humidity	Evapotranspiration Runoff Soil moisture
GCM's ability			
Hydrological importance			

(Source: Xu, 1999)

The field of earth system science has fostered the development of large-scale, synoptic views of the earth's hydrology to assess the impact of climate change on hydrology. In the most general sense, macro-scale hydrological modelling (MHM) is simply the application of hydrological models over a large spatial domain, ranging from a 'large' basin (over 104 km^2), through a continent, to the entire land surface of the globe (Wood, 1998). The basic interests of hydrologist to study hydrological processes at larger scales are enumerated below (Arnell, 1993).

i. To correct perceived weaknesses in the representation of hydrological processes in regional and global atmospheric models. The two important areas in development MHM are the explicit treatment of variability within an atmospheric model grid cell and the routing of water along a river network within and between grid cells.

ii. An interest in simulating riverflows in large river basins for a variety of operational and planning purposes.

Currently two types of macro scale hydrological models; macro-scale water-balance models (MWB) and macro-scale land-surface hydrological models are developed. The MWB, (Engeland *et al*., 2001; Graham, 2004) focuses on the catchment water balance and provide no

coupling with GCMs or RCMs and run "off-line". MHM, (Liang *et al*., 1994; Chen and Dudhia, 2001) have a primary purpose of improving the land-surface hydrological characteristics of global climate models, regional climate models and meso-scale meteorological models. The MHM uses the energy balance as its primary concept and it could be coupled with GCMs/RCMs, and therefore it could run with smaller time steps. Dolman *et al.* (2001), and Singh and Frevert (2002) reported a discussion of the critical issues involved in MHMs. The coupling of macro models with the GCM produce a better representation of the recorded flow regime than GCMs predictions of runoff for world's large river basins.

2.8 SUMMARY

On the basis of the literature presented in this chapter, following important points are inferred:

i. The studies based on the analysis of historical data may help to address the issue of climate change vulnerability. However it has been established that global or continental scale study of historical climate are not very useful for local or regional scale climatic predictions and subsequent planning. Hence the analysis of hydrometeorological trends at the basin scale is important in studying the impacts of climate change for water resources planning and management.

ii. The study of Indian summer monsoon variability is one of the important scientific themes that receive lot of attention because of its complexity. El Niño has been known to be one of the most important forcing's of the Indian monsoon variability.

iii. In view of expected global changes in climate and environment for the future due to anthropogenic greenhouse forcing, it is crucial to understand hydrological changes on a regional scale. Hence various downscaling techniques have been developed to obtain information on regional and even local scales from global GCMs.

iv. The overreliance on a single GCM with one scenario could lead to high uncertainty in prediction of hydrometeorological variables. Hence use of multi-modal ensemble predictions is suggested in climate change impact studies.

v. In climate-change studies, a macro scale hydrologic model operating over large scales can be an important tool in developing consistent hydrological variability estimates over large basins. They can provide a connection between GCMs and water resource systems on large spatial scales and temporal scales.

CHAPTER 3: SPATIO-TEMPORAL ANALYSIS OF METEOROLOGICAL VARIABLES

3.1 GENERAL

Hydrometeorological variables represent the basin characteristics of periodic events occurring at different time scales in the basin. Changes in climatic and hydrologic time series are usually detected by trend analysis. Several studies have used trend analysis technique to study changes in hydrometeorological variables such as temperature (Kothyari and Singh, 1996; Arora *et al.,* 2005; Fall *et al.*, 2011; Mishra *et al.*, 2012c; Khattak *et al.*, 2011), rainfall (Türkeş, 1996; Douglas *et al.*, 2000; Yue *et al.*, 2003; Burn *et al.*, 2004; Partal and Kahya, 2006; Basistha *et al.*, 2008; Kumar and Jain, 2011; Mishra and Lettenmaier, 2011; Jain and Kumar, 2012; Murumkar *et al.*, 2013; Wagesho *et al.* 2013; Khattak *et al.*, 2011; Taxak *et al.*, 2014), evaporation (Chattopadhyay and Hulme, 1997; Burn and Hesch 2007; Bandyopadhyay *et al.*, 2009) and streamflow (Lettenmaier *et al.*, 1994; Zhang *et al.*, 2001; Burn and Hag Elnur, 2002; Kahya and Kalayci, 2004; Cigizoglu *et al.*, 2005; Wagesho *et al.* (2012)) at regional and global scale.

The Mann-Kendall (MK) test (Mann, 1945; Kendall, 1955) is one of the most widely used nonparametric test for trend analysis (Steele *et al.*, 1974; Hirsch *et al.*, 1982; Taylor and Loftis, 1989; Douglas *et al.*, 2000; Kahya and Kalayci, 2004). Autocorrelation is commonly found in hydrologic or climatic records (Haan, 1995). A detailed analysis of the effect of autocorrelation on trend and *vice-versa* has been presented by Yue *et al*. (2002b). The Modified Mann-Kendall (MMK) test was suggested to make the Mann Kendall test suitable for autocorrelated series (Hamed and Rao, 1998; Rao *et al.*, 2003).

The wavelet transform is a strong mathematical tool that provides a time–frequency representation of a signal (Daubechies, 1992; Polikar, 1999) and is used for analysing non-stationarity of hydrometeorological variables (Pisoft *et al.*, 2004). Wavelet transformations have been successfully applied to climate characteristics analysis, such as streamflow characterization (Smith *et al.*, 1998), relationship between North Atlantic Oscillation and sea level changes (Yan *et al.*, 2004), inter-annual temperature events and shifts in the global temperature (Park and Mann, 2000), inter-decadal and inter-annual variations of annual and

extreme precipitations (Penalba and Vargas, 2004) and to study ENSO (Torrence and Compo, 1998).

An increase in the average global surface temperatures by approximately 0.6°C since the late 19th century with an increase in the rate of rise in the temperature in the most recent decades (Houghton *et al*., 2001). Several studies have reported that the trends of warming are not uniform. Furthermore, lesser warming in maximum temperatures and substantial warming in minimum temperatures have been reported (Dai *et al*., 1997; Easterling *et al*., 1997). The increased atmospheric moisture content associated with warming might lead to increased global mean precipitation. Global annual mean precipitation in land areas showed a small, but uncertain, upward trend over the 20th century of approximately 1.1 mm per decade (Vose *et al*., 1992; Mitchell and Jones, 2005). However, the record is characterized by large inter-decadal variability, and the global annual land mean precipitation shows a non-significant decrease since 1950 (IPCC, 2007). Runoff tends to increase where precipitation has increased and decrease where precipitation has decreased over the past few years. Variations in inter-annual flow have been found to be much more strongly related to precipitation changes than to temperature changes (Krasovskaia, 1995; Risbey and Entekhabi, 1996).

The trend and magnitude of warming over the Indian sub-continent over the last century is broadly consistent with the global trends of temperatures (Arora *et al*., 2005; Dash *et al*., 2007). In relation to changing rainfall pattern, there is no clear increasing or decreasing trend in the average amounts of rainfall over Indian subcontinent (Mooley and Parthasarathy, 1984; Thapliyal and Kulshrestha, 1991; Lal, 2001; Kumar *et al*., 2010). Significant increasing or decreasing trends have been found in monsoon rainfall at regional scales (Koteswaram and Alvi, 1969; Jagannathan and Parthasarathy, 1973; Raghavendra, 1974; Chaudhary and Abhyankar, 1979; Kumar *et al*., 2005; Dash *et al*., 2007; Kumar and Jain, 2010). Narayanan *et al.*, 2013 reported that there is a significant rise in the pre-monsoon rainfall over the north-west part of India. There is a sudden shift in annual and monsoon rainfall pattern after 1964 in the Indian Himalayas resulting in decreased rainfall (Basistha *et al*., 2007, 2009). While conducting similar study in Orissa, Patra *et al*., 2012 observed a long term insignificant declining trend of annual as well as monsoon rainfall during 1871-2006. A significant decreasing trend was observed in grass reference evapotranspiration during 1971-2002 across India by Bandyopadhyay *et al*., 2009.

The analysis of rainfall trends is important in studying the impacts of climate change for water resources planning and management (Haigh, 2004). It has been recognized that global or continental scale observations of historical climate are less useful for local or regional scale planning (Barsugli *et al*., 2009; Brekke *et al*., 2009; Raucher, 2011).

3.2 OBJECTIVES

Climate has large spatial and temporal variations in India, due to its vast size and geographical complexity (Dash 2007). Rainfall and temperature are the major indicators in the climate change impact studies which influences water resources systems and agriculture sector of the region. It is also recognized that rainfall is one of the key climatic variables that affect both the spatial and temporal patterns of water availability (De Luis *et al*., 2000). Therefore, this chapter examines the historical variations in seasonal and annual meteorological variables in the Bhima basin to assess the impact of climate change through trend analysis. The specific objectives of the chapter are:

i.   To analyse the temporal and spatial variability of gridded temperature data (minimum, maximum and mean) during 1969-2009, and rainfall data on seasonal and annual scale during 1901-2004 and 1961 to 2004.
ii. To test the homogeneity of temperature and rainfall trends.

3.3 STUDY AREA

3.3.1 Bhima Basin

The Bhima River is a major river in the central India. It flows for about 861 km through Maharashtra, Karnataka, and Telangna states (newly carved state from Andhra Pradesh) before joining the Krishna River (Figure 3.1). The river originates in the Sahyadri Range (known as the "Western Ghats") in Maharashtra with an average elevation of around 1,000 m. The river merges in the Krishna River near Kudlu in Raichur districts of Karnataka state. Ghod, Sina and Kagini are left bank tributaries whereas Bhama, Indrayani, Mula-Mutha and Nira are right bank tributaries of the Bhima River as shown in figure 3.1.
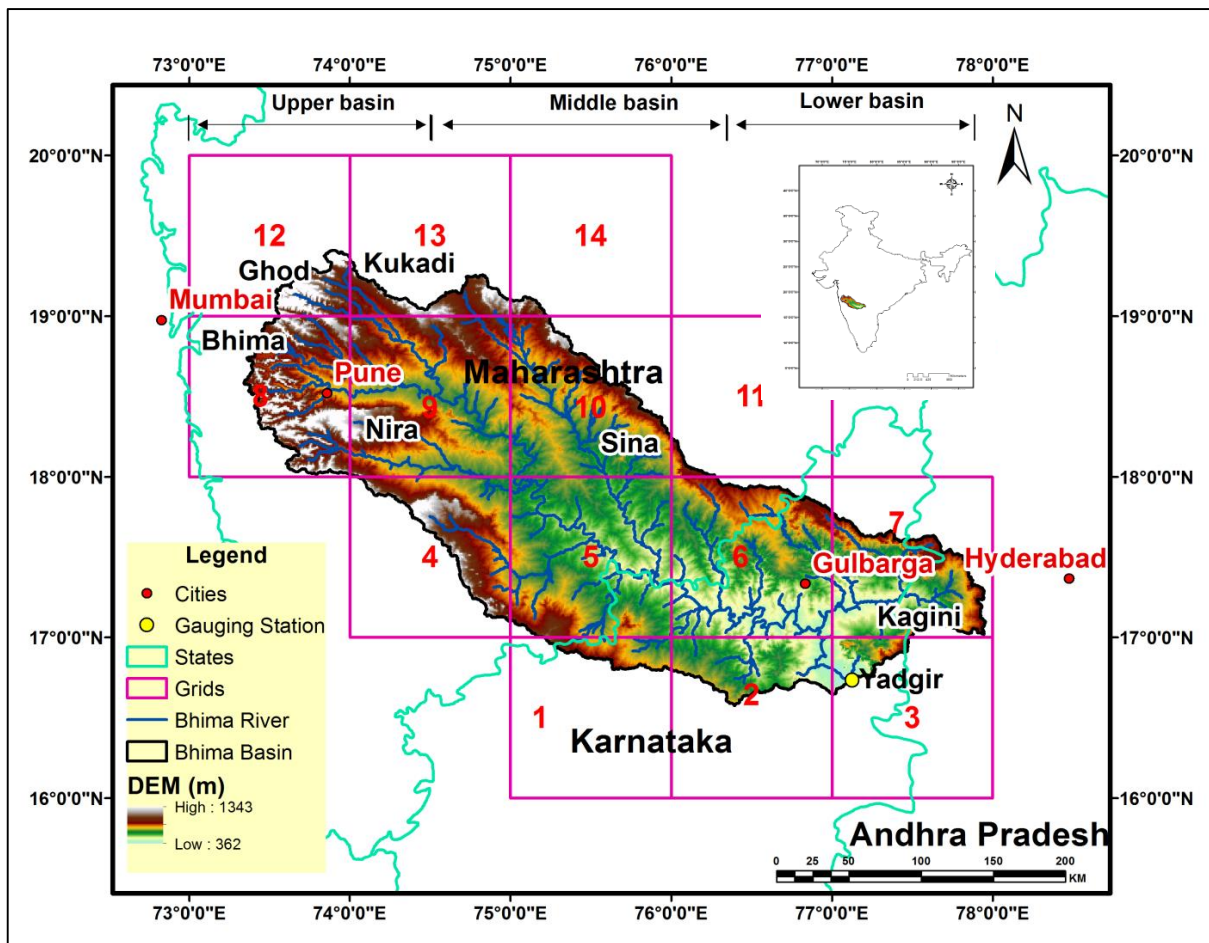
Figure 3.1 Drainage map of the Bhima basin with digital elevation map in the background

(Note: Andhra Pradesh has been divided into two states namely Telangna and Seemant Andhra, recently. The part shown above as Andhra Pradesh now lies in newly carved out state Telangna).

The Bhima basin is the second largest sub-catchment in the Krishna River basin and lies between 73° 18' 26.64" E to 77° 56' 22.83" E longitude and 16° 24' 55.62" N to 19° 25' 26.64" N latitude, covering an area of about 70,614 km^2. Seventy-five percent (48,631 km^2) of the basin lies in the state of Maharashtra. It is an important basin in the context of serving inter-sectorial demands including drinking and agricultural water supply and hydropower generation.

3.3.2 Climate

The basin has a diverse climate mainly caused by the interaction between monsoon and the Western Ghats mountain range. Figure 3.2 represents the annual climate of the basin. The mean annual rainfall of the basin is 642 mm ranging from 380 to 1120 mm. According to the India Meteorological Department (IMD), four prominent seasons namely (i) winter (December to

February), (ii) summer (March to May), (iii) monsoon (June to September) and (iv) post-monsoon (October and November) are observed in the basin. The average temperature of the basin varies from 20.7°C (December) to 29.3°C (May).
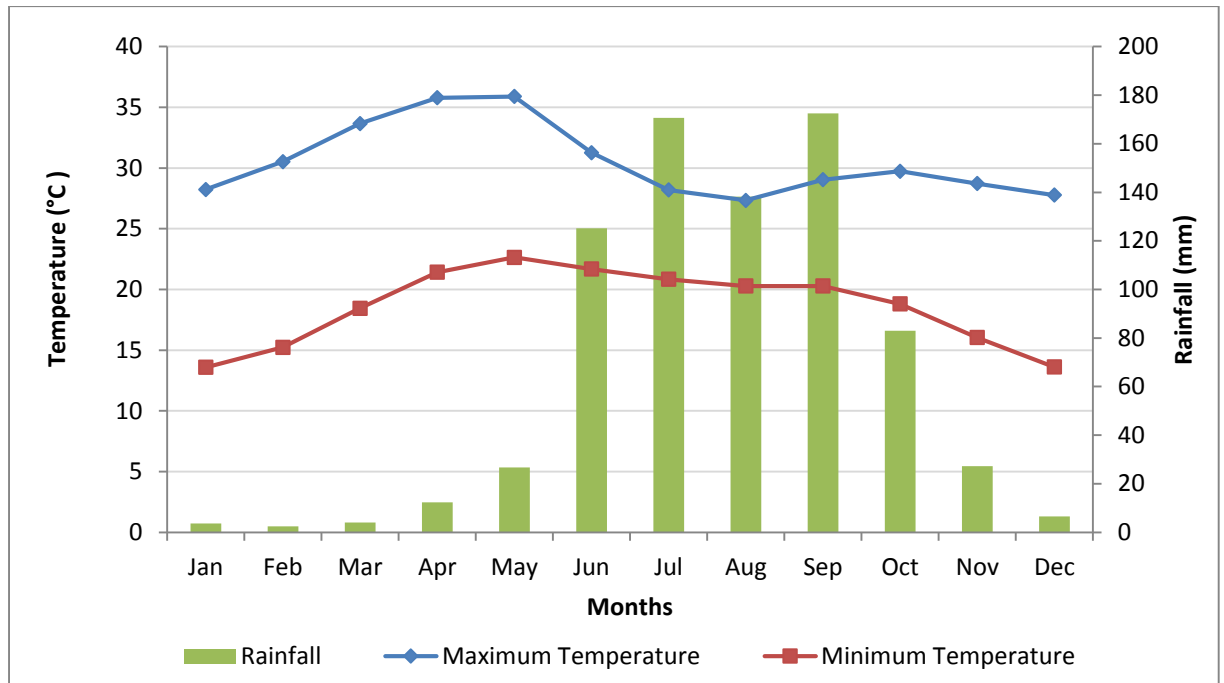
Figure 3.2 Average climate graph of the Bhima basin

3.4 DATA USED

High-resolution 1°×1° gridded daily temperature (1969-2009) and rainfall (1901-2004) data was obtained from IMD, Pune. These dataset was developed using observed temperature data of 395 stations and rainfall data of 1384 stations (Rajeevan *et al*., 2006; Rajeevan *et al*., 2008; Srivastava *et al*., 2009) for the entire country. The Bhima basin is covered in 14 grids of 1°×1° resolution as shown in figure 3.1.

Daily minimum, maximum and mean temperature data (1969-2009) were extracted for all the grids from the IMD gridded dataset. Monthly averages of minimum temperature, maximum temperature and mean temperature were computed from the daily data. Seasonal and annual temperature series for each grid were prepared using monthly averages. The seasonal and annual temperature series of the basin were prepared by averaging temperatures of the 14 grids of the basin.

23

Daily rainfall data were extracted for 14 grids for 104 years i.e. from 1901 to 2004. Monthly rainfall series were prepared from the daily rainfall data for each grid and for the entire basin. Similarly, seasonal rainfall series of four seasons (summer, monsoon, post-monsoon and winter) and annual rainfall series were prepared from monthly rainfall series for each grid and for the entire basin. The area weighted average method was used for preparation of rainfall series of the grids partially lying in the catchment using equation 3.1.

$$R = \frac{\sum_{i=1}^{n} R_i * A_i}{A}$$
(3.1)

Where R_i is the rainfall of grid i, A_i is the area of grid i and A is the total area of the basin.

The seasonal and annual partial duration series from 1961-2004 were obtained from entire duration series.

3.5 METHODOLOGY

The trend analysis of temperature data was performed on 14 grids of the basin during 1969-2004. Grid wise trend analysis is presented in the beginning of the section whereas for the entire basin is presented towards the end of the section. The trend analysis of rainfall was performed for two durations: 1901-2004 and 1961-2004. The duration from 1961-2004 was chosen to find the changes in recent trends compared to the overall trends. Seasonal and annual changes in streamflow of the Bhima River were also performed. Statistical significance of the trend was tested at 10% significance level. Step-wise methodology of trend analysis of hydrometeorological variables is given below:

(1) Significance of autocorrelation was detected by using student's t-test at lag-1 in seasonal and annual hydrometeorological series (Appendix I).
(2) Mann-Kendall (MK)/Modified Mann-Kendall (MMK) tests were applied to the non-autocorrelated/ autocorrelated series to detect the presence of trend in seasonal and annual hydrometeorological series (Appendix II).
(3) Magnitude of a trend was estimated by Theil and Sen's slope estimator test (Appendix III).
(4) Changes over a mean were calculated as percent change during 104 years and 44 years in annual and seasonal rainfall and streamflow series (Appendix III).

24

(5) Study of the spatial pattern of temperature and rainfall trend results was carried out using ArcGIS.

(6) Homogeneity in annual and seasonal trends were tested by Van Belle and Hughes' homogeneity trend test to obtain global trend over a basin (Appendix IV).

3.6 RESULTS

3.6.1 Spatio-temporal Variability Analysis of Temperature Trends

Preliminary analysis of the temperatures data (1969-2009) shows that annual average minimum temperature varies from 18.4ºC (grid #13) in upper region to 21.2ºC (grid #3) in lower zone. Figures 3.3 to 3.5 represent the spatial pattern of average minimum, maximum and mean temperatures over the entire basin. The annual average maximum temperature varies from 29.6ºC (grid #1) in lower region to 33.5ºC (grid #11) in upper zone. The annual mean temperature varies from 25.4ºC (grid #4) in upper region to 27.2ºC (grid #3) in lower zone. In general, the north-western (upper) and south-eastern (lower) parts of the basin show relatively higher temperatures as compared to the central parts. An uniform temperature gradient can be observed across the basin, with higher temperatures on the south-eastern edge and decreasing in the north-west direction. This gradient is more prominent in mean annual temperatures and the maximum temperatures.
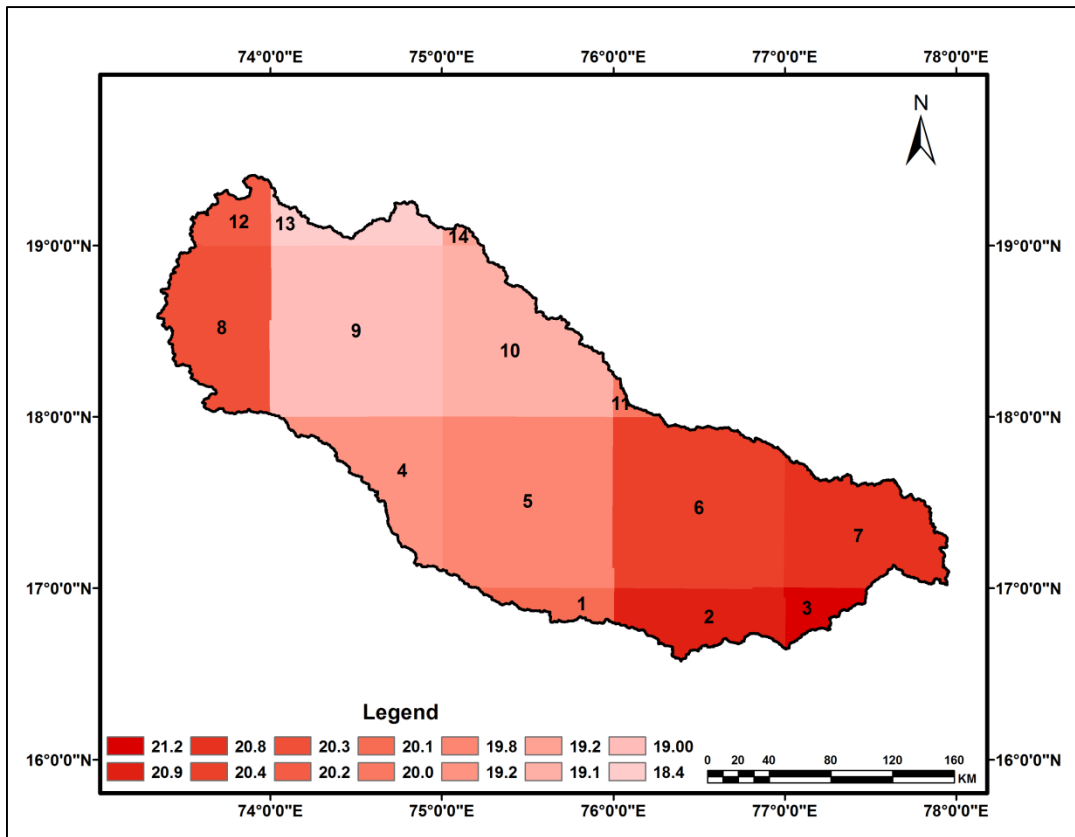
Figure 3.3 Spatial pattern of annual average minimum temperature over the basin
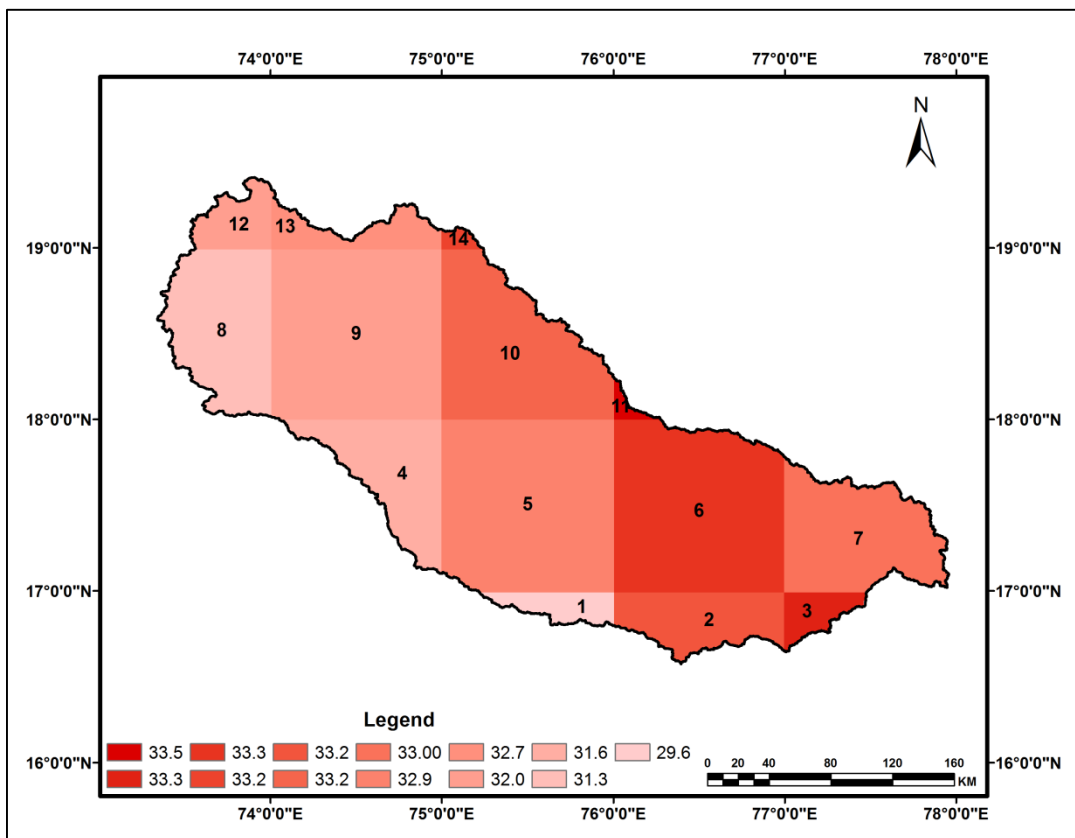
Figure 3.4 Spatial pattern of annual average maximum temperature over the basin

26
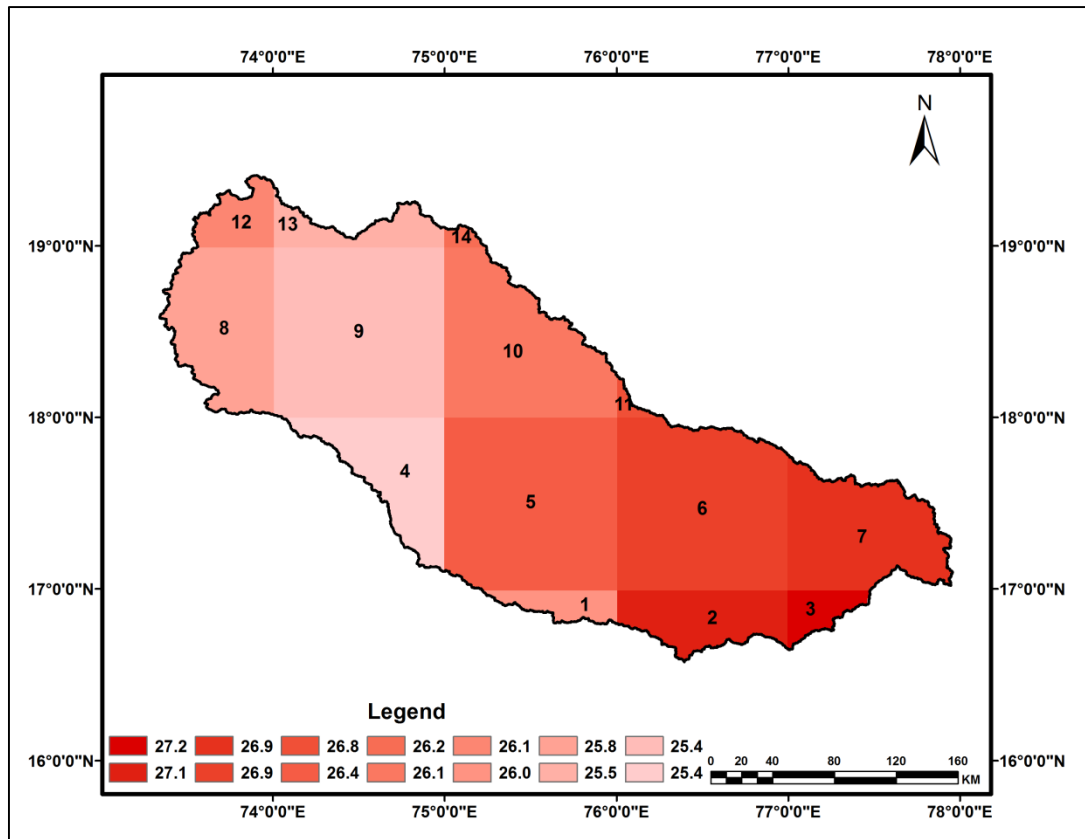
Figure 3.5 Spatial pattern of annual mean temperature over the basin

3.6.1.1 Seasonal and annual changes in average minimum temperature

Results of autocorrelation analysis, Z-statistics of MK/MMK test and Sen's slope calculated for seasonal and annual average of minimum temperature of all the grids during 1969-2009 are given in table 3.1. The sign of MK/MMK test statistics indicate increasing trend (+ve sign) and decreasing (-ve sign) trend. The sign of Sen's slope indicates an increasing (positive slope) or decreasing (negative slope) trend, as well.

Autocorrelation was found in eight seasonal temperature series at 10% level. Hence, trend analysed was performed using MMK test for these series. Significant decreasing trends were observed in summer season in grid #5 and grid #6. Eight out of 14 grids exhibited decreasing trends for winter season. In monsoon season, significant increasing trends were found in four grids shown in bold in table 3.1. During post-monsoon season, eight temperature series out of 14 show non-significant increasing trends.

Significant autocorrelation was found in annual minimum temperature data of five grids. An increasing trend was observed in nine grids, out of which only grid #8 exhibited

statistically significant increasing trends. Grid #8 is located in the upper basin in Western Ghats. Remaining five grids, which are located in the middle and lower basin exhibited non-significant decreasing trends.

Table 3.1 Result of MK /MMK test and Sen's slope estimator test of seasonal and annual average minimum temperature during 1969-2009

Series	Annual		Seasonal							
			Summer		Monsoon		Post-Monsoon		Winter	
Grids	MK/ MMK	Sen's Slope	MK/ MMK	Sen's Slope	MK/ MMK	Sen's Slope	MK /MMK	Sen's Slope	MK/ MMK	Sen's Slope
1	-0.887	-0.006	-1.134	-0.007	0.000	0.000	-0.393	-0.005	-0.827	-0.001
2	-0.438	-0.003	-1.067	-0.009	0.730	0.003	-0.483	-0.005	-0.617	-0.008
3	0.124	0.000	-0.505	-0.005	**1.966**	0.009	0.056	0.001	-0.478	-0.009
4	-1.123	0.000	-1.359	-0.011	0.685	0.003	-0.056	-0.001	-0.361	-0.006
5	-0.573	-0.006	**-1.876**	-0.017	-0.303	-0.001	-0.146	-0.002	-0.664	-0.013
6	-0.55	-0.004	**-1.921**	-0.015	0.865	0.005	-0.685	-0.007	-0.268	-0.005
7	0.416	0.002	-0.887	-0.006	**2.213**	0.012	0.056	0.001	-0.082	-0.001
8	**1.898**	0.012	0.168	0.002	**2.617**	0.015	0.595	0.009	0.897	0.008
9	1.022	0.008	-0.236	-0.002	1.404	0.008	0.303	0.004	0.315	0.006
10	0.089*	0.001	-1.089*	-0.011	0.607*	0.009	0.000	0.000	0.082	0.001
11	0.106*	0.001	-1.426	-0.012	1.471	0.009	-0.416	-0.007	-0.268	-0.004
12	1.008*	0.015	0.820*	0.006	**1.663***	0.018	0.955	0.018	1.573	0.019
13	0.405*	0.008	-0.213*	-0.002	0.560*	0.007	0.573	0.010	0.874	0.001
14	0.196*	0.005	-1.404*	-0.011	0.673*	0.012	0.034	0.001	0.548	0.007
Note: *indicates presence of autocorrelation in the temperature series; Bold numbers represent significant increasing and decreasing trends in the series.										

Figure 3.6 presents the box and whisker plot of the magnitude of Sen's slope of seasonal and annual average minimum temperature in the basin. The median of the slopes of summer and winter seasons are in negative zone, as seen in figure 3.6, and in positive zone for monsoon and post-monsoon seasons. Thus, summer and winter seasons seem to be getting cooler while monsoon and post-monsoon seasons seem to be getting warmer.

The median of the magnitude of the slopes of annual temperature lies in the positive zone (Figure 3.6). It indicates that an overall increase in the average annual minimum temperature is observed in the entire basin.
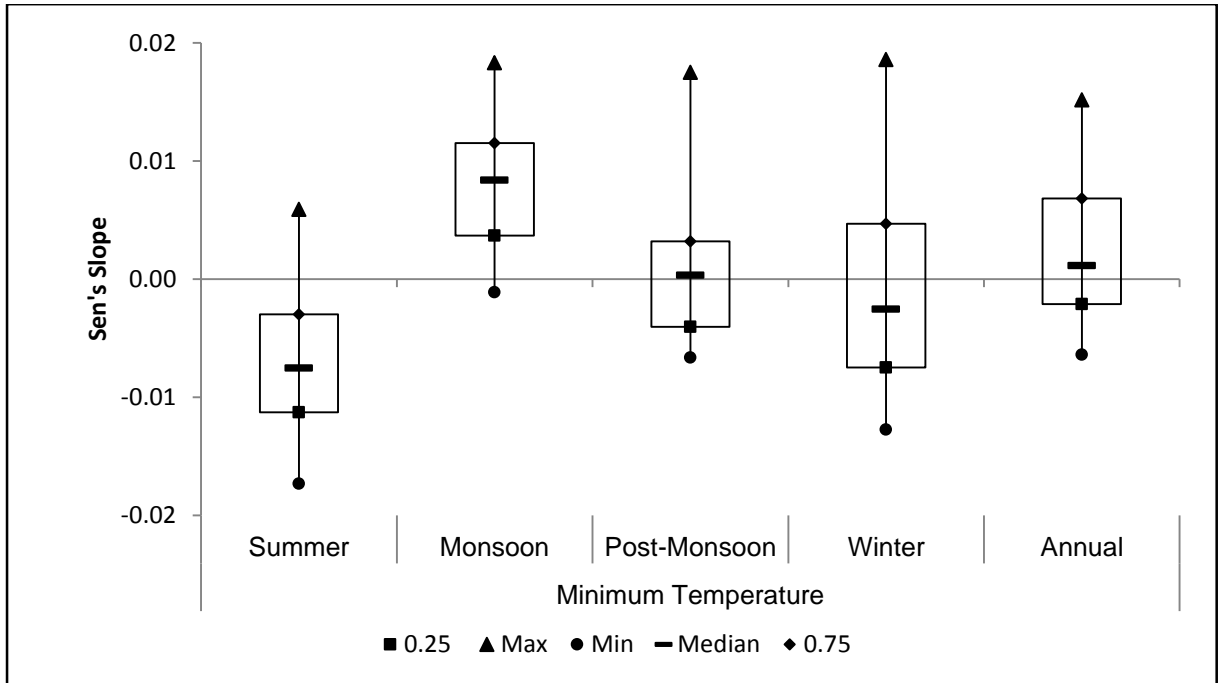
Figure 3.6 Box-and-Whisker plot of the magnitude of Sen's slope of average minimum temperature

Spatial pattern of changes in annual average minimum temperatures using the magnitude of Sen's slope over the basin is shown in figure 3.7. Upper basin, which is on Western Ghats, shows rise in annual average minimum temperatures. On the contrary, middle and lower parts of the basin show reduction in minimum temperature. Thus, it is concluded that the upper basin experienced warming whereas the middle part of the basin experienced cooling.
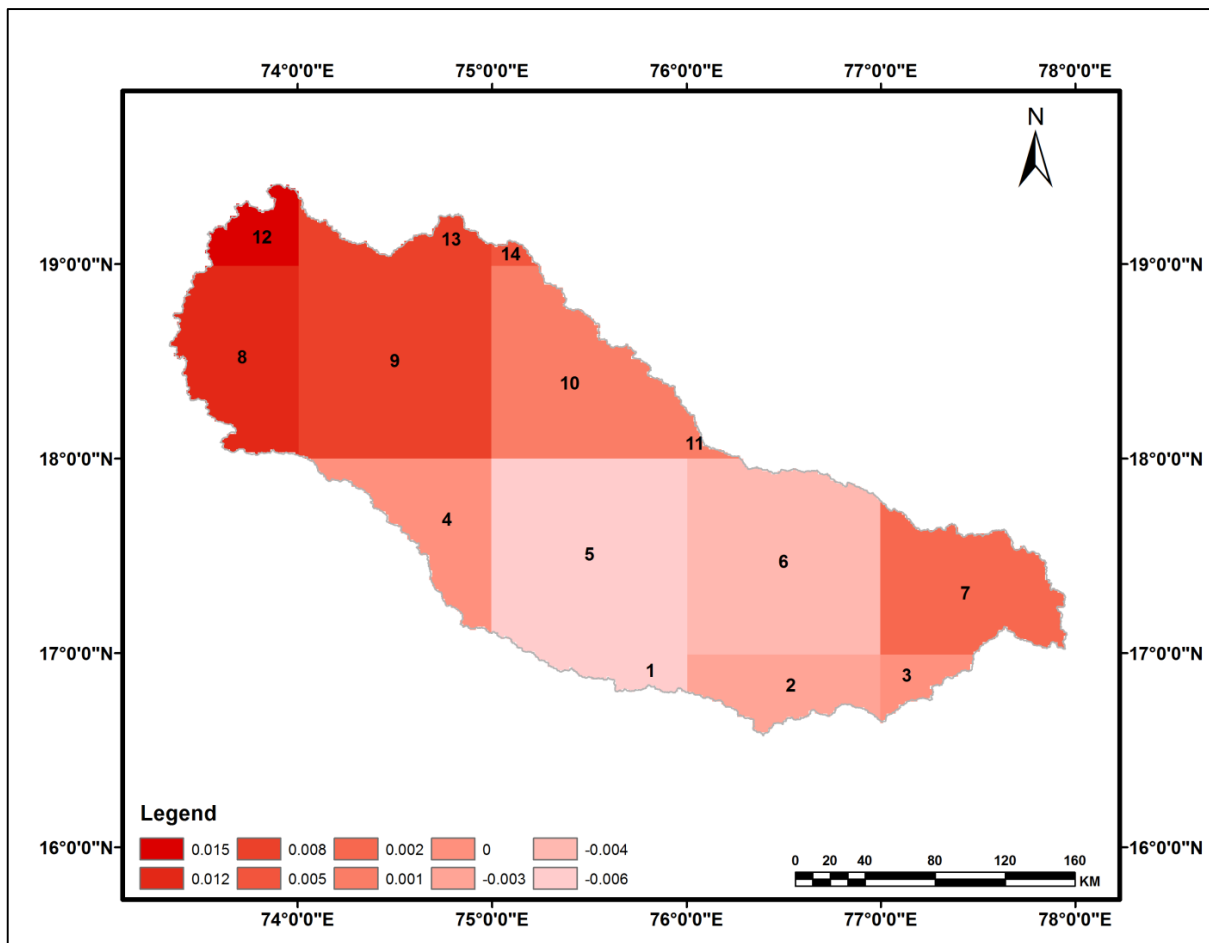
Figure 3.7 Spatial variability in annual average minimum temperature in the Bhima basin

3.6.1.2 Seasonal and annual changes in average maximum temperature

The results of autocorrelation analysis, MK/MMK and Sen's slope for seasonal and annual series of average maximum temperatures are given in table 3.2. No significant autocorrelation was found in seasonal average maximum temperature.

All the 14 grids of the basin exhibit rise in average maximum temperature during all the seasons. The significant increasing trends were observed during post-monsoon and winter seasons in most of the grids. The highest rise of 0.04°C (in 41 years) was observed in grid #8 in post-monsoon season, and in grids #3 (0.043°C) in winter season.

Significant autocorrelation in annual average maximum temperatures was found in five grids. All grids of the basin exhibit rise in annual maximum temperatures with significant rise in eight grids as seen in the table 3.2. An average rise of 0.02°C was observed in 41 years in the basin.

30

Table 3.2 Result of MK /MMK test and Sen's slope estimator test of seasonal and annual average maximum temperature during 1969-2009

Series	Annual		Seasonal							
			Summer		Monsoon		Post-Monsoon		Winter	
Grids	MK/ MMK	Sen's Slope	MK/ MMK	Sen's Slope	MK/ MMK	Sen's Slope	MK/ MMK	Sen's Slope	MK/ MMK	Sen's Slope
1	**3.336**	0.014	1.067	0.007	**1.718**	0.012	**1.876**	0.021	**3.510**	0.027
2	1.281*	0.016	1.450	0.010	1.561	0.014	**2.235**	0.024	**4.110**	0.035
3	1.321*	0.021	**1.700**	0.015	**1.990**	0.018	**2.752**	0.030	**4.160**	0.043
4	**3.426**	0.019	1.224	0.013	**2.010**	0.016	**2.258**	0.024	**3.200**	0.029
5	**2.707**	0.014	0.820	0.007	1.426	0.013	**1.970**	0.022	**2.690**	0.026
6	1.222*	0.016	0.620	0.006	1.000	0.012	**2.392**	0.029	**3.880**	0.037
7	1.245*	0.017	0.460	0.006	1.157	0.011	**2.684**	0.029	**4.020**	0.037
8	**2.976**	0.023	1.450	0.012	**1.853**	0.017	**2.370**	0.035	**3.550**	0.030
9	**2.640**	0.019	1.270	0.015	1.471	0.017	**2.505**	0.030	**3.040**	0.027
10	**2.100**	0.011	0.520	0.007	0.620	0.007	1.430	0.020	**2.060**	0.022
11	0.826*	0.012	0.530	0.005	0.393	0.004	**1.990**	0.023	**3.160**	0.034
12	**3.560**	0.018	**1.760**	0.013	1.202	0.010	**2.030**	0.022	**3.250**	0.026
13	**2.864**	0.012	1.380	0.010	0.730	0.008	**1.700**	0.020	**2.440**	0.025
14	1.364	0.007	0.240	0.002	**3.370**	0.000	0.980	0.015	**1.970**	0.023
Note: *indicates presence of autocorrelation in the temperature series; Bold numbers represent significant increasing and decreasing trends in the series.										

Box-and-Whisker plot of magnitude of Sen's slope for seasonal and annual average maximum temperature of the basin are shown in figure 3.8. The median of the slope of seasonal and annual series are in positive zone that indicates rise in maximum temperature. Spatial pattern of the changes in the annual average maximum temperature is shown in figure 3.9. As seen, the upper and lower parts of the basin show high rise in average maximum temperature compared to middle part of the basin.
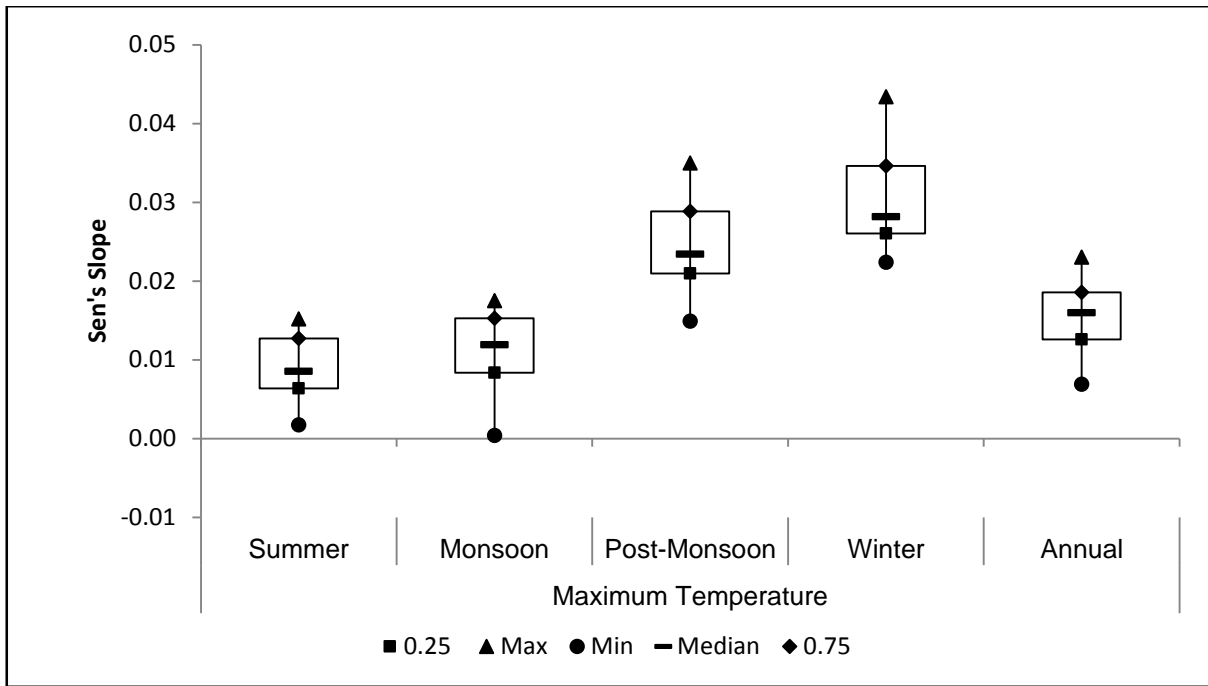
Figure 3.8 Box-and-Whisker plot of the magnitude of Sen's slope of average maximum temperature
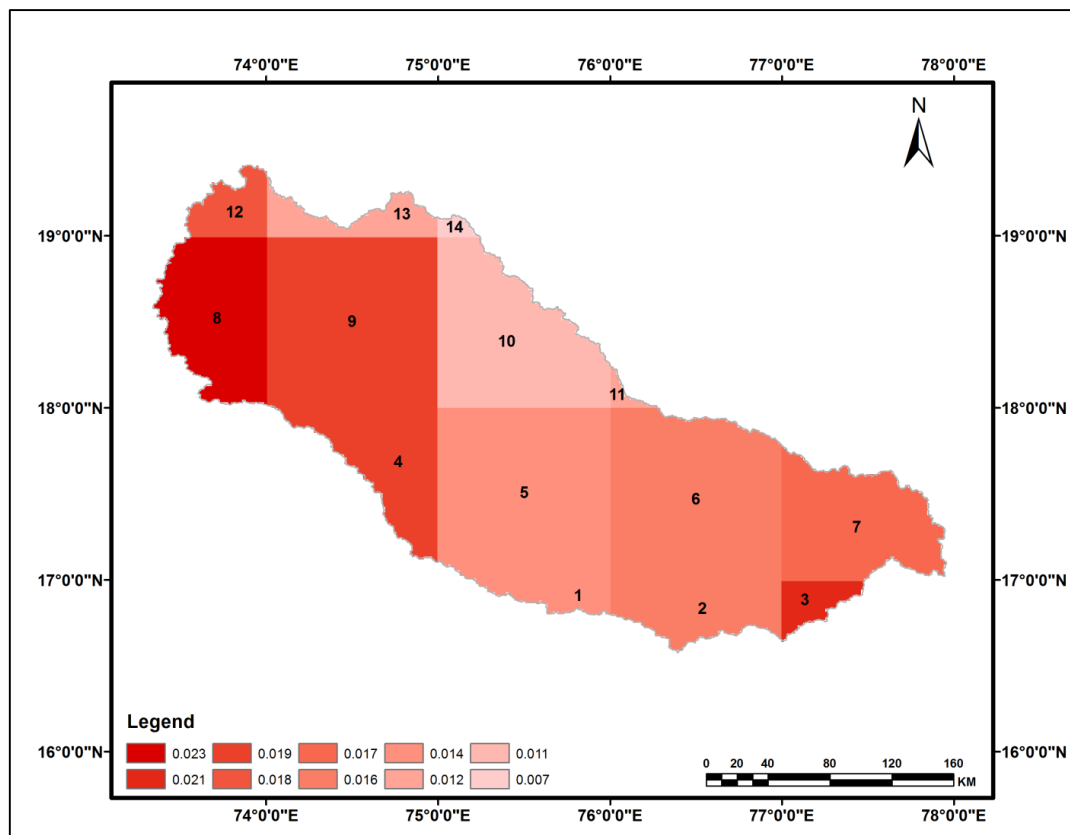
Figure 3.9 Spatial variability in annual average maximum temperature in the Bhima basin

3.6.1.3 Seasonal and annual changes in average mean temperature of the basin

Results of autocorrelation analysis, MK/MMK test and trend analyses for seasonal and annual average mean temperature series are given in table 3.3. There was no significant autocorrelation found in the seasonal mean temperature. All seasonal series excluding summer season indicate rise in average mean temperature. Non-significant decreasing trend was found in six grids (grid #5, #6, #7, #10, #11 and #14) in summer season.

Out of 14, only two grids (grid #12 and #14) show significant autocorrelation in annual average mean temperature at 10% level. All grids show increasing trend in annual average mean temperature however significant trend was found only at four grids (grid #3, #8, #9, and #13). Sen's slopes also demonstrate rising trend in annual average mean temperature.

Table 3.3 Result of MK /MMK test and Sen's slope estimator test of seasonal and annual average mean temperature during 1969-2009

Series	Annual		Seasonal							
			Summer		Monsoon		Post-Monsoon		Winter	
Grids	MK/ MMK	Sen's Slope	MK/ MMK	Sen's Slope	MK/ MMK	Sen's Slope	MK/ MMK	Sen's Slope	MK/ MMK	Sen's Slope
1	1.000	0.006	0.168	0.001	0.702	0.012	0.977	0.013	**1.806**	0.011
2	1.337	0.007	0.000	0.000	0.685	0.010	0.932	0.010	**1.666**	0.013
3	**2.190**	0.011	0.505	0.004	0.808	0.015	**1.696**	0.016	**1.992**	0.018
4	1.471	0.008	0.303	0.001	0.460	0.008	0.708	0.008	1.48	0.010
5	0.393	0.002	-0.842	-0.005	0.538	0.005	0.236	0.004	0.431	0.006
6	0.797	0.006	-0.505	-0.004	0.560	0.008	0.887	0.010	1.363	0.015
7	0.218	0.010	-0.034	0.000	0.734	0.011	**1.606**	0.019	**1.900**	0.019
8	**2.932**	0.016	1.224	0.009	**2.145**	0.017	1.494	0.017	**2.388**	0.021
9	**2.078**	0.010	0.753	0.005	0.719	0.014	1.044	0.012	1.363	0.016
10	0.528	0.004	-0.044	-0.001	0.550	0.009	0.753	0.011	0.664	0.005
11	0.977	0.005	-0.240	-0.003	1.112	0.007	0.865	0.012	1.27	0.013
12	1.219*	0.015	1.202	0.009	0.821	0.015	1.247	0.015	**2.901**	0.024
13	**1.651**	0.009	0.281	0.003	0.932	0.005	0.932	0.013	**2.132**	0.022
14	0.640*	0.005	-0.240	-0.003	0.797	0.006	0.236	0.004	1.200	0.013

Note: *indicates presence of autocorrelation in the temperature series; Bold numbers represent significant increasing and decreasing trends in the series.

Box-and-Whisker plot of the magnitude of slope (Figure 3.10) for seasonal and annual average mean temperature series show that the medians of the slopes are on the positive side. It indicates that the average mean temperature has gone up in the basin. Maps depicting spatial pattern of the changes in annual mean temperatures is given in figure 3.11. Temperature distribution, as seen in the map, shows higher rise in upper and lower zones compared to middle zone of the basin.
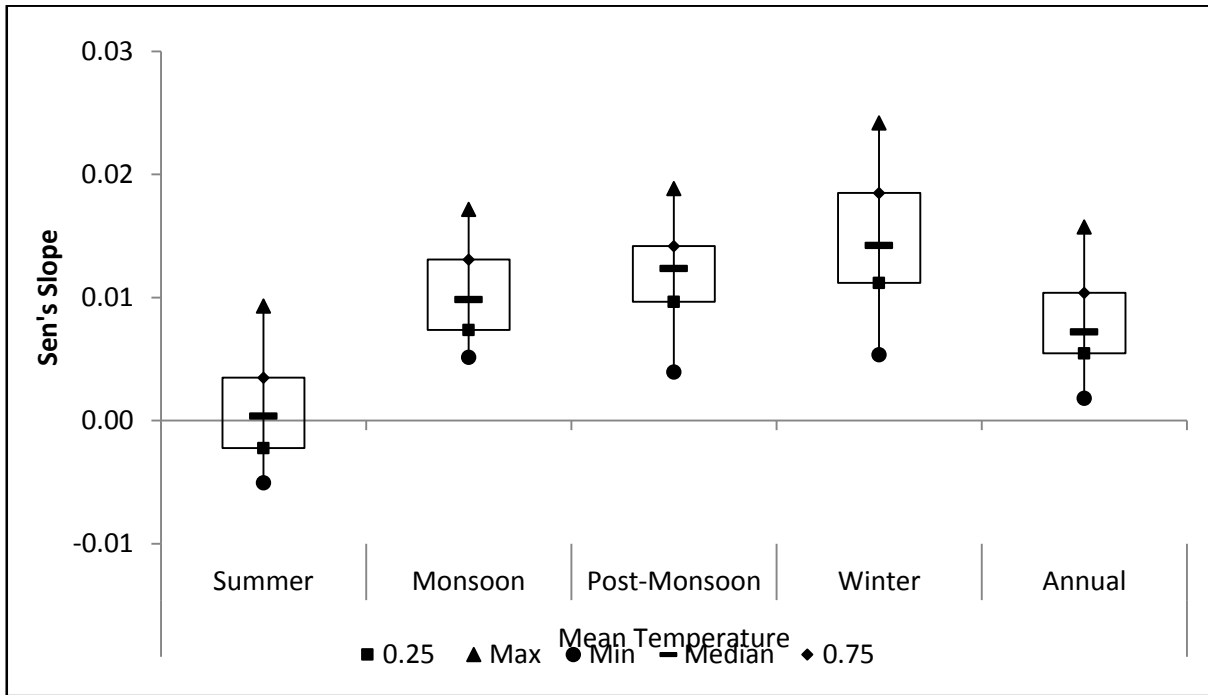
Figure 3.10 Box-and-Whisker plot of the magnitude of Sen's slope of average mean temperature
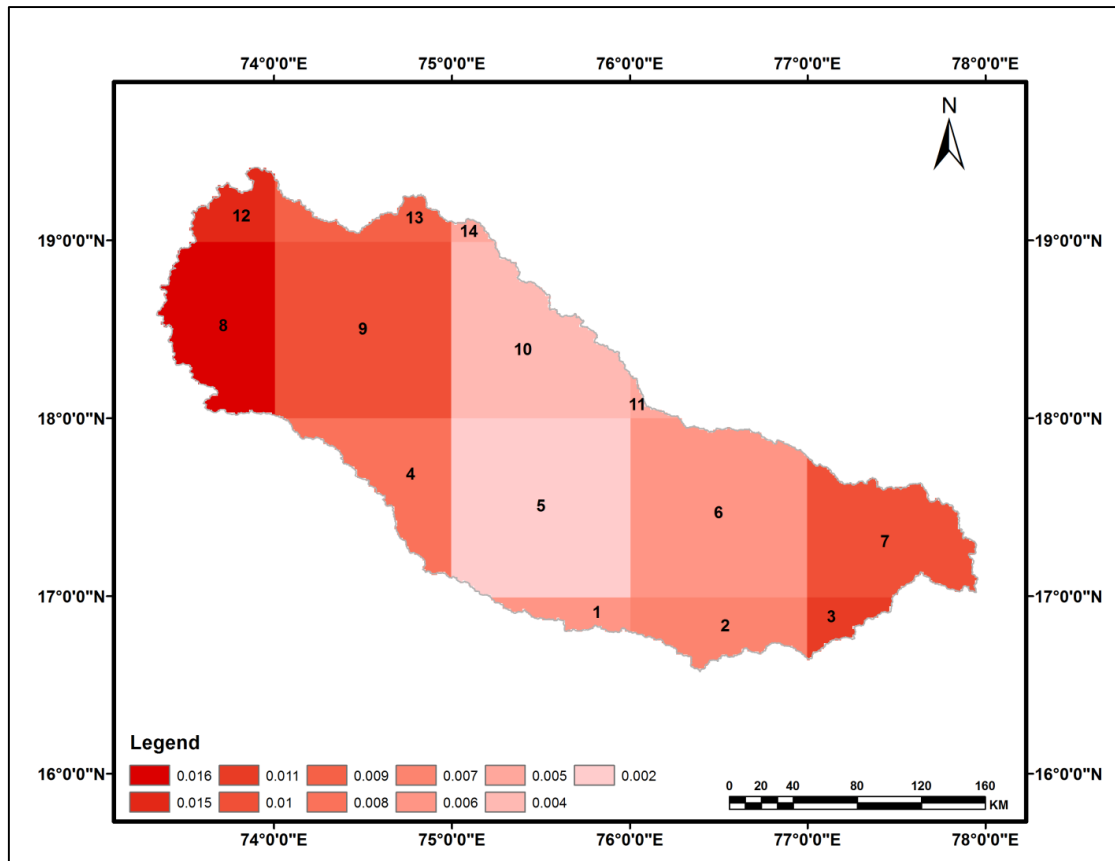
Figure 3.11 Spatial variability in annual average mean temperature in the Bhima basin

3.6.1.4 Homogeneity of seasonal and annual trends of temperature

Van Belle and Hughes' homogeneity of trend test was used to test the homogeneity of the trends in seasonal and annual temperatures. The results of the test are given in table 3.4. The null hypothesis - the trends are homogeneous across the basin - was tested at 10% significance level. The table show that the null hypothesis was accepted for all seasonal as well as annual trends of temperatures. In other words, the increasing/decreasing trends determined in the previous sections are homogeneous across all the grids.

Table 3.4 Results of homogeneity of trend test in the Bhima basin

Series	Test	$\chi^2_{homogenous}$		
	Temperature	**Minimum**	**Maximum**	**Mean**
Seasonal	**Summer**	8.01*	3.22*	4.59*
	Monsoon	9.09*	7.21*	2.25*
	Post-monsoon	2.74*	3.07*	2.50*
	Winter	6.42*	6.78*	5.52*
Annual		8.74*	12.22*	7.65*
Note: *indicates statistically significant homogeneous trend				

3.6.1.5 Seasonal and annual trends of average basin temperature

The average basin series of seasonal and annual temperature were prepared by averaging temperatures of the 14 grids. Results of autocorrelation analysis, MK/MMK test and Sen's slope of the entire basin are given in table 3.5.

Seasonal analysis of average minimum temperature of the entire basin shows a decreasing trend in summer, post-monsoon and winter seasons except monsoon season as seen in the table. An increasing trend was observed in average maximum and average mean temperature of the entire basin for all the seasons. Significant increasing trend was found in annual maximum temperature, however, non-significant increasing trends were observed in annual minimum and mean temperatures in the basin (Table 3.5).

Sen's slope test results indicate that the highest increase took place in the maximum temperature. Over a period of 41 years, it is 0.027°C for winter season indicating that the winters are becoming warmer; and, it is 0.014°C for annual temperature indicating that the Basin, in general, is getting warmer. The increase in the mean temperature also indicates the same but the values are very small. Since most of the seasonal and annual temperature series show increasing trends, it is concluded that the basin has become warmer during the past 41 years.

Table 3.5 Result of MK /MMK test and Sen's slope estimator test of seasonal and annual temperature over the entire Bhima basin

Series	Test	Minimum	Maximum	Mean
Summer	MK/MMK	-1.134	1.07	0.168
	Sen's slope	-0.007	0.007	0.001
Monsoon	MK/MMK	**1.786***	**1.718**	0.837*
	Sen's slope	0.008	0.012	0.011
Post-Monsoon	MK/MMK	-0.034	1.88	0.977
	Sen's slope	-0.0004	0.021	0.013
Winter	MK/MMK	-0.105	3.51	1.806
	Sen's slope	-0.002	0.027	0.011
Annual	MK/MMK	0.281*	**3.34**	1.449*
	Sen's slope	0.002	0.014	0.007
Note: *indicates presence of autocorrelation and bold numbers represent significant trends				

3.6.2 Spatio-temporal Analysis of Rainfall Data

Figures 3.12 and 3.13 represent the spatial pattern of average annual and average monsoon rainfall over the Bhima basin. Preliminary analysis of the rainfall data shows that the average annual/monsoon rainfall varies from 2264/2127 mm to 502/356 mm during 1901-2004 as seen in the figures. Spatial rainfall pattern shows that the upper and lower basin receives higher rainfall then the middle part, in general.
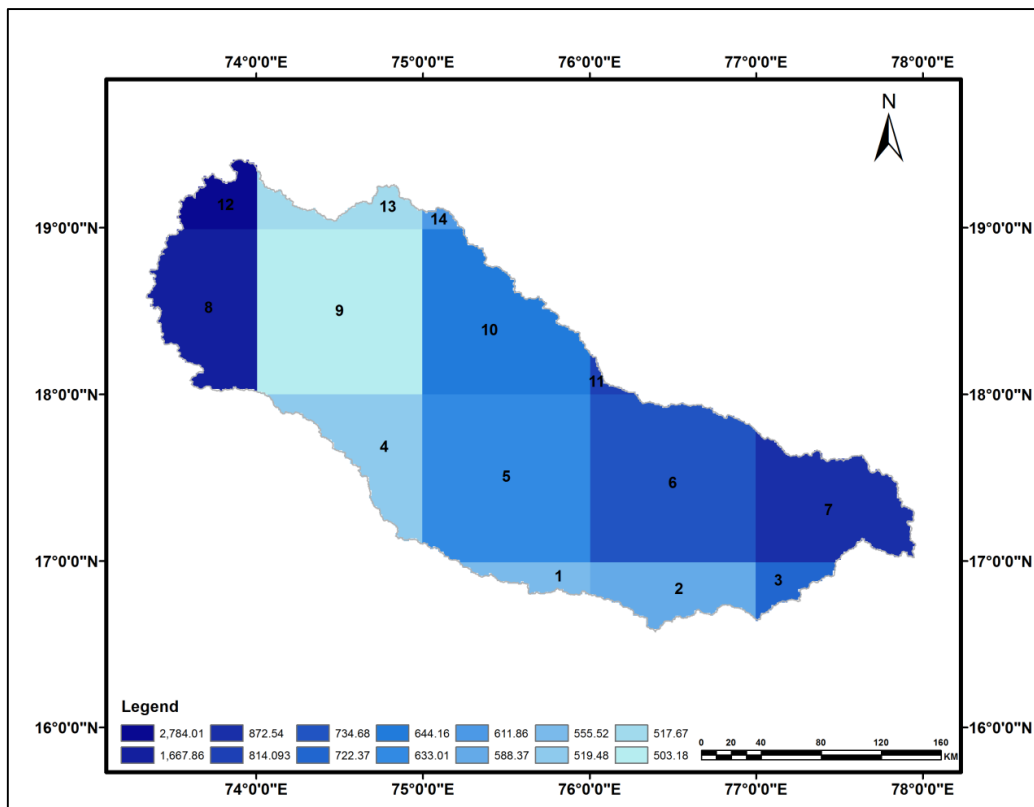
Figure 3.12 Spatial pattern of annual rainfall in the Bhima basin during 1901 – 2004
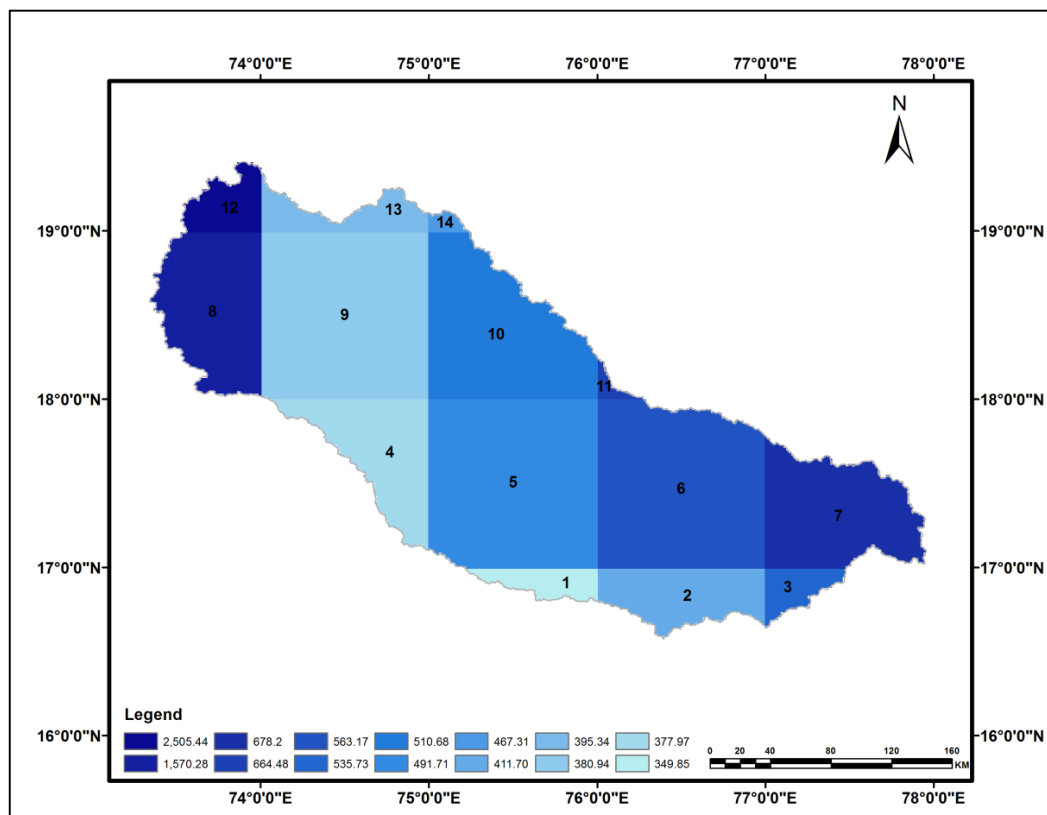
Figure 3.13 Spatial pattern of monsoon rainfall in the Bhima basin during 1901 – 2004

3.6.2.1 Changes in seasonal rainfall patterns

The results of autocorrelation analysis of seasonal rainfall series are given in table 3.6 along with Z statistics of MK/MMK test and magnitude of Sen's slope test. Statistically, monsoon rainfall of grid #8 was found autocorrelated at 10% significance. Hence, MMK test was used for grid #8 rainfall series. Trend analysis of summer season shows non-significant decreasing trends in eight grids while remaining grids show increasing trend. Significant increasing trend was found in monsoon season in three grids and non-significant decreasing trend was observed in grids #7, #12 and #14. Increasing trend was observed for all the grids (significant in grid #1, #2, #7 and #11) for post-monsoon season whereas decreasing trend was detected for winter season (significant in grid #2, #4, #7, #9, #10, #13 and #14).

Table 3.6 also shows the percent changes over mean values in seasonal rainfall. The maximum percent increase in rainfall was observed in summer, monsoon and post-monsoon season at grid #2, #9 and #7, respectively. Maximum percent decrease was found in summer, monsoon and winter seasons at grid #4, #12 and #7, respectively.

Over the 104 years, the rainfall decreased in summer seasons and increased during the monsoon and post-monsoon seasons. The change in summer rainfall ranged from -3.7% to -28.7% in 8 out of 14 grids and from 0% to 21% at the other 6 grids. Thus, almost half of the basin received below normal rainfall during the summer season indicating water scarcity in summers. The monsoon rainfall on the other hand shows an increase of 0.5% to 23.6% at 11 out of 14 grids. The effects of this increase may be positive or negative impacts depending upon the timing and intensity of rainfall. The change in post-monsoon rainfall ranged from 15% to 65% at 12 out of 14 grids. Such a large increase may not have much impact in the basin as magnitude of post-monsoon rains is small in the total rainfall. The winter season rainfall doesn't seem to change much across the basin.

Monsoon rainfall contibutes more than 80% to the annual rainfall. Therefore spatial pattern of percent changes in monsoon rainfall only is shown in figure 3.14. Highest positive magnitude of Sen's slope is seen in grids #9 and highest negative magnitude of Sen's slope in grid #12. The middle zone shows higher percent change in monsoon rainfall, as seen in the figure, which decreases towards the upper and lower parts of the basin. Overall, an increasing trend was found in most of the grids in monsoon season.

Table 3.6 Result of MK (MMK) test and percent change of seasonal rainfall during 1901-2004

Seasons	Summer			Monsoon			Post-Monsoon			Winter		
Grids	MK/MMK	Sen's Slope	% change	MK/MMK	Sen's Slope	% change	MK/MMK	Sen's Slope	% change	MK/MMK	Sen's Slope	% change
1	0.169	0.03	3.69	0.601	0.22	6.57	**1.944**	0.51	41.26	-1.074	0.00	-1.29
2	1.483	0.13	21.02	**1.790**	0.69	18.63	**1.775**	0.45	37.87	**-1.761**	0.00	-3.62
3	1.084	0.12	21.13	0.444	0.24	4.58	1.489	0.37	32.49	-0.643	0.00	0.00
4	-1.463	-0.14	-28.70	1.430	0.60	17.97	0.851	0.18	16.83	**-2.089**	0.00	0.00
5	0.002	0.00	0.55	**1.823**	0.86	19.51	1.290	0.31	26.64	-1.225	0.00	-2.12
6	-0.188	-0.02	-3.66	0.278	0.16	2.99	1.542	0.35	32.95	-1.516	-0.02	-13.51
7	1.081	0.12	19.67	-0.143	-0.06	-0.91	**2.761**	0.67	65.17	**-1.743**	-0.05	-29.16
8	0.180	0.01	2.19	0.392*	1.59	10.94	1.115	0.25	23.82	-1.213	0.00	0.00
9	-1.311	-0.06	-22.60	**2.067**	0.81	23.62	1.497	0.34	33.42	**-2.234**	0.00	-1.24
10	-0.303	-0.01	-4.21	1.050	0.64	13.30	1.115	0.24	26.15	**-2.701**	-0.02	-18.82
11	-1.171	-0.08	-21.05	0.053	0.03	0.53	**1.944**	0.40	45.73	-1.624	-0.03	-17.76
12	-1.149	0.00	0.00	-0.756	-1.71	-6.73	0.135	0.02	2.08	-1.071	0.00	0.00
13	-1.045	-0.03	-16.97	1.014	0.46	12.03	1.109	0.19	22.09	**-2.203**	-0.01	-7.55
14	-1.450	-0.05	-24.65	-0.576	-0.30	-6.29	0.430	0.08	10.10	**-2.656**	-0.02	-14.67

Note: *indicates the presence of autocorrelation in the series; Bold values represent the significant trend; Cyan colour shows the highest percent increase and yellow colour shows the highest decrease in a series
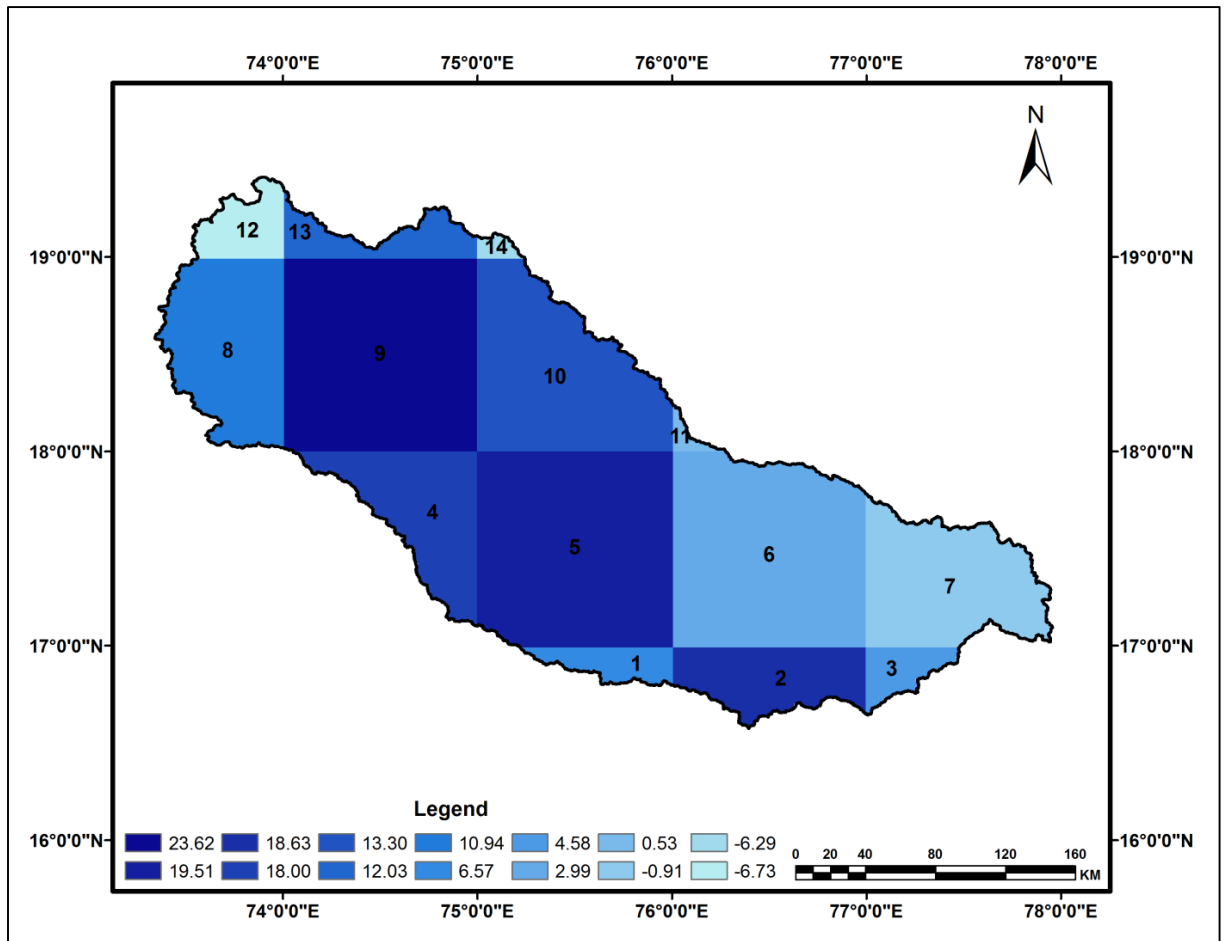
Figure 3.14 Spatial variability map of monsoon rainfall represented by the Sen's slope in the Bhima basin during 1901-2004

An increase in anthropogenic activities was observed all over the world during 1960-1990 (Kittel *et al*., 1995; Hulme *et al*., 1999). Therefore to find the effect of these activities, trend analysis was also performed for a shorter time span of 44 years i.e. during 1961-2004. The results of trend analysis are presented in table 3.7 along with Z statistics of MK/MMK test and percent change in magnitude over the mean. Only, two grids show presence of autocorrelation in summer season. Most of the grids show decreasing trends for summer and monsoon season rainfall and increasing trends for post-monsoon and winter season rainfall. The significant decreasing trends were observed at grids #1, grid #9 and #14 in summer season and at grid #7 in monsoon season. Spatial pattern of percent change in monsoon rainfall over the mean is shown in figure 3.15. It shows a decreasing monsoon rainfall over the entire basin as the negative slopes were found in most of the grids. The highest increase was found at grid #9 in monsoon rainfall whereas the highest decrease at grid #8. The grid #9 is located on the leeward side of the Western Ghats in the Basin. Since, grid #8 partially falls in the Bhima basin

41

and partially on the windward side of the Ghats; its geographical location might be playing a role in getting these results. Spatially, a decreasing monsoon rainfall trend is observed from the upper to the lower basin.
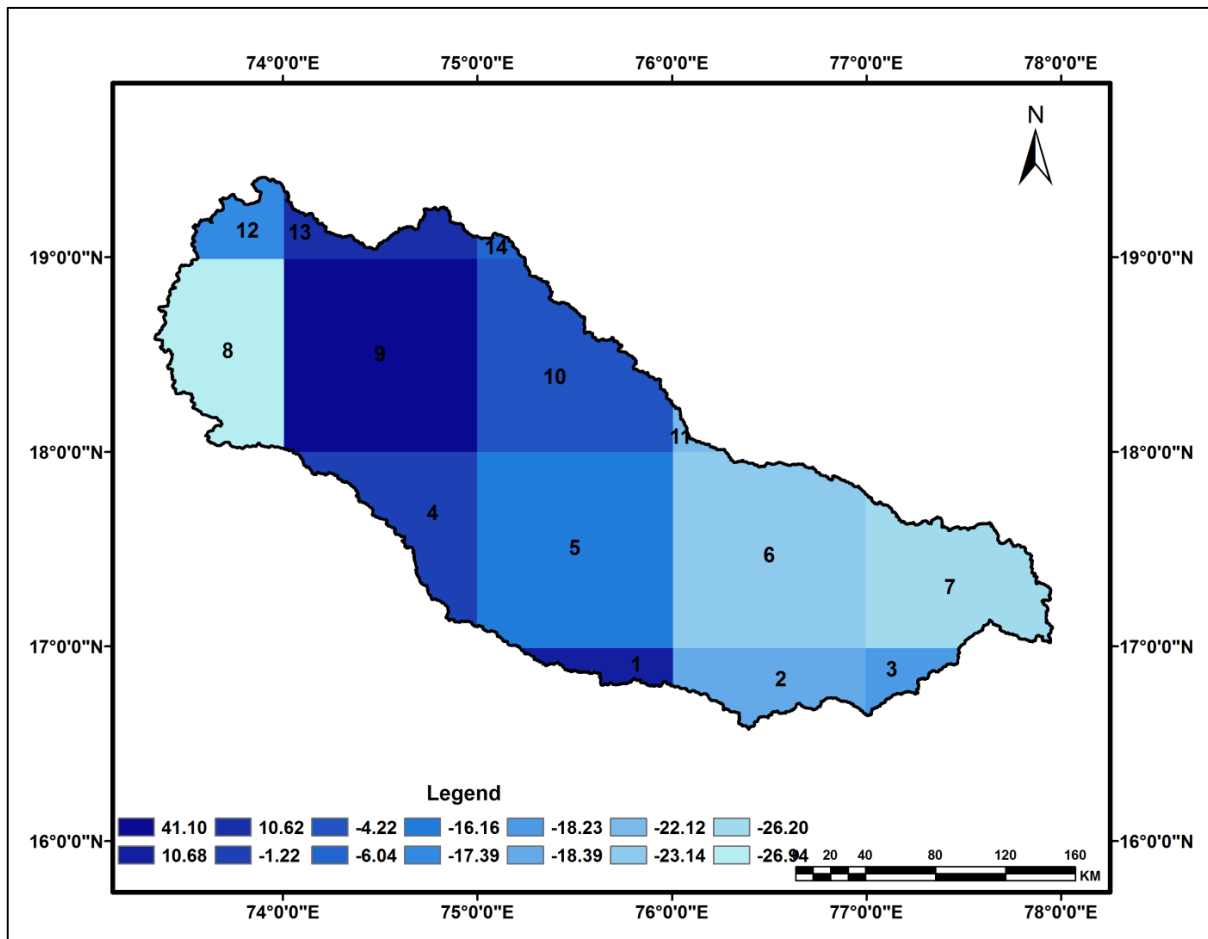
Figure 3.15 Spatial variability map of monsoon rainfall represented by the Sen's slope in the Bhima basin during 1961-2004

Table 3.7 Result of MK (MMK) test and percent change of seasonal rainfall during 1961-2004

Seasons	Summer			Monsoon			Post-Monsoon			Winter		
Grids	MK/ MMK	Sen's Slope	% change	MK/ MMK	Sen's Slope	% change	MK/ MMK	Sen's Slope	% change	MK/ MMK	Sen's Slope	% change
1	**-1.851**	-0.87	-55.11	0.637	0.85	10.68	-0.202	-0.11	-3.46	0.627	0.00	0.00
2	0.293	0.20	12.62	-1.123	-1.72	-18.39	0.759	0.69	21.57	0.718	0.00	0.00
3	-0.597	-0.30	-20.04	-1.588	-2.22	-18.23	0.179	0.26	8.63	0.85	0.02	7.51
4	-2.62	-0.95	-91.95	-0.071	-0.11	-1.22	0.253	0.16	6.12	-0.152	0.00	0.00
5	-0.354	-0.14	-14.59	-0.941	-1.81	-16.16	0.212	0.17	5.49	0.374	0.00	0.00
6	-0.446*	-0.60	-53.14	-1.305	-2.96	-23.14	0.577	0.44	15.90	-0.051	0.00	0.00
7	-0.435	-0.21	-14.09	**-1.689**	-4.04	-26.20	1.467	1.44	49.88	-0.091	0.00	0.00
8	-1.396	-0.40	-54.40	-1.79	-9.61	-26.94	0.00	-0.01	-0.45	0.485	0.00	0.00
9	**-1.882**	-0.42	-69.60	2.134	3.56	41.10	0.799	0.60	23.74	0.506	0.00	0.00
10	-1.345*	-0.41	-47.76	-0.104*	-0.49	-4.22	0.657	0.53	22.64	0.040	0.00	0.00
11	-0.658	-0.57	-69.24	-1.387	-3.34	-22.12	0.091	0.11	4.75	0.334	0.00	0.00
12	-0.516	0.00	0.00	-1.325	-9.90	-17.39	1.163	0.83	42.85	-0.354	0.00	0.00
13	-1.286	-0.16	-38.04	0.374	0.95	10.62	0.839	0.55	27.38	-0.263	0.00	0.00
14	**-1.831**	-0.26	-59.55	0.455	-0.64	-6.04	0.9	0.59	32.27	-0.384	0.00	0.00

Note: *indicates the significant presence of autocorrelation in the series; Bold values represent the significant trend; Cyan colour shows the highest percent increase and yellow colour shows the highest decrease in a series

The rainfall trend observed during the recent duration represents different trends in the seasonal rainfall. The range of percent change in summer rainfall during recent years was -15% to -92% at 12 out of 14 grids. The recent duration analysis shows a decreasing summer rainfall similar to the 104 year duration analysis. However, the percent decrease in rainfall has gone up. This reduction during summer season necessitates a better water resources planning and management to deal with the water scarcity. The monsoon season rainfall during the recent period shows a decreasing trend at 11 out 14 grids with percent change ranging between -1% to -27%. These results are in contrast to the results of 104 year duration analysis where it shows increasing trend in the monsoon season. The post-monsoon and winter season rainfalls show similar trends during the recent period as those during the 104 year period. Overall, the analysis of recent duration trends have shown relatively dryer summer and monsoon seasons in the basin.

3.6.2.2 Changes in annual rainfall pattern

The results of autocorrelation analysis of annual rainfall series for the two durations i.e. 1901-2004 and 1961-2004 are presented in table 3.8 along with Z statistics of MK/MMK test and Sen's slope. Only six out of 28 annual rainfall series were found autocorrelated at 10% significance level. Of the six, five series were from 1901-2004 duration. During 1901-2004, most of the annual rainfall series exhibited an increasing trend; only two series (grid #2 and grid #10) trends were found significant. On the Contrary, recent duration i.e. 1961-2004 shows a non-significant decreasing trend in most of the grids except in grid #9 (significant, increasing) and grid #13 (non-significant, increasing).

Table 3.8 also shows the percent changes over mean values in annual rainfall. For 104 years duration, highest percent increase/decrease in annual rainfall were observed at grid #9 (27.6%)/grid #12 (-8.7%). For recent duration, grid #8 shows the highest percent reduction (-26.8%) while grid #9 shows the highest percent increase (30.1%) in annual rainfall. In general, the grids located at higher elevations (Western Ghats) showed decrease in rainfall pattern during recent years.

Table 3.8 Results of annual rainfall trend analysis including MK/ MMK test statistics and percent change over 1901-2004 and 1961-2004

Annual Rainfall Grids#	1901-2004			1961-2004		
	MK/MMK	Sen's slope	% change	MK/MMK	Sen's slope	% change
1	1.416	0.664	12.5	-0.071	-0.10	-0.7
2	**2.455**	1.384	24.5	-0.172	-0.55	-3.8
3	1.407	0.802	11.5	-0.920	-1.95	-11.5
4	1.528	0.803	16.1	-0.405	-1.12	-9.0
5	0.674*	1.446	23.8	-0.496	-1.36	-8.7
6	0.89	0.601	8.5	-1.588	-4.23	-24.9
7	1.623	0.635	7.6	-1.537	-2.92	-14.5
8	0.401*	2.145	13.4	-0.603*	-10.51	-26.8
9	0.687*	1.335	27.6	**1.952**	3.62	30.1
10	**1.761**	1.171	19.00	-0.071	-0.12	-0.8
11	0.149*	0.36	4.6	**-1.649**	-4.37	-23.6
12	-1.104	-2.33	-8.7	-1.224	-9.10	-15.3
13	1.357	0.758	15.3	0.941	1.83	15.6
14	-0.164*	-0.397	-6.8	-0.880	-1.94	-14.7

Note: *indicates the significant presence of autocorrelation in the series; Bold values represent the significant trend; Cyan colour shows the highest percent increase and yellow colour shows the highest decrease in a series

Spatial variability of the changes in annual rainfall with respect to mean for both durations (1901-2004 and 1961-2004) are shown in figure 3.16 and 3.17. A comparision of the spatial patterns seen in these figures brought out the fact that the grids in the middle zone of the basin show an increase in rainfall during 104 years and a decrease in rainfall during the recent duration. Also, the figures clearly show that these changes are dominant in valley portion of the basin than the higher elevations near the boundry.
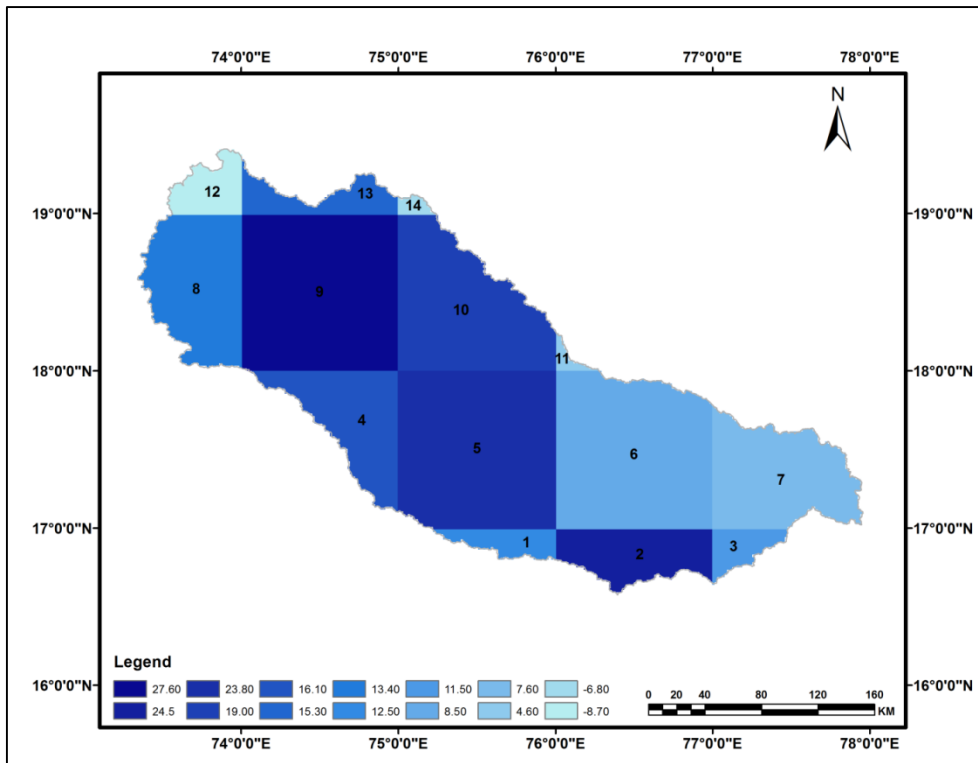
Figure 3.16 Spatial variability map of annual rainfall represented by the Sen's slope in the
Bhima basin during 1901-2004
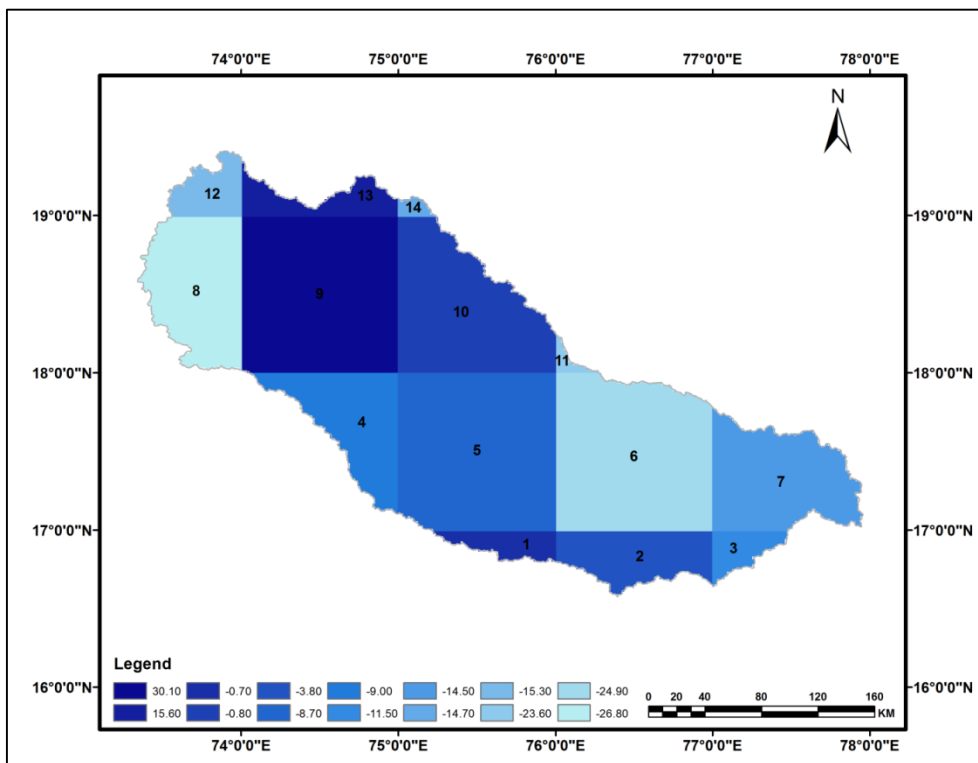
Figure 3.17 Spatial variability map of annual rainfall represented by the Sen's slope in the
Bhima basin during 1961-2004

3.6.2.3 Analysis of magnitude of slope in sesaonal and annual rainfall trends

The box-plots of Theil-Sen's slopes for seasonal and annual rainfall series over the basin are shown in figure 3.18 and figure 3.19 for the two time periods i.e 1901-2004 and 1961-2004, respectively. At the seaonal and annual scales, the medians of slopes are located above zero line during 1901-2004 and below the zero line during 1961-2004 (except for the post-monsoon season). This concludes that the rainfall is found increasing during 1901-2004 and decreasing during 1961-2004.
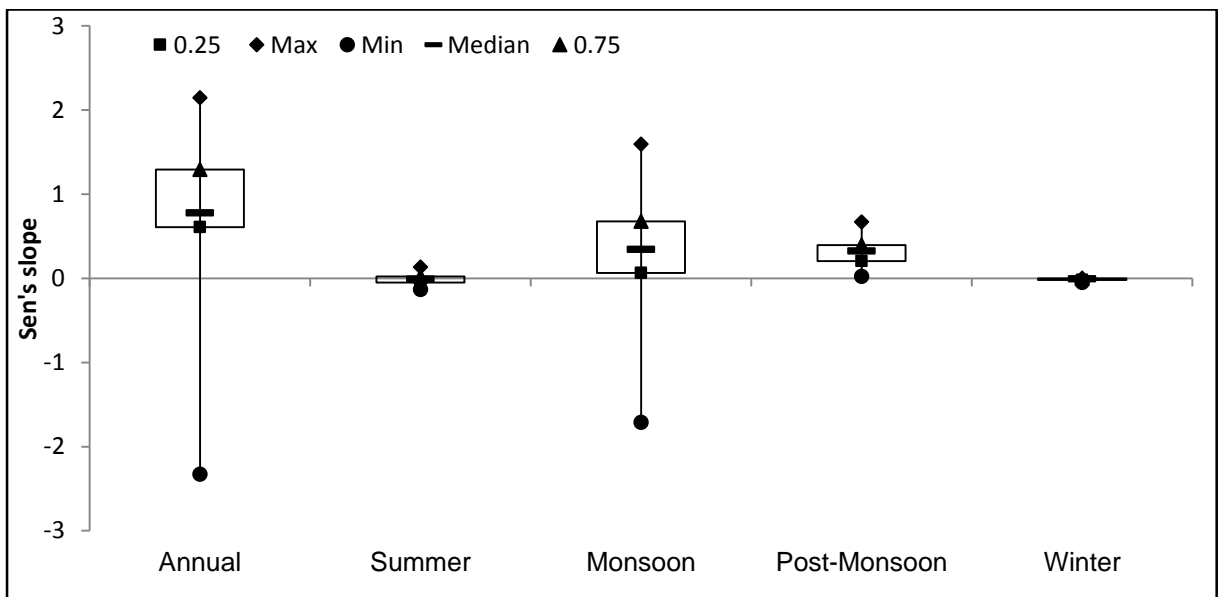
Figure 3.18 Box-and-Whisker plot of the magnitude of Theil and Sen's slope during 1901-2004
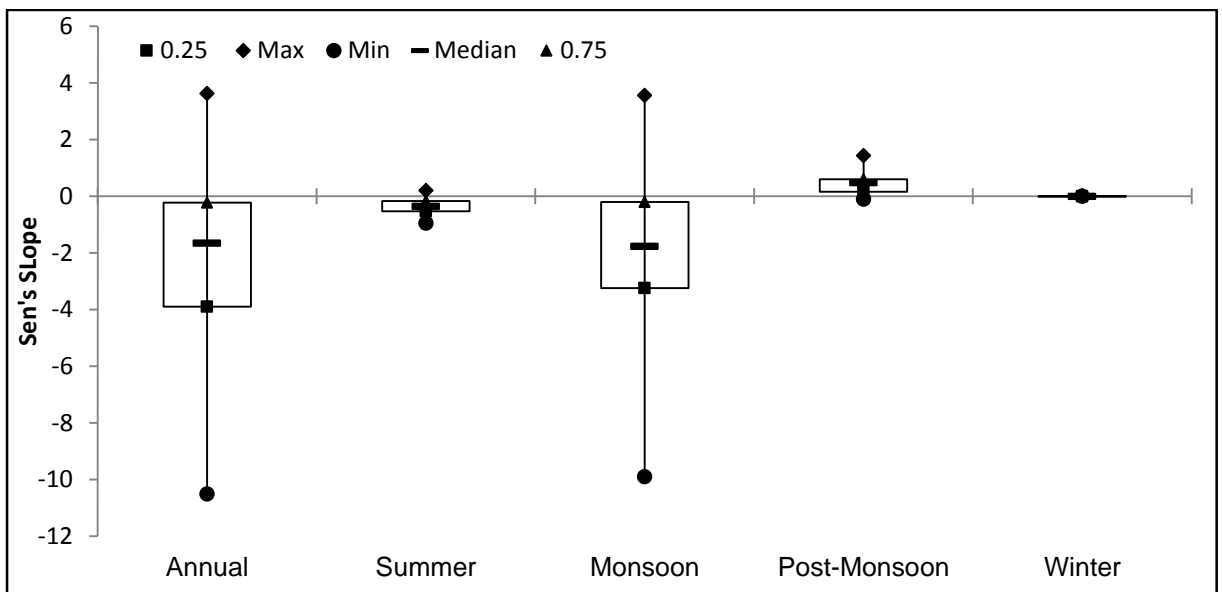
Figure 3.19 Box-and-Whisker plot of the magnitude of Theil and Sen's slope during 1961-2004

3.6.2.4 Analysis of homogeneity of seasonal and annual rainfall trends

To test homogeneity of trends across seasonal and annual rainfall, Van Belle and Hughes' homogeneity trend test was applied on all rainfall series of all the grids. Results of the test are given in table 3.9. At 10% significance level, null hypothesis of homogeneity of trends is accepted for seasonal and annual rainfall trends during 1901-2004 and 1961-2004. It concluded that the trends in seasonal and annual rainfall obtained in previous sections are homogeneous trends across the all grids.

Table 3.9 Results of homogeneity of seasonal and annual rainfall trends

Series	Test	$\chi^2_{homogenous}$	
	Duration	**1901-2004**	**1961-2004**
Seasonal	**Summer**	13.29*	8.34*
	Monsoon	10.35*	17.17*
	Post-monsoon	5.70*	2.96*
	Winter	5.02*	2.25*
	Annual	10.85*	13.00*
Note: *indicates significant homogeneous			

3.6.2.5 Seasonal and annual rainfall trend analysis over the entire Bhima basin

The results of autocorrelation analysis with Z statistics of MK/MMK test, Sen's slope and % change for seasonal and annual rainfall series are given in table 3.10. Statistically non-significant increasing trends were found in all seasonal series except winter during 1901-2004. Statistically non-significant decreasing trends were found in summer, monsoon and annual rainfall over the entire basin during the period 1961-2004. An overall increase of 15.9% during 1901-2004 duration and decrease of 11.0% during the period 1961-2004 (Table 3.10) in the annual rainfall were observed in the Bhima basin.

Table 3.10 Results of rainfall trend analysis over the entire basin including MK/ MMK test statistics and percent change over 1901-2004 and 1961-2004

Series		1901-2004			1961-2004		
		MK/ MMK	Sen's Slope	% Change	MK/ MMK	Sen's Slope	% Change
Seasonal	Summer	0.034	0.00	0.9	-1.244	-0.40	-41.7
	Monsoon	1.508	0.60	10.3	-1.305	-1.95	-13.7
	Post-Monsoon	1.542	0.33	31.4	0.415	0.47	17.6
	Winter	**-1.914**	0.00	-2.6	0.233	0.01	3.7
Annual		0.568*	1.178	15.9	-1.163	-1.99	-11.0
Note: *indicates the significant presence of autocorrelation in the series; Bold values represent the significant trend							

3.7 SUMMARY AND DISCUSSION

The spatio-temporal variability analysis of meteorological variables in the Bhima basin was carried out using 1°x1° gridded temperature data (minimum, maximum and mean; 1969-2009) and rainfall data (1901-2004). The MK/MMK test was applied for detection of trends in the non-autocorrelated/autocorrelated variables. Theil and Sen's slope estimator was used for estimation of magnitude of trend of meteorological variables. The major findings are described below:

3.7.1 Changes in Temperature of the Basin

i.   Analysis of seasonal minimum temperature of 14 grids of the basin revealed decreasing trends during summer and winter seasons and increasing trends during monsoon and post-monsoon seasons.

ii.   Seasonal maximum and seasonal mean temperatures of the 14 grids of the basin showed rising trends in all seasons across all the grids with an exception of mean temperature of summer season during which was found to be decreasing trends at 6 grids.

iii. All annual temperature series of the all the grids showed an increasing trends except in grids #1, #2, #4, #5 and #6 which have shown a decreasing trend in average minimum temperature.

iv. Over the duration (1969-2009), on an average an increase of 0.002°C, 0.014°C and 0.007°C were found in annual minimum, maximum and mean temperatures of the entire basin, respectively.

v. General spatial pattern of changes in average annual temperatures indicates that the upper and lower basins experienced warming in comparison to middle part of the basin.

3.7.2 Changes in Rainfall of the Basin

i. Trend analysis of seasonal rainfall during 1901-2004 showed non-significant decreasing trend in eight grids in summer season, significant decreasing trends in grids #2, #4, #7, #8, #9, #13 and #14 in winter season, increasing trend in monsoon season (significant at grid #2, #5 and #9), and increasing trend in post-monsoon season (significant at grid #1, #2, #7 and #11).

ii. Trend analysis of seasonal rainfall during 1961-2004, showed decreasing trends in summer, monsoon and winter season rainfall for most of the grids. An increasing trend was found during post-monsoon seasons. In recent duration trends analysis, monsoon season shown a reverse trend.

iii. The annual rainfall series for the duration of 1901-2004 showed increasing trends in most of the grids. However, annual rainfall series of the duration of 1961-2004, showed decreasing trends in most of the grids.

iv. Analysis of rainfall data of the entire basin, showed an increase of 15.9% in annual rainfall during the period 1901-2004 and decrease of 11% during 1961-2004.

v. Spatial patterns of monsoon and annual rainfall indicated an increase in rainfall in middle zone grids during 104 years and decrease in rainfall during the recent duration.

Pant and Kumar (1997) reported increasing trend of about 0.4°C/100 years in Indian region. The increasing tendency of mean temperature is mainly caused by the increase in maximum temperature (Kumar *et al.*, 1994). Arora *et al.* (2005) also reported a significant increasing trend over India during the 1940 to 2000 at the rate of 0.42, 0.92 and 0.09°C/100 years in annual mean temperature, mean maximum temperature and mean minimum temperature, respectively. Though the magnitude of slope in the temperatures trends are not much higher with the findings of other researchers, but the pattern of temperature trends are in agreement.

Monsoon and annual rainfall showed increasing trend over the 114 years which got reversed during recent durations. The observed trends over the Bhima basin are consistent with the findings of many researchers. Ramesh and Goswami (2007) analysed daily gridded observed rainfall data of India for the period 1951–2003 and found decreasing trends in both early and late monsoon rainfall over India. Pattanaik (2007) found decreasing trend in monsoon rainfall over northwest and central India during 1941–2002. Trend in annual rainfall in the Krishna River basin also shows decreasing trend wherein Kumar *et al*. (2010) predicted more droughts events. As the Bhima basin, a sub-basin of the Krishna River basin, have similar trends in the annual rainfall analysed at Bhima basin scale to those of the Krishna River basin scale, the Bhima sub-basin may also face water scarcity as indicated by Kumar *et al*. (2010).

CHAPTER 4: ASSOCIATION AND IMPACT ANALYSES OF ENSO ON MONSOON RAINFALL

4.1 GENERAL

El Niño Southern Oscillation (ENSO), a naturally occurring phenomenon, refers to the variations in atmospheric pressure between the east and west tropical Pacific that accompany both El Niño and La Niña events in the Pacific Ocean. The warm sea surface temperature conditions in the tropical Pacific Ocean are described by 'El Niño', while the 'Southern Oscillation' is the see-saw of the atmospheric pressure differences between Australian-Indonesian region and eastern tropical Pacific Ocean (Chiew and McMohan, 2002). The term 'El Niño' is widely used specifically for the warming of sea surface temperature that occurs every few years and 'La Niña' is the term used for events cooler-than-normal sea surface temperature in the equatorial Pacific. ENSO is one of the dominant feature of climate variability on inter-annual timescales.

El Niño and La Niña occurrences are commonly known to be linked with extreme climate around the globe (Kane 1997, 1999) and affects mean annual streamflow (Dettinger and Diaz, 2000; Misir *et al*., 2013), monthly streamflow (Robertson and Wang, 2013) and peak flows (Ward *et al*., 2010; Lim *et al*., 2012). These oscillations cause extreme weather (such as floods and droughts) in many regions of the world. Severe floods and droughts associated with ENSO occur in different parts of the world negatively affecting important economic activities of many countries such as, agriculture and tourism etc. ENSO influences climate and hydrologic conditions on timescales ranging from seasons to decades (Poveda and Mesa, 1997). It is essential to have at least two ENSO indices, and perhaps more to approximately describe the character of ENSO events. In reality, ENSO simulation is a crucial task in the climate system (Latif, 2001).

Indian rainfall variability is the result of a series of complex interactions between ocean and atmospheric phenomenon. The cross-equatorial pressure gradients resulting from differential heating of land and ocean, modified by the rotation of the earth and the exchange of moisture among the ocean, atmosphere, and land are the fundamental driving mechanisms of the monsoon cycle (Webster 1987). A distinct asymmetry to the summer monsoons of the

Northern and Southern hemispheres results from strong thermal forcing due to the Himalayas and the Tibetan Plateau (Yanai and Li 1994; Webster *et al.*, 1998).

India is an agrarian economy and the agricultural production is constrained every year by the summer monsoon rains in India (Krishna *et al.*, 2006). Hence, a strong emphasis is currently on studying the association between Indian climate and ENSO (Kumar *et al.*, 2007). Commonly, ENSO has negative correlations with inter-annual variability of Indian monsoon (June to September) (Yadav, 2009a, 2009b) and positive correlation with northwest Indian winter precipitation (Yadav *et al.*, 2010; Webster and Palmer, 1997; Webster and Yang, 1992; Krishna *et al.*, 1999).

4.2 ENSO Indices

There are many ENSO indices used world-wide. Indices namely: Southern Oscillation Index (SOI), Multivariate ENSO Index (MEI) and Niño 3.4 (N3.4) are commonly used for studying ENSO events, their association and impacts. These indices are described below:

4.2.1 Southern Oscillation Index

SOI is used to quantify the strength of the Walker circulation across the Pacific at the source of the phenomenon. This index is published and updated regularly by the Australian Bureau of Meteorology and is computed using a method developed by Troup (1965), as the standardized anomaly of monthly Mean Sea Level Pressure (MSLP) differences, measured at Papeete, Tahiti (149.6°W, 17.5°S) and Darwin, Australia (139.9°E, 12.4°S). It is calculated as follows:

$$SOI = 10 * \frac{[P_{diff} - P_{diffave}]}{SD(P_{diff})}$$
(4.1)

Where P_{diff} = Tahiti MSLP – Darwin MSLP

$P_{diffave}$ = long term average of pressure difference for the month

$SD(P_{diff})$ = standard deviation of pressure difference for the month

4.2.2 Multivariate ENSO Index

Multivariate ENSO Index (MEI) is based on six observed variables over the tropical Pacific *viz.*: sea-level pressure, zonal and meridional components of the surface wind, sea surface temperature, surface air temperature, and total cloudiness fraction of the sky. The MEI is computed separately for each of the twelve sliding bi-monthly seasons (Dec/Jan, Jan/Feb,…, Nov/Dec). After spatially filtering the individual fields into clusters (Wolter, 1987), the MEI is calculated as the first un-rotated Principal Component (PC) of all six observed fields combined (Wolter and Timlin, 1993).

4.2.3 Niño 3.4 Index

The N3.4 index is defined as a three-month average of sea surface temperature departures from normal for a critical region of the equatorial Pacific extending from 120° W to 170° W and 5° N to 5° S. El Niño (La Niña) is a phenomenon in the equatorial Pacific Ocean characterized by a five consecutive 3-month running mean of sea surface temperature (SST) anomalies in the Niño 3.4 region that is above (below) the threshold of +0.5°C (-0.5°C).

4.3 OBJECTIVES

Following are the specific objectives of this chapter:

  i.   To investigate the association between ENSO and monsoon rainfall of the basin.
 ii.   To understand the variations in the monsoon rainfall occurrence during different ENSO phases.

Rainfall data only during monsoon were considered for analysis since most of the rainfall occurs during this season.

4.4 DATA USED

4.4.1 Rainfall Data

Rainfall data of the monsoon season (June, July, August and September) as described in section 3.4 were used.

4.4.2 ENSO Indices Data

Three ENSO indices data were downloaded from National Oceanic and Atmospheric Administration (NOAA) (www.esrl.noaa.gov) and National Centre for Atmospheric Research (NCAR) (www.cgd.ucar.edu) web portals.

4.4.3 ENSO Phases Data

Years arranged in ENSO phases based on SOI were downloaded from the website http://www.longpaddock.qld.gov.au/products/australiasvariableclimate/ensoyearclassification.html and are listed in Appendix V. The years in each category correspond to the first three months of the ENSO year i.e. October, November and December. For example, the ENSO year 1970 starts with October 1970 and ends in September 1971.

4.5 METHODOLOGY

Step-by-step methodology used to carry out the analysis is given below:

i.   The daily rainfall data of 14 grids (1°x1°) covering the entire Bhima basin were extracted for the period of 1901-2004 from the gridded rainfall data of India.

ii. Monthly monsoon rainfalls (June, July, August and September) series were derived from daily rainfall data to match the time scale of ENSO indices for each grid. As ENSO indices are in normalized form, the rainfall series of each grid were also normalized using the mean and standard deviation of the series using equation 4.2.

$$z = \frac{X - \mu}{\sigma}$$

(4.2)

Where, z, X, μ and σ are normalized rainfall, monthly rainfall value, mean and standard deviation

Seasonal mean monsoon rainfall series for each grid was then derived from normalized monsoon rainfall data.

iii. ENSO indices were rearranged into three groups corresponding to the seasons winter (ONDJ i.e October, November, December and January), summer (FMAM i.e.February, March, April and May) and monsoon (JJAS i.e June, July, August and September).

56

iv. Pearson's correlation coefficients, r, were computed between normalized mean monsoon rainfall and ENSO indices to study the relationships between monsoon rainfall and ENSO. The t-statistic was used to find the statistical significance of 'r' at 5% significance level as given below:

$$t = r\sqrt{\frac{n-2}{1-r^2}}$$
(4.3)

Where, test statistic t has a t-distribution with (n-2) degrees of freedom. If $|t| \geq t_{\alpha/2}$, the null hypothesis about 'there is the correlation between variables' was accepted at α (5%) significance level.

v. Monsoon rainfall series of each grid and of the entire basin were further divided into three sub series corresponding to La Niña, Neutral and El Niño events to investigate changes during these phases on the basis of SOI index.

vi. The parametric ANOVA ((H$_0$: $\mu_{La\ Niña}$= $\mu_{Neutral}$= $\mu_{El\ Niño}$ i.e. population means are homogeneous; H$_1$: $\mu_{La\ Niña}\neq \mu_{Neutral} \neq \mu_{El\ Niño}$ i.e. population means are heterogeneous) was used to test the hypothesis that there is no difference among the monsoon rainfalls occurring during the three different ENSO phases.

vii. Percentage change in average monsoon rainfall of each grid and basin occurring in La Niña/ El Niño phase were computed with respect to the average monsoon rainfall of the neutral phase.

4.6 RESULTS

4.6.1 Correlation Analysis between ENSO Indices and Monsoon Rainfall

The result of the correlation analysis between monsoon rainfall and seasonal ENSO indices are given in table 4.1a. As seen in the table, weak correlations were found with winter and summer ENSO indices, and strong and statistically significant correlation were found with monsoon ENSO indices. Rainfall of grids #8 and # 12 did not show significant correlation with monsoon SOI, and grids #4, #8 and #9 did not show significant correlation with MEI and N3.4. The highest positive correlation was found with SOI at grid #10 and highest negative with MEI and N3.4 at grid #11 with monsoon indices. It concludes that there is a strong association between monsoon rainfall and monsoon ENSO indices.

Figure 4.1 (a-c) are the season wise plots of the r values. Monsoon rainfall of all grids are found to be negatively correlated with the winter SOI and positively correlated with the winter MEI and N3.4 as shown in figure 4.1a. No definite relationship was found between monsoon rainfall and summer ENSO indices (Figure 4.2b). A positive correlation was found between monsoon rainfalls and monsoon SOI, whereas a negative correlation was found with monsoon MEI and N3.4 indices as seen in figure 4.1c. Overall, significant 'positive' association between monsoon rainfall and monsoon SOI and significant 'negative' association between monsoon rainfall MEI and N3.4 were found.

Table 4.1 also gives the percentage variability of rainfall with monsoon ENSO indices. It is useful because it gives the proportion of the variance (fluctuation) of monsoon rainfall that is predictable using the ENSO indices. Percentage monsoon variability is not higher in winter and summer ENSO indices in comparison with monsoon ENSO indices. It concludes that the impact of monsoon rainfall can be predicted using monsoon ENSO indices. Percentage variability of monsoon rainfall is better explained by SOI than the other indices. Therefore, SOI is a more suitable ENSO index for studying the impact of ENSO on monsoon rainfall in the basin.

Table 4.1 Pearson's correlation coefficient between rainfall and monsoon ENSO indices with t-statistics and variability in monsoon rainfall explained by ENSO indices

	Indices	SOI			MEI			N3.4		
Season	Grids	r	t	Var	r	t	Var	r	t	Var
ONDJ	1	-0.18	1.84	3.21	0.17	1.77	2.97	0.15	1.51	2.34
	2	-0.17	1.70	2.75	0.14	1.39	1.86	0.12	1.13	1.32
	3	-0.14	1.45	2.01	0.04	0.44	0.19	0.05	0.49	0.25
	4	-0.14	1.47	2.08	0.17	1.72	2.82	0.14	1.33	1.82
	5	-0.12	1.24	1.48	0.13	1.33	1.70	0.10	1.00	1.05
	6	-0.02	0.25	0.06	-0.03	0.35	0.12	-0.02	0.20	0.04
	7	-0.07	0.69	0.46	-0.01	0.14	0.02	0.00	0.02	0.00
	8	-0.21	2.21	4.56	0.14	1.47	2.06	0.10	0.95	0.95
	9	-0.15	1.58	2.40	0.18	1.81	3.10	0.10	1.00	1.04
	10	-0.25	2.57	6.07	0.23	2.36	5.17	0.19	1.91	3.71
	11	-0.12	1.26	1.54	0.07	0.66	0.43	0.07	0.73	0.56
	12	-0.15	1.57	2.35	0.12	1.22	1.45	0.14	1.41	2.04
	13	-0.04	0.42	0.18	0.00	0.04	0.00	-0.02	0.21	0.05
	14	-0.11	1.08	1.12	0.04	0.39	0.15	0.04	0.40	0.17
	Basin	-0.20	2.06	4.01	0.15	1.58	2.38	0.12	1.19	1.47
FMAM	1	-0.07	0.69	0.46	0.02	0.24	0.05	0.01	0.10	0.01
	2	-0.01	0.11	0.01	0.06	0.56	0.31	0.03	0.34	0.12
	3	0.00	0.05	0.00	-0.05	0.46	0.20	-0.06	0.56	0.33
	4	-0.04	0.44	0.19	0.02	0.20	0.04	0.03	0.30	0.09
	5	-0.01	0.14	0.02	0.05	0.49	0.24	-0.01	0.06	0.00
	6	0.05	0.49	0.24	-0.10	0.98	0.93	-0.09	0.87	0.78
	7	0.13	1.34	1.72	-0.12	1.21	1.42	-0.14	1.36	1.92
	8	-0.05	0.55	0.29	0.13	1.31	1.65	0.09	0.93	0.90
	9	-0.13	1.32	1.69	0.11	1.15	1.29	0.07	0.72	0.54
	10	-0.02	0.24	0.06	0.12	1.26	1.52	0.07	0.70	0.51
	11	0.07	0.71	0.49	-0.02	0.20	0.04	-0.05	0.44	0.20
	12	0.04	0.42	0.18	0.05	0.54	0.28	0.08	0.75	0.59
	13	0.13	1.27	1.56	-0.09	0.91	0.80	-0.10	1.01	1.06
	14	0.05	0.47	0.21	-0.02	0.19	0.03	-0.03	0.32	0.10
	Basin	-0.02	0.23	0.05	0.06	0.63	0.38	0.03	0.26	0.07

Note: Cells in yellow colour represents significant correlation of monsoon rainfall with ENSO indices at 5% significance level. Bold numbers show highest percentage of variability of monsoon rainfall explained by ENSO indices.

Season	Indices Grids	SOI			MEI			N3.4		
		r	t	Var	r	t	Var	r	t	Var
JJAS	1	0.32	3.38	10.08	-0.27	2.83	7.27	-0.24	2.42	5.80
	2	0.29	3.02	8.23	-0.20	2.07	4.02	-0.22	2.16	4.67
	3	0.38	4.13	14.31	-0.31	3.28	9.55	-0.37	3.88	13.65
	4	0.23	2.34	5.09	-0.16	1.62	2.51	-0.14	1.41	2.05
	5	0.36	3.93	13.15	-0.26	2.71	6.72	-0.31	3.17	9.55
	6	0.39	4.22	14.87	-0.36	3.91	13.05	-0.35	3.68	12.49
	7	0.42	4.70	17.80	-0.42	4.65	**17.49**	-0.44	4.73	19.07
	8	0.14	1.39	1.86	-0.10	0.97	0.92	-0.19	1.91	3.70
	9	0.20	2.05	3.95	-0.10	1.04	1.06	-0.13	1.32	1.80
	10	0.46	5.27	**21.41**	-0.33	3.49	10.66	-0.40	4.21	15.72
	11	0.44	4.96	19.43	-0.41	4.61	17.22	-0.46	5.08	**21.36**
	12	0.14	1.41	1.91	-0.26	2.66	6.51	-0.28	2.82	7.70
	13	0.33	3.54	10.92	-0.31	3.30	9.63	-0.33	3.46	11.20
	14	0.34	3.63	11.45	-0.31	3.28	9.57	-0.34	3.47	11.23
	Basin	0.39	4.26	15.09	-0.33	3.49	10.65	-0.38	4.04	14.64

Note: Cells in yellow colour represents significant correlation of monsoon rainfall with ENSO indices at
5% significance level. Bold numbers show highest percentage of variability of monsoon rainfall
explained by ENSO indices.

The correlation between monsoon rainfall of the entire basin and seasonal ENSO indices are also given in table 4.1. The monsoon rainfall of the entire basin was found statistically significantly correlated with winter SOI whereas non-significantly with winter MEI and N3.4. Weak and non-significant correlations were found with winter and summer season indices.
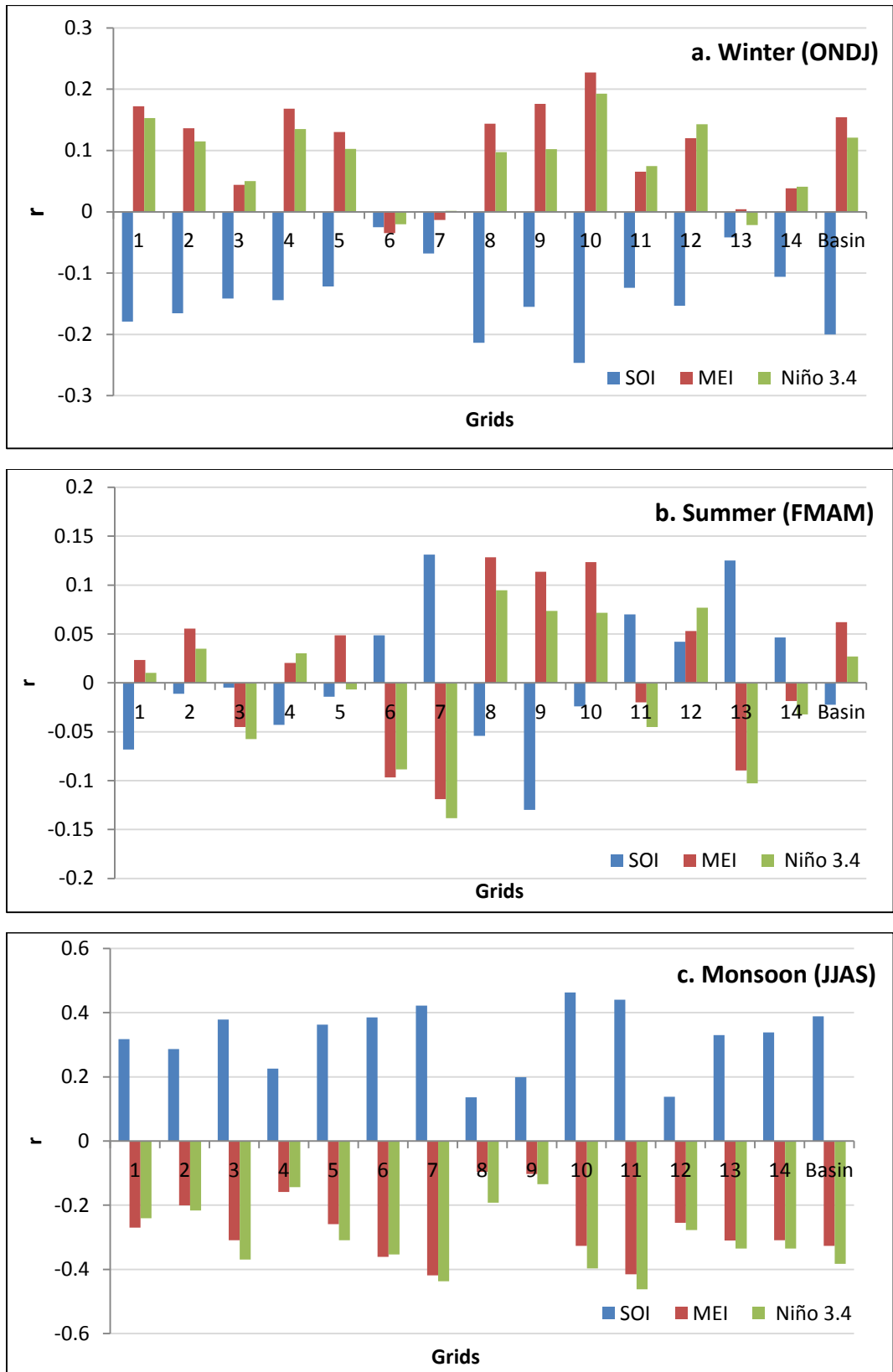
Figure 4.1 Plots of correlation coefficients between monsoon rainfall and seasonal ENSO indices at each grid and in Bhima basin

4.6.2 Impact of ENSO Phases on Monsoon Rainfall

The monsoon rainfall series of each grid and the entire basin were divided into three sub-series matching to ENSO phases (La Niña phase, Neutral phase and El Niño phase). The average monsoon rainfall of each phase was computed for grids and the basin. Representative graph of ENSO phases and rainfall for a sample grid (#9) and for the entire basin are shown in figure 4.2a-b. The blue triangles, red squares and green circles show La Niña, El Niño and neutral ENSO years, respectively. Dotted blue line, dotted-dashed red lines and solid green line show the average rainfall during La Niña, El Niño and neutral phases, respectively. The figure depicts that the average monsoon rainfall which occurred during the La Niña/El Niño phase in the sample grid and the entire basin are above/below the average rainfall of neutral phase.
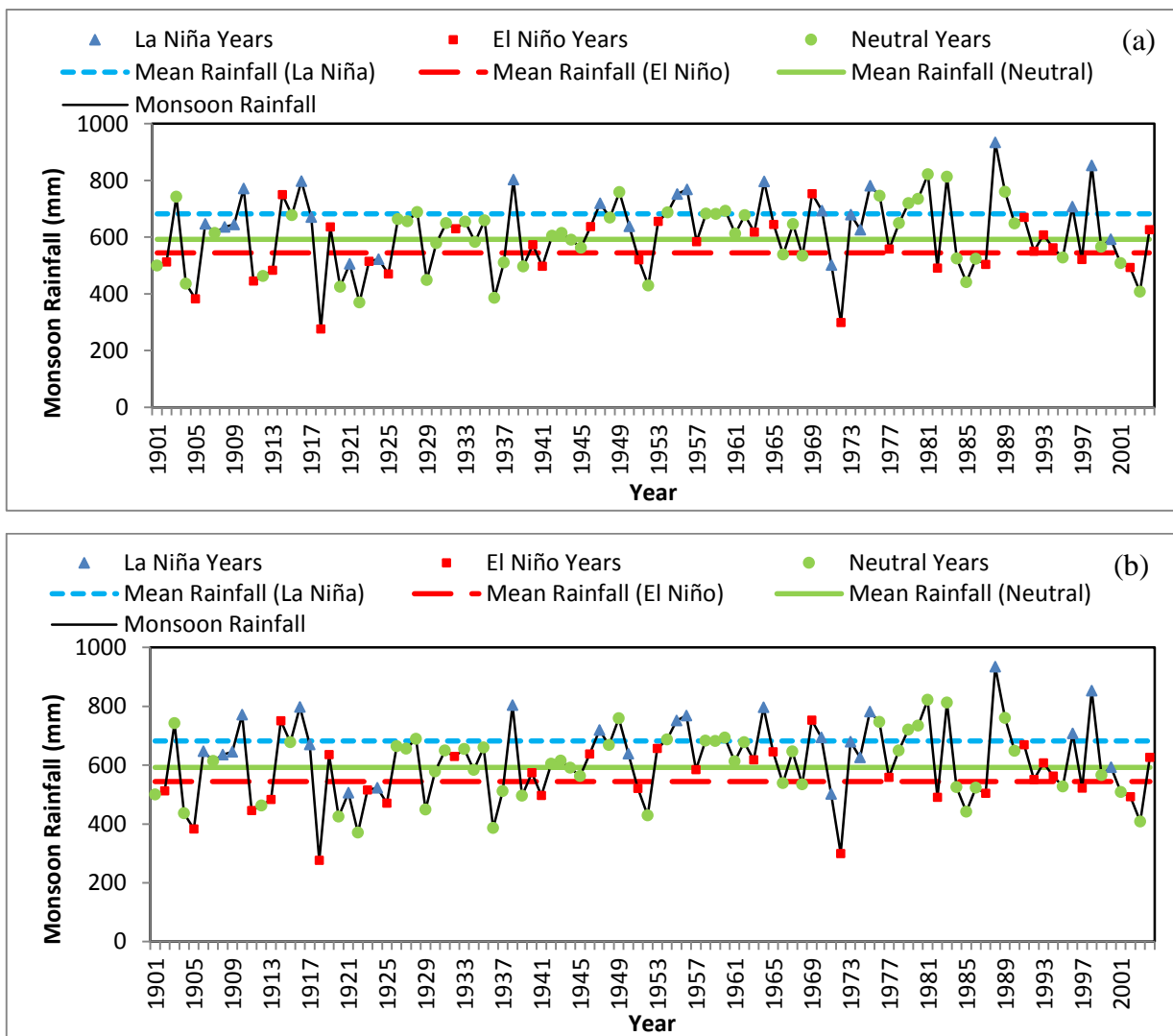
Figure 4.2 Average monsoon rainfall occurred during various ENSO phases (a) at a sample grid #9 and (b) for the entire basin

Figure 4.3 shows the summary of the rainfall which occurred during various ENSO phases in all the grids and in the entire basin with bar graphs. The graph shows that the average rainfall which occurred during the La Niña/El Niño phase is above/below the average monsoon rainfall of the neutral phase for all the grids except for grids #8 and #12. It is therefore concluded that the monsoon rainfall in La Niña phase is more than the monsoon rainfall occurred in El Niño phase in the basin.
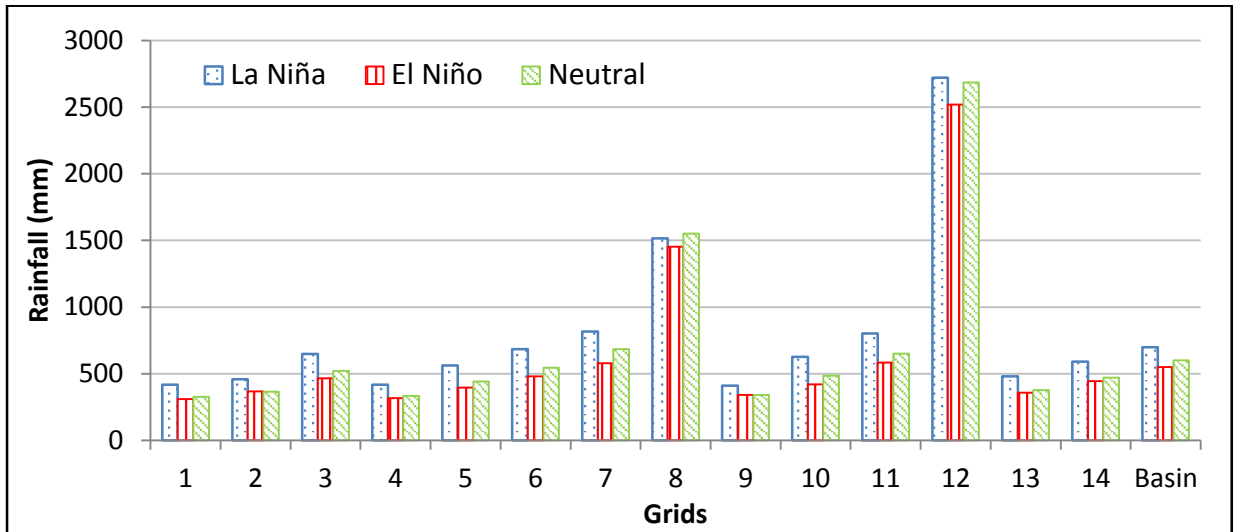
Figure 4.3 Average monsoon rainfall occurred during ENSO phases in all the grids and in the entire basin.

Homogeneity analysis of average monsoon rainfall which occurred during the three ENSO phases was carried out using ANOVA. The F-statistics of ANOVA test are given in table 4.2. Alternate hypothesis is accepted at 5% significance level for all the grids and basin except grids #8 and #12. Thus, it is concluded that the rainfall which occurred during the ENSO phases were significantly different from each other.

Table 4.2 Homogeneity analysis of monsoon rainfall of all grids and for the entire basin

Grids	1	2	3	4	5	6	7	8	9	10	11	12	13	14	Basin
F-statistics	8.77	7.304	13.599	5.62	10.153	10.937	11.619	0.606*	2.939	12.605	11.786	1.161*	7.344	7.704	11.592

Note: * indicates acceptance of null hypothesis at 5% significance level

63

Percentage change in average monsoon rainfall of La Niña and El Niño phases with respect to average monsoon rainfall of neutral phase were computed and are shown using bars in figure 4.4. The average % change in La Niña and El Niño phases are shown lines in the figure. It is clearly seen in the figure that the percentage change in monsoon rainfalls during La Niña phase are 15% higher and the rainfall occurred during El Niño phase are 9.5% lower than the rainfall of neutral phase in the Bhima basin.
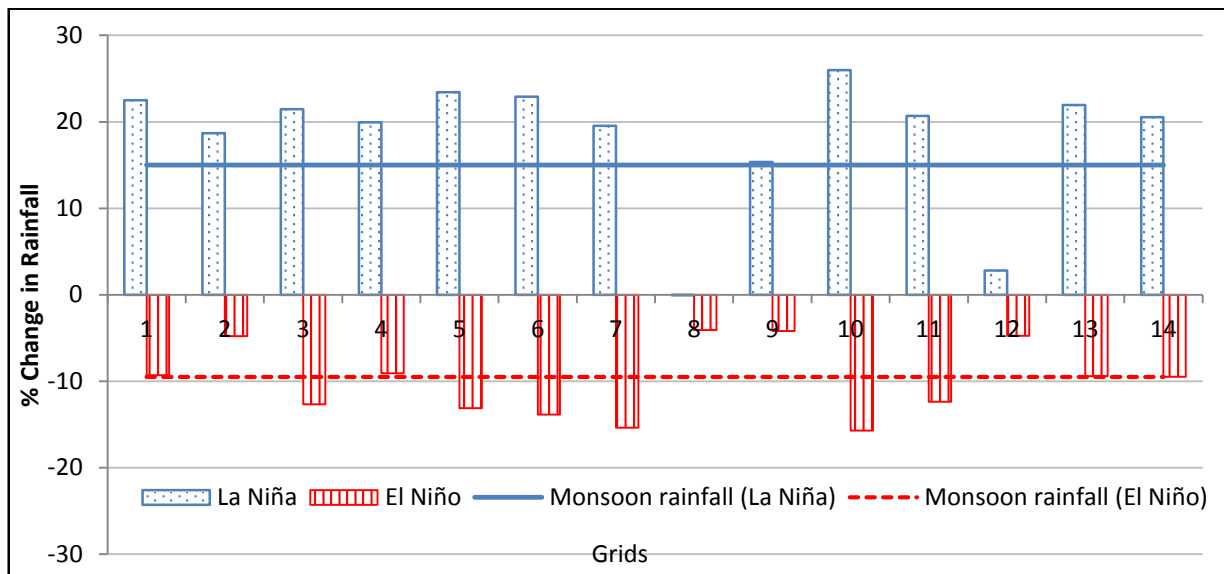
Figure 4.4 Percentage change in monsoon rainfall during La Niña and El Niño phases

4.7 DISCUSSION AND SUMMARY

The major findings of this chapter drawn from the analysis of monsoon rainfall and ENSO indices are enumerated below:

i. Monsoon rainfall shows significant correlation with only monsoon ENSO indices at most of the grid as well as for the entire basin at 5% significance level.

ii. The monsoon rainfall shows significant positive correlation with the monsoon SOI and a negative correlation with monsoon MEI and N3.4 index.

iii. Average monsoon rainfall which occurred during the three ENSO phases are significantly different from each other and the rainfall of the La Niña/El Niño phase is usually above/below the monsoon rainfall of the neutral phase.

iv. On an average 15% more rainfall is received during La Niña years and 9% less in El Niño years in comparison with the average monsoon rainfall of the neutral years.

v. Overall the strong/weak monsoon is associated with La Niña/ El Niño events, respectively.

Many studies reported that ENSO has negative correlations with Indian monsoon (Yadav, 2009a, 2009b) and positive correlation with northwest Indian winter precipitation (Yadav *et al*., 2010; Webster and Palmer, 1997; Webster and Yang, 1992; Krishna *et al*., 1999) and that the El Niño is associated with a weak Indian monsoon with an overall reduction in rainfall (Webster and Palmer, 1997; Kothawale *et al*., 2010). On the other hand, La Niña strengthens the Indian monsoon and increases the rainfall (Sikka 1980; Rasmussen and Carpenter, 1983). The results summarised above confirm all these general findings valid for the Bhima basin, too.

CHAPTER 5: DOWNSCALING AND ANALYSIS OF PROJECTED METEOROLOGICAL VARIABLES

5.1 GENERAL

GCMs simulate the present and future climate of Earth under different climate change scenarios (SRES, 2000). The computational grid of GCMs is having coarse resolution hence the outputs are unable to skilfully model the sub-grid scale climate features like topography or clouds (Wilby *et al*., 2002). Ability of GCM declines from coarse resolution to fine resolutions whereas hydrological importance of the climate data increases from course resolution to high resolution (Xu, 1999). Hence, there is a need for downscaling the coarse resolution GCM outputs to fine resolution or even to station scale.

The available downscaling methodologies are broadly grouped into statistical and dynamical categories. Among the statistical downscaling methods, the use of stochastic weather generators is very popular. They are computationally less demanding, simple to apply and provide station scale information (Coulibaly *et al*., 2005; Kilsby *et al*., 2007). The weather generators are basically statistical models which are used to generate a long synthetic time series, fill in missing data and produce different realizations of the same data (Wilby, 1999). They use the observed time series of a station as input.

Stochastic weather simulation is not new and has a history starting from 1950s, as reported by Racsko *et al.* (1991). Among some researchers who contributed to its evolution are Bruhn *et al*. (1980), Nicks and Harp (1980), Richardson (1981), Richardson and Wright (1984) and Schoof *et al*. (2005). Wilby (1999) has presented a comprehensive review of its theory and evolution over time. Weather generators have been employed to obtain long timeseries of hydrometeorological variables which are then used by crop growth model to forecast agricultural production (Riha *et al*., 1996; Hartkamp *et al*., 2003) and assessment of risk associated with climate variability (Semenov, 2006; Bannayan and Hoogenboom, 2008). When the climate scientists started looking for low cost, computationally less expensive and less demanding and quick methods for impact assessment, the weather generator emerged as the most viable solution (Wilks, 1992; Wilks and Wilby, 1999).

The four major sources of uncertainty in the downscaled climate projections (Tabor and Williams, (2010) are: i) uncertainties in future green-house gas emissions and atmospheric composition (scenario uncertainty), ii) uncertainties in modelling the climate response (GCM uncertainty), iii) uncertainties in the observational data sets used as the base map for the debiasing procedure (observational uncertainty), and iv) uncertainty over the validity of the assumptions underlying the change-factor approach (change-factor uncertainty). Representation and quantification of uncertainty in climate change impact studies are a difficult task.

The availability of downscaled simulations from multiple models is valuable for inter-model comparisons and assessments of inter-model variability. Identifying a single, most reliable model for regional studies is not possible (Martinez-Meyer, 2005). The level of uncertainty in GCM outputs cannot be determined quantitatively and is essentially unknown; however, by using the range of predictions available from all current generation GCMs, it is possible to determine the lower bound of the uncertainty (Wood *et al*., 1997). Using multi-model ensemble means for regional studies has proven superior to using any single climate model because averaging the model projections reduces both mean errors and variance in the models (Pierce *et al.,* 2009).

Over the past 15 years, many researchers used ensemble forecast to predict quantitatively the probability of the state of the atmosphere in future around the world (Agrawal *et al*., 2003; Ghosh and Mujumdar, 2009; Roy *et al*., 2009; Raje and Mujumdar, 2010; Raje and Mujumdar, 2010a; Raje and Mujumdar, 2011; Mahmood and Babel, 2012; Mittal *et al*., 2013). These predictions can be used for several applications ranging from climate change impact assessments at continental scales (IPCC, 2001, 2007) to risk assessments in small urban areas (Vojinovic, 2010).

The primary weather variables - temperature and precipitation - obtained from GCM simulations for the current and future have been used for assessment of impact of climate change on water resources (Gleick, 1989; Mearns *et al*. 1990; Yu *et al*., 2002; Thodsen, 2007; Singhrattna and Babel, 2011; Singhrattna *et al*. 2012; Rehana and Mujumdar, 2013) and for impact assessment on agriculture with climate change (Jin *et al*., 1995; Lin *et al*., 1997; Thomas, 2000, Babel *et al*., 2011 Mishra *et al*. 2013). Long Ashton Research Station Weather Generator (LARS-WG) is a stochastic weather generator specially designed for climate change impact studies (Semenov and Barrow, 1997). It has been tested for diverse climates and found

better than many others as reported by Semenov *et al.*, (1998). A recent study by Semenov (2009) tested the LARS-WG for rainfall modelling at different sites across the world and has shown its ability to model rainfall extremes with reasonable skill.

Therefore LARS-WG was adopted for downscaling the daily rainfall and temperature (maximum and minimum) data from GCM outputs to assess the impact of climate change on meteorological variables of the Bhima basin.

5.2 OBJECTIVES

Following are the specific objectives of the chapter:

i.   To downscale the daily meteorological variables of 14 grids of the Bhima basin using 15 GCMs for three emission scenarios in three time spans using LARS-WG.

ii. To analyse uncertainty in GCM projections using change factor approach with respect to baseline period.

iii. To analyse the impact of climate change on projected meteorological variables.

5.3 DESCRIPTION OF LARS-WG

Stochastic weather generators were originally developed for two main purposes:

i.   To provide a means of simulating synthetic weather timeseries with statistical characteristics corresponding to the observed statistics at a site, but which were long enough to be used in an assessment of risk in hydrological or agricultural applications.

ii. To provide a means of extending the simulation of weather time-series to unobserved locations, through the interpolation of the weather generator parameters obtained from running the models at neighbouring sites.

LARS-WG is a stochastic weather generator which can be used for the simulation of weather data at a single site (Racsko *et al.*, 1991; Semenov *et al.*, 1998; Semenov and Brooks, 1999), under both current and future climate conditions. It uses a semi-empirical distributions for the lengths of wet and dry day series, daily precipitation and daily solar radiation. The semi-empirical distribution Emp = $\{a_0, a_i; h_i, i=1,\ldots,10\}$ is a histogram with ten intervals, $[a_{i-1}, a_i]$, where $a_{i-1} < a_i$, and h_i denotes the number of events from the observed data in the ith interval. Random values from the semi-empirical distributions are chosen by first selecting one of the

intervals (using the proportion of events in each interval as the selection probability), and then selecting a value within that interval from the uniform distribution. Such a distribution is flexible and can approximate a wide variety of shapes by adjusting the intervals [a_{i-1}, a_i].

The cost of this flexibility, however, is that the distribution requires 21 parameters (11 values denoting the interval bounds and 10 values indicating the number of events within each interval) to be specified compared with, for example, 3 parameters for the mixed-exponential distribution used in an earlier version of the model to define the dry and wet day series (Racsko *et al*., 1991). The intervals [a_{i-1}, a_i] are chosen based on the expected properties of the weather variables. For solar radiation, the intervals [a_{i-1}, a_i] are equally spaced between the minimum and maximum values of the observed data for the month, whereas for the lengths of dry and wet series and for precipitation, the interval size gradually increases as *i* increases. In the latter two cases, there are typically many small values but also a few very large ones and this choice of interval structure prevents a very coarse resolution being used for the small values.

The simulation of precipitation occurrence is modelled as alternate wet and dry series, where a wet day is defined to be a day with precipitation > 0.0 mm. The length of each series is chosen randomly from the wet or dry semi-empirical distribution for the month in which the series starts. In determining the distributions, observed series are also allocated to the month in which they start. For a wet day, the precipitation value is generated from the semi-empirical precipitation distribution for the particular month independent of the length of the wet series or the amount of precipitation on previous days.

There are 15 GCMs incorporated in LARS-WG. The detailed description of each GCM is given in Appendix VI (Meehl, 2007a; Semenov and Stratonovitch, 2010). The availability of GCMs in three emission scenarios and in three time spans (i.e. 2011-2030 centred at 2020, 2046-2065 centred at 2055 and 2080-2099 centred at 2090) are given in table 5.1. These emission scenarios represent a range of possible future scenarios explored by the IPCC (Nakicenovic and Swart 2000, Meehl *et al.,* 2007b) with no explicit probability attached to any of these.

Table 5.1 List of GCMs in different emission scenarios for each time span

2011-2030			2046-2065			2080-2099		
A1B	**A2**	**B1**	**A1B**	**A2**	**B1**	**A1B**	**A2**	**B1**
BCM2	CNCM3	BCM2	BCM2	CNCM3	BCM2	BCM2	CNCM3	BCM2
CGMR	GFCM21	CSMK3	CGMR	GFCM21	CSMK3	CGMR	GFCM21	CSMK3
CNCM3	HADCM3	FGOALS	CNCM3	HADCM3	FGOALS	CNCM3	HADCM3	FGOALS
CSMK3	HADGEM	GFCM21	CSMK3	HADGEM	GFCM21	CSMK3	INCM3	GFCM21
FGOALS	INCM3	GIAOM	FGOALS	INCM3	GIAOM	FGOALS	IPCM4	GIAOM
GFCM21	IPCM4	HADCM3	GFCM21	IPCM4	HADCM3	GFCM21	MPEH5	HADCM3
GIAOM	MPEH5	INCM3	GIAOM	MPEH5	INCM3	GIAOM	NCCCSM	INCM3
HADCM3	NCCCSM	IPCM4	HADCM3	NCCCSM	IPCM4	HADCM3		IPCM4
HADGEM	NCPCM	MIHR	HADGEM	NCPCM	MIHR	INCM3		MIHR
INCM3		MPEH5	INCM3		MPEH5	IPCM4		MPEH5
IPCM4		NCCCSM	IPCM4		NCCCSM	MIHR		NCCCSM
MIHR			MIHR			MPEH5		
MPEH5			MPEH5			NCCSM		
NCCSM			NCCSM					
NCPCM			NCPCM					

5.3.1 Outline of the Stochastic Weather Generation Process

The process of generating the weather data can be divided into three distinct steps:

i. Model Calibration **- SITE ANALYSIS -** observed weather data are analysed to determine their statistical characteristics.

ii. Model Validation - **QTEST-** the statistical characteristics of the observed and synthetic weather data are analysed to determine if there are any statistically-significant differences.

iii. Generation of Synthetic Weather Data **- GENERATOR-** the parameters derived from observed weather data during the model calibration process are used to generate synthetic weather data having the same statistical characteristics as the original observed data, but differing on a day-to-day basis.

Synthetic data corresponding to a particular climate change scenario may also be generated by applying global climate model-derived changes in precipitation, temperature and solar radiation data.

71

Three statistical tests for comparison of observed and synthetic weather data used in LARS-WG are t-test for comparison of mean of observed and synthetic data, F-test for checking equality of variance of observed and synthetic data and Kolmogorov-Smirnov (KS) test for comparing probability distribution rainfall and temperature timeseries. These tests are described in detail in Appendix VII. As the variability is high in rainfall than the temperature data, LARS-WG computes F statistics only for the rainfall data.

5.4 DATA USED

The 1°x 1° resolution daily rainfall and temperature (minimum and maximum) of 14 grids of the Bhima basin were used to downscale the GCMs outputs to analyse the impact of climate change at the river basin scale. Details of the data used in this chapter are described in the section 3.4 of the Chapter 3.

5.5 METHODOLOGY

Keeping the above objectives in view, the following stepwise approach was undertaken to carry out the analysis:

  i.   Preparation of daily meteorological data series for all 14 grids of the Bhima basin.
 ii.   Application of a stochastic weather generator model (LARS-WG version 5.5) for downscaling daily meteorological variables from 15 GCMs for three emission scenarios (A1B, A2 and B1) in three time spans 2020s, 2055s and 2090s.
iii.   Calculation of change factor (CF) for rainfall and temperature (minimum and maximum) data with respect to the baseline period (1961-1990) for each GCM in each emission scenarios on seasonal and annual basis at each grid.
       The equation of change factor for rainfall and temperature are given below:

$$\Delta p = (p'-p)/p \qquad\qquad (5.1)$$

Where p' is the future predicted rainfall at a grid, p is the rainfall of the baseline period at that grid and Δp is the CF for rainfall

$$\Delta t = (t'-t) \qquad\qquad (5.2)$$

Where t' is the future predicted temperature at a grid, t is the temperature of the baseline period at that grid and Δt is the CF for temperature. The relative change in rainfall was calculated using equation below:

$$\% \text{ Change} = \Delta p \times 100 \tag{5.3}$$

iv. Analysis of uncertainty in projected meteorological variables data using box-plot graphs in each time spans on seasonal and annual basis.

v. Assessment of the impact of climate change on rainfall and temperature data.

The flow chart describing the approach used in downscaling and projection of daily rainfall and temperature (minimum and maximum) of each grid of the basin is given in the form of a flowchart as shown in the figure 5.1.
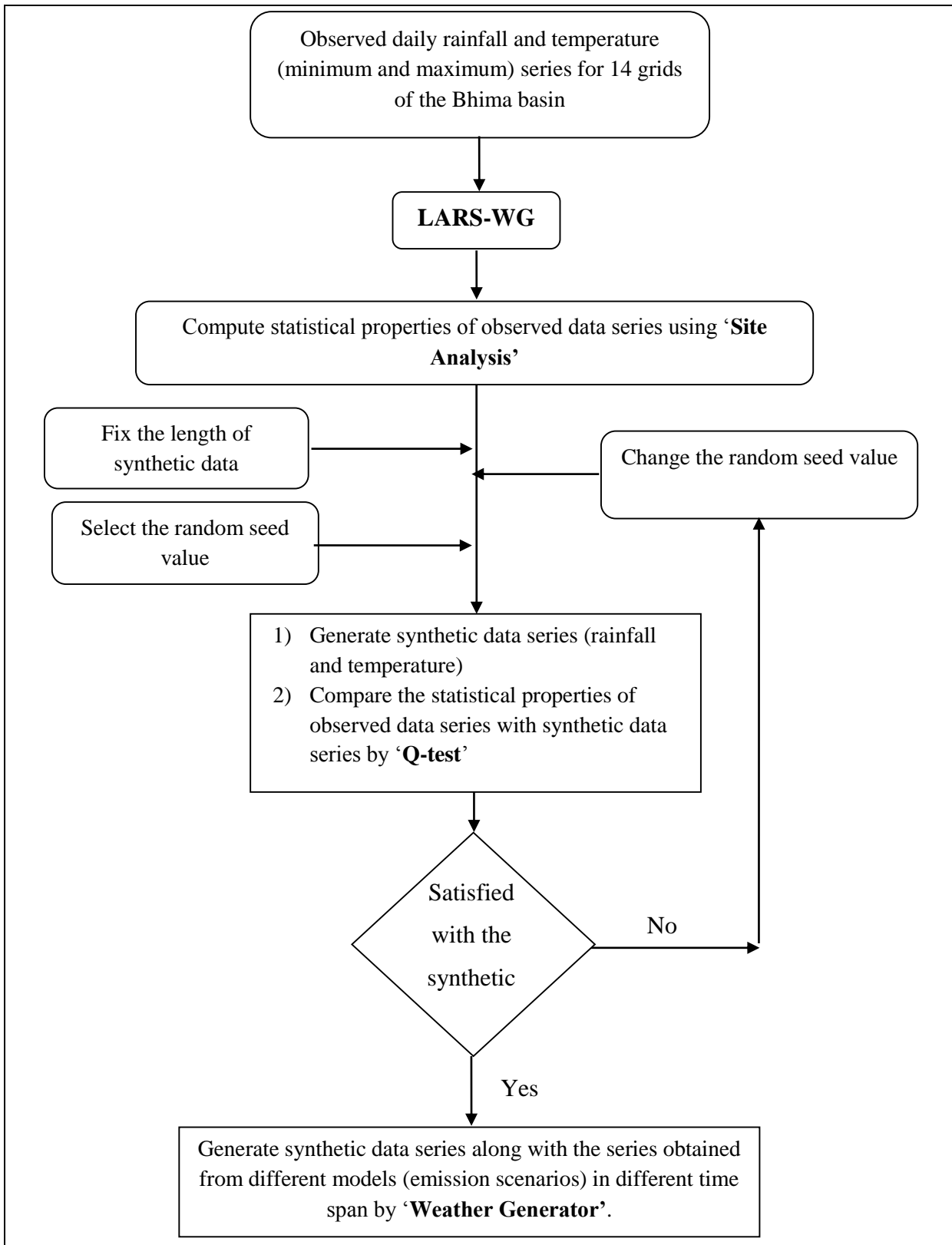
Figure 5.1 Flow chart for downscaling of daily meteorological variables by LARS-WG

5.6 RESULTS

5.6.1 Calibration of the model

A range of prime numbers between 500 and 1500 was suggested by the developer of LARS-WG for seed values. The different number of runs with different seed values was performed for calibration of LARS-WG along with the grid data.

Table 5.2 summarizes the results of KS test for daily minimum and maximum temperatures and daily rainfall, in all 14 grids of the basin. The analysis was conducted at a significance level of 0.05. The empirical distributions for each month were compared with the synthetic data distributions using the χ^2 statistic. The p-value indicates the significance of the fitted distribution. A p-value greater than 0.05 indicates a good fit while a p-value less than 0.05 indicates poorly fitted distribution. Table 5.2 shows a good fit of daily rainfall distribution in most of months across all the grids. Similar results were obtained for the minimum and maximum temperature distributions across all 14 grids as shown in the table.

Table 5.2 Results of KS test for rainfall and temperature data distribution

Grid	Test/ Months	Jan	Feb	Mar	Apr	May	Jun	Jul	Aug	Sep	Oct	Nov	Dec
1	Min. Temperature	√	√	√	√	√	√	√	√	√	√	√	√
	Max. Temperature	√	√	√	√	√	√	√	√	√	√	√	√
	Rainfall	√	x	√	√	√	√	√	√	√	√	√	√
2	Min. Temperature	√	√	√	√	√	√	√	√	√	√	√	√
	Max. Temperature	√	√	√	√	√	√	√	√	√	√	√	√
	Rainfall	√	√	√	√	√	√	√	√	√	√	x	√
3	Min. Temperature	√	√	√	√	√	√	√	√	√	√	√	√
	Max. Temperature	√	√	√	√	√	√	√	√	√	√	√	√
	Rainfall	√	√	√	√	√	√	√	√	√	√	√	√
4	Min. Temperature	√	√	√	√	√	√	√	√	√	√	√	√
	Max. Temperature	√	√	√	√	√	√	√	√	√	√	√	√
	Rainfall	√	√	x	√	√	√	√	√	√	√	√	√
5	Min. Temperature	√	√	√	√	√	√	√	√	√	√	√	√
	Max. Temperature	√	√	√	√	√	√	√	√	√	√	√	√
	Rainfall	√	√	√	√	√	√	√	√	√	√	√	√
6	Min. Temperature	√	√	√	√	√	√	√	√	√	√	√	√
	Max. Temperature	√	√	√	√	√	√	√	√	√	√	√	√
	Rainfall	√	√	√	√	√	√	√	√	√	√	√	√
7	Min. Temperature	√	√	√	√	√	√	√	√	√	√	√	√
	Max. Temperature	√	√	√	√	√	√	√	√	√	√	√	√
	Rainfall	√	x	√	√	√	√	√	√	√	√	√	√
8	Min. Temperature	√	√	√	√	√	√	√	√	√	√	√	√
	Max. Temperature	√	√	√	√	√	√	√	√	√	√	√	√
	Rainfall	x	√	√	√	√	√	√	√	√	√	√	√
9	Min. Temperature	√	√	√	√	√	√	√	√	√	√	√	√
	Max. Temperature	√	√	√	√	√	√	√	√	√	√	√	√
	Rainfall	√	√	√	√	√	√	√	√	√	√	√	√
10	Min. Temperature	√	√	√	√	√	√	√	√	√	√	√	√
	Max. Temperature	√	√	√	√	√	√	√	√	√	√	√	√
	Rainfall	√	√	√	√	√	√	√	√	√	√	√	√
11	Min. Temperature	√	√	√	√	√	√	√	√	√	√	√	√
	Max. Temperature	√	√	√	√	√	√	√	√	√	√	√	√
	Rainfall	√	√	√	√	√	√	√	√	√	√	√	√
12	Min. Temperature	√	√	√	√	√	√	√	√	√	√	√	√
	Max. Temperature	√	√	√	√	√	√	√	√	√	√	√	√
	Rainfall	√	√	√	√	√	√	√	√	√	√	√	√
13	Min. Temperature	√	√	√	√	√	√	√	√	√	√	√	√
	Max. Temperature	√	√	√	√	√	√	√	√	√	√	√	√
	Rainfall	√	√	√	√	√	√	√	√	√	√	√	√
14	Min. Temperature	√	√	√	√	√	√	√	√	√	√	√	√
	Max. Temperature	√	√	√	√	√	√	√	√	√	√	√	√
	Rainfall	√	√	√	√	√	√	√	√	√	√	√	√

The cumulative distribution functions (CDFs) for the lengths of dry and wet series of observed and synthetic rainfall data for June, July and August (JJA) months and September, October and November (SON) months were generated by LARS-WG. The wet series distributions derived for the quarters of JJA and SON months at a sample grid #9 which fully lies in the basin are shown in figure 5.2 (a-b). Figure 5.3 (a-b) shows the CDFs derived for the lengths of dry series of observed and synthetic rainfall data during JJA and SON quarters. The wet/dry series distribution plots show that all lengths of wet/dry series distributions are reproduced correctly at grid #9 for JJA and SON months. Similar results were obtained across all the fourteen grids of the basin. Thus, it was concluded that LARS-WG was able to reproduce daily distribution of the observed rainfall and the length of wet/dry series well.
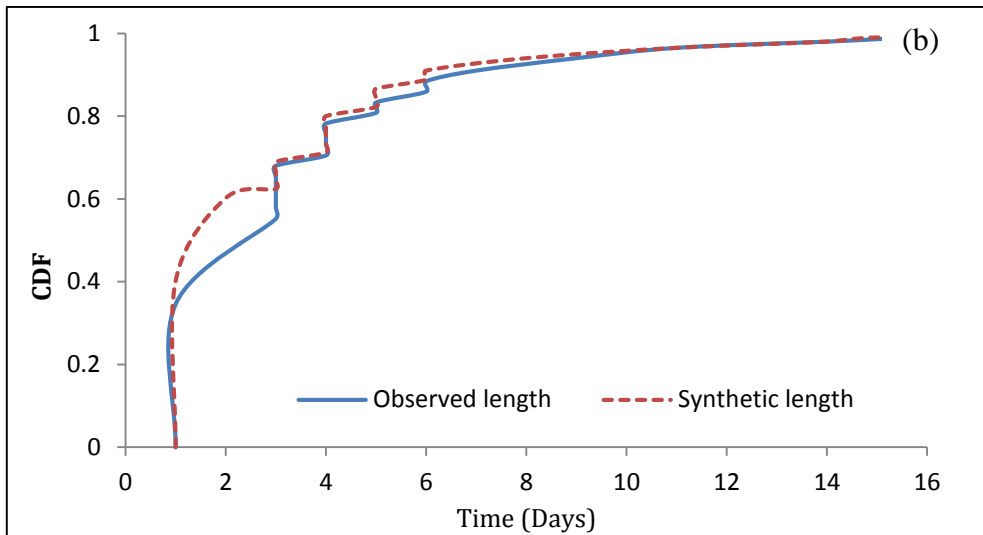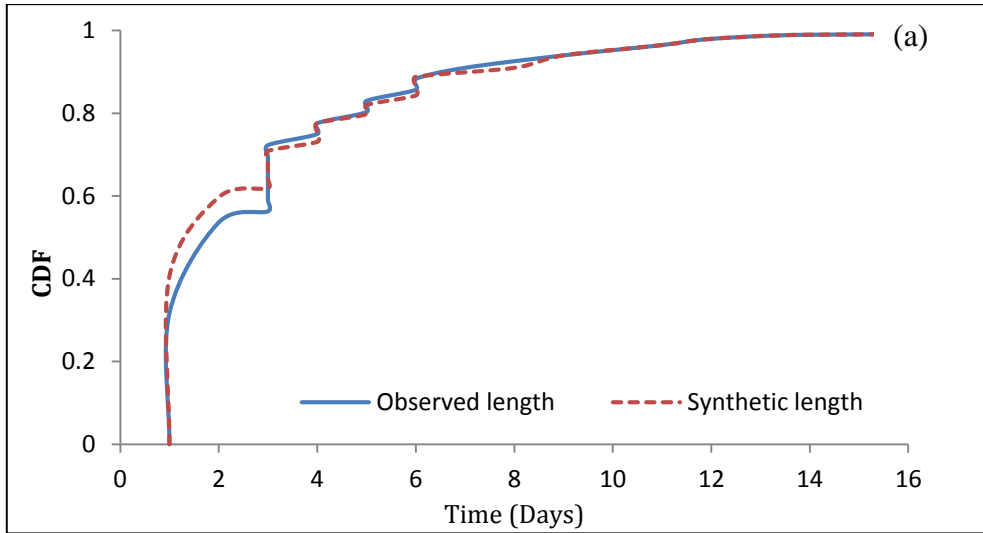
Figure 5.2 CDF wet series of rainfall at grid #9 during a) JJA and b) SON quarters
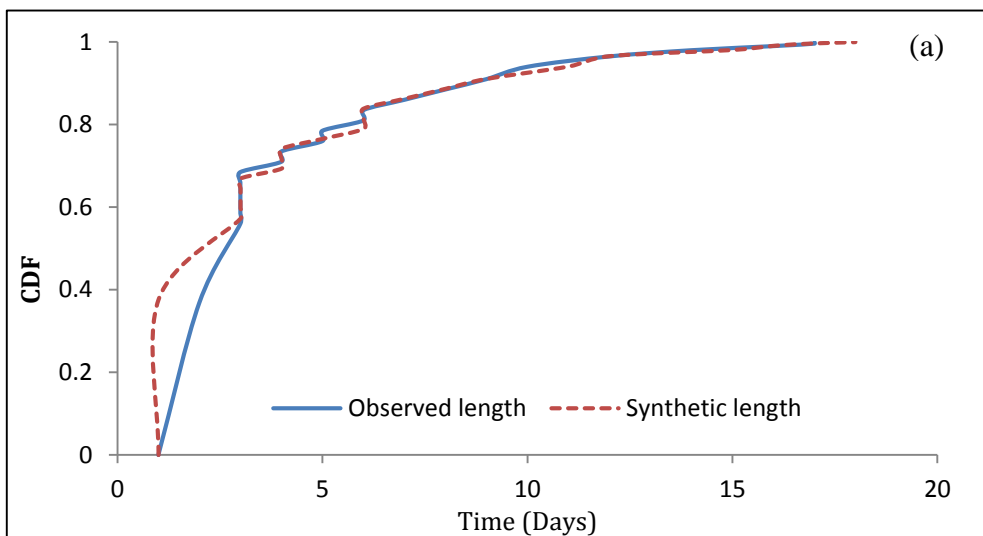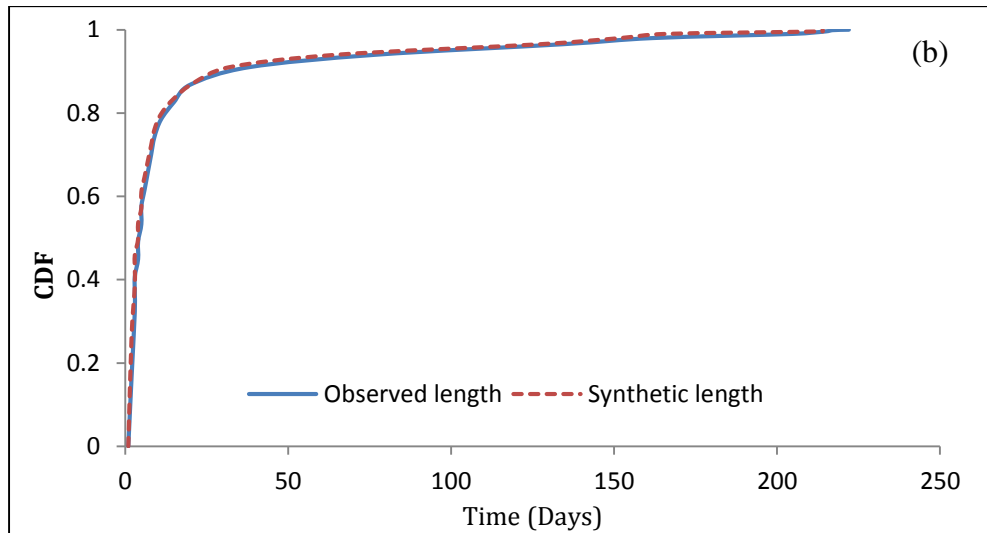
Figure 5.3 CDF of dry series of rainfall at grid #9 during (a) JJA and (b) SON quarters

Daily minimum and maximum temperatures are considered as stochastic processes with daily means and daily standard deviations conditioned on the wet or dry status of the day (Semenov and Brown, 2002). The technique used to simulate the process in LARS-WG was presented by Racsko *et al*. (1991). Table 5.3 summarizes the results of t-tests of the observed and synthetic series of minimum temperatures. The months marked with ($\surd$) indicate p-value > 0.05 and suggest that the two means are equal. The months marked with (x) indicate p-value < 0.05 and hence the null hypothesis of equal means was rejected. Table 5.3 shows that the means of minimum temperatures were not equal for winter (February, March, April) and post-monsoon (September, October) months across most of the grids.

Table 5.3 Comparison of observed and synthetic minimum temperature in each grid

t-test/ Months	Jan	Feb	Mar	Apr	May	Jun	Jul	Aug	Sep	Oct	Nov	Dec
1	√	√	√	√	√	√	√	√	√	√	√	√
2	x	√	√	√	√	√	√	√	√	√	√	√
3	x	√	x	√	√	√	√	√	√	√	√	√
4	√	√	√	x	√	√	√	√	√	x	√	√
5	√	√	x	x	√	√	√	√	√	x	√	√
6	√	√	x	√	√	√	√	√	√	√	√	√
7	√	√	x	√	√	√	√	√	x	√	√	√
8	√	√	√	√	√	√	√	√	√	√	√	√
9	√	√	√	√	√	√	√	√	√	x	√	√
10	√	√	√	x	√	√	√	√	x	√	√	√
11	√	√	√	√	√	√	√	√	x	√	√	√
12	√	√	√	√	√	√	√	√	√	√	√	√
13	√	x	√	√	√	√	√	√	x	x	√	√
14	√	x	√	√	√	√	x	√	√	√	√	√
Note: √ indicate p value >0.05 and x <0.05												

Table 5.4 summarizes the results of t-tests to compare the monthly means of the observed and synthetic series of maximum temperatures. The months marked with (√) indicate p-value > 0.05 and suggest that the two means are equal. The months marked with (x) indicate p-value < 0.05 and hence we reject the null hypothesis of equality of means. Table 5.3 shows that the means of maximum temperatures were not equal for winter (January, February) across most of the grids. Means of monsoon (June, July) months of few grids were not found equal, too.

Table 5.4 Grid-wise comparison of observed and synthetic maximum temperature

Test/ Months	Jan	Feb	Mar	Apr	May	Jun	Jul	Aug	Sep	Oct	Nov	Dec
1	√	x	√	√	√	√	√	√	√	√	√	√
2	x	x	√	√	√	√	√	√	√	√	√	√
3	x	x	√	√	√	√	x	√	√	√	x	√
4	√	√	√	√	√	√	√	√	√	√	√	√
5	√	x	√	√	√	√	√	√	x	√	x	√
6	√	x	√	√	√	√	x	√	√	√	√	√
7	x	x	√	√	√	√	√	√	√	√	x	√
8	√	√	√	√	√	x	x	√	√	√	√	√
9	√	√	√	√	√	x	√	√	√	√	√	√
10	√	√	√	√	√	√	√	√	√	√	√	√
11	x	x	√	√	√	x	√	√	√	√	x	√
12	√	√	√	x	√	x	√	√	√	√	√	√
13	√	x	√	√	√	√	√	√	√	x	√	√
14	√	√	√	√	√	√	x	√	√	√	√	√

Note: √ indicate p value >0.05 and x <0.05

The means and standard deviations of the observed rainfall data at each grid were compared with those of the synthetic data using t-test and F-test, respectively. The results based on the t-test and F-test statistics and calculated p values are summarized in Table 5.5. Months in which the p values of t-test and F-test were less than the significance level of 0.05 (indicating poor performance of the model) are marked with (x). The months marked with (√) indicate p-values greater than the significance level of 0.05 and hence suggest a good agreement between the means and/or standard deviations of the observed and the synthetic data.

Table 5.5 Grid-wise comparison of observed and synthetic mean monthly rainfall

Grid	Test/Months	Jan	Feb	Mar	Apr	May	Jun	Jul	Aug	Sep	Oct	Nov	Dec
1	t-test	√	√	√	√	√	√	√	√	√	√	√	√
1	F-test	x	√	√	√	√	√	x	x	√	√	√	√
2	t-test	√	√	√	√	√	√	√	√	√	√	√	√
2	F-test	√	√	√	√	√	√	x	√	√	x	√	√
3	t-test	√	√	√	√	√	√	√	√	√	√	√	√
3	F-test	√	x	√	√	√	√	√	√	√	√	√	x
4	t-test	√	√	√	√	√	√	√	√	√	√	√	√
4	F-test	√	√	√	√	√	√	x	x	x	√	√	x
5	t-test	√	√	√	√	√	√	√	√	√	√	√	√
5	F-test	√	√	√	√	√	√	x	√	√	x	√	√
6	t-test	√	√	√	√	√	√	√	√	√	√	√	√
6	F-test	√	√	√	√	√	√	x	√	√	√	√	√
7	t-test	√	√	√	√	√	√	√	√	√	√	√	√
7	F-test	√	√	√	√	√	√	x	√	√	√	√	√
8	t-test	√	√	√	√	√	√	√	√	√	√	√	√
8	F-test	√	√	√	√	√	√	x	x	√	√	√	√
9	t-test	√	√	√	√	√	√	√	√	√	√	√	√
9	F-test	x	√	√	√	√	√	x	x	√	√	√	√
10	t-test	√	√	√	√	√	√	√	√	√	√	√	√
10	F-test	√	√	√	√	√	√	x	√	√	√	√	√
11	t-test	√	√	√	√	√	√	√	√	√	√	√	√
11	F-test	√	√	√	√	√	√	x	√	√	√	√	√
12	t-test	√	√	√	√	√	√	√	√	√	√	√	√
12	F-test	√	√	√	√	√	√	x	x	x	√	√	√
13	t-test	√	√	√	√	√	√	√	√	√	√	√	√
13	F-test	√	√	√	√	√	√	x	x	x	x	√	√
14	t-test	√	√	√	√	√	x	√	√	√	√	√	√
14	F-test	x	√	√	√	√	√	x	x	√	√	√	√

Note: √ indicate p value >0.05 and x <0.05

A good agreement was observed between the means of observed and synthetic data in most of the grids during most of the months. However, the inter-annual variability represented by the standard deviations of monthly data, was not well reproduced for monsoon months particularly for July across all the grids. This is in conjunction with the recommendations of Semenov *et al.* (1998), who reported that all weather generators have limited capability of reproducing inter-annual variability.

Figure 5.4 (a-c) shows example plots of means and standard deviations (SD) of monthly minimum and maximum temperatures, and rainfall calculated for synthetic and observed data at grid #9. The plots show that the model performed well in reproducing the synthetic data having similar statistical properties as of the observed data. Similar results were observed for all the months across all 14 grids of the basin.

Based on the results obtained for all the grids during the calibration and validation, it was concluded that the LARS-WG has reproduced the temperature data and rainfall data well. However, the model poorly represented the inter-annual variability of monthly rainfall for the monsoon months. Overall, the calibration and validation results were found satisfactory and the seed values were considered final for further application of LARS-WG for generation of temperature and rainfall for future scenarios.
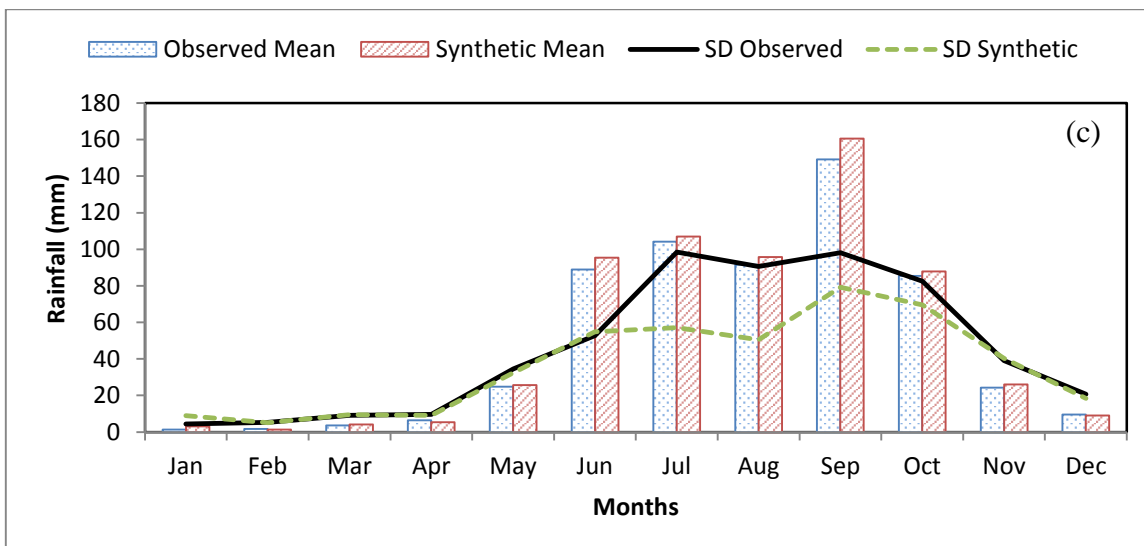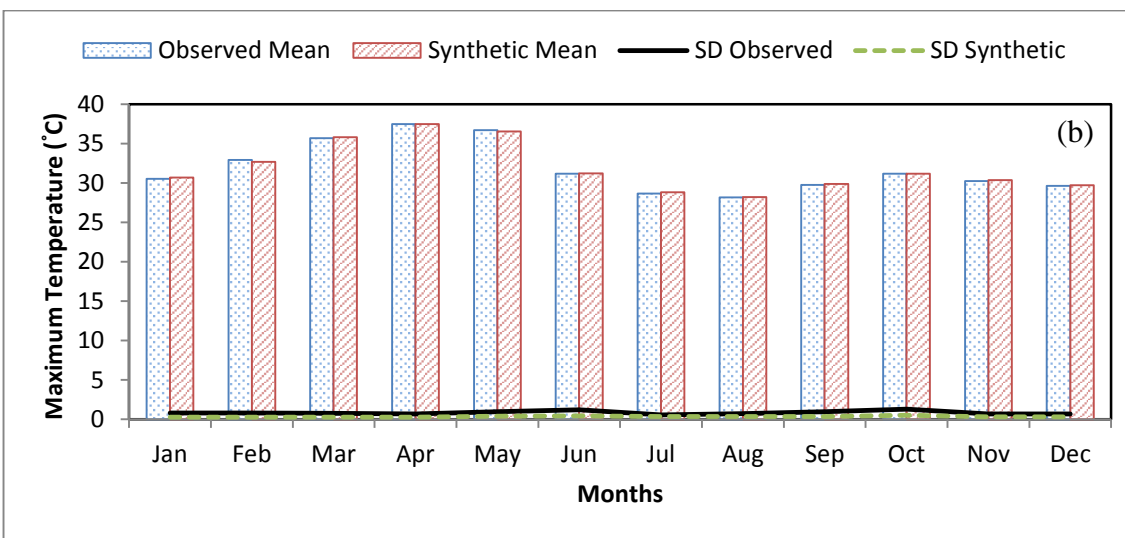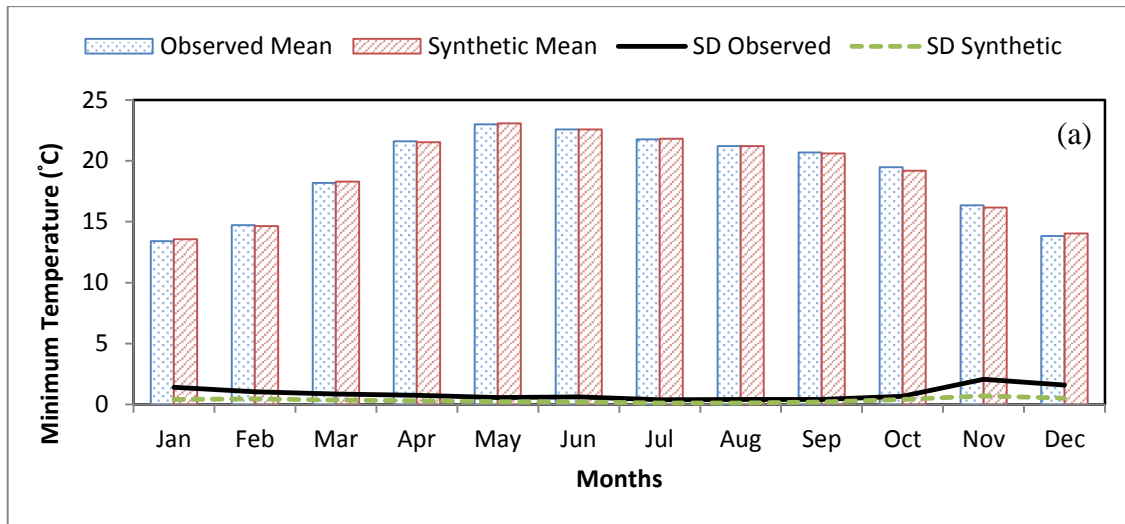
Figure 5.4 Mean and standard deviation (SD) of observed and synthetic data (a) monthly minimum temperature (b) monthly maximum temperature and (c) monthly rainfall for grid #9

5.6.2 Uncertainty in Projection of Meteorological Variables

Future meteorological data from 15 GCMs at each grid of the basin were generated for all three scenarios in three time spans, as stated earlier, using GENERATOR module. The CFs were calculated on the basis of seasonal and annual changes in meteorological variables with respect to baseline period to assess the impact of climate change. It was found that all the projections were different from each other. The statistics of CFs of temperature (minimum and maximum) and rainfall obtained for all GCMs for all emission scenarios A1B, A2 and B1 and for all time spans 2020s, 2055s and 2090s for both seasonal and annual are illustrated in the Box-plots in the figures 5.5 (a-c) for a sample grid #9.

In the figures Sum, Mon, Pmon and Win represent the summer, monsoon, post-monsoon and winter seasons, respectively. The CFs display considerable inter-model variation in projections. The CFs for minimum and maximum temperatures is projected by various GCMs range from 0.5 to 6ºC. Though different models show agreement in terms of suggesting a future rise in minimum (Figure 5.5a) as well as maximum temperatures (Figure 5.5b), they show strong disagreement in sign and the magnitude of the change in rainfall (Figure 5.5c).

The variations in CFs for rainfall projections seem to be smaller compared to those of temperatures. Unlike temperature projections, the boxplots of seasonal as well as annual rainfall projections CFs lie in the positive as well as negative regions. This implies that some GCMs are predicting an increase in future annual as well as seasonal rainfall, while others a decrease.

High variability was observed among GCM projections for the period of 2090s compare to 2020s and 2055s. The variability among GCMs is particularly high for temperature projections. Based on these observations, it may be concluded that relying on one particular GCM projection may either cause underestimation or overestimation of climate change impacts. Hence, the results presented in the subsequent sections are based on the ensemble mean of all the GCMs for each meteorological variable. This assumes that an ensemble of all the GCMs projections is a better representation of the projected climate in order to reduce uncertainty as seen in figure 5.5.
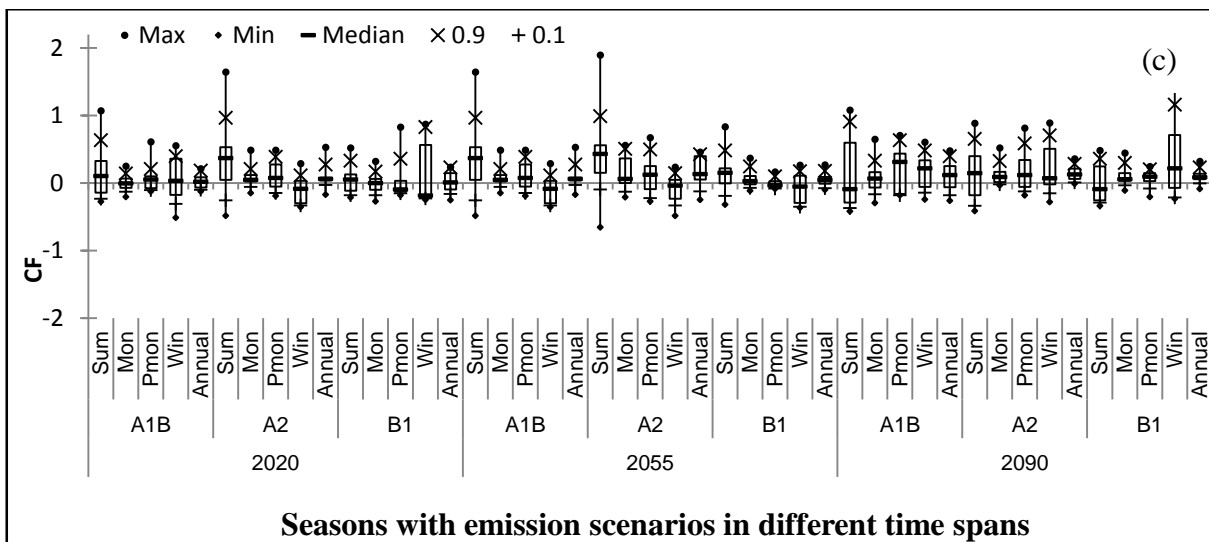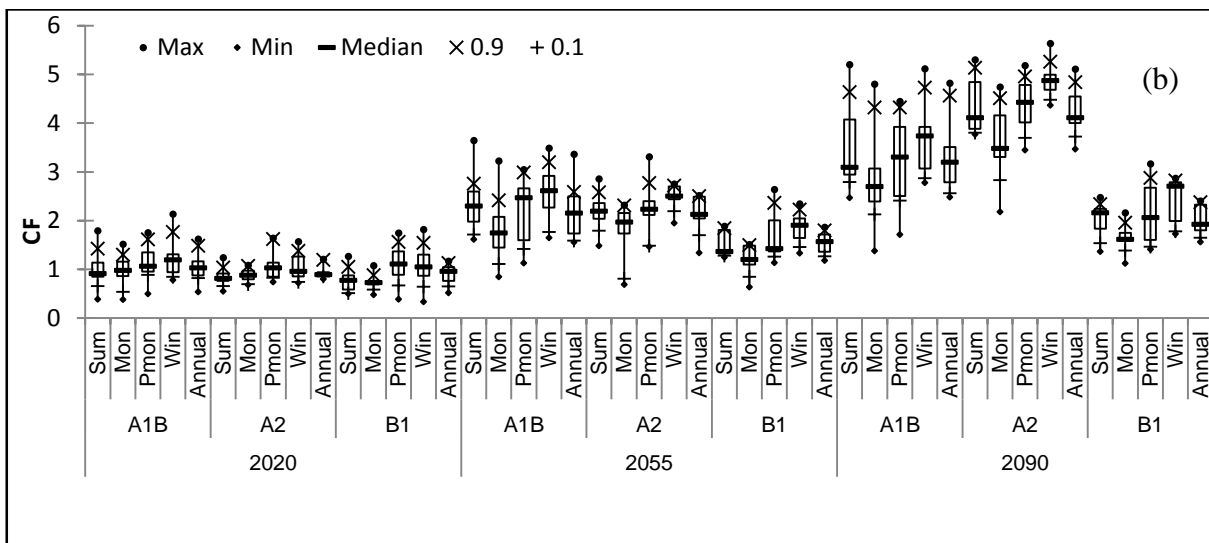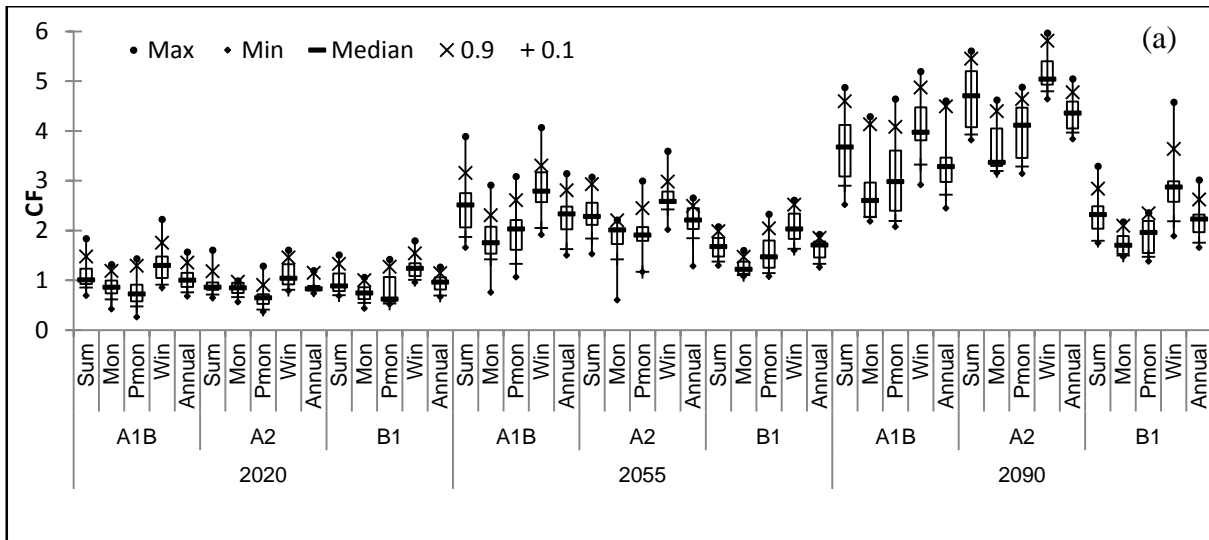
Figure 5.5 Changes in seasonal and annual a) minimum temperature b) maximum temperature c) rainfall projected by 15 GCMs for A1B, A2 and B1 emissions scenario for 2020s, 2055s and 2090s compared with the baseline scenario at grid #9

5.6.3 Projected Changes in Minimum Temperature

5.6.3.1 Analysis of CFs of Seasonal Minimum Temperature

The CFs for the 'entire' basin were obtained by calculating averages of CFs for all the grids and are summarized in Table 5.6. The CF for the entire basin ranged from 0.75°C to 4.65°C. The projected changes in mean seasonal minimum temperature are shown in figure 5.6(a-d) for summer, monsoon, post-monsoon and winter seasons, respectively. The mean minimum temperatures of all seasons show increasing trend in the future with highest increase in A2 scenario at all the grids and the lowest increase in B1 scenario. The highest increase in minimum temperature was observed during winter season as compared to the other seasons for all the scenarios and time spans. The lowest increase in minimum temperatures was observed during monsoon season for all three scenarios and the three time spans.

Table 5.6 Ensemble mean of CFs (°C) of seasonal minimum temperature of the 'entire' Basin

Season	Scenarios	A1B	A2	B1
Summer	2020	1.00	0.85	0.94
	2055	2.32	2.16	1.47
	2090	3.45	4.39	2.21
Monsoon	2020	0.84	0.77	0.75
	2055	1.72	1.73	1.17
	2090	2.73	3.47	1.67
Post-monsoon	2020	0.90	0.75	0.99
	2055	2.02	1.96	1.59
	2090	3.04	3.86	1.92
Winter	2020	1.14	0.94	1.15
	2055	2.50	2.40	1.82
	2090	3.67	4.65	2.64
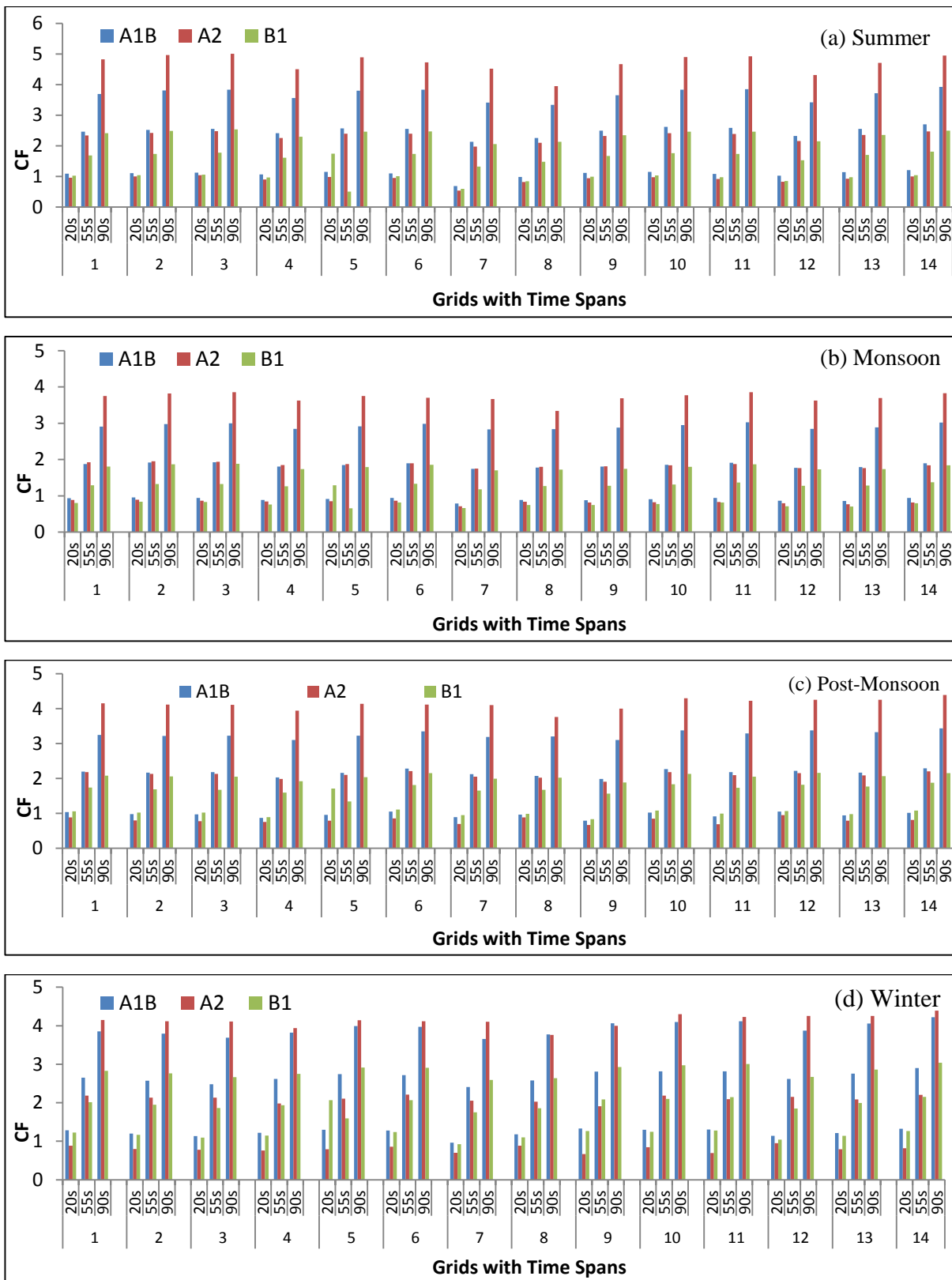
Figure 5.6 Seasonal change factors of minimum temperature for A1B, A2 and B1 scenarios during three time spans (centred at 2020s, 2055s and 2090s) for all the grids

The CFs for 'annual' minimum temperature are shown in figure 5.7 with respect to the baseline period. It shows that there is good agreement about the increase in minimum temperature between among various projections of different scenarios as increasing trend is seen across all the scenarios and time spans. Among the scenarios, A2 scenario is expected to predict high increase in annual minimum temperature followed by A1B and B1, respectively. All grids show similar pattern of increasing trend of annual minimum temperature.
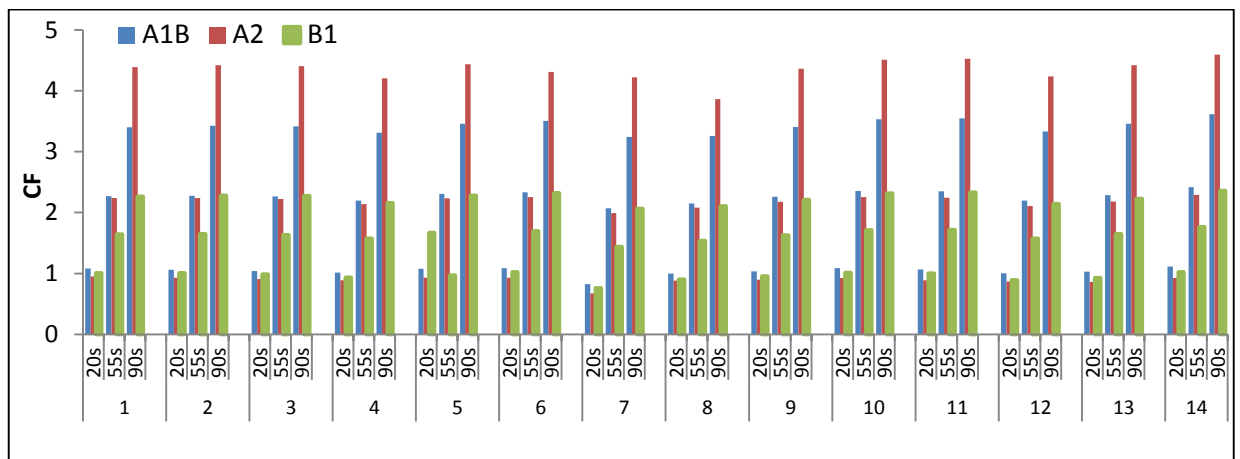
Figure 5.7 Annual change factors of annual minimum temperature for A1B, A2 and B1 scenarios during three time spans (centred at 2020s, 2055s and 2090s) for all the grids

Figure 5.8 shows the spatial pattern of the CFs for annual minimum temperature. Intra-basin CFs analysis of the grids indicate almost equal changes across the grids, scenarios and time spans except for B1 scenarios where minimum temperature increases in the central part of the basin in 2020s and then decreases in 2055s before it is stabilised in 2090s. In general the time span of 2090s was associated with the highest CFs, followed by the 2055s and the 2020s. The magnitude of CFs did not vary much among the three scenarios during 2020s as during 2090s and 2055s. This variation is clearly visible in figure 5.8. In other words, a noticeable variation among scenarios was observed only for CFs during 2090s, with B1 scenario being the lowest and A2 scenario being the highest.
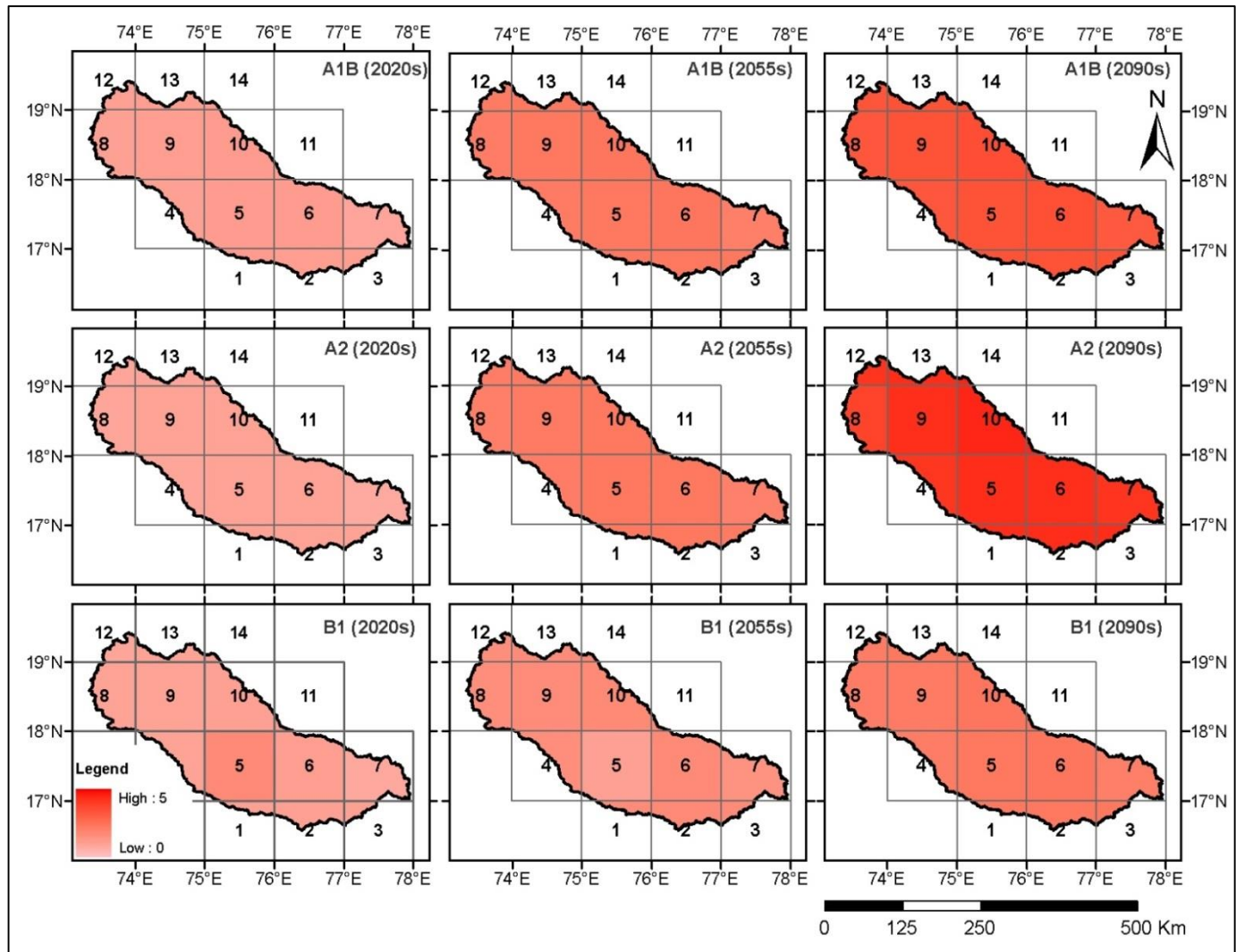
Figure 5.8 Spatial pattern of the projected changes in annual minimum temperature for three scenarios and three time spans

A summary of the observations of the analysis of CFs of the minimum temperature is presented below:

- In general, within each scenario, the CFs increased from 2020s to 2055s to 2090s. CFs for annual minimum temperatures ranged from 0.67°C to 4.59°C across all scenarios and all time spans.

- In 2020s, the CFs ranged from 0.67°C to 1.67°C. In 2055s, the CFs ranged from 0.97°C to 2.42°C. And in 2090s, the CFs ranged from 2.06°C to 4.59°C.

- For A1B scenario, the CFs ranged from 0.82°C to 3.62°C. For A2 scenario, the CFs ranged from 0.67°C to 4.59°C. And for B1 scenario, the CFs ranged from 0.76°C to 2.36°C.

- On an average the annual minimum temperature is projected to increase by 1.04, 0.89, 1.01°C in 2020s; by 2.27, 2.19, 1.58°C in 2055s and by 3.42, 4.35, 2.24°C in 2090s for A1B, A2 and B1 scenarios, in the respective order.

5.6.4 Projected Changes in Maximum Temperature

5.6.4.1 Analysis of CFs of Seasonal Maximum Temperature

The CFs for the 'entire' basin were obtained by calculating average of the CFs for all the grids and are summarized in Table 5.7. The CFs for the entire basin ranged from 0.74°C to 4.45°C. The projected changes in mean seasonal maximum temperature are shown in figure 5.9(a-d) for summer, monsoon, post-monsoon and winter seasons, respectively. The mean maximum temperatures of all seasons show increasing trends in all future time spans with highest increase in A2 scenario at all the grids in the basin and the lowest increase in B1 scenario. Among the seasons, the highest increase in maximum temperatures was observed in winter season. The lowest increase in maximum temperatures was observed during monsoon season across the scenarios and time spans.

Table 5.7 Ensemble mean of CFs (°C) of seasonal maximum temperature of the 'entire' Basin

Season	Scenarios	A1B	A2	B1
Summer	2020	0.95	0.84	0.77
	2055	2.18	2.11	1.48
	2090	3.33	4.16	1.96
Monsoon	2020	0.95	0.87	0.74
	2055	1.73	1.71	1.17
	2090	2.76	3.40	1.59
Post-monsoon	2020	1.09	1.00	1.07
	2055	2.09	2.12	1.61
	2090	3.08	4.08	2.03
Winter	2020	1.12	0.93	0.98
	2055	2.33	2.26	1.70
	2090	3.44	4.45	2.21
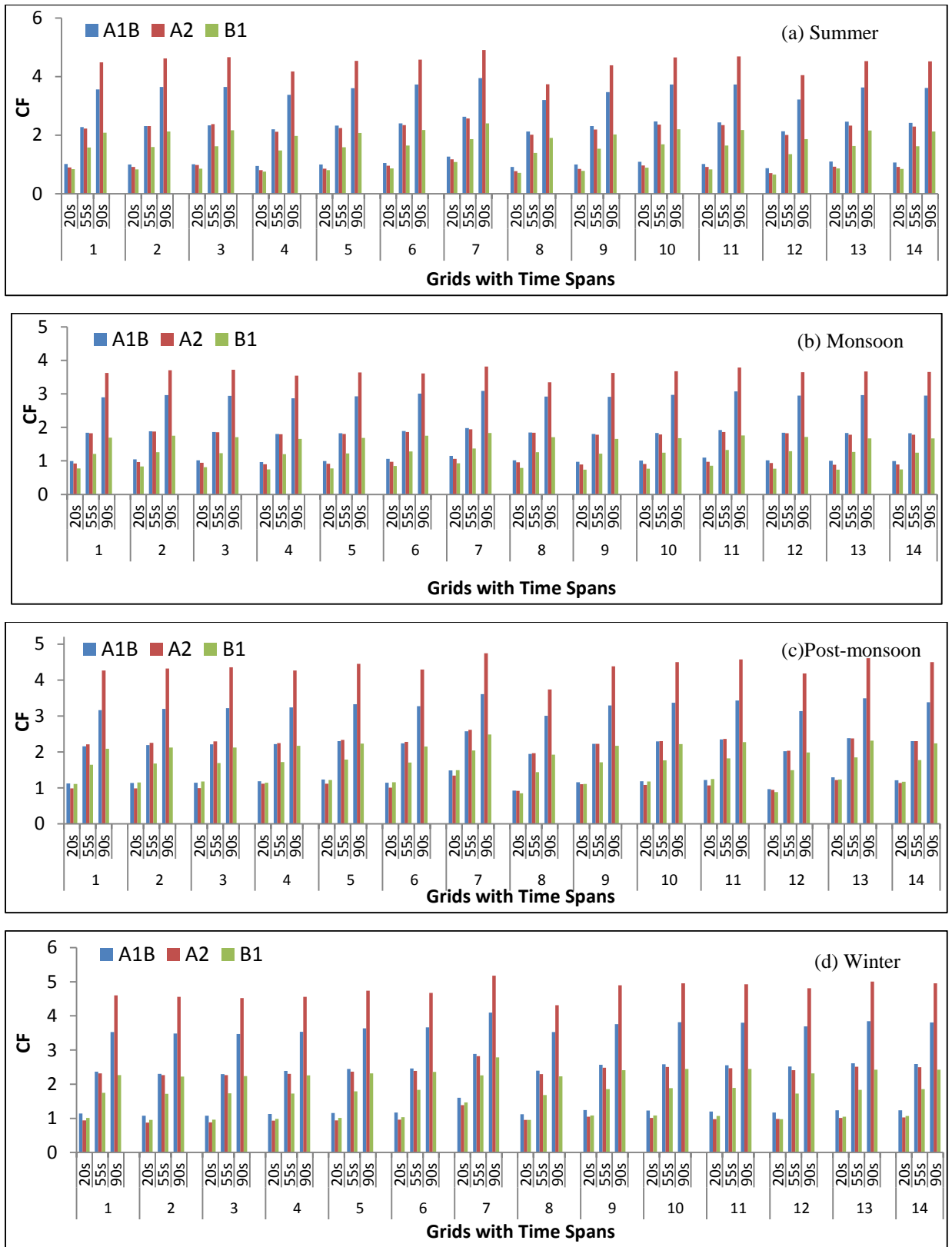
Figure 5.9 Seasonal change factors of maximum temperature for A1B, A2 and B1 scenarios during three time spans (centred at 2020s, 2055s and 2090s) for all the grids.

5.6.4.2 Analysis of CFs of Annual Maximum Temperature

The CFs for annual maximum temperatures are shown in figure 5.10 with respect to the baseline period. Projections of different scenarios show an increasing trend across all the scenarios and time spans. Among the scenarios, A2 scenario is expected to predict high increase in annual maximum temperature followed by A1B and B1, respectively. All grids show similar pattern of increasing trend of annual maximum temperature as seen in the figure.
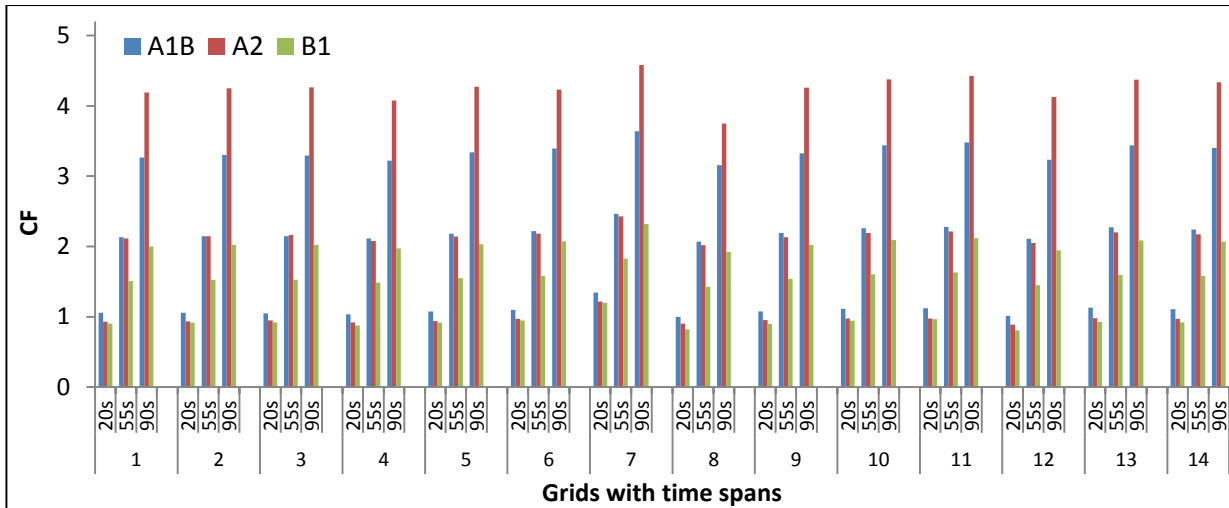
Figure 5.10 Annual change factors of annual maximum temperature for A1B, A2 and B1 scenarios during three time spans (centred at 2020s, 2055s and 2090s) for all the grids

Figure 5.11 shows the spatial pattern of the CFs for annual maximum temperatures. Intra-basin CFs analysis of the grids indicated almost equal changes across the grids, scenarios and time spans. In general the time span of 2090s was associated with the highest CFs, followed by the CFs in 2055s and the 2020s. A noticeable variation among the scenarios was observed for CFs during 2090s, with A2 scenario being the highest and B1 scenario being the lowest.

A summary of the observations of the analysis of CFs of the maximum temperature is given below:

- In general, within each scenario, the CFs increased from 2020s to 2055s to 2090s. CFs for annual maximum temperatures ranged from 0.81°C to 4.58°C across all scenarios and all time spans.

- In 2020s, the CFs ranged from 0.81°C to 1.35°C. In 2055s, the CFs ranged from 1.43°C to 2.47°C. And in 2090s, the CFs ranged from 1.92°C to 4.58°C.

- For A1B scenario, the CFs ranged from 1°C to 3.64°C. For A2 scenario, the CFs ranged from 0.89°C to 4.58°C. And for B1 scenario, the CFs ranged from 0.81°C to 2.32°C. On an average the annual maximum temperatures are projected to increase by 1.09, 0.96, 0.93°C in 2020s; by 2.2, 2.16, 1.56°C in 2055s and by 3.35, 4.25, 2.05°C in 2090s for A1B, A2 and B1 scenarios, in the respective order.
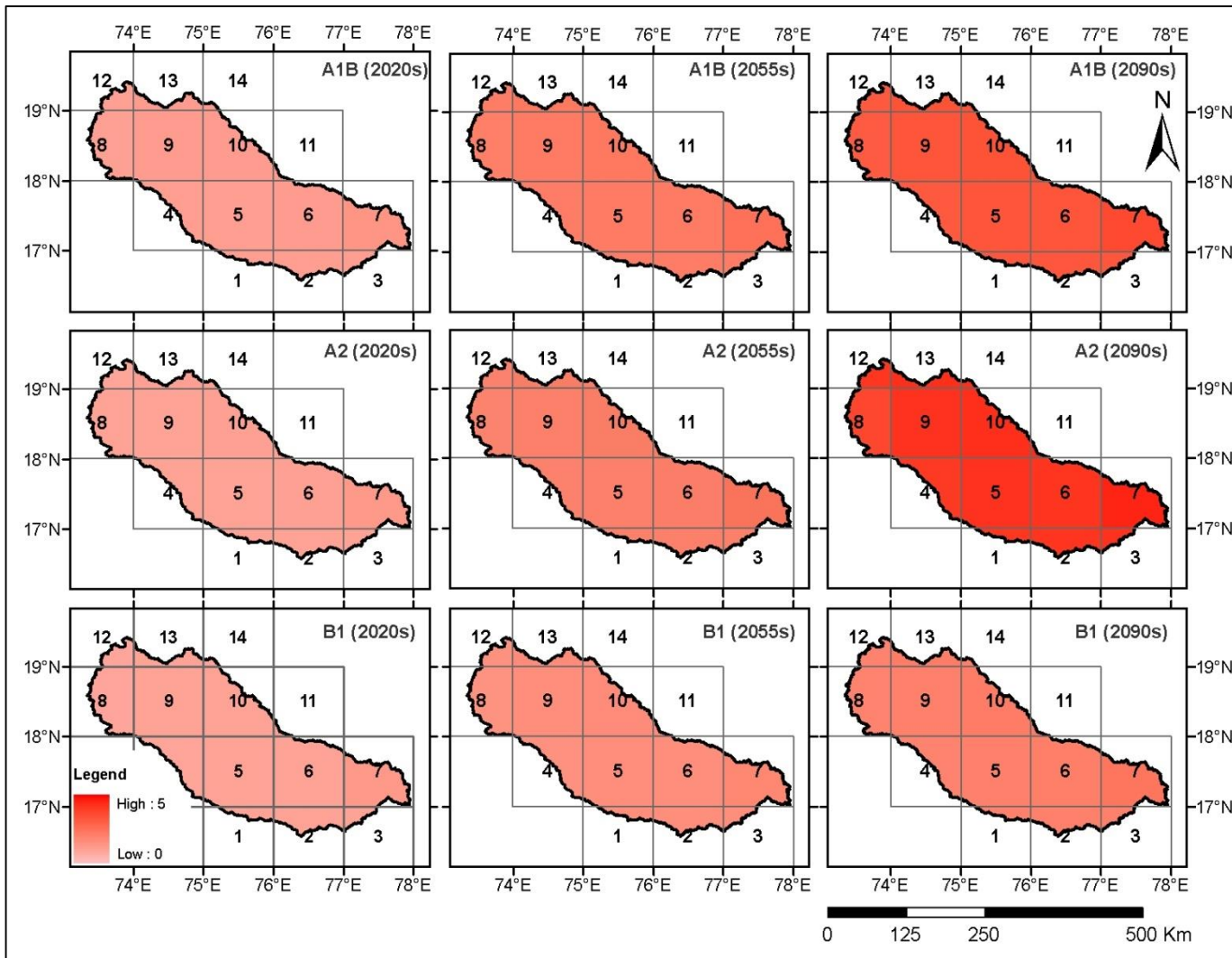
Figure 5.11 Spatial pattern of projected changes in annual maximum temperature for three scenarios and three time spans

5.6.5 Projected Changes in Rainfall

5.6.5.1 Analysis of CFs of Seasonal Rainfall

The projected changes in seasonal rainfall at each grid of the basin are shown in figure 5.12 (a-d). The summer rainfall is projected to increase in future with the highest changes observed in A2 scenario - the average of percent CFs of 14 grids are 17.2, 22.6 and 11.8 during 2020s, 2055s and 2090s. A2 scenario is followed by A1B and B1 scenarios. In both, A1B and A2 scenarios, rainfall was found increasing by 2055s and then it decreased. In B1 scenario, rainfall was projected to increase continuously with the average of percent CFs of 14 grids as 2.7 (2020s), 6.7 (2055s) and 7.1 (2090s). Among three time spans, summer rainfall was projected to increase the highest in 2055s. A decrease in the summer rainfall was projected at grids #1 to #6 for B1 scenario, mainly during 2020s and 2055s.

The monsoon rainfall projections indicated -6 to +50% changes compare to the base period. Similar to the summer season, an increasing trend was observed in monsoon rainfall from 2020s to 2055s to 2090s at all grids under B1 scenario (Figure 5.12b). However, under A1B and A2 scenarios, the rainfall increased from 2020s to 2055s and decreased from 2055s to 2090s at all the grids. The spatial pattern of percent changes in monsoon rainfall across all grids under three scenarios and in three time spans is shown in figure 5.13. As seen in figure 5.13, the grids located in the middle region showed higher percent change in rainfall. The spatial variability increases from 2020s to 2055s and then seems to have decreased from 2055s to 2090s. Among the scenarios, the A2 scenario seemed to project the highest spatial variability in the projected monsoon rainfall, followed by A1B scenario and A2 scenario. Thus, it is concluded that the monsoon rainfall is projected to increase in the basin in future.

Unlike summer and monsoon seasons where A2 scenario showed the highest changes, the post-monsoon rainfall showed the highest percent change for A1B scenario in most of the grids (Figure 5.12c). The averages of the percent change are 3.1, 14.5 and 16.8 during 2020s, 2055s and 2090s, respectively. It is followed by A2 and B1 scenarios. The decrease in rainfall was projected at grids #1 to #4, #7 and #10 under B1 scenario, mainly during 2020s and 2055s.

The winter rainfall, which is less than 10% of the total rainfall in the basin, showed the maximum variation in the future rainfall pattern as seen in figure 5.12(d). Projections under A2 and B1 scenarios indicated a decrease in rainfall at most of the grids during 2020s and 2055s. During the time span 2090s, most of the scenarios project an increase in the winter rainfall. The projections were found mostly positive under A1B scenario suggesting an increase in winter rainfall at most of the grids.
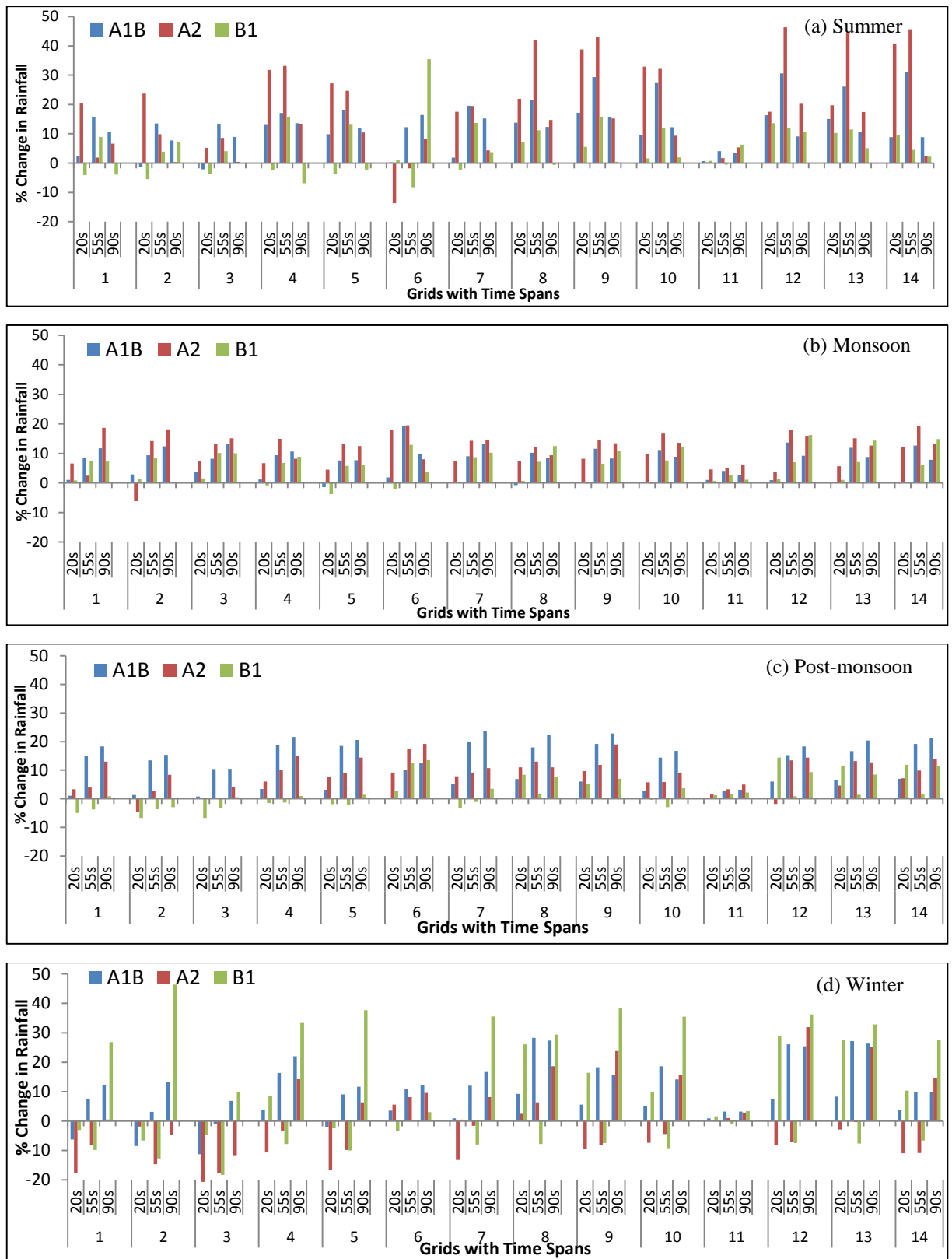
Figure 5.12 Grid-wise percent seasonal changes in rainfall for A1B, A2, and B1 scenarios and during three time spans (2020s, 2055s, and 2090s) (a) summer (b) monsoon (c) post-monsoon (d) winter rainfall
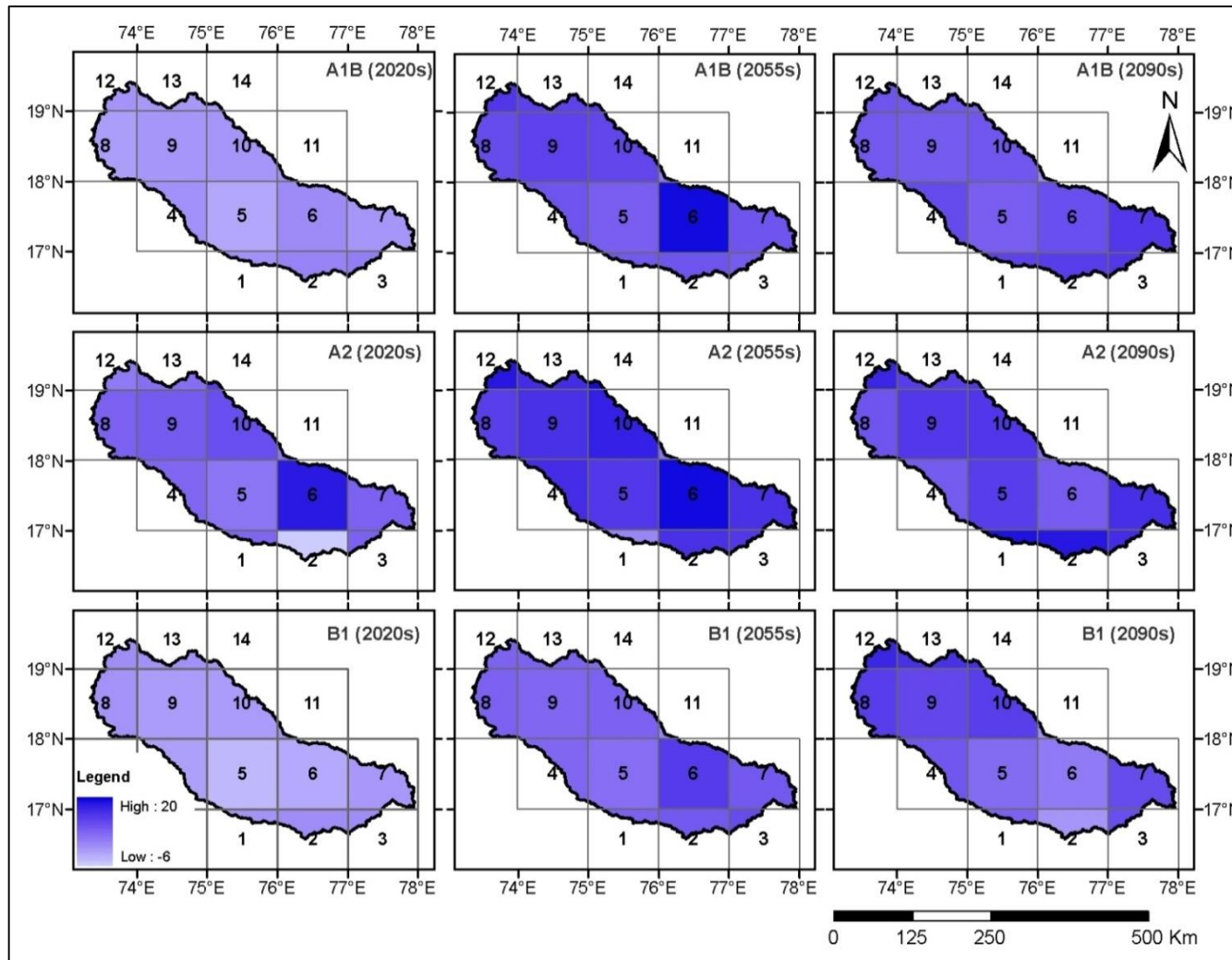
Figure 5.13 Spatial patterns of percent changes in projected monsoon rainfall for A1B, A2 and B1 scenarios during 2020s, 2055s and 2090s

5.6.5.2 Analysis of CFs of Annual Rainfall

The percent changes in projected average annual rainfall in each grid of the basin are shown in figure 5.14. The annual rainfall projections indicated -3.2 to +18.4% changes compared to the base period. The annual rainfall is projected to increase in future in most of the grids from 2020s to 2090s. Among the scenarios, highest increase was observed in A2 scenario (7% in 2020s, 13.4% in 2055s, and 13.1% in 2090s) followed by A1B scenario (1.4% in 2020s, 11.8% in 2055s, and 11.4% in 2090s) and B1 scenario (1.6% in 2020s, 6% in 2055s, and 9.3% in 2090s).
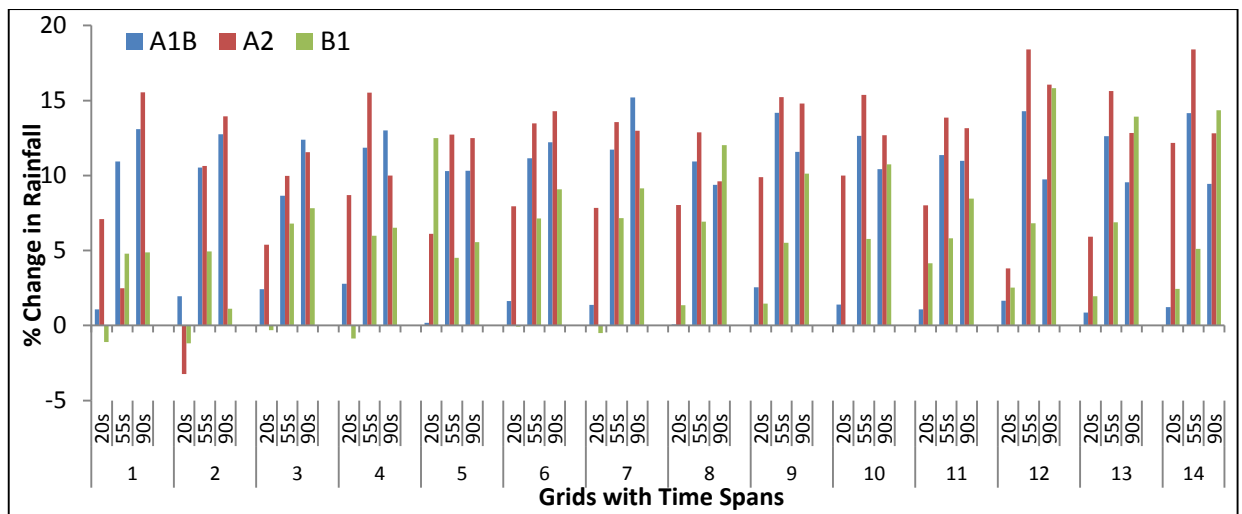
Figure 5.14 Percent change in annual rainfall for A1B, A2 and B1 scenarios during three time spans (centred at 2020s, 2055s and 2090s) for all the grids

The spatial pattern of percent changes in annual rainfall across all grids of the basin are shown in figure 5.15. This confirms the increasing trend of rainfall across most grids from 2020s to 2090s for A1B and B1 scenarios and the increasing trend is not uniform for the grids. However, for A2 scenario, the rainfall seems to increase from 2020s to 2055s and then decreased from 2055s to 2090s across most of the grids. Furthermore, the A2 scenario is associated with the highest percent change in rainfall during all three time spans. Overall, an increase in annual rainfall was projected across the entire basin and the magnitude of percent increase seems to be higher in the middle part of the basin.
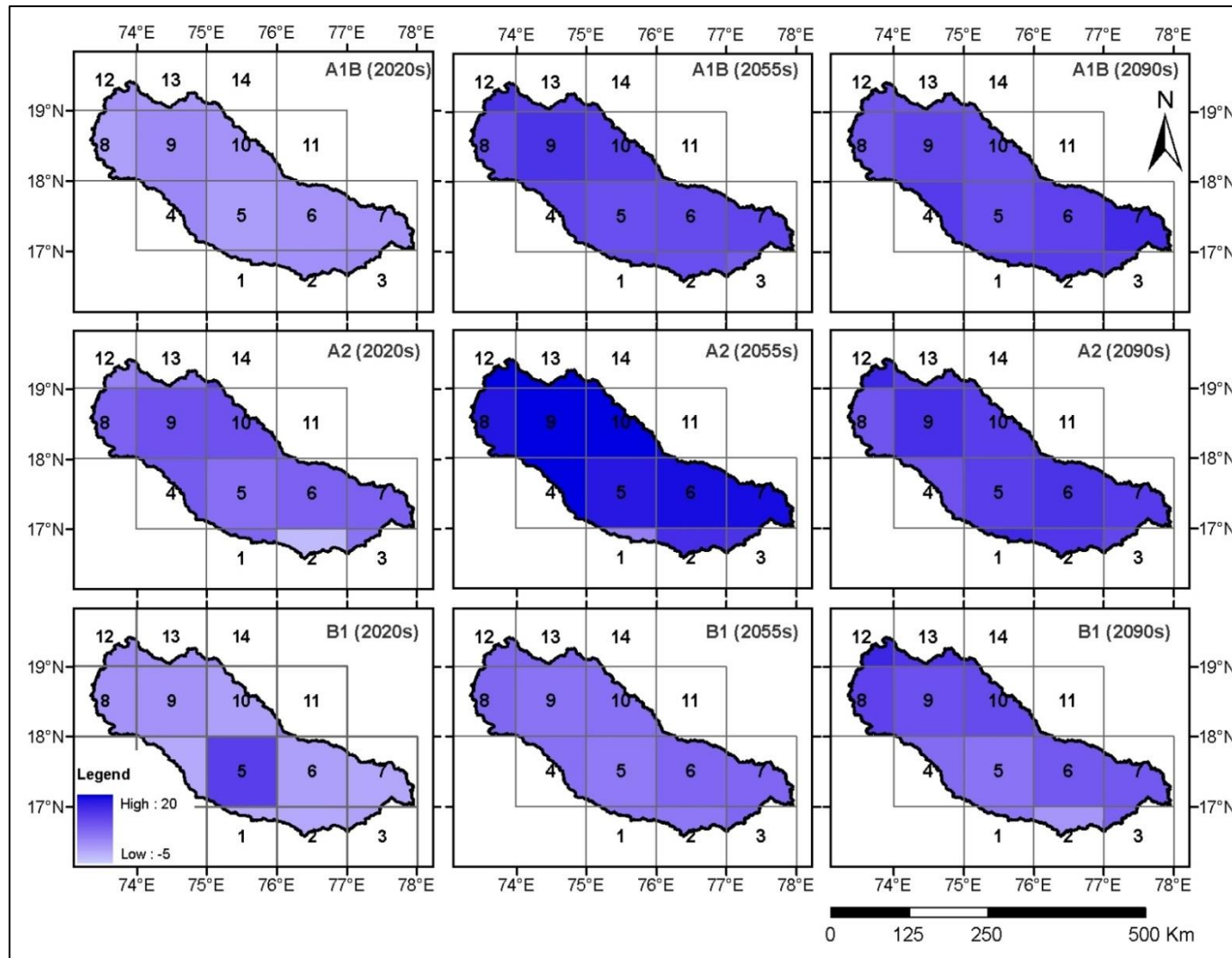
Figure 5.15 Spatial pattern of projected changes in annual rainfall for A1B, A2 and B1 during 2020s, 2055s and 2090s timespans

5.7 SUMMARY AND DISCUSSION

The main objective of this chapter was to assess the impact of climate change on meteorological variables in the Bhima basin. A weather generator LARS-WG was used to downscale and project the meteorological variables namely rainfall, minimum and maximum temperature considering three emission scenarios during three time spans. Major findings from the objective are summarized below:

5.7.1 Projected Changes in Temperature

i. The average minimum and maximum temperatures of all seasons show increasing trend in future with highest increase in A2 scenario and the lowest increase in B1 scenario.

ii. The highest/lowest increase in seasonal minimum and maximum temperatures was observed during winter/monsoon season as compared to the other seasons for all the scenarios and time spans.

iii. The analysis shows an agreement about the increase in annual minimum and annual maximum temperatures across the scenarios and time spans.

iv. High increase in annual minimum and maximum temperatures is predicted in A2 scenario followed by A1B and B1. All grids show similar pattern of increasing trend in annual minimum and maximum temperatures.

v. In general the time span of 2090s was associated with the highest CFs, followed by the 2055s and the 2020s.

vi. The spatial pattern of the CFs for annual minimum temperature indicates almost equal changes across all the grids, scenarios and time spans except for B1 scenario where minimum temperature increases in the central part of the basin in 2020s and then decreases in 2055s before stabilising in 2090s.

vii. The spatial pattern of the CFs for annual maximum temperature also indicates almost equal changes across the grids, scenarios and time spans. In general the time span of 2090s was associated with the highest CFs, followed by 2055s and the 2020s. A noticeable variation among the scenarios was observed for CFs during 2090s, with A2 scenario being the highest and B1 scenario being the lowest.

5.7.2 Projected Changes in Rainfall

i. In A1B and A2 scenarios, summer rainfall is expected to increase until mid-century and decrease. Whereas in B1 scenarios summer rainfall is projected to increase continuously from 2020s to 2055s.

ii. The monsoon rainfall is projected to increase in the basin in future ranging from -6% to +50% changes compare to the base period.

iii. Similar to the summer season, an increasing trend was observed in monsoon rainfall from 2020s to 2090s at all grids under B1 scenario. However, under A1B and A2 scenarios, the rainfall increased from 2020s to 2055s and decreased from 2055s to 2090s at all the grids.

iv. The spatial variability increases from 2020s to 2055s and then seems to have decreased from 2055s to 2090s. Among the scenarios, the A2 scenario seemed to project the highest percent change in the projected monsoon rainfall, followed by A1B scenario and A2 scenario.

v. The post-monsoon rainfall showed the highest percent change for A1B scenario in most of the grids. The averages of the percent change are 3.1, 14.5 and 16.8 during 2020s, 2055s and 2090s, respectively.

vi. The winter rainfall, which is less than 10% of the total rainfall in the basin, showed the maximum variation in the future rainfall pattern.

vii. Projections under A2 and B1 scenarios indicated a decrease in winter rainfall at most of the grids during 2020s and 2055s. The projections were found mostly positive under A1B scenario suggesting an increase in winter rainfall at most of the grids. During the time span 2090s, most of the scenarios are projecting an increase in the winter rainfall.

viii. The annual rainfall projections indicated -3.2 to +18.4% changes. Among the scenarios, highest increase was observed in A2 scenario followed by A1B scenario and B1 scenario.

ix. The spatial pattern of percent changes in annual rainfall across all grids of the basin confirms the increasing trend of rainfall across most grids from 2020s to 2090s for A1B and B1 scenarios and the increasing trend is not uniform for the grids. However, for A2 scenario, the rainfall seems to increase from 2020s to 2055s and then decreased from 2055s to 2090s across most of the grids.

x. Overall, an increase in annual rainfall was projected across the entire basin and the magnitude of percentage increase seems to be higher in the middle part of the basin.

All GCMs considered in this study shows agreement in future temperature rise in the Bhima basin, however, they show strong disagreement in sign and magnitude of future changes in rainfall of the basin. This is consistent with the projections of meteorological variables on global scales as well as on continental scale (Meehl et al., 2007b; Bastola, 2013). The range of CFs for temperature and rainfall of the Bhima basin is highest for A2 scenario and lowest for B1 scenario. This is also in agreement with many researchers findings around the world (Anadhi, 2010; Bastola, 2013). The projected rise in annual minimum and maximum temperatures of the Bhima basin (i.e. 1ºC to 4.5ºC approximately from 2020s to 2090s) is consistent with the findings reported in India's second national communication to United Nations Framework Convention on Climate Change in 2012 (Publication by Ministry of Environment and Forest, Government of India, New Delhi).

CHAPTER 6: CLIMATE CHANGE IMPACT ON STREAMFLOW

6.1 GENERAL

Hydrological modelling is a conceptual representation of natural phenomena that influence primarily the water and energy balances of a basin. The primary aim of hydrological modelling is to develop an understanding of the hydrological system in order to provide reliable information for managing water resources in a sustained manner. Its value lies in its ability, when correctly chosen and adjusted, to extract the maximum amount of information from the available data. Hydrologic models are simplified conceptual representations of a part of the hydrologic cycle. According to Singh (1988), the classification of hydrological models is given in figure 6.1.
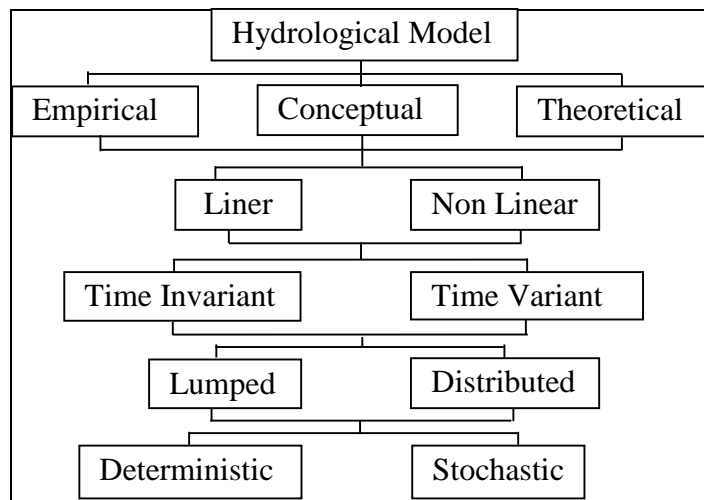
Figure 6.1 Classification of hydrological models

The hydrological models are broadly classified into deterministic and stochastic models. Stochastic models possess some inherent randomness. The same set of parameter values and initial conditions will lead to an ensemble of different outputs.
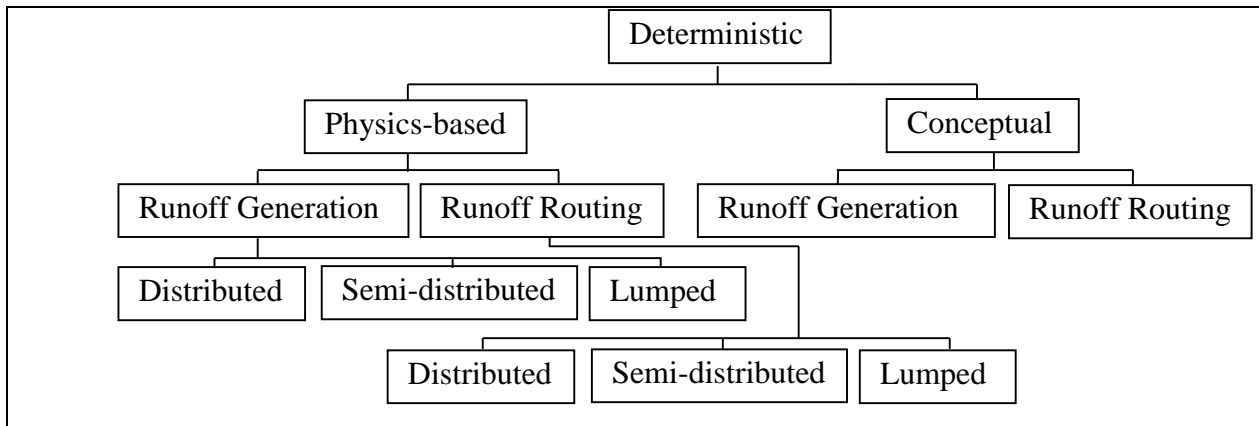
Figure 6.2 Classification of deterministic models

In deterministic models, the output of the model is fully determined by the parameter values and the initial conditions. As shown in figure 6.2 deterministic hydrological models are further classified into three categories: lumped, semi-distributed and distributed hydrological models (Cunderlik, 2003). The lumped model assesses the catchment response simply at the outlet without counting for individual sub-basins responses. These models do not characterize physical characteristic of the hydrologic processes. The semi-distributed model is partly permitted to change in space with division of catchment into an amount of sub-basins. It requires lesser amount of input data in contrast with the fully distributed model. The distributed model has its parameters permitted to change in place at a resolution normally chosen by the client. However it requires large amount of data for setup and parameterization (Arnold *et al*., 1998).

Models are increasingly used in hydrology to study changes in catchment management, to extend datasets and to evaluate the impacts of external influences (such as climate change and land cover change). HEC-HMS (Hydrologic Engineering Centre-Hydrologic Modelling System), Variable infiltration Capacity model (VIC), MIKE-SHE and SWAT (Soil and Water Assessment Tool) are some of the popular hydrological models.

6.1.1 Climate Change and Hydrological Models

To simulate the present climate and to predict future climate changes, GCMs have been developed. It demonstrates changes with coarser resolution at the continental and hemispheric spatial scales. The regional subgrid-scale characteristics and dynamics are not captured by GCMs due to its coarser resolution (Wigley *et al*., 1990; Carter *et al*., 1994). The mismatch

between GCMs and hydrological models is challenging problem in the field of climate change studies. Therefore macro-scale hydrological modelling approaches has been used for simulation of river flows in large river basins considering weaknesses in the representation of hydrological processes in GCMs.

A distributed model could be more appropriate than lumped model for a large basin. Distributed models are applied to analyse the hydrological response to possible landuse changes, while it is difficult to do so with the lumped models (Yao et al., 1998). In the past decade macro-scale hydrological models (MHMs) have been developed to model the land surface hydrologic dynamics of continental-scale river basin (Russell and Miller 1990; Kuhl and Miller 1992; Dümenil and Todini 1992; Liang et al., 1994, 1996; Miller et al., 1994; Sausen et al., 1994; Liston et al., 1994; Abdulla et al., 1996; Nijssen et al., 1997; Wood et al., 1997; Kite 1998; Yao and Terakawa, 1999; Yao and Hashino, 2001; Mishra et al., 2010). MHMs are closely related to the land surface parameterization schemes (LSPs) in general circulation models, but they focus more on modelling of runoff and streamflow and their interaction with other components in the land surface water budget. They can act as a link between global atmospheric models and water resource systems on large spatial scales (250-600 km) and long (seasonal to inter-annual) timescales (Hamlet and Lettenmaier, 1999).

6.1.2 Review on Impact of Climate Change on Hydrologic processes

Yao et al., 1995 proposed a step-wise regression method for predicting future climate change under the global warming. By using this regression, future climatic situation around 2030 was predicted for 2°C temperature rise, which shows that annual rainfall may increase by 1.4%, annual net radiation will decrease by 11.4%, average humidity will decrease by 8.5% and average wind speed will increase by 38.8%, compared to present (1980) level for Shrirakawatani basin in Western Tokushima, Japan. It was found that annual evapotranspiration in this basin would decrease by 11%, while annual runoff would increase by 4.8%.

Yao et al., 2005 used a Soil-Vegetation-Atmosphere Transfer (SVAT) model to simulate the effect of climate change on evapotranspiration of major crops in China. The model reflected dynamic connections of canopy temperature, leaf moisture potential and soil temperature to environmental factors.

Ghosh and Mujumdar (2008) focused on modelling GCM and scenario uncertainty using possibility theory in projecting streamflow of Mahanadi River, at Hirakud, India. A downscaling method based on fuzzy clustering and Relevance Vector Machine (RVM) was applied to project monsoon streamflow from three GCMs with two greenhouse emission scenarios. Possibilities are assigned to all the GCMs with scenarios based on their performance in modelling the streamflow of the recent past (1991 – 2005). The results show that the value of streamflow at which the cumulative distribution function (CDF) reaches 1 decrease with time. This indicates the reduction in probability of occurrence of extreme high flow events in future.

Yao *et al*., 2009 analysed the potential hydrological impacts of climate change on long-term water balances for Harp Lake and its catchment in Ontario by using monthly water balance analyses. Two climate change scenarios based on extrapolation of long-term trends of monthly temperature and precipitation from a 129-year data record, and another based on a Canadian GCM prediction was used. The first scenario with a warmer and wetter climate predicted a smaller magnitude of change than the second scenario. Ghosh *et al*., 2010 assessed the impact of global climate change on hydrology and water resources at river basin scales.

Raje and Mujumdar, 2010 studied the impact of climate change on a multipurpose reservoir performance and derived adaptive policies for possible future scenarios. Outputs from three GCMs for three emission scenarios (A1B, A2 and B1) were downscaled to simulate monsoon streamflow in the Mahanadi River for two future time slices, 2045–65 and 2075–95. Increased irrigation demands, rule curves dictated by increased need for flood storage and downscaled projections of streamflow from the ensemble of GCMs and scenarios were used for projecting future hydrologic scenarios.

Bhave *et al*., 2013 used high resolution (25 km) climatic projections from four RCMs and their ensemble based on the A1B emission scenario for the mid-21st century period to force the WEAP model to project the effect of three options: check dams, increasing forest cover and combined of both, on future (2021–2050) streamflow. All three adaptation options are reported to reduce the streamflow of Kangsabati river catchment in India

Meenu *et al*., 2013 used HEC-HMS 3.4 for the hydrological modelling of the Tunga-Bhadra river basin. Linear-regression-based Statistical Downscaling Model was used to downscale the daily maximum and minimum temperatures, and daily precipitation in four sub-basins using Hadley Centre Coupled Model version 3 for A2 and B2 scenarios in three future

periods: 2011–2040, 2041–2070, and 2071–2099. Results of the study suggested increasing precipitation and runoff and decreasing actual evapotranspiration over the sub-basins in the study area.

Wagesho *et al*., 2013 studied the possible impact of climate change on runoff generation at two agricultural watersheds in the Rift Valley Lakes Basin in Ethiopia. A statistical downscaling model was applied to downscale large-scale atmospheric variables into localized weather variables from the Bjerknes Center for Climate Research and Commonwealth Scientific and Industrial Research Organization (CSIRO) Mark (MK) 3.0 GCM outputs. SWAT model was used to simulate runoff for current and future climate scenarios. The simulated runoff varied from −4 to 18% and −4 and 14%, respectively in two watersheds.

Dhadwal *et al*., 2010 used VIC model to study the hydrology of Mahanadi river basin of India. An increase of 4.53% (3514.2 x 106 m^3) in the annual streamflow was found at the outlet from 1972 to 2003. This was attributed to decrease in forest cover by 5.71%.

Mishra *et al*., 2010a examined the relative effect of regional LULC patterns and future climate change on hydrologic processes. Past, present and future land cover data were used in the VIC model using observed meteorological forcing data for 1983 – 2007 over Wisconsin (USA). Downscaled and bias-corrected projected future climate forcing from three different GCMs namely HadCM3, PCM and GFDL was used as meteorological inputs to the model. Sensitivity analysis performed on a single grid cell show that the annual average surface runoff and baseflow were increased by 8 and 6 mm; respectively, while evapotranspiration was reduced by 15 mm when a fully forested grid was converted to cropland. Results also indicate that annual average net radiation and sensible heat flux were reduced considerably due to forest-to-cropland conversion, and the reduction was more prominent in winter and spring seasons due to effect of snow albedo.

Mishra *et al*., 2010b used VIC to identify regional-scale droughts and associated severity, areal extent, and temporal extent under historic and projected future climate using reconstructed soil moisture data and gridded climatology for the period 1916–2007 in the Midwestern United States. Results indicate that precipitation, minimum air temperature, total column soil moisture, and runoff have experienced upward trends, whereas maximum air temperature, frozen soil moisture, and snow water equivalent have experienced downward trends.

Mishra *et al*., 2011c applied VIC model with a physically based lake algorithm to simulate thermal conditions of lakes at regional scale during the open water period of 1916-2007 to study the impacts of climate variability and lake ice cover feedbacks on the seasonal thermal dynamics of inland lakes. Results suggested the climate warming may lead to increased rate of evaporation that is driven by feedbacks of ice cover and snow storage.

Frans *et al*., 2013 used VIC model to assess the hydrologic implications of climate and LULC changes between 1918 and 2007 in the Upper Mississippi River Basin (UMRB). At local scales, modelled annual runoff decreased (increased) by up to 9% (5%) where grasslands (forests) were replaced by croplands. It emphasized climate change as the dominant driver of runoff change in the UMRB.

6.2 OBJECTIVES

The explicit objectives of this chapter are given below:

i.   To calibrate and validate VIC model for the Bhima River basin
ii.   To simulate future streamflows under various emission scenarios for three time spans centred at 2020s, 2055s and 2090s using projected meteorological variables.
iii.   To analyse impact of future climate on streamflows in the Bhima River basin.

6.3 DESCRIPTION OF VIC MODEL

The first description of Variable Infiltration Capacity (VIC) model is found in Wood et al. (1992). They describe a method to generalize the bucket representation of land-surface hydrology based on a model that represents the variation in infiltration capacity within a GCM grid cell. They presents an alternative land-surface parameterization for GCMs that represents subgrid variability in infiltration capacity, a drainage term for interstorm runoff and a nonlinear evaporation term. They explored the model through direct observations and found VIC model runoff are in much more agreement to the observed flows.

Liang *et al.* (1994) described investigation of VIC model for incorporating land surface water and energy fluxes in GCM. VIC model which incorporates a two-layer description of the soil column is formulated for a fully coupled application within a GCM. The upper layer is characterized by the typical VIC spatially distributed scheme of soil moisture capacities, and the layer below is spatially lumped, and uses the Arno (Francini and Pacciani, 1991) drainage term.

The model partitions a grid cell into N+I land cover types; and for each land cover type the fraction of roots in the upper and lower soil is specified. Evaporation and transpiration are parameterized by a Penman- Monteith technique, applied separately to bare soil and vegetation classes. Evaporation from water intercepted by the vegetation is also represented. In addition, the model contains an energy-based snow accumulation and ablation parameterization.

Liang *et al*. (1996a) found that evaporation computed by two-layer Variable Infiltration Capacity (VIC-2L) model was less in comparison with the equilibrium results of weekly soil moisture measurements (one year data) due to low soil moisture availability in its upper soil layer. They described a modified version, with new feature to allow diffusion of moisture between soil layers, and a 0.1 m thin soil layer on top of the previous soil layers and LAI and fraction vegetation cover are allowed to vary at each time step. With these modifications the structural deficiencies in the earlier version of model are resolved.

Liang *et al*. (1996) incorporate a representation of sub-grid variability in precipitation into the VIC-2L model, using an analytical one-dimensional statistical dynamic representation for partial area coverage of precipitation. This allows the effect of sub-grid scale spatial variability of precipitation on surface fluxes, runoff production, and soil moisture to be represented explicitly. The approach gives better results than the pixel-based approach, and is superior to the uniform precipitation approach.

Wood *et al*. (1997) describes the development of VIC-2L model for simulation of continental-scale basins and inclusion of soil-vegetation-atmospheric-transfer (SVAT) land surface parameterization scheme in atmospheric general circulation models (AGCMs). Results from application of VIC model demonstrate the ability of the model to simulate hydrological fluxes for large continental-scale river basins.

Nijssen *et al*. (1997) described a grid network version of the VIC-2L macroscale hydrologic model to accurately predict monthly hydrographs for continental scale river basins. Annual runoff volumes as well as hydrograph shape were simulated with a considerable degree of accuracy, with mean annual runoff volumes predicted to within 11.8% for Columbia River (10 latitude-longitude spatial resolution) and 1.4% for the Delaware River (0.50 resolution) during the test. The model failed in the arid region for the Snake River apparently owing to the absence of an infiltration excess mechanism in the model as well as strong ground surface water interaction in the particular region.

113

Variable infiltration capacity model is designed to represent surface energy and hydrological fluxes and states at scales ranging from large river basins to the entire globe. It is a grid based semi distributed hydrological model which quantifies the dominant hydro-meteorological processes taking place at the interface of the land surface atmospheric. Typically grid resolution ranges from 1/8 to 2 degree. VIC computes the vertical energy and moisture flux in grid cells based on specification at each grid cell considering soil properties and vegetation coverage. Also it includes the representation of sub grid variability in soil infiltration capacity and all mosaic of vegetation classes in any grid cell. The resultant runoff and base flow is routed via a separate channel routing module to produce stream flow at a selected point within the model domain. A two layer model was modified to a three layer by adding one thin surface layer along with a canopy layer to achieve better representation of bare soil evaporation processes.

	RL - Long wave radiation,
	RS – Shortwave radiation,
	G – Ground heat flux,
	L – Latent heat flux,
	S – Sensible heat flux
	Q – Percolation,
	E - Evaporation from soil layer,
	Et – Evapotranspiration,
	Ec – Canopy interception Evapotranspiration,
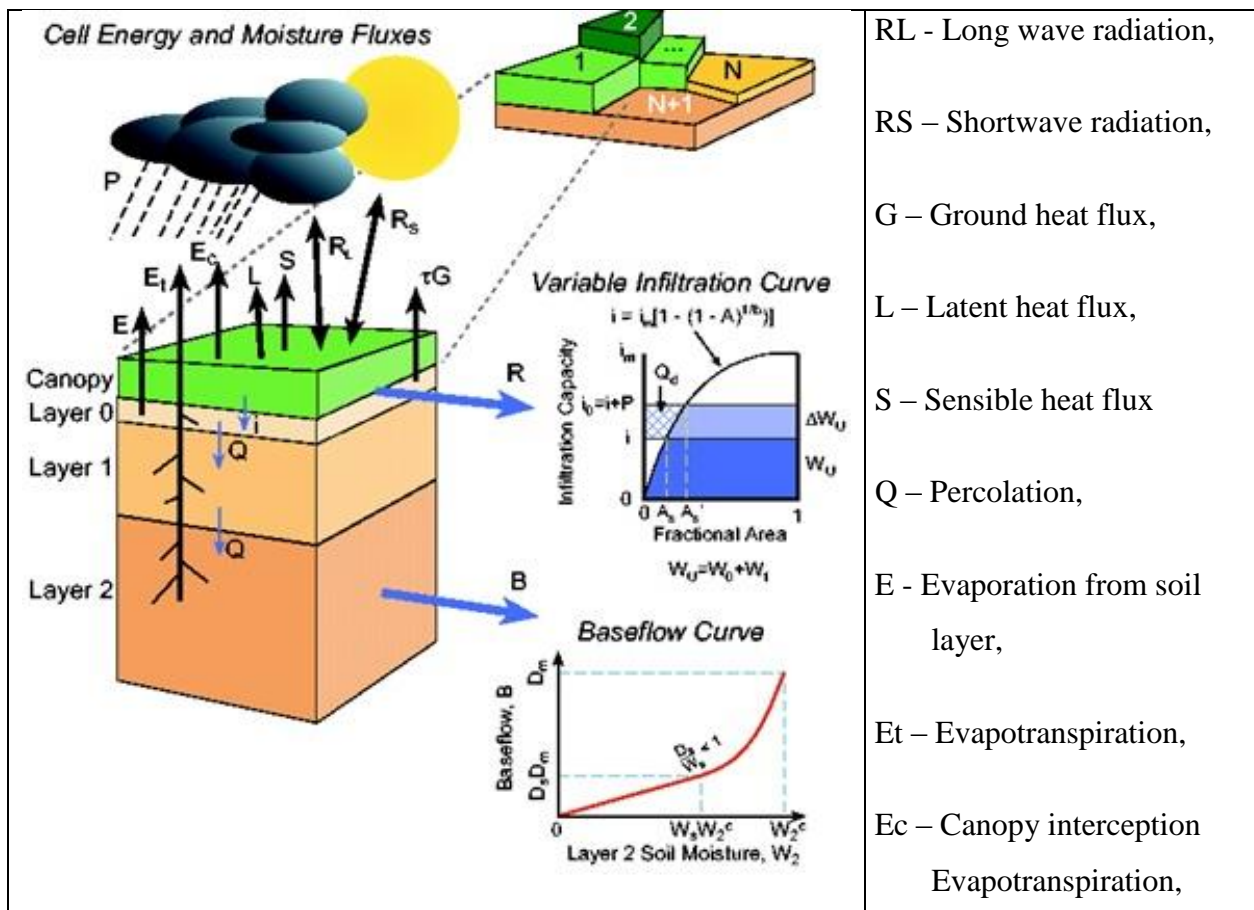
Figure 6.3 Schematic of the VIC-3L model with mosaic representation of vegetation coverage

(Source: www.hydro.washington.edu/Lettenmaier/Models/VIC/images/VIC_grid_cell_schematic.gif)

114

Figure 6.3 illustrates the schematic of the VIC model with a mosaic representation of vegetation coverage and three soil layers. The surface of each grid cell is described by N+1 land cover tiles, where n = 1, 2, … , N represents N different tiles of vegetation, and n = N+1 represents bare soil. For each vegetation tile, the vegetation characteristics, such as Leaf Area Index (LAI), albedo, minimum stomatal resistance, architectural resistance, roughness length, relative fraction of roots in each soil layer, and displacement length (in the case of LAI) are assigned. Evapotranspiration is calculated according to the Penman-Monteith equation, in which the evapotranspiration is a function of the net radiation and vapor pressure deficit. Total actual evapotranspiration is the sum of canopy evaporation and transpiration from each vegetation tile and bare soil evaporation from the bare soil tile, weighted by the coverage fraction for each surface cover class. Associated with each land cover type are a single canopy layer, and multiple soil layers. The canopy layer intercepts rainfall according to a Biosphere-Atmosphere Transfer Scheme (BATS) parameterization (Dickinson *et al*., 1986) as a function of LAI. The top two soil layers are designed to represent the dynamic response of soil to the infiltrated rainfall, with diffusion allowed from the middle layer to the upper layer when the middle layer is wetter. The bottom soil layer receives moisture from the middle layer through gravity drainage, which is regulated by a Brooks-Corey relationship (Brooks and Corey, 1988) for the unsaturated hydraulic conductivity. The bottom soil layer characterizes seasonal soil moisture behaviour and it responses to short-term rainfall only when the top soil layers are saturated. The runoff from the bottom soil layer is according to the drainage described by the Arno model (Franchini and Pacciani, 1991). Moisture can also be transported upward from the roots through evapotranspiration. Although vegetation subgrid-scale variability is a critical feature for the VIC model, the soil characteristics (such as soil texture, hydraulic conductivity, etc.) are held constant for each grid cell. In the model, soil moisture distribution, infiltration, drainage between soil layers, surface runoff, and subsurface runoff are all calculated for each land cover tile at each time step. Therefore for each grid cell, the total heat fluxes (latent heat, sensible heat, and ground heat), effective surface temperature, and the total surface and subsurface runoff are obtained by summing over all the land cover tiles weighted by fractional coverage.

6.3.1 Various Modes of VIC Model

6.3.1.1 Water balance

Water balance mode assumes that land surface temperature equals air temperature. Although it does not solve the full surface energy balance, exception is the snow algorithm that still solves the surface energy balance to determine the fluxes needed to drive accumulation and ablation processes. It requires comparatively less time for computation than other modes due to removal of the ground heat flux solution and iterative procedure needed to close the surface energy balance. The time step ranges from hourly to daily.

The daily water balance mode is significantly faster than sub-daily simulations. Parameters required for daily solutions are different from those used for sub-daily solutions. Although the daily water balance model can be used to simulate discharge from a basin, calibration parameters for the daily water balance model are unlikely to be transferable to any model run with a sub-daily time step. Usually daily water balance model experiences higher evaporation, resulting in lower soil moistures and base flows.

6.3.1.2 Energy balance

Full energy balance mode calculates all water and energy fluxes near the land surface, and run time step may be one or three hours. The surface energy balance is closed by an iterative process which tries to find a surface temperature which adjusts surface energy fluxes (sensible heat, ground heat, ground heat storage, outgoing long wave and indirect latent heat). Hence this mode requires more computational time than water balance as well as require sub-daily simulation time step. Finally this mode simulates the surface energy fluxes, which are important to understand the hydrologic cycle as well as land surface-atmosphere interactions in a basin. It has been proved that moisture fluxes generated from both energy balance and water balance modes are similar.

6.3.1.3 Frozen soil

Frozen soil affects on both moisture and energy fluxes. It solves thermal fluxes at nodes through the soil column using the finite difference method as well as it computes the maximum unfrozen water content at each soil node based on the nodal temperature. Also ice content for each soil moisture layer is computed from the nodal values and is used to restrict infiltration

116

and soil moisture drainage. In addition to that the nodal ice contents are also used to derive the soil thermal conductivity and volumetric heat capacity for the next model time step. It has been observed that frozen soil algorithm increases peak flows in the spring and decreases base flow in the winters.

6.3.2 VIC Model Components

6.3.2.1 Water balance

The water balance in the VIC model follows the continuous equation for each time-step

$$\frac{\partial S}{\partial t} = P - E - R \tag{6.1}$$

Where dS/dt, P, E, and R are the change of water storage, precipitation, evapotranspiration, and runoff, respectively. Within the time step, all units of above variables are mm. Over vegetated areas, the water balance equation in the canopy layer (interception) is

$$\frac{\partial W_i}{\partial t} = P - E_c - P_t \tag{6.2}$$

Where W_i is canopy intercepted water (mm), Ec is evaporation from canopy layer (mm), and Pt is throughfall (mm).

6.3.2.2 Evapotranspiration

Three types of evaporation which are evaporation from canopy layer of each vegetation class, transpiration from each vegetation class and evaporation from the bare soil are considered to calculate total evapotranspiration over a grid cell. Penman-Monteith formula given below is used to calculate the evapotranspiration for each class. Figure 6.4 represents the different energy components of VIC model.

$$\lambda_v E_p = \frac{\Delta(R_n - G) + \rho_a c_p (e_s - e_a) / r_a}{\Delta + \gamma} \tag{6.3}$$

where λv is the latent heat of vaporisation (J kg-1), Rn is the net radiation (W m-2), G is the soil heat flux (W m-2), (es - ea) represents the vapor pressure deficit of the air (Pa), ρa is the

117

density of air at constant pressure (kg m-3), cp is the specific heat of the air (J kg-1 K-1), Δ represents the slope of the saturation vapor pressure temperature relationship (Pa K-1), and γ is the psychrometric constant (66 Pa K-1).

6.3.2.3 Infiltration

This model assumes that infiltration capacity of the soil is not uniform. Hence runoff generation and evaporation vary within an area owing to variations in topography, soil and vegetation. It also considers that infiltration capacity is storage and not a rate. Sub-grid variability scheme in infiltration is used to account variable infiltration capacity. This uses a spatial probability distribution to represent variable infiltration capacity as a function of relative saturated area of the grid cell. VIC uses infiltration formula used in Xinanjang model which assumes that precipitation in excess of the available infiltration capacity forms surface runoff. Figure 6.4 shows the variable infiltration capacity curve.

Spatial variation of infiltration capacity is expressed as,

$$i = i_m \; [1-(1-A)^{1/bi}] \tag{6.4}$$

where, i = Infiltration capacity upto which the soil is filled, i_m = Maximum infiltration capacity, A = represents the saturated fraction of the grid cell ($0 = A = 1$), b_i = shape parameter.

6.3.2.4 Baseflow

The formulation of baseflow (sub surface runoff, Q_b), which used the Arno model formulation, (Franchini and Pacciani, 1991), is expressed as

$$Q_b = \begin{cases} \dfrac{D_S D_m}{W_S \theta_S} \cdot \theta_3, & 0 \le \theta_3 \le W_S \theta_S \\[4mm] \dfrac{D_S D_m}{W_S \theta_S} \cdot \theta_3 + (D_m - \dfrac{D_S D_m}{W_S})(\dfrac{\theta_3 - W_S \theta_S}{\theta_S - W_S \theta_S})^2, & \theta_3 \ge W_S \theta_S \end{cases} \tag{6.5}$$

where D_m is the maximum subsurface flow (mm d^{-1}), D_S is a fraction of D_m,, and W_S is the fraction of maximum soil moisture (soil porosity) θ_s, θ_3 is volumetric soil moisture content of soil layer 3. The base flow recession curve is linear below a threshold ($W_S\;\theta_s$) and nonlinear

above the threshold. The first derivative at the transition from the linear to nonlinear drainage is continuous.
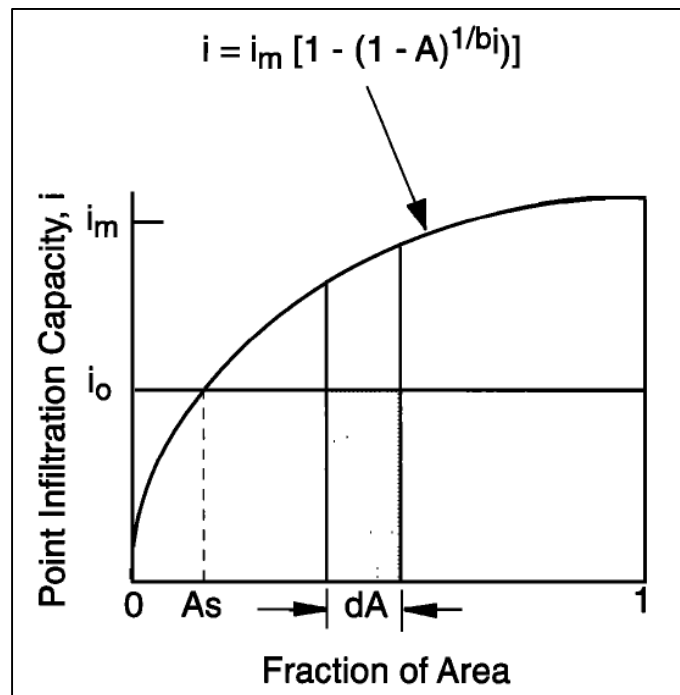
Figure 6.4 Variable Infiltration capacity curve (Source: Liang *et al.* 1994)

6.3.2.5 Vegetation Cover

In VIC each grid cell's land cover is divided into arbitrary number of "tiles", each corresponding to the fraction of the cell area covered by that land cover type. The surface of each grid cell is described by N+1 land cover tiles, where n = 1, 2, ... , N represents N different tiles of vegetation, and n = N+1 represents bare soil. For each vegetation tile, the vegetation characteristics, such as albedo, LAI, minimum stomatal resistance, displacement length (in the case of LAI) etc. are assigned. To get the total flux and storage with a cell, fluxes and storages are averaged together (weighted by area fraction) for writing to output file. Grid cell vegetation coverage is shown in figure 6.5.
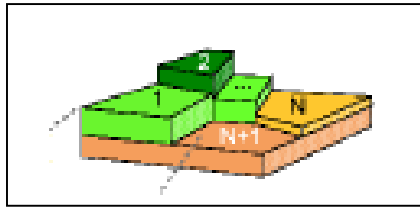
Figure 6.5 Grid cell vegetation coverage (Source: Liang *et al.* 1994)

6.3.2.6 Elevation Bands

VIC can consider spatial heterogeneity in precipitation, arising from either storm fronts/local convection or topographic heterogeneity. Here we consider the influence of topography, via elevation bands (Figure 6.6). Each grid cell is sub-divided into random no. of elevation bands, to account for difference of elevation within each grid cell. In each elevation band, meteorological forcing are lapsed from grid cell average elevation to band average elevation.
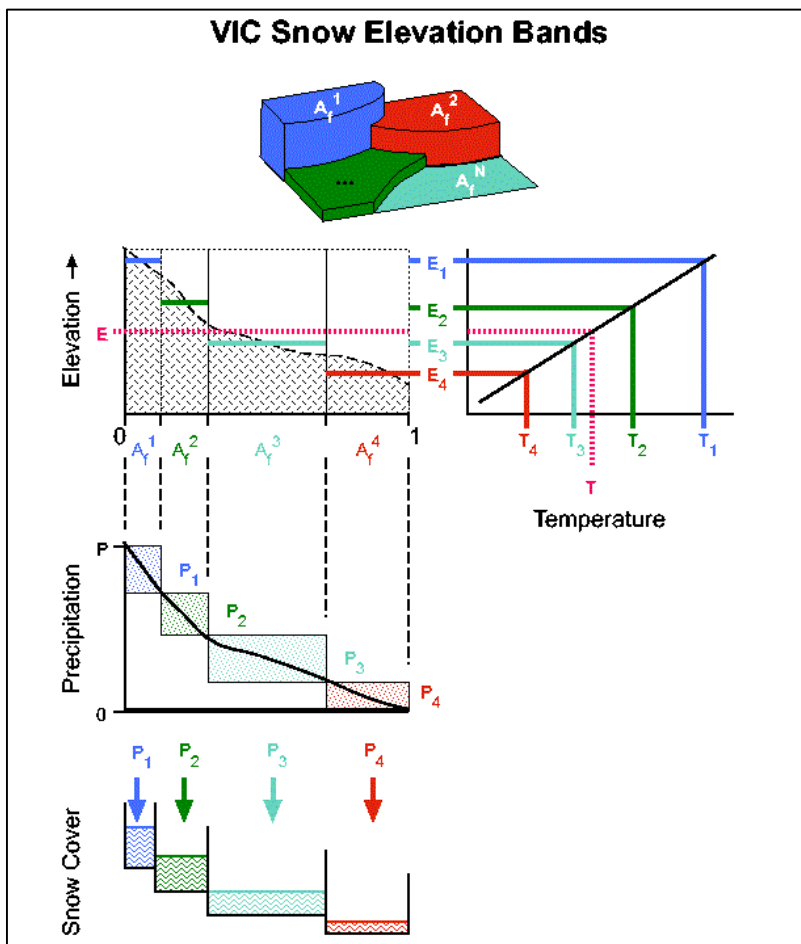
Figure 6.6 VIC snow elevation bands

(Source: www.hydro.washington.edu/Lettenmaier/Models/VIC/images/VIC_dist_prec_schematic.gif)

6.3.2.7 Distributed Rainfall

VIC model considers the sub-grid variability of rainfall which is distributed throughout all or a portion of grid cell as a function of rainfall intensity as shown in figure 6.7. Rainfall distribution is expressed as follows,

$$\mu = (1-e^{-aI}) \tag{6.6}$$

where, I = Rainfall intensity, a = coefficient which describes the effect of grid cell size and geography

Change in rainfall intensity of a storm changes the fractional coverage accordingly. When intensity increases, the fractional coverage over a grid cell increases and when decreased fractional coverage decreases. Before the occurrence of a storm the soil water content throughout the grid cell is set to average. However, forcing data plays an important role and accordingly simulation can be done hourly, 3 hourly, daily or monthly.
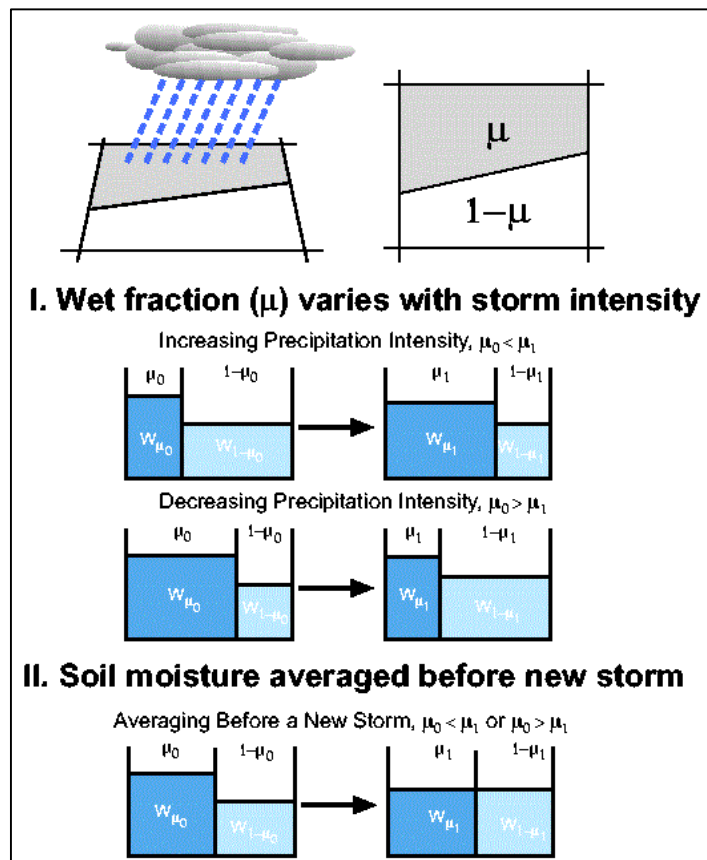
Figure 6.7 VIC distributed precipitation

(Source: www.hydro.washington.edu/Lettenmaier/Models/VIC/images/VIC_dist_prec_schematic.gif)

6.3.3 Routing Model

In the VIC model, each grid cell is modelled independently without horizontal water flow. The grid-based VIC model simulates the timeseries of runoff only for each grid cell, which is non-uniformly distributed within the cell. Therefore, a stand-alone routing model (Lohmann., *et al.*, 1996, 1998) is employed to transport grid cell surface runoff and baseflow to the outlet of that grid cell then into the river system. In the routing model, water is never allowed to flow from the channel back into the grid cell. Once it reaches the channel, it is no longer part of the water budget. Figure 6.8 shows the schematic of the routing model. A linear transfer function model characterized by its internal impulse response function is used to calculate the within-cell routing. Then by assuming all runoff exits a cell in a single flow direction, a channel routing based on the linearized Saint-Venant equation is used to simulate the discharge at the basin outlet.
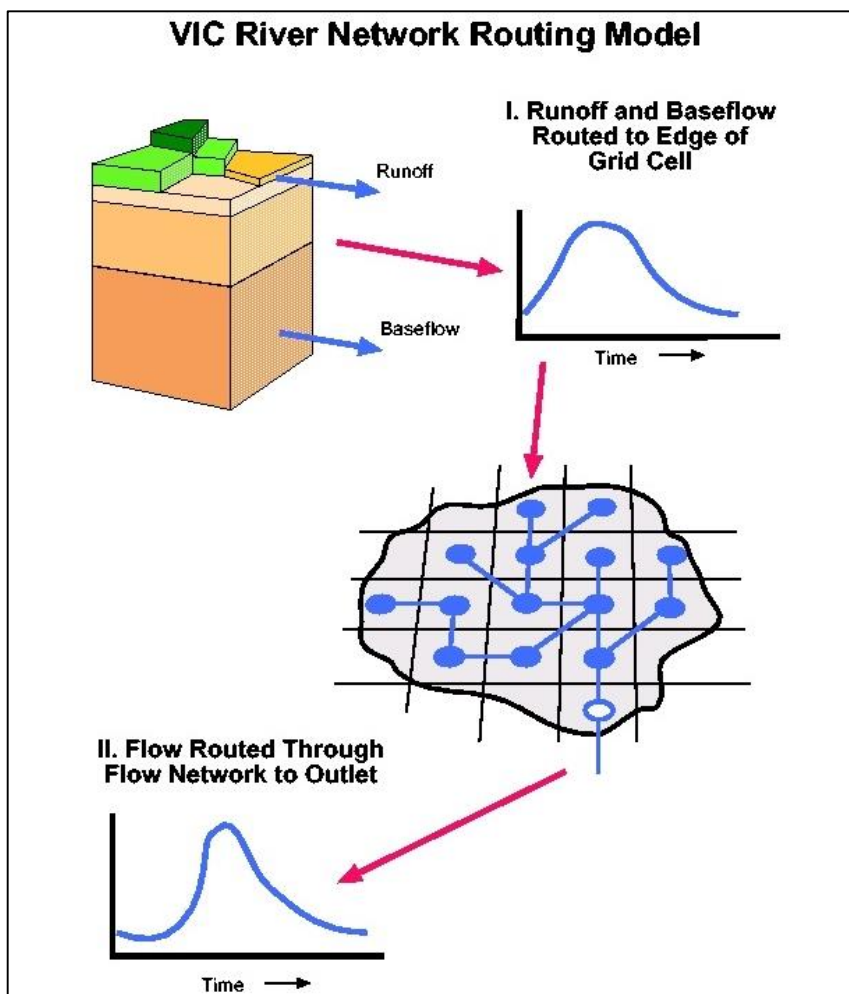
Figure 6.8 Schematic of VIC network routing model
(Source: www.hydro.washington.edu/Lettenmaier/Models/VIC/images/VIC_river_routing_model.gif)

The routing model is described in detail by Lohmann *et al*. (1996, 1998). It essentially calculates the concentration time for runoff reaching the outlet of a grid cell as well as the channel flow in the river network. It is assumed that most horizontal flow within the grid cell reaches the channel network within the grid cell before it crosses the border into a neighbouring grid cell. Flow can exit each grid cell in eight possible directions but all flow must exit in the same direction. The flow from each grid cell is weighted by the fraction of the grid cell that lies within the basin. Once water flows into the channel, it does not flow back out of the channel and therefore it is removed from the hydrological cycle of the grid cells. The daily surface runoff and baseflow produced by the VIC model from each grid cell is first transported to the outlet of the cell using a triangular unit hydrograph, and then routed to in the river network to the basin outlet.

Both parts of the routing scheme (within grid cell and river routing) are constructed as simple linear transfer functions. The routing model extends the FDTF-ERUHDIT (First Differenced Transfer Function-Excess Rainfall and Unit Hydrograph by a Deconvolution Iterative Technique) approach (Duband *et al*., 1993) with a time scale separation and a simple linear river routing model. The model assumes that the runoff transport is linear, causal, stable, and time invariant. It also assumes the impulse response function is never negative. The following summarizes the within grid and river network routing respectively according to the modelling algorithms cited from Lohmann *et al*., (1996; 1998).

6.3.3.1 Routing within a Grid Cell

To simulate the in-grid-dynamic of the horizontal routing process, one first separates the fast and slow components of the measured discharge with the linear model described in Duband *et al*., (1993).

$$\frac{dQ^S(t)}{dt} = -k \cdot Q^S(t) + b \cdot Q^F(t)$$

(6.7)

where $Q^S(t)$ is the slow flow, $Q^F(t)$ is the fast flow, and $Q(t)$ is the total flow with $Q(t) = Q^S(t) + Q^F(t)$.

For each river basin, the parameters b and k are assumed to be constant over the period of calculation. The ratio of b over k represents the ratio of water in the slow flow over water in the fast flow. The fast and slow components are analytically connected by:

$$Q^S(t) = b \int_0^t \exp(-k(t-\tau)) Q^F(\tau) d\tau + Q^S(0) \exp(-kt)$$

(6.8)

6.3.3.2 River Routing

The linearized Saint-Venant equation is used in simple linear river routing model to model the transport of water in channels. The model assumes that water is transported out of the grid box only in the form of river flow. The linearized Saint-Venant equation, where C and D are parameters denote wave velocity and diffusivity, respectively, as follows:

$$\frac{\partial Q}{\partial t} = D \frac{\partial^2 Q}{\partial x^2} - C \frac{\partial Q}{\partial x}$$

(6.9)

Either from measurements or by estimation from geographical data of the river bed, C and D are regarded as effective parameters since there are often times more than one river in one grid cell. This way each grid cell ultimately ends up with one C and one D value, which characterize the water transport within the cell.

The Saint-Venant equation is solved with convolution integrals

$$Q(x,t) = \int_0^t U(t-s) h(x,s) ds$$

(6.10)

where

$$h(x,t) = \frac{x}{2t\sqrt{\pi D}} \exp\left(-\frac{(Ct-x)^2}{4Dt}\right)$$

(6.11)

is the impulse response function of the Saint-Venant equation with h(x,0)=0 when x>0 and h(0,t)=δ(t) for t≥0. Because this solution scheme is linear and numerically stable, the influence from human activities (e.g., dams, irrigation water use) can be easily implemented in each node.

6.4 METHODOLOGY

For the calibration and validation of VIC model, the model was setup with past data. The past meteorological data and parameter files were supplied to the model and the model was calibrated and validated with trial and error method. The file preparation and data used for VIC and routing model are described in section 6.6 and 6.7.

The flowcharts of the methodology adopted for modelling of hydrological components and study of impact of climate change on streamflows of the basin is given in figure 6.9 and step-wise methodology is described in subsequent sections.

To study impact of future climate change on streamflows the projected daily rainfall and temperature (maximum and minimum) from 15 GCMs ensemble is used as explained in chapter 5. The validated VIC model was run with these meteorological data for the projection of future streamflows.

6.4.1 VIC model calibration using soil parameters

In any hydrological model, values of few model parameters are unknown and are not measurable. The value of these parameters are obtained by running the model with an initial value and adjusted by comparing the predicted discharge with observed data until it reaches the best fit. These values are called calibrated values and these variables are called calibrated parameters. The calibrated values are selected based on Nash-Sutcliffe Efficiency (NSE), Percent bias (PBIAS) and ratio of root mean square error to the standard deviation of measured data (RSR).
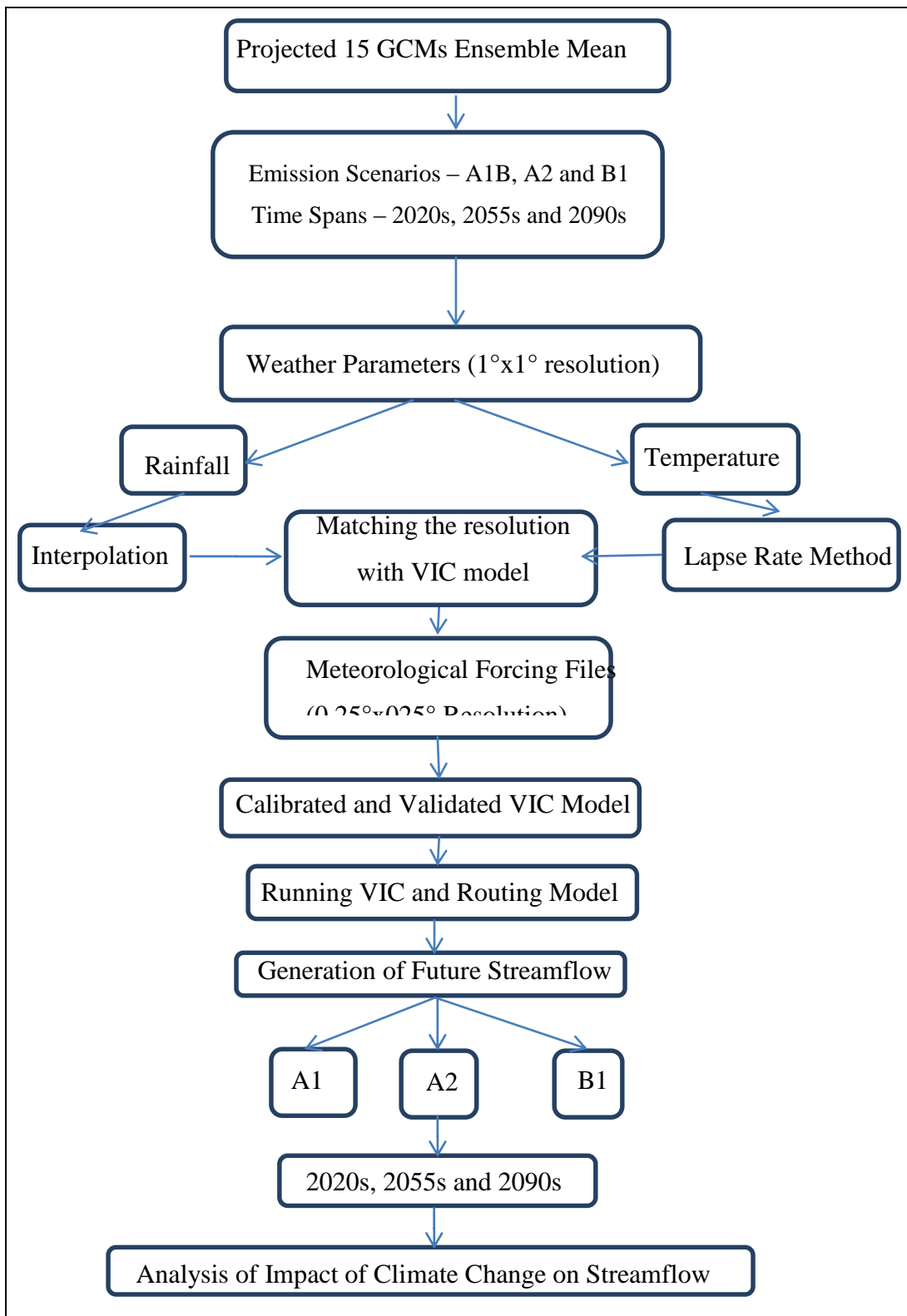
Figure 6.9 Flow chart of methodology to study impact of climate change on streamflows

Yuan, 2004 reported that the following six model parameters of the VIC -3L model need to be calibrated because they cannot be determined well based on the available soil information:

i. Ds_{max} (>0 to ~30): This is the maximum baseflow that can occur from the lowest soil layer (in mm/day). It depends on hydraulic conductivity.

ii. Ds (>0 to 1): This is the fraction of Ds_{max} where non-linear (rapidly increasing) baseflow begins. With a higher value of Ds, the baseflow will be higher at lower water content in the lowest soil layer.

iii. Ws (>0 to 1): This is the fraction of the maximum soil moisture (of the lowest soil layer) where non-linear baseflow occurs. This is analogous to Ds. A higher value of Ws will raise the water content required for rapidly increasing, non-linear baseflow, which will tend to delay runoff peaks.

iv. b_i (>0 to ~0.4): This parameter defines the shape of the Variable Infiltration Capacity curve. It describes the amount of available infiltration capacity as a function of relative saturated grid cell area. A higher value of b_i gives lower infiltration and yields higher surface runoff.

v. Soil Depth (of each layer) (typically 0.1 to 1.5 meters): Soil depth affects many model variables. In general, for runoff considerations, thicker soil depths slow down (baseflow dominated) seasonal peak flows and increase the loss due to evapotranspiration. The maximum soil moisture storage capacity is dynamically determined by the change of soil thickness. The thicker the soil depths are (resulting in more soil moisture stored in the soil layers), the less runoff is generated.

6.4.2 Model efficiency

Three criteria vz.: Nash-Sutcliffe efficiency (NSE), Percent bias (PBIAS) and Ratio of the root mean square error to the standard deviation of measured data (RSR) were selected for evaluating the model calibration (Moriasi *et al*., 2007).

(i) Nash-Sutcliffe efficiency

The Nash-Sutcliffe efficiency (NSE) is the ratio of residual variance to measured data variances (Nash and Sutcliffe, 1970). The Nash-Sutcliffe is computed using equation

$$NSE = 1 - \left[\frac{\sum\limits_{i=1}^{n} (x_i^{obs} - x_i^{sim})^2}{\sum\limits_{i=1}^{n} (x_i^{obs} - x_{mean}^{obs})^2} \right]$$

(6.12)

Where x_i^{obs} = i^{th} observation value of streamflow, x_i^{sim} = i^{th} simulated value streamflow, x_{mean}^{obs} = mean of observed streamflow, n = total number of observations

(ii) Percent bias efficiency

The Percent bias (PBIAS) measures the average tendency of the simulated data to be smaller or larger than their observed counterparts (Gupta *et al*., 1999). The PBIAS is calculated using equation (6.20). The optimal value of PBIAS is 0.0, with low-magnitude values indicating accurate model simulation. Positive values indicate model underestimation, and negative values indicate model overestimation (Gupta *et al*., 1999).

$$RE = \left[\frac{\sum\limits_{i=1}^{n} (x_i^{obs} - x_i^{sim})}{\sum\limits_{i=1}^{n} (x_i^{obs})} \right] *100$$

(6.13)

(iii) Root mean square error

The ratio of root mean square error to the standard deviation of measured data (RSR) is calculated as the ratio of the Root Mean Square Error (RMSE) and standard deviation of the observed data (Moriasi *et al*., 2007), as shown in equation below:

$$RSR = \frac{RMSE}{STDEV_{obs}} = \left[\frac{\sqrt{\sum\limits_{i=1}^{n} (x_i^{obs} - x_i^{sim})^2}}{\sqrt{\sum\limits_{i=1}^{n} (x_i^{obs} - x_{mean}^{obs})^2}} \right]$$

(6.14)

Graphical technique was also used for evaluation of model performance. Graphical

128

techniques provide a visual comparison of simulated and measured data and a first overview of model performance (ASCE, 1993). A hydrograph is a time series plot of predicted and measured flows throughout the calibration and validation periods. Hydrograph helps to identify model bias (ASCE, 1993) and can identify differences in timing and magnitude of peak flows and the shape of recession curves.

6.4.3 Basin Boundary Delineation and Grid Generation

To delineate the basin boundary ArcSWAT extension was used in ArcGIS 10.1. Basin delineation was done using SRTM DEM for the station Yadgir for which observed streamflow data were available (Figure 6.10).

In order to capture the effects of topography, soil and land use, a grid resolution of 0.25°x0.25° was selected for the VIC model to simulate micro-scale processes that play key role in the overall water budget. A square grid mesh of resolution 0.25°x0.25° was created covering the Bhima basin boundaries. As a result, a total of 124 grids were generated as seen in figure 6.10.
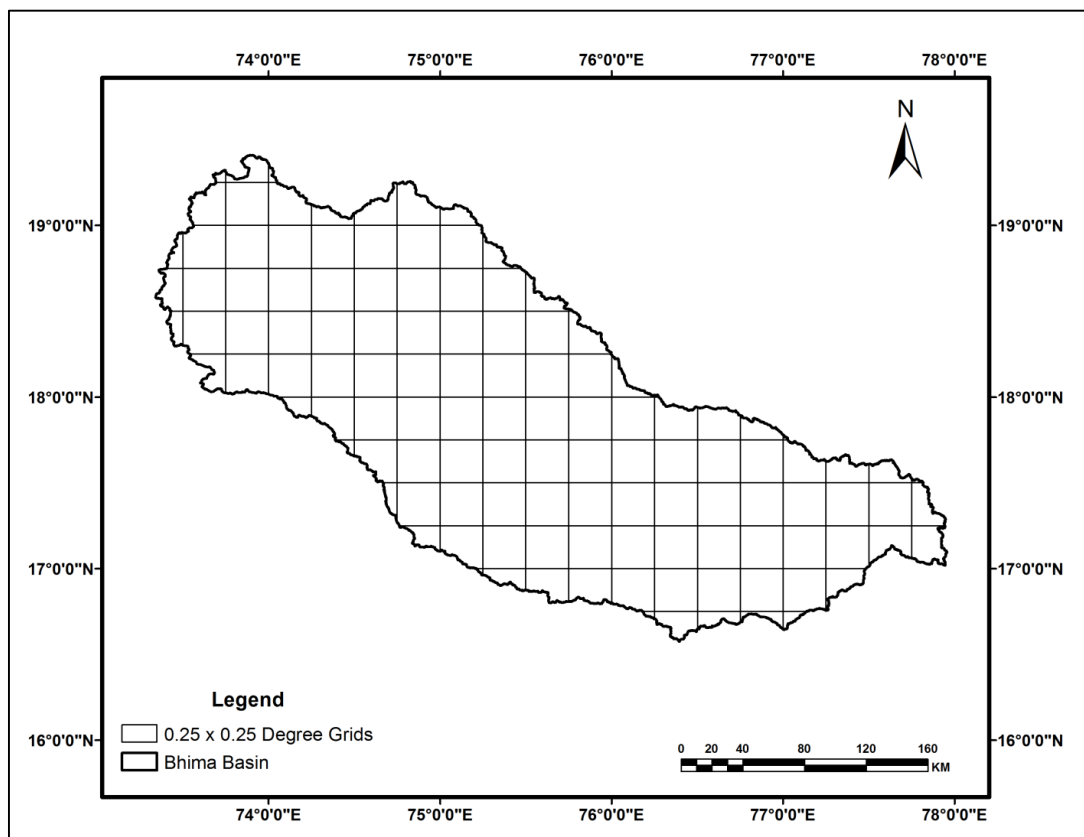
Figure 6.10 Grid mesh used in VIC model (0.25°x 0.25° resolutions) in the Bhima basin

6.5 Data used and Input file preparation for VIC model

The VIC model input database contains five major input files: soil parameter file, vegetation library file, vegetation parameter file, elevation band file and forcing files. Besides, a global parameter file is used to control the model run. These are described in subsequent sections.

6.5.1 Global parameter file

This is the main control file of the model. It contains all the necessary information and settings to run VIC model like name, path and format of input and output files, run time options, start and end date of simulation, number of soil layers, number of nodes, time step, mode of operation, soil temperature parameters, precipitation parameters, turbulent flux parameters, meteorological forcing disaggregation parameters, forcing files and parameters, land surface file parameter, output file parameter, miscellaneous parameters etc.

Global control file was created for the basin. The start and end dates of the model run were set as required during various analysis phases. The number of soil layers and number of soil thermal nodes were set to 3. VEGPARAM_LAI was set to true as monthly LAI for each vegetation class per grid was provided in vegetation parameter file.

6.5.2 Soil parameter file

The basic grid information like grid cell number, latitude-longitude of the grids (which serves as a link to other parameter files) etc. are defined in the soil parameter file. It describes the characteristics of each soil layer for each grid cell. The different soil hydrologic and thermal properties needed for VIC model are also provided in the same file. The initial soil moisture conditions are defined to be used in the absence of an initial state file.

The digital soil map of the world (1:5000000 scale) prepared by FAO (http://www.fao.org) was used to extract the soil information for the Bhima basin. Soil map of the Bhima basin is shown in figure 6.11. Detailed soil class information was taken from the site http://www.fao.org/ag/agl/agll/key2soil.stm. VIC mesh was overlaid on FAO Global soil layer to know the dominant soil class in each grid. Soil hydraulic properties index defined in VIC documentation (http://www.hydro.washington.edu) was used for deriving soil properties of various soil types found in the Basin.
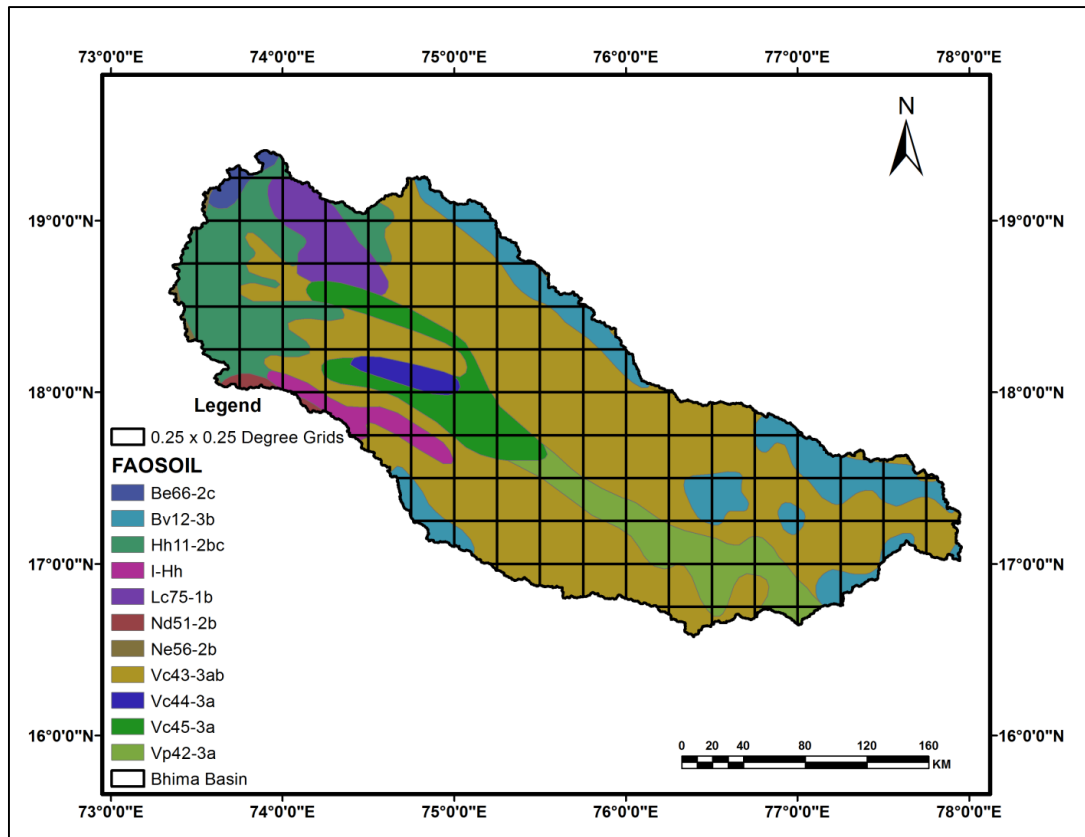
Figure 6.11 Soil map of the Bhima basin

6.5.3 Vegetation library file

In vegetation library file class identification number, architectural resistance, minimum stomatal resistance, LAI, albedo, vegetation roughness length, vegetation displacement height, height at which wind is measured, radiation attenuation factor etc. are defined . LAI and albedo for each class in 12 months are provided in this file. LAI is defined as the one-sided green leaf area per unit ground surface area in broadleaf canopies. Albedo is defined as the ratio of upwelling to downwelling radiative flux at the surface. LAI and albedo for each class was extracted from MODIS 15A02 and MOD 43B3 products, respectively for the year 2007.

The 8 daily data were downloaded from NASA's Goddard Space Flight Centre website (http://modis-land.gsfc.nasa.gov) for year 2007. Each weekly file was projected to UTM projection system (UTM zone 43) and then multiplied with correction factor (0.1 for LAI and 0.001 for albedo) to get 8 daily LAI and albedo files. Multiple files obtained so were mosaicked to cover the entire Bhima basin. These 8 daily files were than averaged to get monthly LAI and albedo values. Average value of LAI and albedo for each month are shown in figure 6.12 and figure 6.13, respectively.

131

For derivation of other variables like roughness length, displacement height, overstory, architectural resistance, minimum stomatal resistance LDAS 8th database (http://ldas.gsfc.nasa.gov/LDAS8th/MAPPED.VEG/web.veg.monthly. table. html) was used.
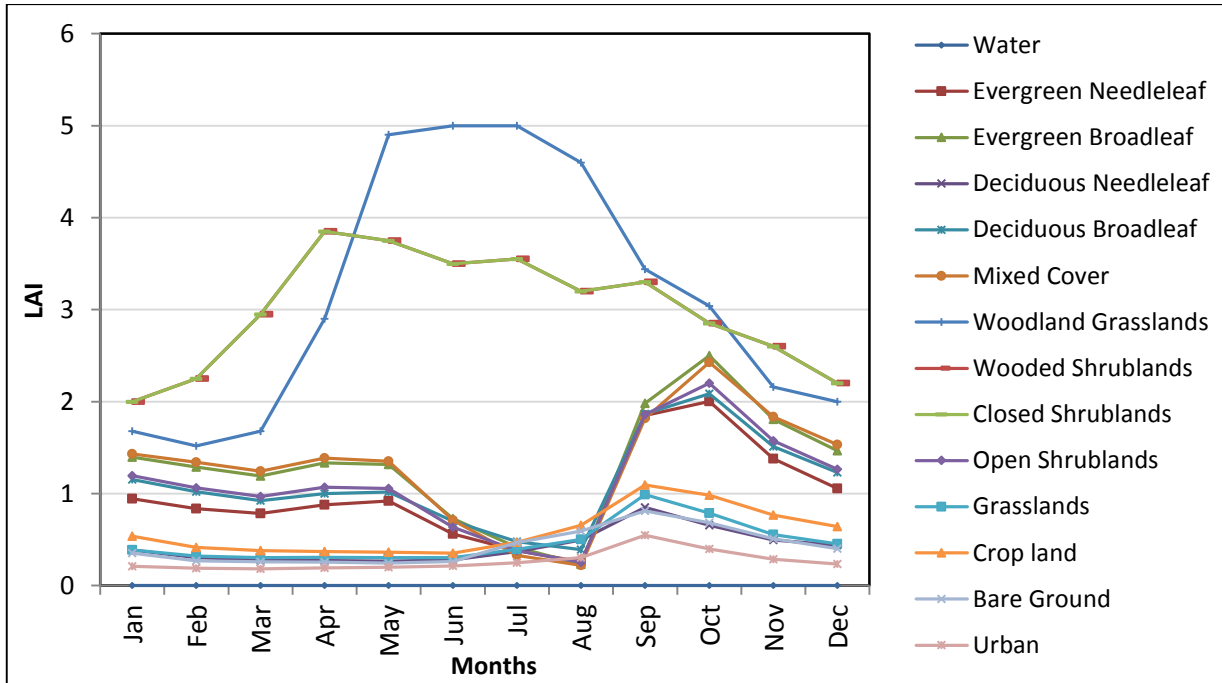
Figure 6.12 Monthly LAI data for various vegetation types in Bhima basin.
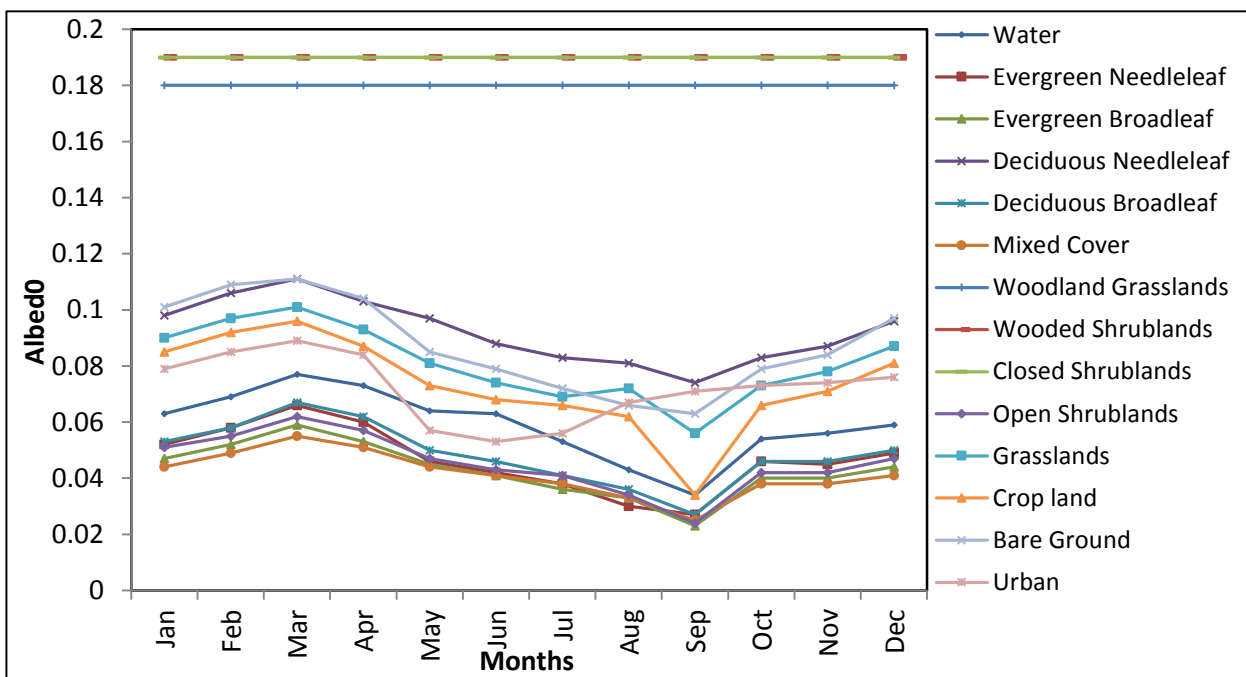
Figure 6.13 Monthly albedo data for various vegetation types in Bhima basin

6.5.4 Vegetation parameter file

The vegetation parameter file describes the vegetative composition of each grid cell. This file cross-indexes each vegetation class (from any land-cover classification scheme) to the classes listed in the vegetation library file.

A global landcover map (GlobCover 2009) developed by European Space Agency (ESA) was used for obtaining landuse/landcover information. GlobCover 2009 was downloaded from the website http://due.esrin.esa.int/globcover/ and extracted within the boundaries of the Bhima basin. The land use/land cover map of the basin is shown in figure 6.14.
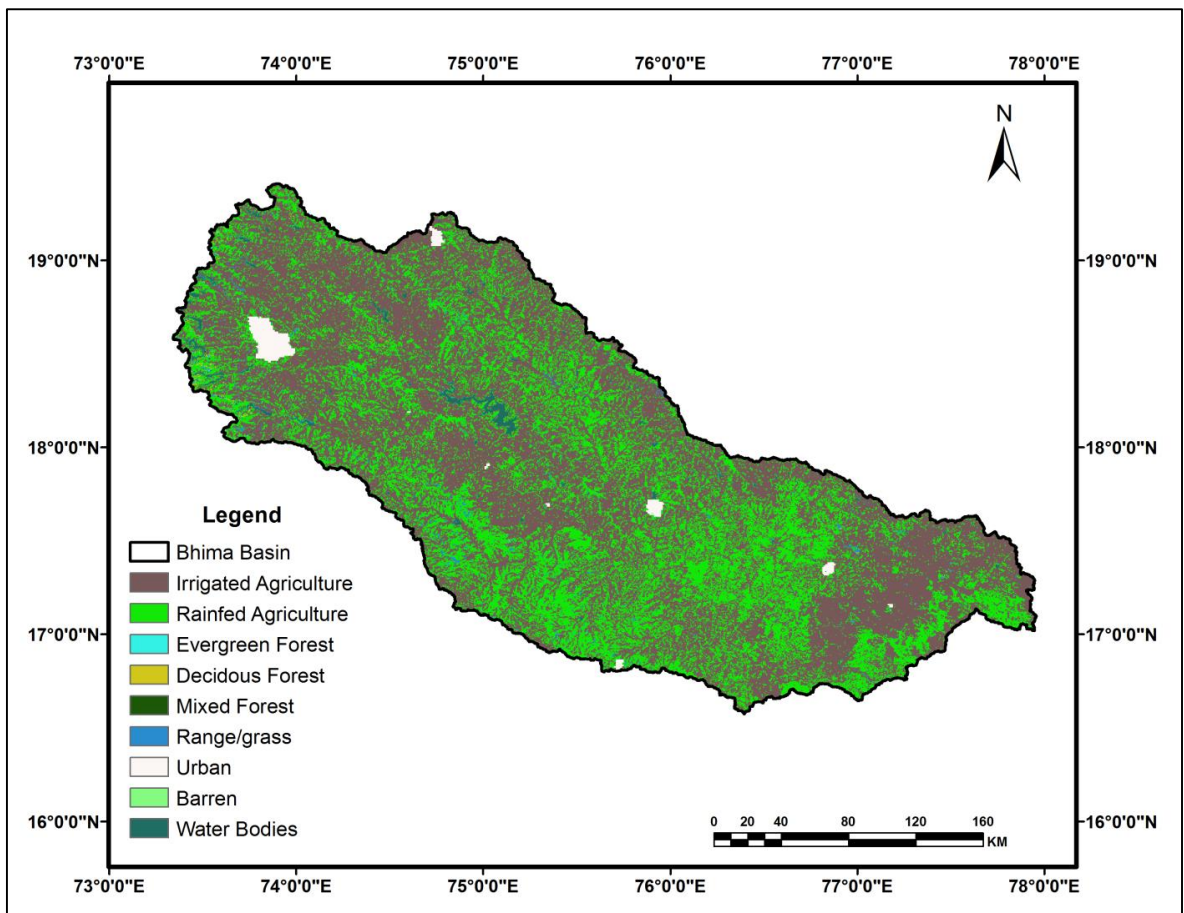
Figure 6.14 LULC map of the Bhima basin

A C++ program was used to read number of vegetation classes in each grid, the relative fraction of each vegetation class in that grid and corresponding monthly LAI value of each vegetation class in the vegetation parameter file.

6.5.5 Elevation band parameter file.

This file contains information needed to define the properties of each elevation band. Elevation range of each grid is divided into number of bands to better simulate the effect of elevation on snow pack accumulation and ablation and distributed precipitation to improve the model's performance in areas with pronounced topography, especially mountainous regions. Mean elevation of each band is used to lapse the grid cell average temperature, precipitation, & pressure to account for local estimate.

The SRTM DEM data was downloaded from the URL http://srtm.csi.cgiar.org/. DEM map of the basin is shown in figure 6.15. SRTM DEM has a spatial resolution of 3 seconds (90m) whereas the grid size is 0.25 degree. Hence, a C++ program was used to read elevation data from the DEM file matching to a particular grid to compute fractional area and average elevation in five bands within the grid. Finally this data was stored in the elevband file of the basin.
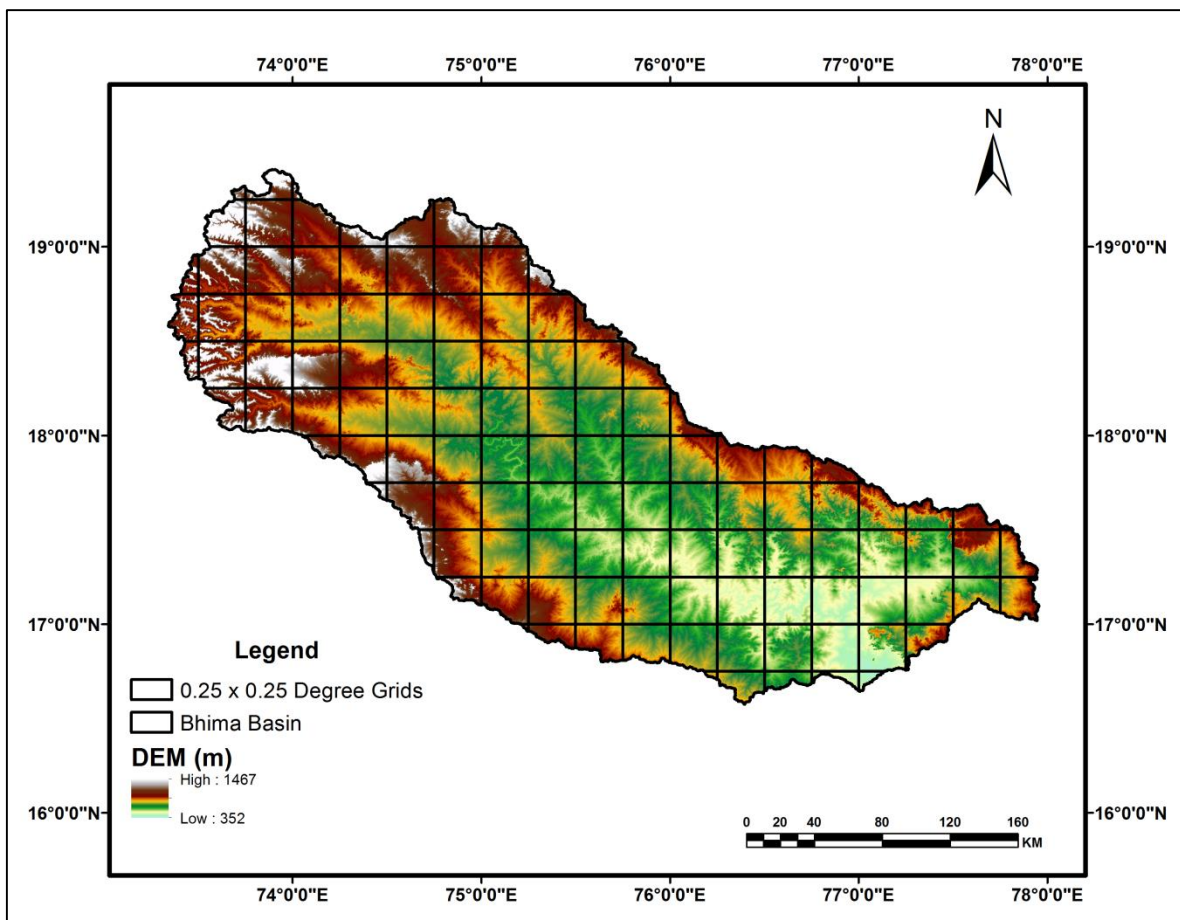
Figure 6.15 Elevation map of the Bhima basin

6.5.6 Meteorological forcing file

The meteorological forcing file contains meteorological inputs viz.: daily rainfall (mm), daily minimum and maximum temperatures (°C). VIC model requires one forcing file for each grid having n*365 rows (indicating days in n year) and 3 columns (for rainfall, minimum and maximum temperatures data) in ASCII format.

6.6.6.1 Past gridded rainfall and temperature data

Daily gridded rainfall data product 'Monsoon Asia APHRO_MA_V1101' available at 0.25°x0.25° resolution were downloaded from APHRODITE's (Yatagai *et al.*, 2012) (http://www.chikyu.ac.jp/precip/ index.html). The gridded daily rainfall data for all grids covering the entire Bhima basin were extracted from this dataset starting from 1971 to 1980.

The description of temperature data used in VIC model is given in the section 3.4 of the chapter 3. Temperature data of 1°x1° resolution was extracted for 14 grids of basin. SRTM 90 m elevation data within the basin boundary were resampled at 1°x1° and 0.25°x0.25° resolutions. Lapse rate method which assumes that the temperature varies with the elevation in the lower atmosphere was used to compute the temperature at 0.25°x0.25° resolutions. Equation 6.12 was used to generate 0.25°x0.25° resolution temperature data.

$$T_{Grid} = T_{Nearest\ point} + 6.5/1000*(Elevation_{Nearest\ point} - Elevation_{Grid}) \quad\quad\quad (6.12)$$

6.6.6.2 Future gridded rainfall and temperature data

The ensemble mean of daily projected meteorological varaibles from 15 GCMs outputs were used to prepare the inputs file for VIC model under different emission scenarios and time spans. Projected rainfall and tempearures data were at 1°x1° resolution. Since, VIC model was set up to run at 0.25°x0.25° resolution, the rainfall and temperature inputs were transformed to the VIC resolution using IDW interpolation method for rainfall and and the lapse rate techniques for the temperature data as described in the previous section.

6.6 Input File Preparation for Routing Model

Routing model requires flow directional, area fraction, station location and VIC output files as the inputs. The 90 m SRTM was used to prepare the flow directional and area fraction files.

6.6.1 Flow direction file

The flow direction file guides the routing model how all of the grid cells are connected in the routing network. The format is an arc/info ASCII grid. Table 6.1 shows direction conversion between Arc GIS and VIC model.

<div align="center">Table 6.1 Flow Directions in Arc GIS and VIC</div>

Arc GIS Direction	Direction	VIC Flow Direction
1	East	3
2	South East	4
4	South	5
8	South West	6
16	West	7
32	North West	8
64	North	1
128	North East	2

6.6.2 Fraction file

The fraction file is gridded information about the fraction of each grid cell that flows into the basin being routed. This allows the user to more accurately define the basin area, since edge cells can contribute more or less than 100% of their runoff and baseflow components to the basin. The format is an arc/info ASCII grid. Accordingly, the fractional file for the Bhima basin was prepared using Arc GIS.

6.6.3 Station Location File

This file contains the location of the grid cells produce output flow data. This file contained information only about one location referring to the Yadgir station.

6.7 Results and Discussion

The discharge data of the Bhima River was downloaded for Yadgir station from India-WRIS (http://www.india-wris.nrsc.gov.in) portal during 1970 to 2006. The India-WRIS web portal is a joint venture of the Central Water Commission (CWC), Ministry of Water Resources, and

Government of India to provide water resources data in India. It includes data on gauge discharge, silt and water quality parameters as recorded by CWC hydrometeorological Stations from 1965.

The VIC model was used to model hydrological components of the basin. Model was calibrated and validated for streamflows at the outlet (Yadgir) using observed data. After satisfactory calibration and validation, the climate change impacts on streamflows were analysed for the emission scenarios A1B, A2 and B1 in near century i.e. 2020s, in mid-century i.e 2055s and in end century i.e. 2090s.

Future streamflow were simulated using the future rainfall and temperature (minimum and maximum) data ensemble from 15 GCMs. Only the forcing data were changed in these simulations and the vegetation and soil parameters were kept same. The effects of climate change on streamflow of the basin were studied by comparing the model outputs with the observed data subsequent section presents the results of model calibration and impact analysis.

6.7.1 Calibration and Validation of VIC model

Calibration of VIC model was done using trial and error method for the Yadgir station of the Bhima basin. VIC model has six calibration parameters namely b_{infilt}, Ds, Dsmax, Ws, d2 and d3. Initial values of bi, Ds, Dsmax, Ws, d2 and d3 were 0.1, 0.1082, 0, 22.3, 1 and 0.2183 respectively. The major variation of streamflow was due to the change in the following three parameters: b_{infilt}, d2 and d3, hence calibration was performed only for these parameters. For the study period 1972-2007, the two years 1970 and 1971 were considered as the warming period for the model. Then the streamflow data during 1972-1976 (5 years) was selected as the calibration period and 1977-1980 (4 years) was selected as the validation period. Calibrated values of b_{infilt} , d2 and d3 were 0.071, 0.567 and 0.01.

The performance of the model in calibration and validation phases of daily and monthly streamflows at Yadgir are given in table 6.2. In general, model simulation is considered satisfactory if NSE > 0.50 and RSR < 0.70, and if PBIAS ±25% for streamflow (Moriasi *et al.*, 2007). For the daily data, NSE, PBIAS and RSR of 0.50, 16% and 0.71 were obtained during calibration period and 0.50, 2% and 0.75 during validation period in the given order. For monthly data, NSE, PBIAS and RSR were 0.85, 17% and 0.93 during calibration period and

0.77, 2% and 0.89 during validation period. The NSE obtained at daily and monthly scales for calibration and validation periods were considered satisfactory.

Table 6.2 Performance of VIC model during calibration and validation periods

Period	Calibration (1972-1976)		Validation (1977-1980)	
Criteria	Daily	Monthly	Daily	Monthly
NSE	0.50	0.85	0.50	0.77
PBIAS (%)	16	17	2	2
RSR	0.71	0.93	0.75	0.89

The plots of observed and simulated daily streamflows shows satisfactory matching during calibration and validation periods (Figure 6.16a-b). Figure 6.17 (a-b) also represents good matching of the observed monthly flows with the simulated flows during calibration and validation period. Final calibrated values of b_{infilt} , d2 and d3 were 0.071, 0.567 and 0.01.
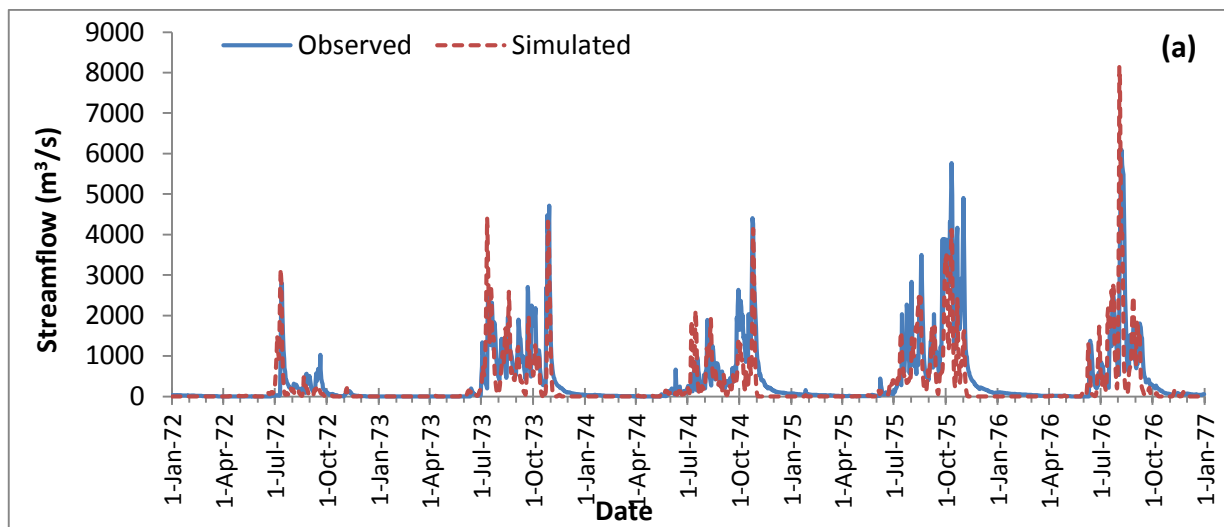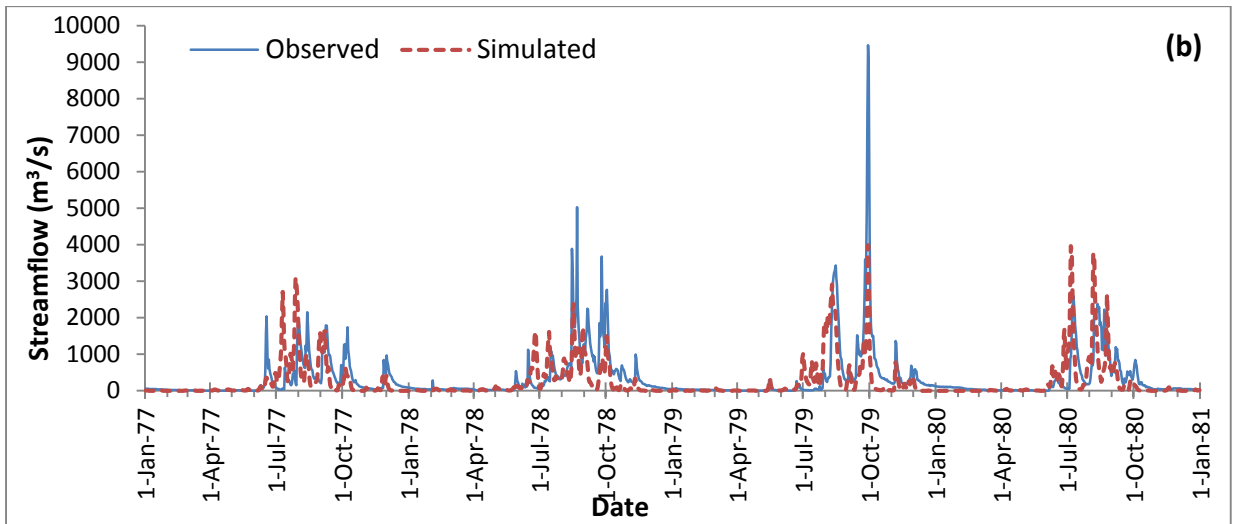
Figure 6.16 Plots of daily observed and simulated streamflow during a) calibration and b) validation of VIC model
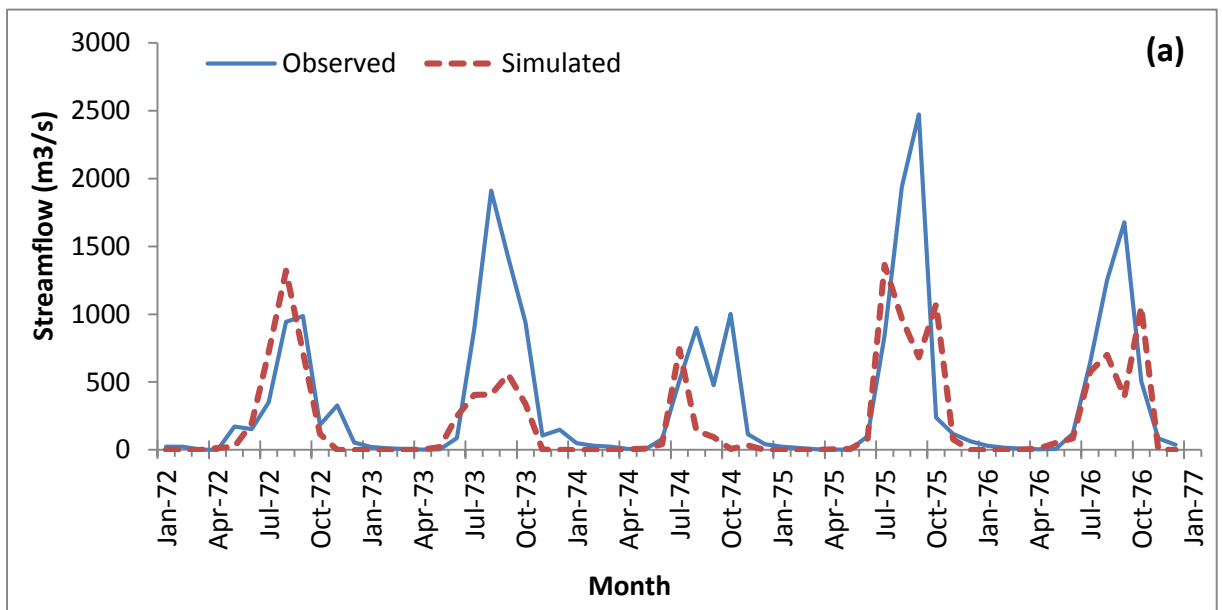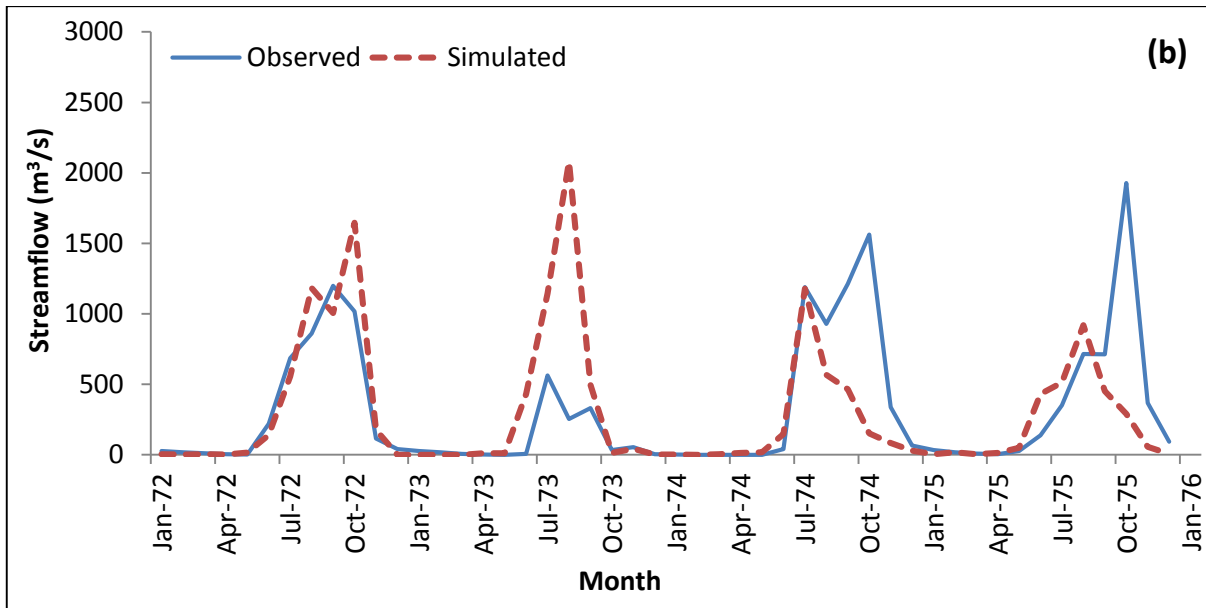
Figure 6.17 Plots of monthly observed and simulated streamflow during a) calibration and b) validation of VIC model

6.7.2 Impact of Climate Change on future Streamflow

VIC model was run from 2011-2030, 2046-2065 and 2080-2099 to simulate future streamflow for three emission scenarios using ensemble mean of daily projected data of the meteorological variables. Daily streamflows were converted into monthly, seasonal and annual streamflow series for A1B, A2 and B1 SRESs and for 2020s, 2055s and 2090s time periods. The changes in simulated monthly, seasonal and annual streamflows are given in subsequent section.

6.7.2.1 Projected changes in monthly streamflow

The plot of monthly streamflows simulated under A1B, A2 and B1 scenarios during 2011-2030, 2046-2065 and 2080-2099 are shown in figures 6.18. A2 scenario shows highest magnitudes of simulated monthly streamflows during 2020s and 2055s whereas in 2090s, the highest magnitude of simulated monthly streamflows is observed in B1 scenarios. No definite pattern was found alongwith the time scale in all the periods. Hence, average monthly streamflows in each time duration were computed to analyse average monthly patterns in a year. The monthly streamflows are expected to increase in May, June, July, August and September in future under all the scenarios and time spans. The monthly streamflows are expected to decrease significantly in October and November months. The highest changes in monthly streamflow was found in A2 scenario during 2055s and B1 during 2090s.

140
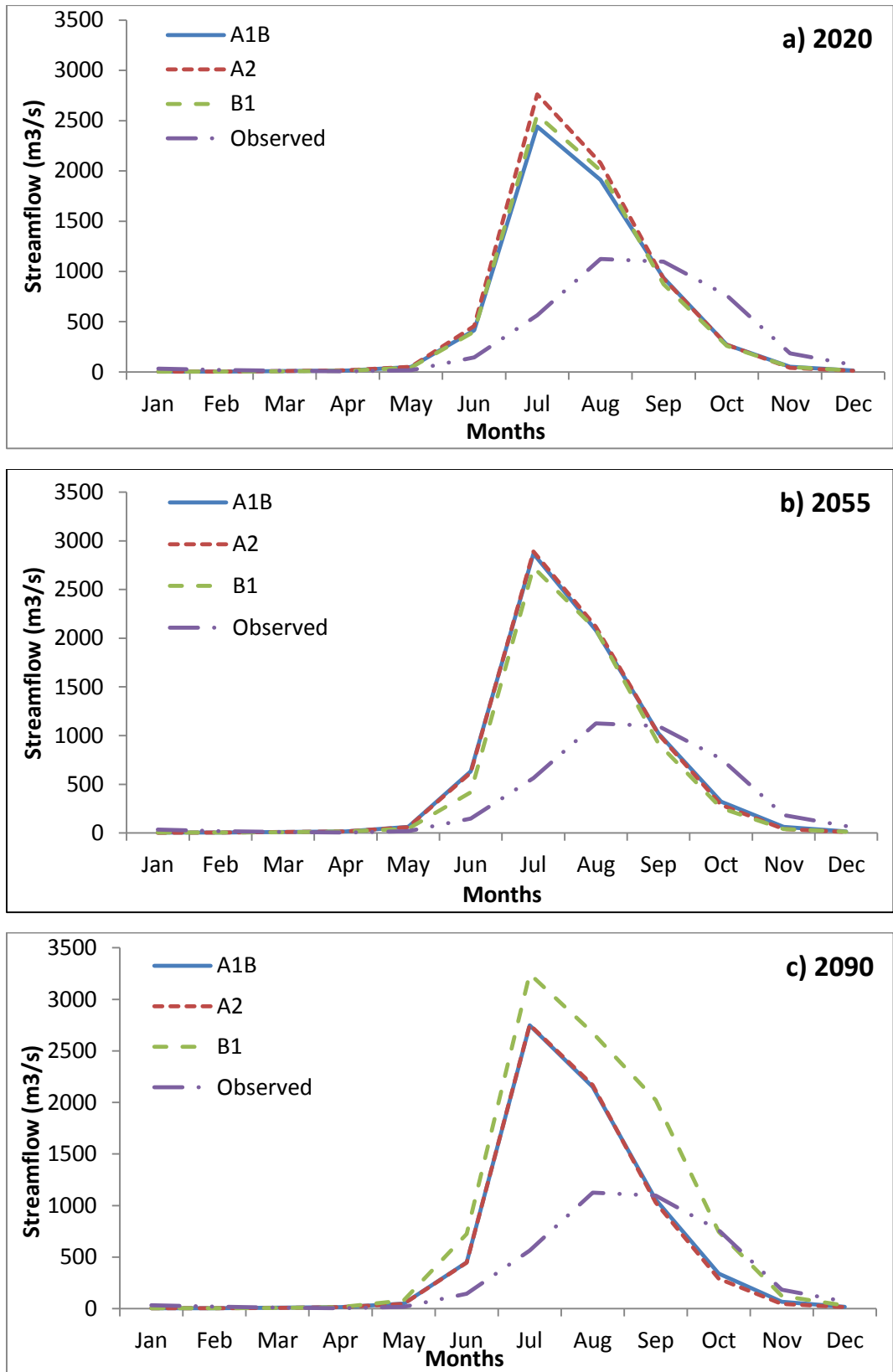
Figure 6.18 Projected changes in monthly streamflow in A1B, A2 and B1 in (a) 2020s, (b) 2055s and (c) 2090s

6.7.2.2 Projected changes in seasonal streamflow

Scenario wise seasonal streamflows computed for all the time spans shown in figure 6.19(a-c). As compared to the present streamflows (1970-1980), shown in blue colour, the streamflows are expected to increase in future for all scenarios during all time spans in summer and monsoon seasons and decrease during post-monsoon and winter season. The results described hare broadly follow the rainfall patterns discussed in Chapter 5.

Monsoon season shows the highest changes followed by the post-monsoon season. The summer/winter streamflows are expected to increase/decrease in future. However the changes are small in comparison to monsoon and post-monsoon seasons. The highest changes were observed in A2 scenario in monsoon streamflows during 2055s and in B1 during 2090s. In both, A1B and A2 scenarios, streamflows were found increasing by 2055s and then it decreases as compare to 2020s and 2090s durations. In B1 scenario, streamflows were projected to increase continuously from 2020s to 2090s.

Unlike summer and monsoon seasons where A2 scenario showed the highest changes, the post-monsoon streamflow showed the highest decrease change for A1B scenario during first two durations and in last durations by B1 scenarios. The winter streamflow is projected to decrease in future with the highest changes observed in A1B scenario during 2055 and B1 during 2090.
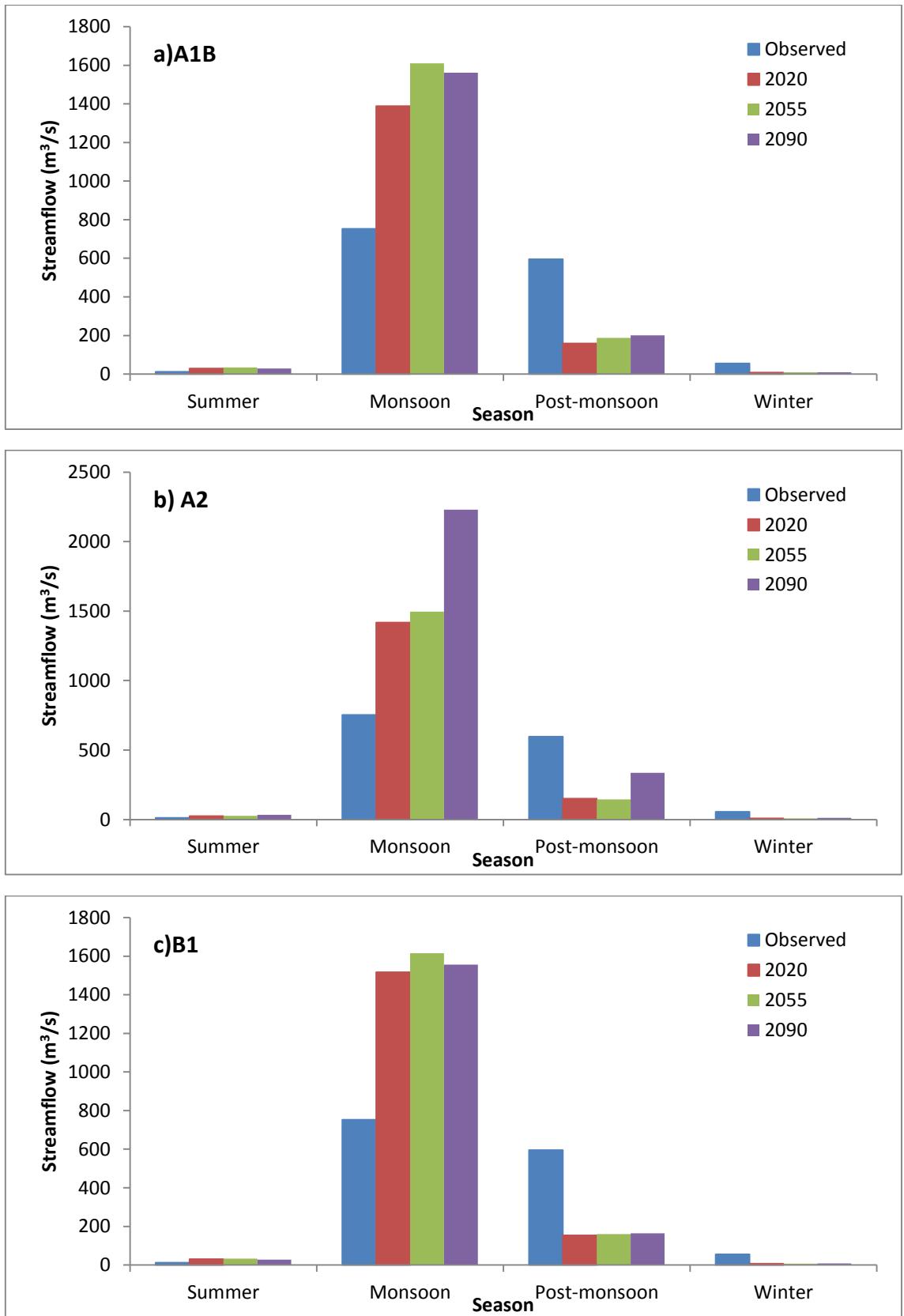
Figure 6.19 Plots of average seasonal streamflows for a) A1B, b) A2 and c) B1 scenarios

6.7.2.3 Projected changes in annual streamflow

The observed and future annual streamflows are plotted for three scenarios in 2020s, 2055s and 2090s (Figure 6.20). It shows annual streamflow of the basin is projected to increase in future. It was expected also as the rainfall is expected to increase in the same pattern. A1B and A2 scenarios project the same trend, i.e. the annual streamflow will increase slightly in 2050s and then decrease in 2090s, while B1 scenario shows continuous increase in annual streamflow. The highest increase in 2020s is observed in A2 scenario, in 2055s in A1B scenario and in 2090s in B1 scenario respectively.
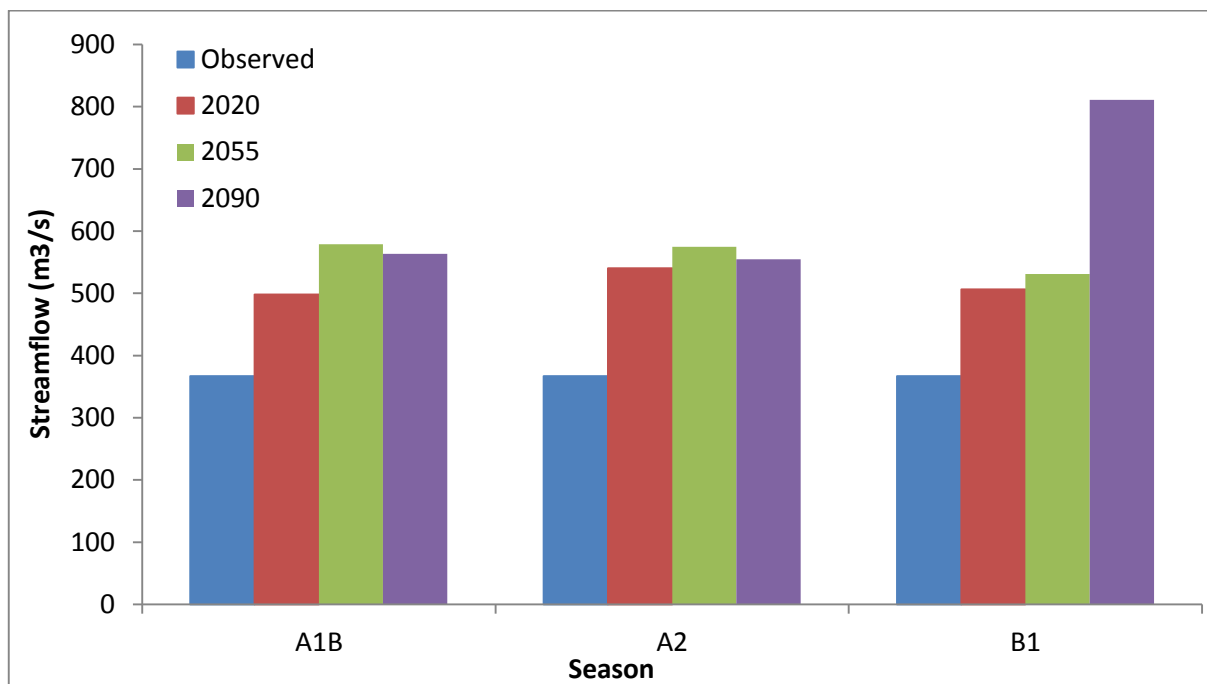
Figure 6.20 Projected changes in mean annual streamflows for A1B, A2 and B1 scenarios

The increase in projected streamflows may be directly attributed to the increasing trends projected in future annual rainfall of the basin under all scenarios for all three time spans.

6.8 SUMMARY AND DISCUSSION

The long term hydrological changes (represented by streamflow at the outlet) due to climate change in the Bhima basin were studied using VIC model. An ensemble of climatic variables predicted by 15 GCMs representing three emission scenarios for three periods was used to generate meteorological forcing files for the VIC model. The calibration and validation results indicate that the model performance was good and is acceptable to simulate the future

144

streamflows of the basin using calibrated and validated VIC model. The major findings are summarized below:

i. A2 scenario shows highest magnitudes of simulated monthly streamflows during 2020s and 2055s whereas in 2090s, the highest magnitude of simulated monthly streamflows is observed in B1 scenarios.

ii. An increasing trend is projected for summer and monsoon streamflows, whereas a decreasing trend in streamflow is projected for post monsoon and winter season.

iii. The highest changes were observed in A2 scenario in monsoon streamflows during 2055s and in B1 during 2090s. In both, A1B and A2 scenarios, streamflows were found increasing by 2055s and then it decreases as compare to 2020s and 2090s durations. In B1 scenario, streamflows were projected to increase continuously from 2020s to 2090s.

iv. Impact of climate change on streamflow shows an increasing trend in projected annual streamflow for all future emission scenarios in all durations.

v. Highest increase in the projected annual streamflow was found in A2 and B1 scenario in duration 2020 and 2090, respectively.

In present study, the projected increase in streamflows are because of the projected increase in rainfall in the basin. Central Indian basins are showing an increasing trend for monsoon surface runoff as reported by many researchers (India's Second National Communications to UNFCC, 2012; Raje *et al*., 2014). Hence, the findings obtained in this chapter are in agreement with other studies carried out on regional scale. It also underline the fact that the impact of climate change on the future streamflow of the Bhima River will influence the water resources availability in the Krishna River basin.

CHAPTER 7: OBSERVED AND GRIDDED RAINFALL ANALYSIS IN THE NIRA RIVER BASIN

7.1 GENERAL

Availability of the sufficient hydrometeorological data is one of the prime concerns in the field of hydrology and climate change. There are many open data sources which provide gridded meteorological data in public domain. It has been experienced that the observed data are not available for all the areas under investigation. However, the gridded datasets and reanalysis datasets are available for the entire globe on varied resolutions. Therefore, an attempt was made to study the differences in long-term rainfall trends based on the observed dataset and gridded dataset. The Nira River basin, a nested sub-basin of the Bhima River basin, was chosen for this comparison solely based on the data availability.

7.2 OBJECTIVES

The analysis presented in this chapter aimed at the following specific objectives:

i. The observed monsoon rainfall data of the Nira River basin was analysed to study the temporal trends in seasonal and annual rainfall, to investigate the association of monsoon rainfall and ENSO, and to study the future rainfall scenarios using LARS-WG.

ii. Comparison of the results obtained using observed rainfall data with the results of gridded rainfall data.

7.3 STUDY AREA AND DATA USED

The Nira River basin is a nested sub-basin of the Bhima River basin which is located in the state of Maharashtra in India having an area of 6900 km^2 (shown red in in figure 7.1) and a total length of about 180 km. Arabian Sea and Western Ghats are located to the west of the Nira basin. The Nira River originates in Sahyadri hills at Bhor and flows through Satara, Pune and Solapur districts. The river flows to the southeast in the plains of the Deccan Plateau, a fertile agricultural region with densely populated riverbanks (Biggs *et. al*., 2007). The basin is located between 445 m and 1410 m above mean sea level elevation with annual rainfall ranging

147

between 500 and 1000 mm. The banks of the Nira River are steep and rocky. The agro industries (especially sugar, distilleries, dairy, paper etc.), automobile and textile industries are dominant in this region. Millet, wheat, sugarcane, maize and all pulses, are the main crops being cultivated in the basin (Neena, 1998). Now a days, horticultural activities are increasing particularly for producing fruits such as orange, sweet limes, grapes, banana etc.
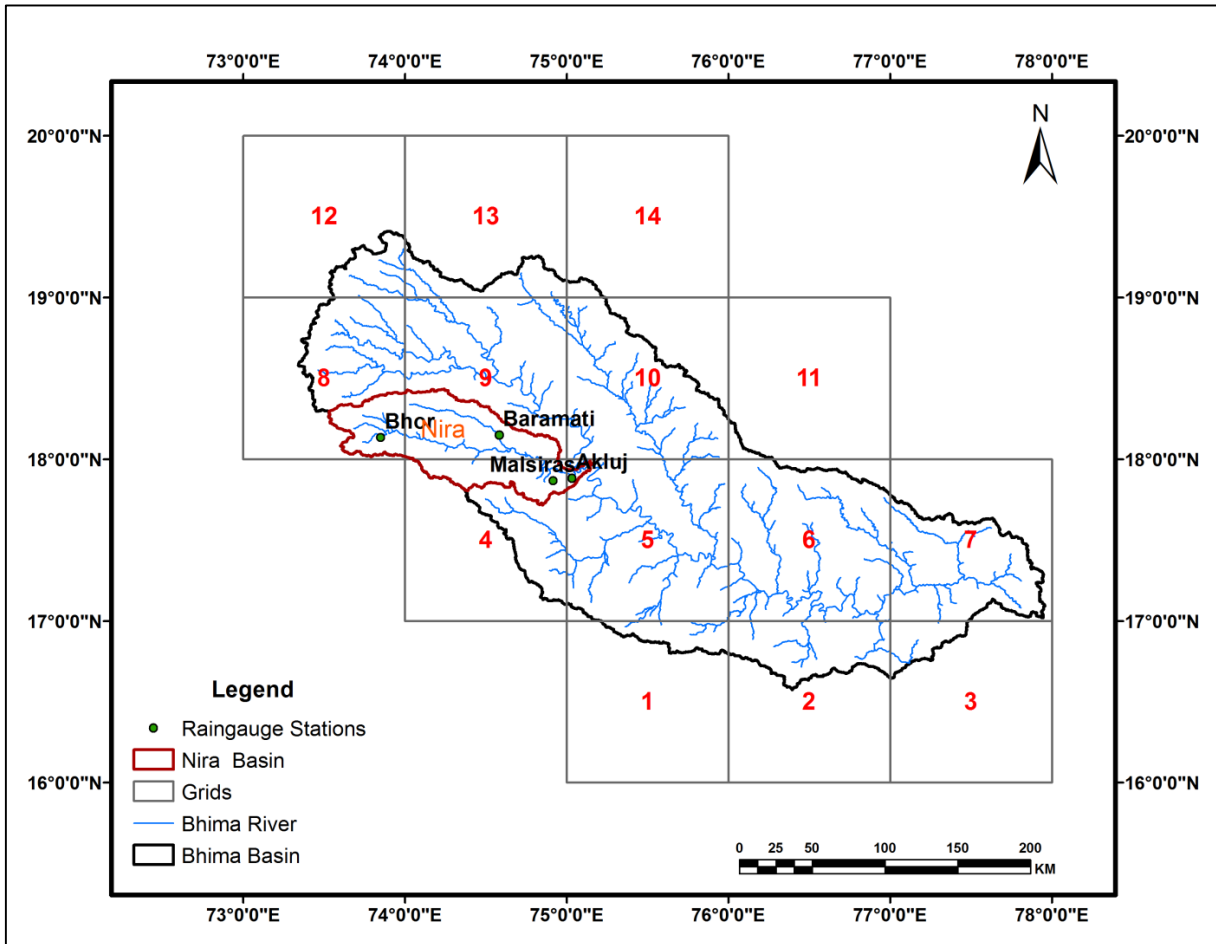
Figure 7.1 Location map of the Nira River basin

7.3.1 Rainfall Data

Daily rainfall data of 104 years (1901-2004) for four raingauge stations namely, Malsiras, Akluj, Bhor and Baramati, as seen in figure 7.1, was obtained from IMD, Pune. Four grids of the Bhima basin i.e. grid #4, #5, #8 and #9 cover the entire Nira basin (Figure 7.1). Malsiras, Akluj, Bhor and Baramati stations falls in the grid #4, #5, #8 and #9, respectively. In this Chapter, the term "observed data" refers to the "station data" obtained from the four raingauge stations as mentioned above. Both these terms have been used interchangeably. The "gridded

data" refers to the grid-based data set obtained from IMD at 1°x1° resolution as explained in Chapter 3.

7.4 METHODOLOGY

7.4.1 Trend Analysis of Seasonal and Annual Rainfall

Monthly rainfall series of four stations were prepared from daily observed data. These series were used to create the seasonal and annual rainfall series of each station. The methodology explained in Section 3.5 of Chapter 3 was then used for performing the trend analysis during 1901-2004. The detailed description of trend analysis tests are also given in appendix (3A-D).

7.4.2 Analysis of Relationship between Monsoon Rainfall and ENSO

Monthly monsoon rainfall series of four stations were derived from daily rainfall data to match the time scale of ENSO indices during 1901-2004. The rainfall series were then normalized using mean and standard deviation of particular month. The methodology described in Section 4.4 of Chapter 4 was used for studying the relationship between observed monsoon rainfall and ENSO in the Nira basin.

7.4.3 Analysis of Future Rainfall Scenarios

The LARS-WG was used to downscale the future rainfall data for three emission scenarios A1B, A2 and B1 using 15 GCMs in three time spans i.e. 2011-2030 (centred at 2020s), 2045-2065 (centred at 2055s), and 2080-2099 (centred at 2090s). Downscaling methodology as explained in Section 5.4 of Chapter 5 was used in this chapter, too.

7.4.4 Comparative of Analysis of Observed and Gridded datasets

Lastly, the results of the observed rainfall data analysis were compared with the results of the gridded rainfall data of the Bhima basin which covers the Nira basin. The trend analysis results of grid #4, #5, #8 and #9 were taken from section 3.6.2.1 and 3.6.2.2 of the Chapter 3. The results of ENSO analysis on gridded monsoon rainfall were taken from section 4.5.1 and 4.5.2 of the Chapter 4. The projected changes in respective gridded rainfall data which are given in section 5.5.5.1 and 5.5.5.2 of the Chapter 5 were used to compare the results obtained in this Chapter.

7.5 RESULTS

7.5.1 Analysis of Rainfall Variability

The results of the autocorrelation analysis and MK test in case of non-autocorrelated series, and MMK test for autocorrelated series for trend detection in annual and seasonal rainfall are given in table 7.1. Significant autocorrelation was found in 10 out of 16 seasonal rainfall series. A significant decreasing trend was observed in summer rainfall season at Malsiras, Akluj, Baramati and non-significant decreasing trend at Bhor station. A significant increasing trend was observed in monsoon rainfall at the stations Malsiras and Bhor whereas non-significant decreasing trend was observed in monsoon rainfall at Akluj. In monsoon seasons, the change in rainfall varied between -7.7% (Akluj) to 31.9% (Bhor). A significant increasing trend was found at all the stations for post-monsoon season. Decreasing trend was observed in winter rainfall season at all the stations, however, significant only at Malsiras and Baramati stations.

Statistically significant increasing trends were observed in annual rainfall series at Akluj, Baramati and Bhor stations. The magnitude of trend and percent change in annual rainfall are also shown in table 7.1. The magnitude of the increasing trends in annual rainfall was ranging from 11.8% (at Malsiras) to 28.0% (at Bhor station). Bhor station (28.02%) shows the maximum increase in percent change in annual rainfall over the 104 years period.

Over the 104 years, the rainfall decreased in summer seasons and increased during the monsoon and post-monsoon seasons. The change in summer rainfall ranged from -22% (Bhor) to -130.6% (Akluj) indicating water scarcity in summers. The decrease in monsoon rainfall at Akluj might affect water availability and agricultural production. The increase in monsoon rainfall at other three stations may have positive or negative impacts depending upon the timing and intensity of rainfall. The winter season rainfall doesn't seem to change much across the basin.

Table 7.1 MK/MMK statistics (Z), Theil and Sen's slope estimator, and % change in seasonal and annual rainfall of the raingauge stations and gridded rainfall

Series	Station	MK (MMK)	Sen's Slope	% change	Grids	MK (MMK)	Sen's Slope	% change
Summer	Malsiras	**-2.079**	-0.15	-48.95	4	-1.463	-0.14	-28.70
Summer	Akluj	**-5.519***	-1.03	-130.61	5	0.002	0.00	0.55
Summer	Bhor	-1.429*	-0.09	-22.44	8	0.180	0.01	2.19
Summer	Baramati	**-3.183**	-0.13	-41.76	9	-1.311	-0.06	-22.60
Monsoon	Malsiras	**2.056***	0.70	32.22	4	1.430	0.60	17.97
Monsoon	Akluj	-0.443*	-0.18	-7.68	5	**1.823**	0.86	19.51
Monsoon	Bhor	**2.969***	2.26	31.91	8	0.392*	1.59	10.94
Monsoon	Baramati	0.454*	0.12	6.54	9	**2.067**	0.81	23.62
Post-Monsoon	Malsiras	**3.202**	0.01	0.39	4	1.290	0.31	26.64
Post-Monsoon	Akluj	**4.909**	1.73	109.58	5	1.542	0.35	32.95
Post-Monsoon	Bhor	**1.943***	0.67	29.12	8	1.115	0.25	23.82
Post-Monsoon	Baramati	**1.758***	0.81	32.24	9	1.497	0.34	33.42
Winter	Malsiras	**-2.326**	0.0	0.00	4	**-2.089**	0.00	0.00
Winter	Akluj	-0.465*	0.0	0.00	5	-1.225	0.00	-2.12
Winter	Bhor	-1.052*	0.0	0.00	8	-1.213	0.00	0.00
Winter	Baramati	**-2.594**	0.0	0.00	9	**-2.234**	0.00	-1.24
Annual	Malsiras	0.934	0.61	11.77	4	1.528	0.803	16.1
Annual	Akluj	**1.667***	1.11	23.04	5	0.674*	1.45	23.8
Annual	Bhor	**3.075***	2.76	28.02	8	0.401*	2.15	13.4
Annual	Baramati	**1.456***	0.81	16.94	9	0.687*	1.34	27.6

(Note: * indicates significant autocorrelated series at 10% significance level and bold values indicate statistically significant trends)

7.5.2 Analysis of Relationship between Monsoon Rainfall and ENSO

7.5.2.1 Correlation analysis between monsoon rainfall and ENSO

Pearson's correlation coefficients (r) between monsoon rainfalls of all the stations and seasonal ENSO indices with t-statistics are given in table 7.2. Analysis of correlation shows that the monsoon rainfall of Baramati station was significantly correlated with winter SOI and MEI indices. Other three stations did not show any significant correlation with winter ENSO indices. No significant correlation was found with the summer ENSO indices, as well.

Correlation analysis indicates that the monsoon rainfall is positively correlated with SOI whereas negatively correlated with MEI and N3.4. The highest positive r is 0.41 between monsoon rainfall of Malsiras and Akluj stations with monsoon SOI. The highest negative r 0.38 was obtained between monsoon rainfalls of Malsiras and monsoon N3.4 index. Monsoon rainfall of three stations shows significant relationship with monsoon SOI, MEI and N3.4 indices - Bhor station did not show a significant relationship. The possible reasons for not finding significant correlation with Bhor station could be its location (located on relatively higher elevation the Western Ghats).

Table 7.2 Pearson's correlation coefficient between monsoon rainfall and seasonal ENSO indices with t-statistic in the Nira basin

Stations/ grids	Test/Season Indices	Winter (ONDJ)			Summer (FMAM)			Monsoon (JJAS)		
		SOI	MEI	N3.4	SOI	MEI	N3.4	SOI	MEI	N3.4
		Observed data								
Malsiras	r	-0.10	0.17	0.12	-0.01	0.04	-0.02	0.41	-0.30	-0.38
	t-statistics	0.99	1.78	1.20	0.12	0.40	0.23	4.49*	3.14*	4.12*
Akluj	r	-0.06	0.04	0.01	0.07	-0.08	-0.11	0.41	-0.32	-0.36
	t-statistics	0.60	0.39	0.08	0.60	0.74	1.03	4.43*	3.25*	3.75*
Bhor	r	0.24	-0.12	-0.11	0.11	-0.06	-0.06	0.11	-0.11	-0.10
	t-statistics	2.45*	1.18	1.14	1.14	0.64	0.57	1.14	1.08	1.06
Baramati	r	-0.20	0.20	0.16	-0.07	0.13	0.08	0.38	-0.22	-0.30
	t-statistics	2.10*	2.09*	1.64	0.74	1.30	0.78	4.11*	2.30*	3.14*
		Gridded data								
Grid #4	r	-0.14	0.17	0.14	-0.04	0.02	0.03	0.23	-0.16	-0.14
	t statistics	1.47	1.72*	1.33	0.44	0.20	0.30	2.34*	1.62	1.41
Grid #5	r	-0.12	0.13	0.10	-0.01	0.05	-0.01	0.36	-0.26	-0.31
	t statistics	1.24	1.33	1.00	0.14	0.49	0.06	3.93*	2.71*	3.17*
Grid #8	r	-0.21	0.14	0.10	-0.05	0.13	0.09	0.14	-0.10	-0.19
	t statistics	2.21*	1.47	0.95	0.55	1.31	0.93	1.39	0.97	1.91
Grid #9	r	-0.15	0.18	0.10	-0.13	0.11	0.07	0.20	-0.10	-0.13
	t statistics	1.58	1.81*	1.00	1.32	1.15	0.72	2.05*	1.04	1.32

Note: *indicates significance of 'r' at 5% level

7.5.2.2 Impact of ENSO phases on monsoon rainfall

The monsoon rainfall series of each station were divided into three sub-series matching to the ENSO phases (La Niña phase, Neutral phase and El Niño phase). The average monsoon rainfall of each phase was computed for all the stations. Graph of monsoon rainfall in each ENSO phase with ENSO events are shown in figure 7.2(a-d). In this figure, the blue squares, red triangles and green circles show La Niña, El Niño and neutral ENSO events, respectively. Dashed, dotted and dotted-dashed lines show the mean rainfall during La Niña, El Niño and neutral phases, respectively. The differences between monsoon rainfall occurred during ENSO phases are clearly visible (except for Bhor station) in these figures. It reveals that the rainfalls occurred during La Niña events are more than the rainfall occurred during El Niño events at Akluj, Baramati and Malsiras stations. The results are opposite for the Bhor station.
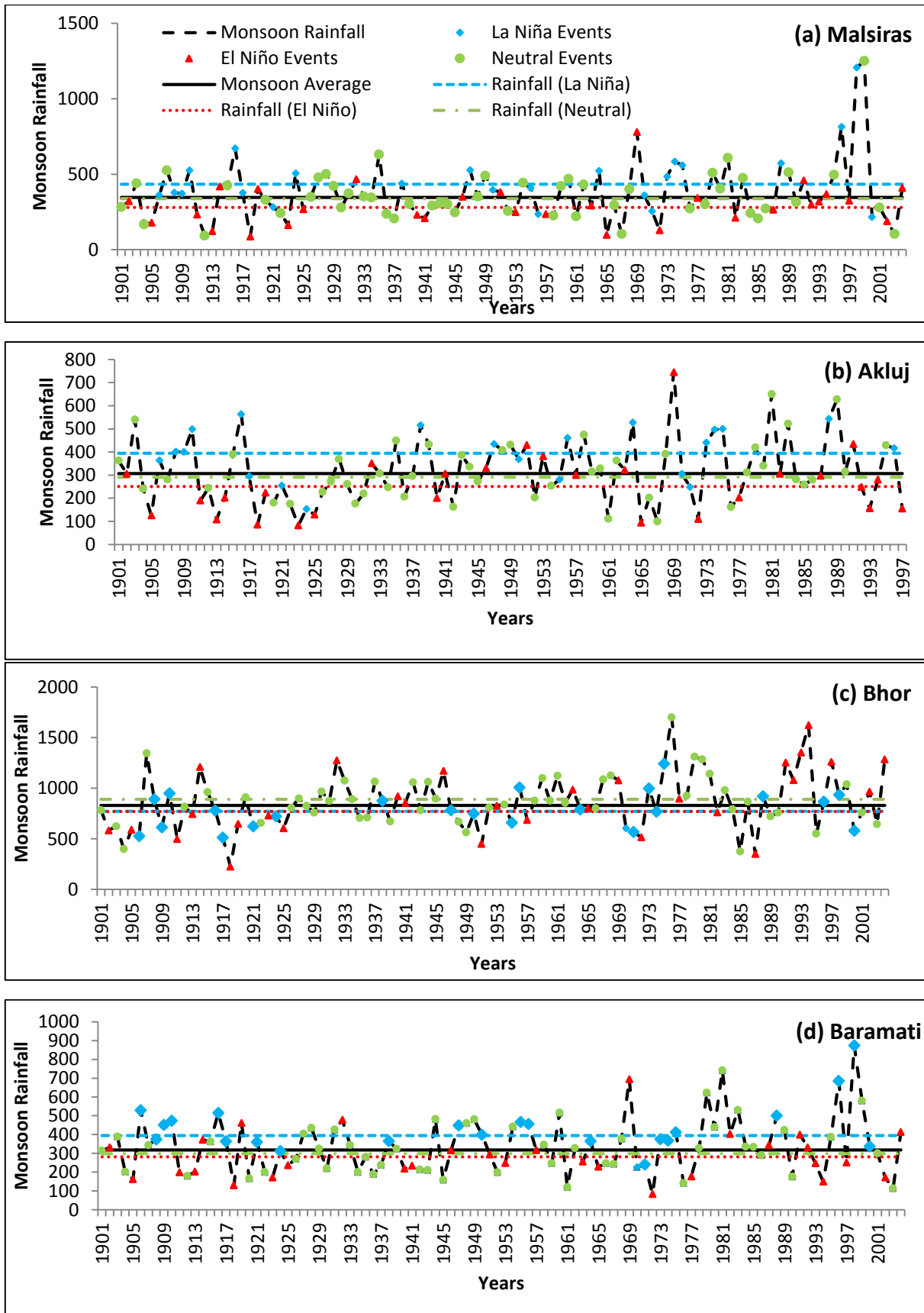
Figure 7.2 Plots of monsoon rainfall during ENSO Phases at (a) Malsiras, (b) Akluj, (c) Bhor and (d) Baramati stations

The results of homogeneity analysis of monsoon rainfall at four stations of the Nira basin during ENSO phases with F statistics of ANOVA test are given in table 7.3. Alternate hypothesis is accepted at 5% significance level for Malsiras, Akluj, and Baramati rain gauge stations except Bhor. It implies that the monsoon rainfalls of La Niña, Neutral and El Niño phases of ENSO are significantly different.

Table 7.3 Homogeneity analysis of monsoon rainfall during ENSO phases using ANOVA

Stations	F statistics	Grids	F statistics
Malsiras	7.290	**4**	5.62
Akluj	8.614	**5**	10.153
Bhor	1.337*	**8**	0.606*
Baramati	7.998	**9**	2.939

*indicates acceptance of null hypothesis at 5% significance level

Percent changes in mean monsoon rainfall during La Niña and El Niño phases with respect to neutral phase were computed and are shown in figure 7.3 (a-b). It shows that the percent change in monsoon rainfall during the La Niña phase is higher than the rainfall occurred during El Niño phase at all stations except Bhor. Malsiras shows higher percentage increase/decrease in monsoon rainfall during La Niña/El Niño phases. As the result of the Bhor station are not consistent with other stations, the changes at this station were not included in computation of overall changes in the Nira basin. Overall, twenty eight % higher rainfall is received during monsoon in La Niña phase and 18 % less in El Niño phase.
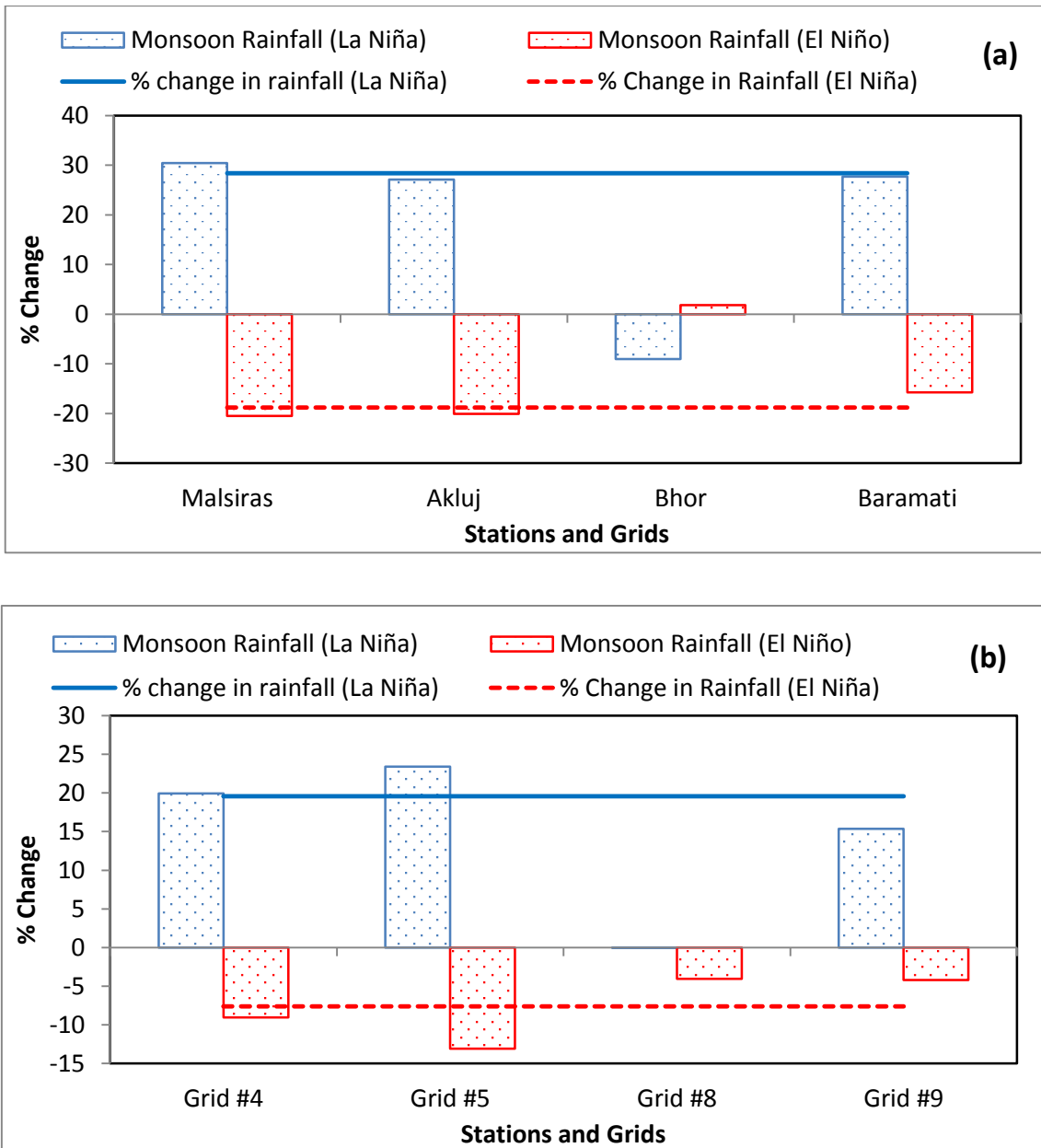
Figure 7.3 Percentage change in monsoon rainfall during ENSO Phases at (a) the stations and at (b) the grids

7.5.3 Analysis of future rainfall scenarios using observed data

7.5.3.1 Calibration of LARS-WG

The daily rainfall data of the duration 1961-1990 were used for calibration of LARS-WG for each station. Care was taken to calibrate the model during monsoon months (June, July and August) as most of the rainfall occurs during these months. The CDFs for the lengths of dry and wet series of observed and synthetic rainfall data for JJA months were generated by LARS-

WG. The days with rainfall greater than 0 mm were classified as wet series, and days with no rainfall were classified into dry series. The wet series distributions derived for the quarters of JJA at each station are shown in figure 7.4 (a-b). The wet/dry series distribution plots show that all lengths of wet/dry series distributions were reproduced correctly at each station for JJA months. Thus, it was concluded that LARS-WG in general, was able to reproduce daily distribution of the observed rainfall and the length of wet/dry series well.
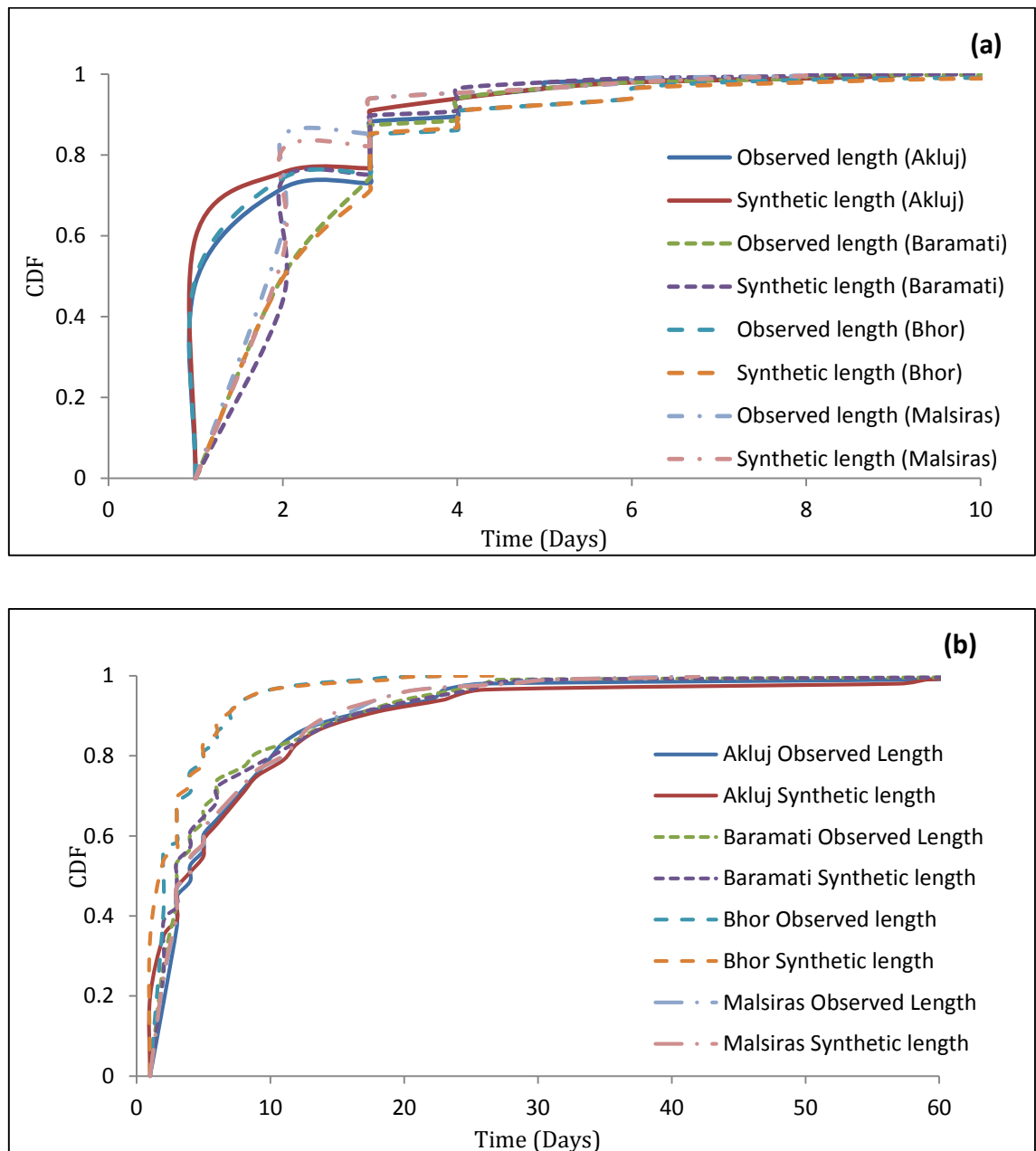
Figure 7.4 CDF of observed and synthetic data during monsoon a) wet series and b) dry series

Means and standard deviations of the observed data at each station were compared with those of the synthetic data using t-test and F-test, respectively. The results based on the t-test and F-test statistic and calculated p values are summarized in table 7.4. Months in which the p values of t and F tests were less than the significance level of 0.05 (indicating poor performance of the model) are highlighted and marked with 'x'. The months marked with '√' indicate p-values greater than the significance level of 0.05 indicating a good agreement between the means and/or standard deviations of observed and synthetic data. A good agreement was observed between the means of observed and synthetic data at all the stations during all the months. However, the inter-annual variability represented by the standard deviations of monthly data, was not well reproduced for few months. In general, LARS-WG performed relatively poor in terms of representing the inter-annual variability of January, March and December months' rainfall of Akluj station; January, February and April months' rainfall of Baramati; and, March, July and August months' rainfall of Bhor and Malsiras stations. This is in conjunction with the recommendations of Semenov *et al*. (1998), who reported that all weather generators have limited capability of reproducing inter-annual variability.

In general, a model is considered calibrated for the generation of synthetic data, if it shows good performance for the months of monsoon and post-monsoon seasons. Table 7.4 shows that the model has reproduced the data well for these two seasons. Therefore the model was considered calibrated.

Table 7.4 Comparison of observed and synthetic monthly rainfall data at the raingauge stations

Month	p-value of t-test (p-value of f-test)							
	Akluj		**Baramati**		**Bhor**		**Malsiras**	
	t-test	F-test	t-test	F-test	t-test	F-test	t-test	F-test
January	√	x	√	x	√	√	√	√
February	√	√	√	x	√	√	√	√
March	√	x	√	√	√	x	√	x
April	√	√	√	x	√	√	√	√
May	√	√	√	√	√	√	√	√
June	√	√	√	√	√	√	√	x
July	√	√	√	√	√	√	√	x
August	√	√	√	√	√	√	√	x
September	√	√	√	√	√	√	√	√
October	√	√	√	√	√	√	√	√
November	√	√	√	√	√	√	√	√
December	√	x	√	√	√	√	√	√
Note: √ indicate p value >0.05 and x <0.05								

7.5.3.2 Analysis of projected changes in rainfall

The calibrated model was used to generate the projected rainfall data corresponding to scenarios A1B, A2 and B1 during three time spans 2011-2030, centred at 2020; 2046-2055, centred at 2055; and 2080-2099; centred at 2090. These data were further analysed to study the impact of climate change on seasonal and annual rainfall using change factor technique. The CFs of rainfall were obtained with respect to the baseline period (1961-1990) for both seasonal and annual rainfall data and are illustrated in figures 7.5 to 7.8. In the figures Sum, Mon, Pmon and Win represent summer, monsoon, post-monsoon and winter seasons, respectively.

Figures 7.5 to 7.8 illustrate the range of uncertainty associated with rainfall projections using different GCM outputs. The longer the length of the box-plot, the more is the uncertainty in the projections. The box-plots for seasonal as well as annual CFs lie on the positive as well as negative sides approximately in between -1 to 2. It indicates that some GCMs are suggesting an increase in seasonal as well as annual rainfall, while others are suggesting a decrease. The mean values in all the box-plots at all the stations are above zero. It indicates that the increase

in rainfall in the future is very likely in the basin. The lengths of box-plots also show the inter-GCM variability of the projections. The variability in the projections is less in annual values compared to that in the seasonal. This may have resulted in greater inter-annual variability, compared to seasonal variability. At seasonal time scale, the summer season is associated with the highest uncertainty compared with other seasons. However, summer season contribution to the total rainfall is very small.
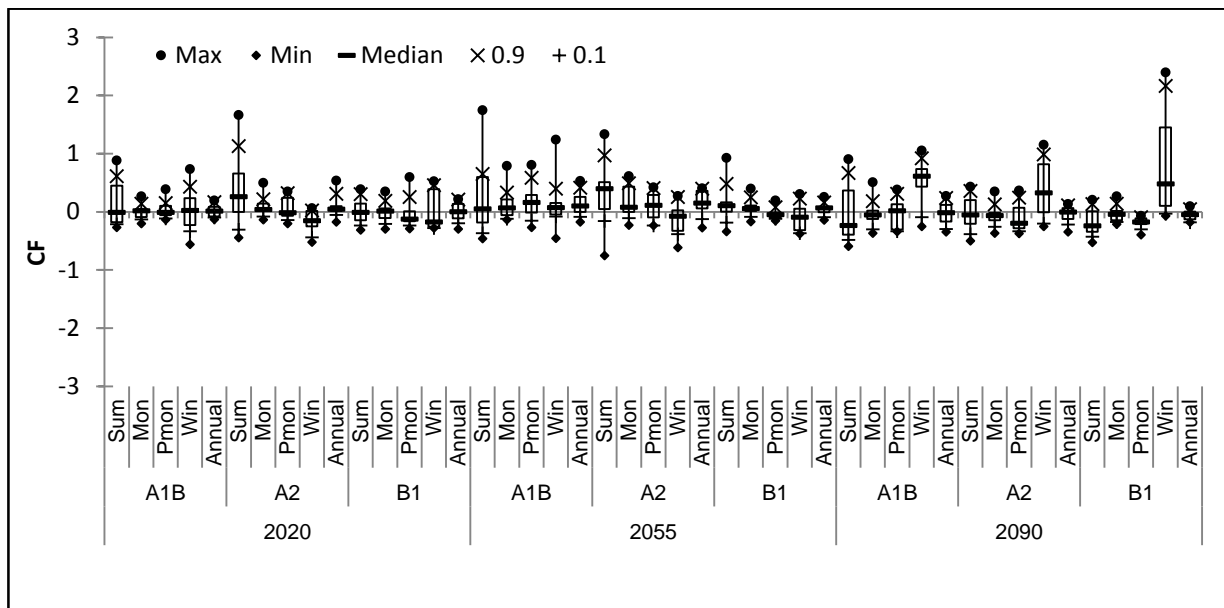
Figure 7.5 Box-plot of the changes in seasonal and annual rainfall at Baramati
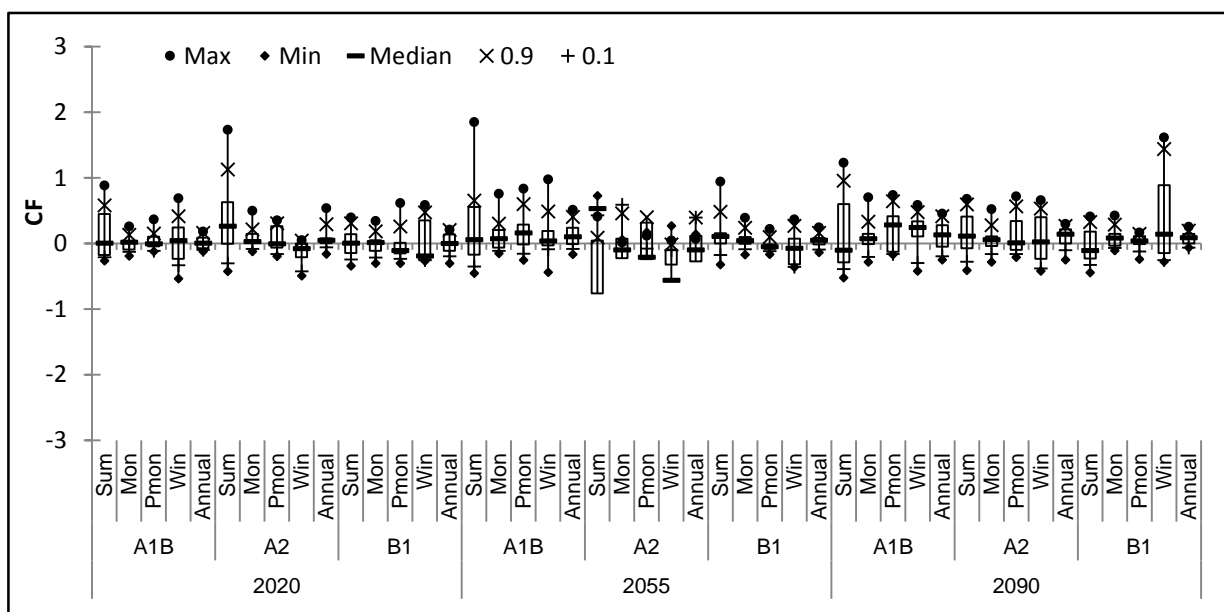
Figure 7.6 Box-plot of the changes in seasonal and annual rainfall at Akluj
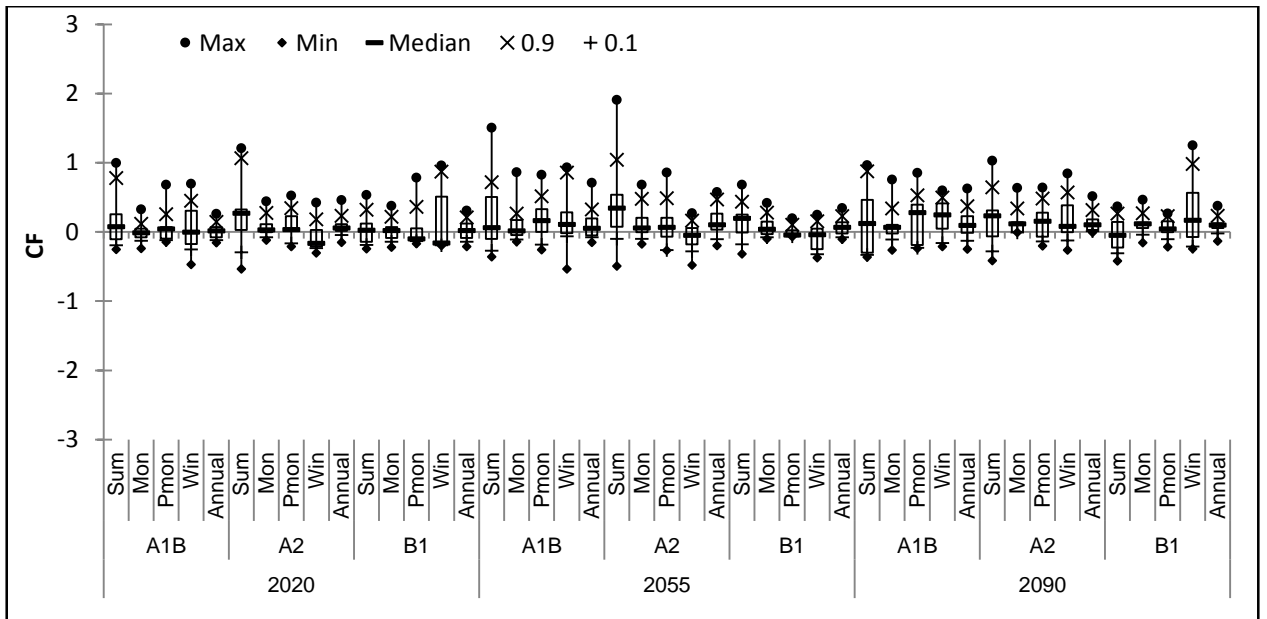
Figure 7.7 Box-plot of the changes in seasonal and annual mean rainfall at Bhor
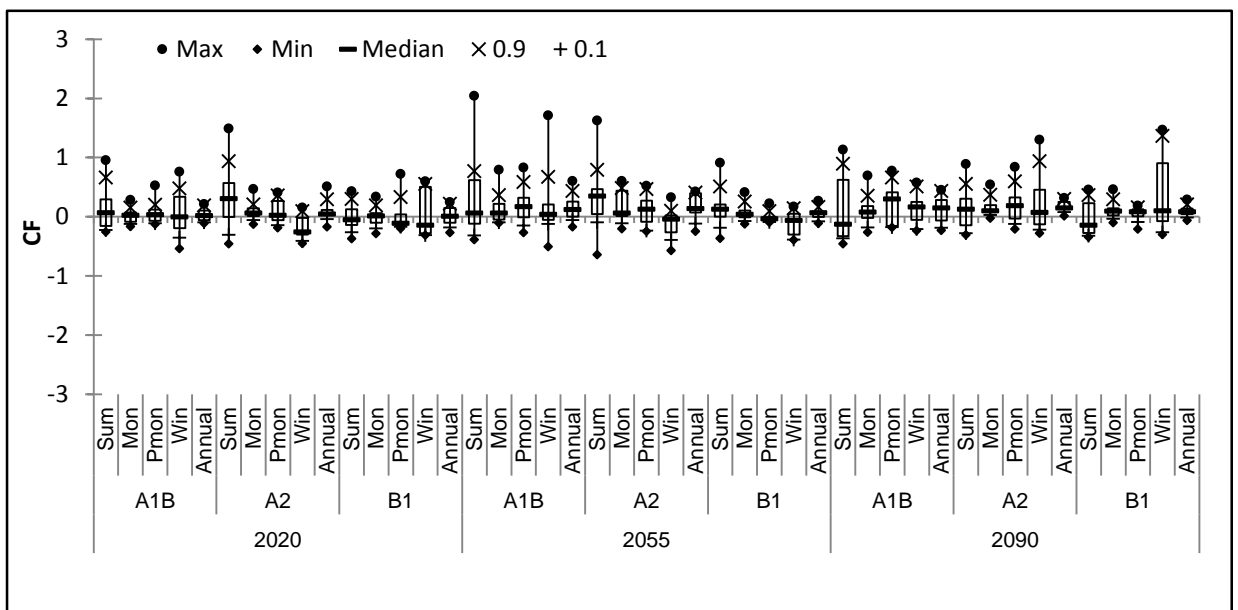
Figure 7.8 Box-plot of the changes in seasonal and annual mean rainfall at Baramati

7.5.3.3 Impact of Climate Change on Seasonal Rainfall

Relying on a particular GCM projection may either cause underestimation or overestimation in estimating the impacts of climate change. An ensemble mean of all GCMs may help in reducing the uncertainty in projections of rainfall. Hence results presented in this section are based on an ensemble of all GCMs for rainfall projection at each station giving equal

weightage in computing the ensemble mean. Ensemble means were also computed using the GCMs available for a particular emission scenario in a particular time span. The percentage changes in seasonal rainfall at four stations and their respective grids in the Nira basin are shown in figure 7.9 (a) to figure 7.12 (a) for A1B, A2 and B1 scenarios centred at 2020s, 2055s and 2090s with respect to the baseline period 1961-1990.

Percent change in projected rainfall in summer season showed an increase at all the stations under all emission scenarios except in B1 scenarios (Figure 7.9a). In B1 scenario summer rainfall is projected to decrease in 2090s for all stations wherein for Malsiras station summer rainfall is projected to decrease for all time periods. In general, the projected rainfall shows an increase from 2020s to 2055s and then decrease in 2090s under A1B and A2 emission scenarios. Amongst the four stations, highest increase in summer rainfall is projected at Bhor (43.8%, A2) followed by Baramati (35.0%, A2), Malsiras (26.2%, A1B) and Akluj (37.6%, A1B).

In monsoon season, the percent change in projected rainfall is highest in A1B scenario in 2055s time period (Figure 7.10a). In A2 scenario rainfall is projected to increase in 2055s from 2020s and then decrease in 2090s at all stations except Akluj. A similar pattern is projected for B1 scenario at Bhor and Baramati stations. However in Malsiras there is a net decrease in rainfall under the B1 scenario for all the three time spans. The highest increase is projected at Baramati station (16.7%, B1 scenario).

In post monsoon season, under A1B scenario, the rainfall is projected to increase from 2020s to 2055s and then decrease in 2090s (Figure 7.11a). Under A2 scenario, however, a continuous decreasing pattern in rainfall is projected from 2020s to 2090s at all stations except Akluj. For B1 scenario, a pattern similar to that for A2 scenario was observed at all stations. The highest change is projected in 2055s at Akluj station (39.1%, A2 scenario).

In winter season, the rainfall decreases from 2020s to 2055s and then increases in 2090s under A1B scenario (Figure 7.12a). In A2 scenario rainfall increases in 2020s, and then decreases in 2055s and 2090s at all the stations except Akluj. In B1 scenario rainfall increases in 2020s, then decreases in 2055s and then increases in 2090s with positive magnitude of change across all time periods. Highest change in winter season is shown at Baramati station (84.7%, B1 scenario).

The following points can be highlighted from the above discussion:

- Decreasing rainfall trend was found in winter season under almost all scenarios during all seasons.
- Summer and winter seasons show maximum variation while monsoon and post-monsoon seasons shows least variation.
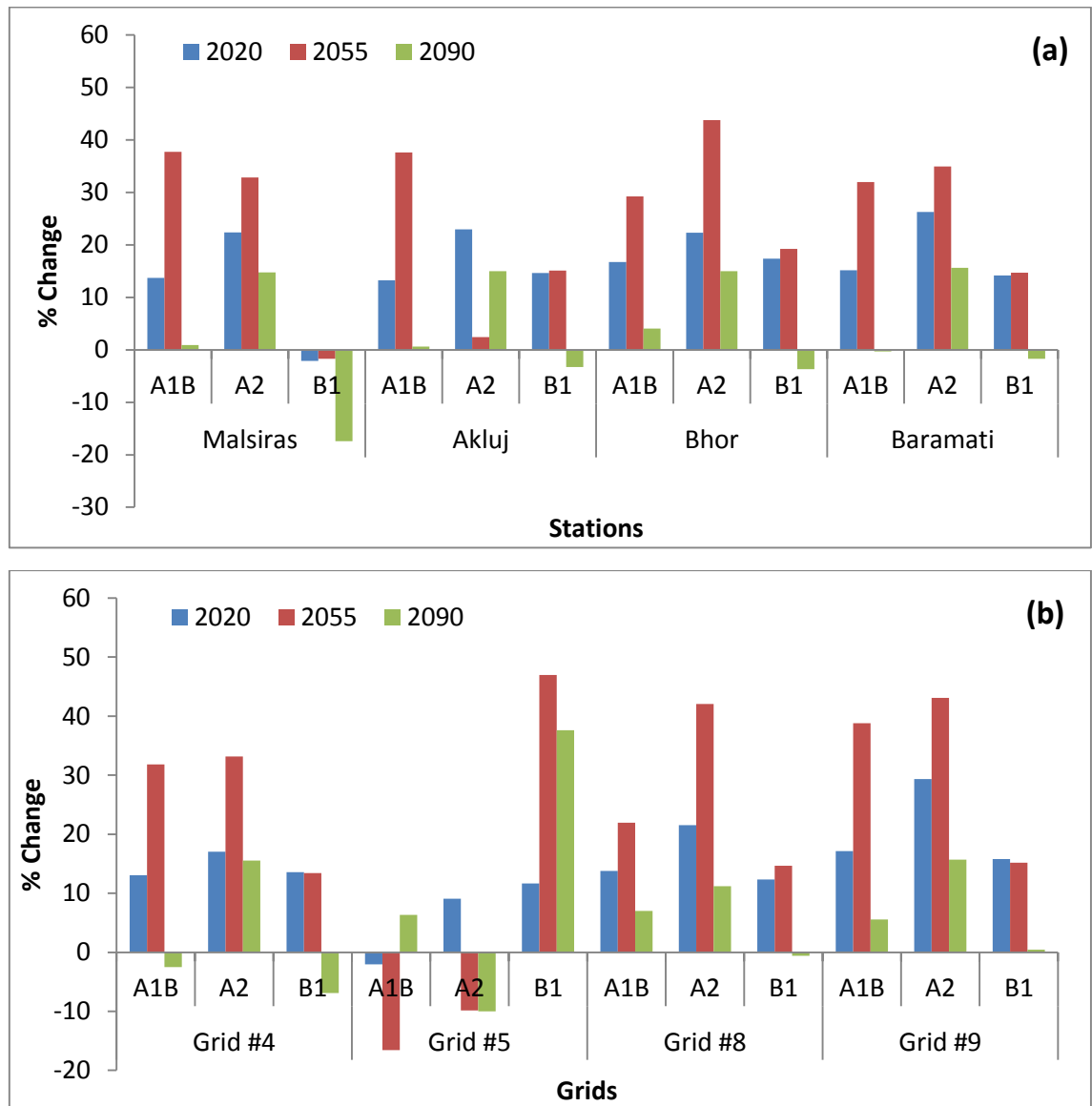
Figure 7.9 Changes in summer rainfall of at each a) stations and b) grid #4
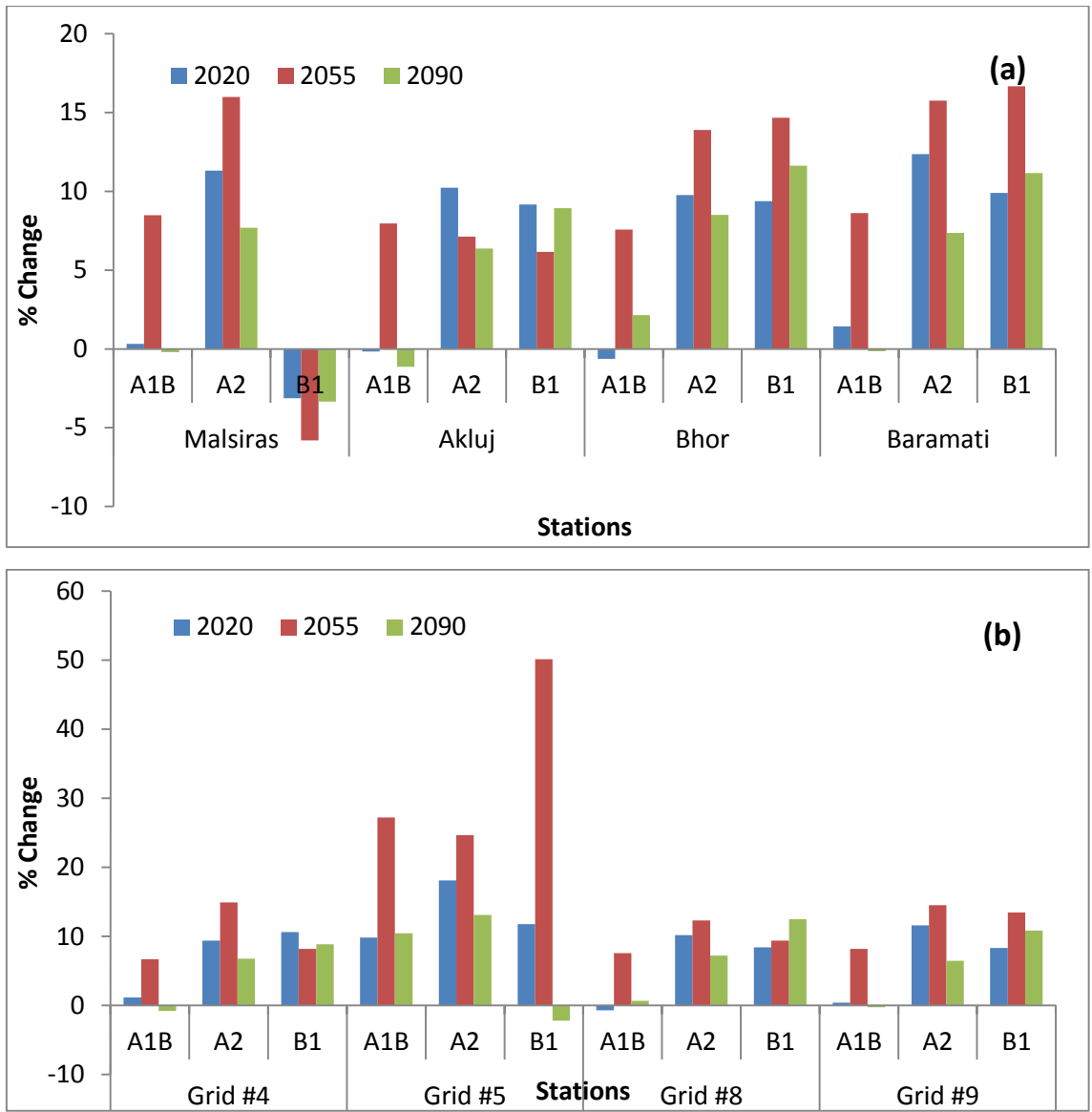
Figure 7.10 Changes in monsoon rainfall of at each a) stations and b) grid #4
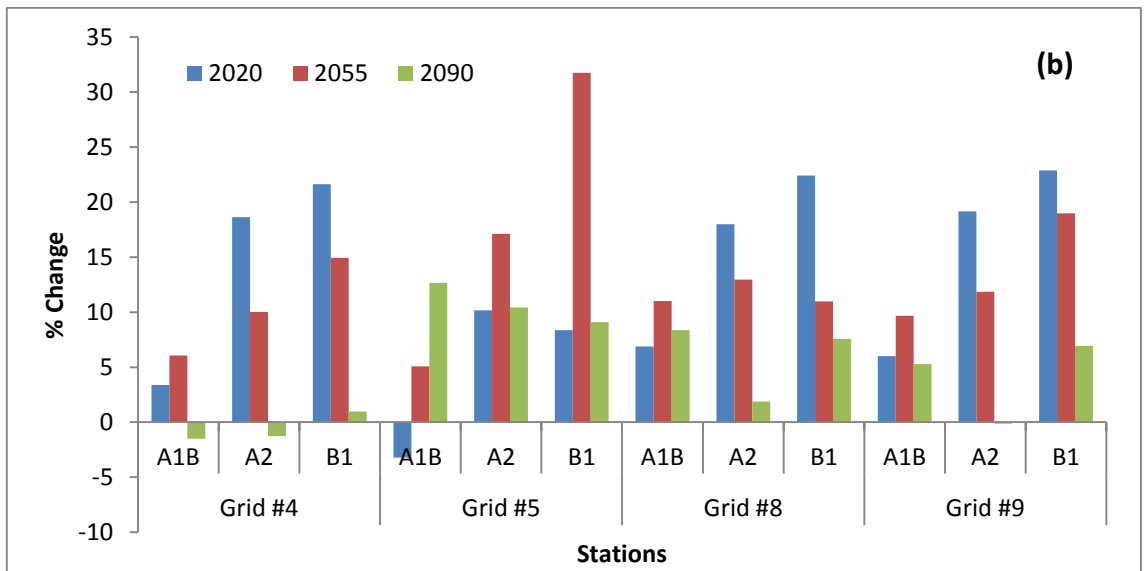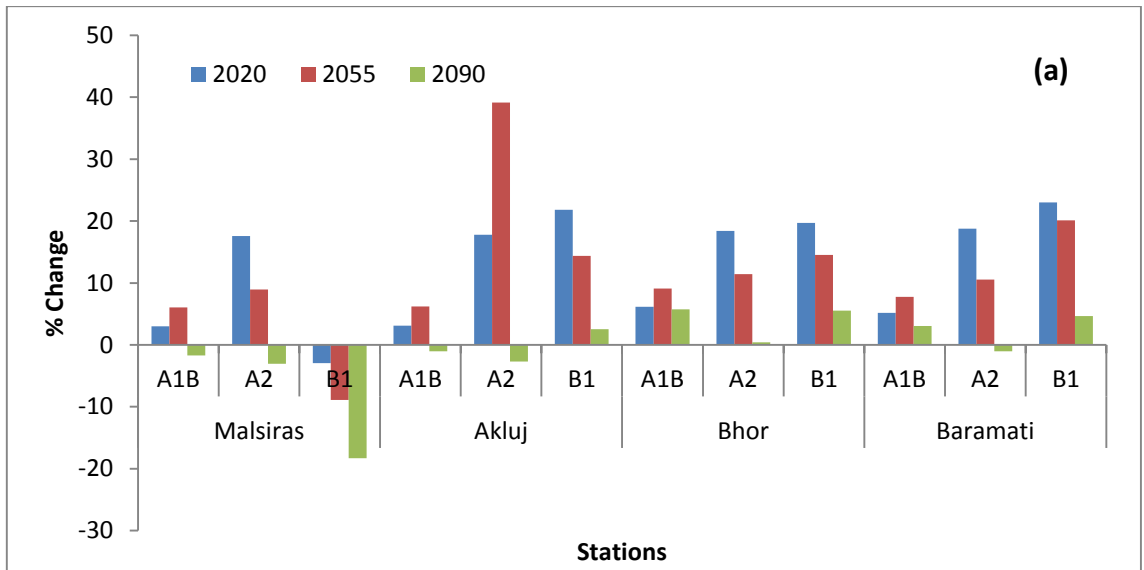
Figure 7.11 Changes in post-monsoon rainfall of at each a) stations and b) grid #4
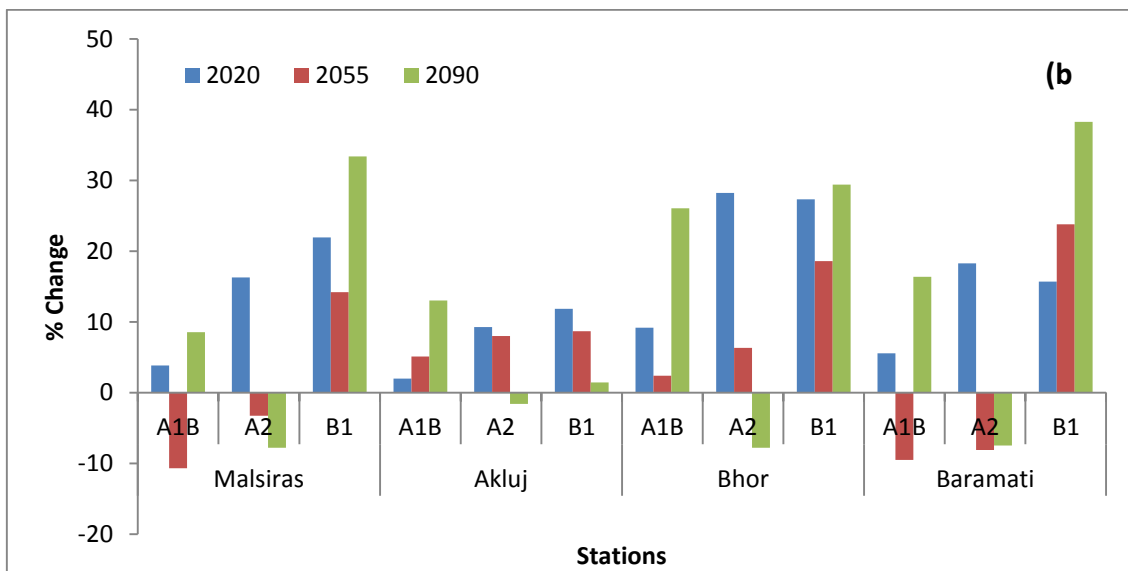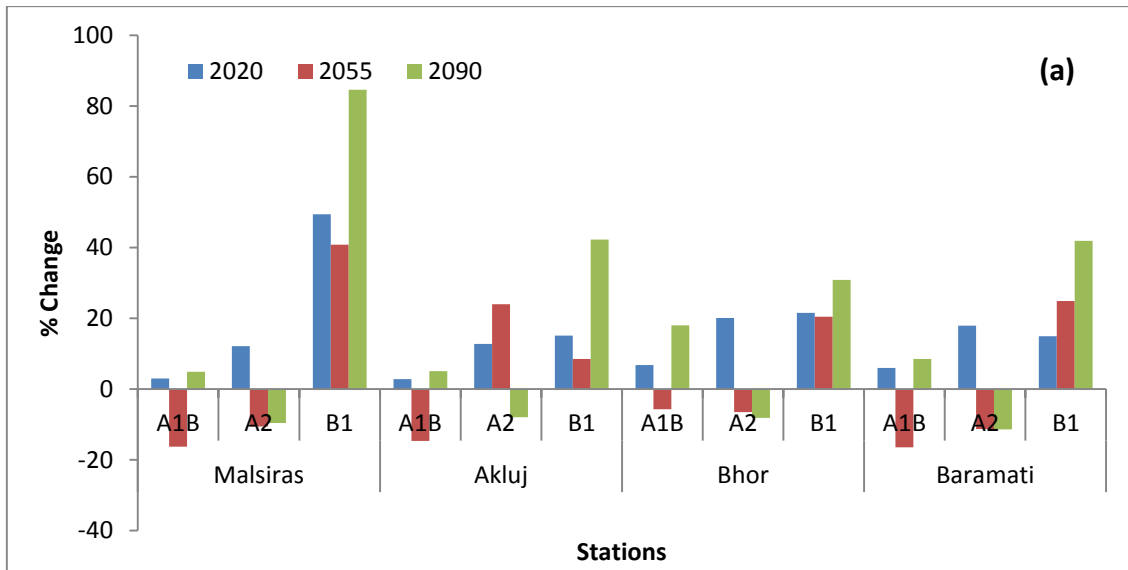
Figure 7.12 Changes in winter rainfall of at each a) stations and b) grid #4

The percent change in annual rainfall calculated at each station and, its corresponding grid are shown in figure 7.13. The annual rainfall is projected to increase for all scenarios over three time spans except at Malsiras for A2 and B1 scenarios in 2090s (figure 7.13a). For each time span, the A2 scenario shows greatest percent change in annual rainfall followed by B1 and A1B scenarios. In 2020s, annual rainfall is projected to change by 1.0 to 3.5% in A1B, 8.7 to 9.6% in A2 and -0.7 to 2.7% in B1 scenarios. In 2055s, annual rainfall is projected to increase by 13.33 to 15.14% in A1B, 13.68-15.26% in A2 and 4.30-7.79% in B1 scenarios. In 2090s, annual rainfall is projected to change by -1.31 to 13.34% in A1B; -4.74 to 17.57% in A2 and -5.29 to 10.28% in B1 scenarios. Overall, it is expected that the annual rainfall will increase in future at all the station as seen in figure 7.13.
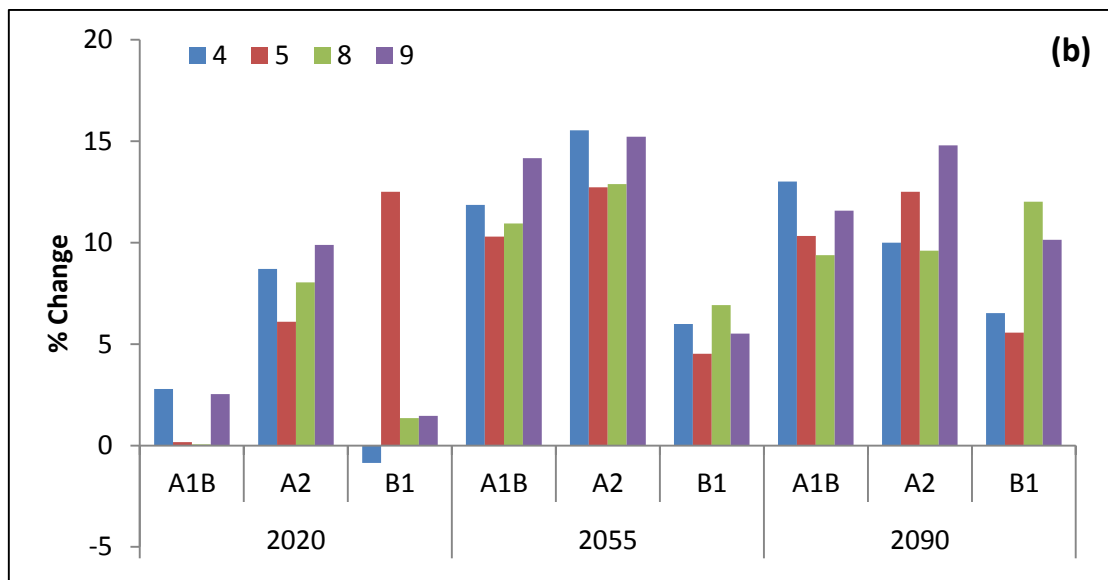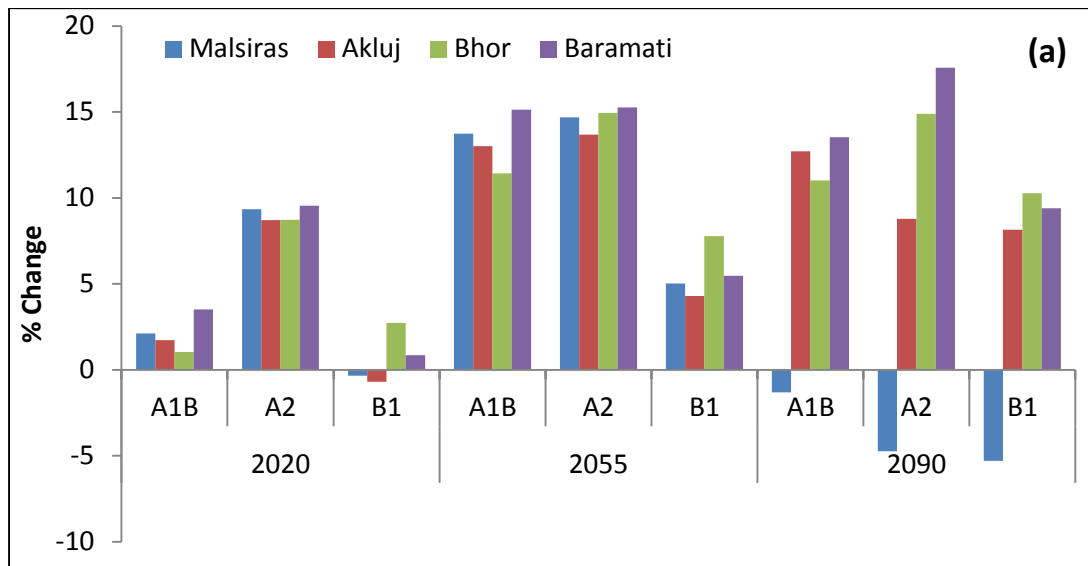
Figure 7.13 Changes in annual mean rainfall at the a) stations and b) grids

7.5.4 Comparison of observed and gridded rainfall data analysis

The results of the trend analysis, ENSO impacts and projected changes in future rainfall using station data were compared with the results obtained using gridded data. The results of gridded data are given in tables and figures of respective sections where the results of the observed data analysis are presented. Subsequent sections present this comparison:

7.5.4.1 Historical changes in Rainfall

The comparison of change in seasonal and annual rainfall between station and their respective grid data is given in table 7.2. The findings of this analysis are given below:

i. The pattern of seasonal trends of rainfall obtained from stations data matches with the trends obtained from respective grids.

ii. With stations data, significant trends were observed in seasonal rainfall whereas non-significant trends were observed in most of the grid-based seasonal rainfall data.

iii. Significant increasing trends were observed in station-based annual rainfall at Akluj, Bhor and Baramati; whereas the corresponding grid-based data resulted in non-significant increasing trends in annual rainfall.

iv. The percent changes in annual as well as seasonal rainfall series were greater in cases of station-based data compared to those from grid-based data.

7.5.4.2 Impact of ENSO on Monsoon Rainfall

i. The results of the tests used for assessing impact of ENSO on monsoon rainfall in grids #4, #8 and #9 matches closely with those for the corresponding stations. Table 7.2 shows that similar values of correlation coefficients were obtained between the monsoon rainfall and seasonal ENSO indices at the stations corresponding to the grids mentioned above. At stations Malsiras and Akluj, the monsoon rainfall has stronger correlation with seasonal ENSO indices as compared to the grid-based correlation.

ii. Monsoon season rainfall series were significantly different during ENSO phases (Table 7.3) at stations as well as their respective grids.

v. The percent changes in mean monsoon rainfall at all four grids during La Niña and El Niño phases are shown in figure 7.3. It is clearly seen that on an average more rainfall has been received during La Niña phase and less during El Niño phase in monsoon season at Malsiras, Akluj and Baramati and at their respective at grids #4, #5 and #9. However, the percentage change is higher in observed rainfall than the gridded rainfall.

7.5.4.3 Projected Changes in Future Rainfall

vi. The similar pattern of changes in seasonal rainfall were obtained between station (Malsiras, Bhor and Baramati) and their respective grid (gird #4, grid #8 and grid #9)

168

data (figure for Malsiras (Figure 7.9(a-b), Figure 7.11(a-b) and Figure 7.12(a-b)) except for Akluj and and its respective grid #4 (Figure 7.109a-b).

i.   The change in projected annual rainfall of stations of the Nira basin follows the similar pattern of change with annual rainfall of respective grids (Figure 7.13).

7.6 SUMMARY AND DISCUSSION

The comparison of observed and gridded rainfall data suggests that though similar patterns of results are obtained, risk is averaging out in gridded data. Observed data give better representation of changes within smaller sub-basin than the gridded data. Thus, it can be recommended that station-based (observed) data should be preferred over the gridded data whenever both are available for a basin. However, in case of limited data availability, gridded data can prove to be reliable in terms of identifying the general trends in the hydrometeorological series, and comparing the relative differences between various scenarios.

Furthermore, if stations are not well-distributed within the basin, they may not provide a clear understanding of spatial differences of climate across the entire basin. If the spatial distribution is important for the study, then a well-distributed station network should be chosen. In cases where such network does not exist, gridded data should be preferred. The resolution of gridded data seems to have direct effect on the magnitude of risk assessment. Also, caution should be used while using gridded data for risk assessments at scales similar to that of the Nira basin.

CHAPTER 8: CONCLUSIONS, LIMITATIONS AND SCOPE FOR FUTURE WORK

8.1 GENERAL

The impacts of future climate change on water resources and agriculture have become a world-wide concern these days. India and many other developing countries are expected to be seriously affected by the consequences of climate change (IPCC, 2001). Consequently, assessment of climate change impacts on hydrology and water resources are becoming an integral part of the water resources management and planning studies. In this context, assessment of the climate change impacts at basin-scale in the Bhima River basin, part of the Krishna River Basin (India), was undertaken as the PhD thesis work. The broad objectives of the work were (i) to study the variability of meteorological variables (i.e. temperature and rainfall) trends and their impacts on the streamflows in changing climate and (ii) to study the association of ENSO with the monsoon rainfall. Due to the limited availability of observed data in Bhima river basin, gridded dataset was used for the assessment of the climate change impacts. A comparison of the analyses performed using observed and gridded data for the nested Nira basin are also presented in the thesis. The major findings and inferences, limitations, and scope for future work are presented in the subsequent sections.

8.2 MAJOR FINDINGS

8.2.1 Spatio-temporal Variability of Meteorological Variables

The analysis of past temperature records showed decreasing trend in minimum temperatures during summer and winter seasons whereas an increasing trend during monsoon and post-monsoon seasons. However, the seasonal maximum and seasonal mean temperatures showed increasing and decreasing trends respectively. On an annual scale, minimum, maximum, and mean temperatures showed an increasing trend. The results indicated that the increase in the minimum temperatures of the basin is more pronounced than the decrease. This conclusion is in corroboration with other similar studies conducted for the Indian sub-continent. It was also observed that the upper and lower basin showed a comparatively higher increase in temperatures than the middle part of the basin.

The rainfall data was analysed in two time periods i.e. 1901-2004 and 1961-2004. This demarcation was done to capture the effect of increased anthropogenic activities in the latter half of the last century. Analysis of the seasonal rainfall data indicated that there is a decrease in the summer and winter rainfall during the 1901-2004 timescale whereas an increase in the monsoon and post monsoon rainfall during the same period. For the second time scale (1961-2004), it was seen that the summer and monsoon rainfall showed a decreasing trend while an increasing trend was found in the rainfall in the other two seasons. The decreasing monsoon rainfall is in consonance with the trends observed in the rest of the country.

The analysis of the data on annual basis shows that the rainfall increased over the last century (15% increase), however there is a decrease in the annual rainfall during 1961-2004 (11% decrease). There is considerable spatial variation in the rainfall data over the basin. While the central parts of the basin showed an increase in rainfall (1901-2004) the upper and lower parts showed decreasing trends of rainfall (1961-2004).

The difference in trends of seasonal rainfall series during the two timescales is indicative of the anthropological climate change in the later part of the century. These results assume a central interest in the water resources planning since most of the rainfall of the basin is concentrated in the monsoon months and the fact that agriculture is highly dependent on this rainfall. The rainfall in the other two seasons (post monsoon and winter) is seen to have increased in the later part of the century. The changes in the pattern of trends in rainfall is prominent in the two timescales, which gives credibility to the fact that the changing climate is affecting basin scale climatic processes and patterns.

8.2.2 Analysis of Relationship of Monsoon rainfall and ENSO

The monsoon rainfall showed significant correlation with the monsoon ENSO indices at majority of grid points in the basin. A significant positive correlation with the monsoon SOI and a negative correlation with monsoon MEI and N3.4 was found. The ANOVA tests implied that the means of monsoon rainfall during the three ENSO phases are significantly different from each other at most of the grids. Monsoon rainfall of the La Niña/El Niño phase was usually above/below the monsoon rainfall of the neutral phase. Overall the strong/weak monsoon rainfall was found associated with La Niña/ El Niño respectively. On an average 15% more rainfall was received during monsoon season during La Niña phase and 9% less during El

Niño phase in the basin. This finding will find prominence in the water allocation and management planning with prior knowledge of an impending La Niña/El Niño phase.

8.2.3 Impact of Climate Change on Meteorological Variables

Downscaling of future climatic conditions from 15 GCMs for three SRES scenarios (A1B, A2, and B1) and three time spans (i.e 2011-2030, 2046-2065 and 2080-2099) was performed using the LARS-WG software. The results were analysed to identify the future changes in the projected meteorological variables. The minimum and maximum temperatures of all seasons are projected to increase with a maximum increase in the A2 scenario and a minimum increase in the B1 scenario. The highest/lowest increases in minimum and maximum temperatures were observed in winter/monsoon season. Spatial pattern of change factors of annual minimum and maximum temperatures over the basin indicated a greater temperature rise in the middle part than that in the upper and lower parts.

There is considerable variation in the rainfall projections of the GCMs. However the seasonal rainfall was projected to increase at most of the grids. The annual rainfall projections indicated 3.2 to 18.4% increase with respect to the baseline period (i.e. 1961-1990). Overall, an increase in annual rainfall is projected across the entire basin, except for a small portion of the upper part of the basin.

8.2.4 Impact of Climate Change on Future Streamflow

The VIC model was setup for the study area using the data from different sources. After the satisfactory calibration and validation, the model was used to simulate future streamflows using the future projections of temperature and rainfall data. The analyses of the results show that the flows are likely to increase across all time spans and scenarios. This is in consonance with the overall trend of future rainfall. Analysis of future seasonal streamflows data indicated that the river flows are likely to increase in all the seasons expect during the post-monsoon season.

8.2.5 Comparative Analysis of Observed and Gridded datasets in Nira basin

Availability of sufficient hydrometeorological data is the major concern in the field of hydrology and climate change. Therefore, an attempt was made to compare the results of the climate change analysis on rainfall in the Nira basin using two rainfall datasets; observed dataset obtained from IMD and gridded dataset obtained from IMD. Four rainfall stations

namely Akluj, Baramati, Bhor and Malsiras were selected on the basis of available observed rainfall data (1901-2004) and the analysis of the records led to the following conclusions.

Significant increasing trends were detected in annual rainfall at 10% significance level for Akluj and Bhor stations. Seasonal rainfall in the basin increased especially during the monsoon and post-monsoon seasons. The monsoon months' rainfall is expected to slightly increase in future as compared to the pre-monsoon rainfall for all scenarios. Assessment of impact of ENSO on monsoon rainfall indicated that the monsoon rainfall in the region is correlated with the monsoon ENSO indices. In general, more rainfall was received during La Niña phase compared to El Niño phase.

The comparison of observed and gridded rainfall data suggested that the observed data give better representation of changes than the gridded data. Thus, it was concluded that the observed data should be preferred over the gridded data whenever both are available for a basin. However, in case of limited data availability, gridded data can also prove to be reliable in terms of identifying the general trends in the hydrometeorological series, and comparing the relative differences between various scenarios. Overall, it was concluded that results of the analysis carried out using observed rainfall data are in agreement with the findings of the gridded data.

8.3 LIMITATIONS OF WORK

The limitations of this research work are mentioned below:

- Trend analysis was carried out in the Bhima basin using only gridded data due to non-accessibility to the observed data.
- Extreme events were not analysed in trend detection.
- A single downscaling technique was used to downscale rainfall and temperature data.
- Long-term temperature trends could not be analysed due to non-availability of the data prior to 1969.
- Temperature datasets were available only at 1°x1° resolution from IMD, which were then interpolated to 0.25°x0.25° resolution using lapse rate to input in VIC model.
- IMD rainfall data at 0.25°x0.25° resolution was not available; hence, interpolated data using inverse distance weighting methods was used.

- The VIC model was calibrated using streamflow data of 1970-80 assuming the flow as natural flows.

- Land use/ land cover changes in future scenario have also not been incorporated.

8.4 SCOPE FOR FUTURE WORK

Following are some areas of future exploration of this work:

- Analysis of trends in hydrometeorological variables such as evaporation, wind speed to study the impact of changing climate
- Detailed study to analyse the differential behaviour of the impact of ENSO on rainfall in grid #8, grid#12 and at Bhor station
- Projection of hydrometeorological variables considering new RCPs
- Incorporation of Land use/ land cover change dynamics in VIC modelling
- Hydrological modelling with recently published 0.25°x0.25° resolution IMD data
- Analyses of irrigation and drinking water requirements and availability in future

Bibliography

Abdulla, F. A., Wood, E. F. and Smith, J. A. (1996). Application of a macro-scale hydrologic model to estimate the water balance of the Arkansas–Red River Basin. Journal of Geophysical Research, 101:7449-7459.

Aerts, J. C. J. H and Droogers, P. (2004). Climate change in contrasting river basins: adaptation strategies for water, food and environment. Wallingfrd: CABI.

Agrawala, S., Ota, T., Ahmed, A. U., Smith, J. and van Aalst. M. (2003). Development and Climate Change in Bangladesh: Focus on Coastal Flooding and the Sunderbans. Organization for Economic Co-operation and Development (OECD), Paris.

Albritton D., Meira Filho, G., Cubasch, U., Dai, X., Ding, Y., Griggs, D., Hewitson, B., Houghton, J., Isaksen, I., Karl, T., McFarland, M., Meleshko, V., Mitchell, J., Noguer, M., Nyenzi, B., Oppenheimer, M., Penner, J., Pollonais, S., Stocker, T. and Trenberth, K. (2001). Technical Summary. Climate Change 2001. The Scientific Basis. Contribution of WG 1 to the Third Assessment Report of the Intergovernmental Panel on Climate Change. J. T. Houghton, Y. Ding, D. J. Griggs, M. Noguer, P. J. van der Linden, X. Dai, K. Maskell, and C. A. Johnson, Eds., Cambridge University Press. 21-83.

Arnell, N. W. (1993). Data requirements for macroscale modeling of the hydrosphere, Macroscale Modeling of the Hydrosphere, IAHS Publ. No. 214:139-149.

Arnold, J.G., Srinivasan, R. Muttiah R.S. and Williams, J.R. (1998). Large are hydrologic modeling and assessment part I: Model development. Journal of American Water Resources Association, 34:73-89.

Arora, M., Goel, N. K. and Singh, P. (2005). Evaluation of temperature trends over India. Hydrological Sciences Journal, 50(1):81-93.

ASCE. (1993). Criteria for evaluation of watershed models. Journal of Irrigation Drainage Engineering, 119(3):429-442.

Babel, M. S., Agarwal, A., Swain, D. K. and Herath, S. (2011). Evaluation of Climate Change Impacts and Adaptation Measures for Rice Cultivation in Northeast Thailand. Climate Research, 46:137-146.

Bandyopadhyay, A., Bhadra, A., Raghuwanshi, N.S. and Singh, R. (2009). Temporal Trends in Estimates of Reference Evapotranspiration over India. Journal of Hydrologic Engineering, 14 (5):508-515.

Bannayan, M. and Hoogenboom, G. (2008). Predicting realizations of daily weather data for climate forecasts using the non-parametric nearest-neighbour re-sampling technique. International Journal of Climatology, 28 (10):1357-1368.

Barsugli, J., Anderson, C., Smith, J.B. and Vogel, J.M. (2009). Options for Improving Climate Modeling to Assist Water Utility Planning for Climate Change. White Paper, Water Utility Climate Alliance.

Basistha A., Arya D. S and Goel, N.K. (2008). Spatial Distribution of Rainfall in Indian Himalayas – A Case Study of Uttarakhand Region. Water Resources Management, doi: 10.1007/s11269-007-9228-2.

Basistha, A., Arya, D.S. and Goel, N.K. (2009). Analysis of Historical rainfall change in Indian Himalayas. International Journal of Climatology, 29:555-572.

Basistha, A., Goel, N.K., Arya, D.S. and Gangwar, S.K. (2007). Spatial Pattern of Trends in Indian Sub-divisional Rainfall. Jalvighyan Sameeksha, (22).

Bastola, S. (2013). Hydrologic impacts of future climate change on Southeast US watershed. Regional Envionmental Change, 13(1):131-139.

Bates, B.C., Kundzewicz, Z.W., Wu, S. and Palutikof, J.P. Eds., (2008). Climate Change and Water. Technical Paper of the Intergovernmental Panel on Climate Change. IPCC Secretariat, Geneva, pp 210.

Bergkamp, G., Orlando, B. and Burton, I. (2003). Change: Adaptation of Water Resources Management to Climate Change. IUCN, Gland, Switzerland

Bhave, A., Mishra, A. and Raghuwanshi, N. S. (2013). A combined bottom-up and top-down approach for assessment of climate change adaptation options. Journal of Hydrology, DOI: 10.1016/j.hydro

Bindoff, N., Willebrand, J., Artale, V., Cazenave, A., Gregory, J., Gulev, S., Hanawa, K., Le Quéré, C., Levitus, S., Nojiri, Y., Shum, C., Talley, L. and Unnikrishnan, A. (2007). Observations: Proof Oceanic climate change and sea level. In Solomon, S., Qin, D., Manning, M., Chen, Z., Marquis, M., Averyt, K. B., Tignor, M. And Miller, H. L. (Eds.) Climate Change 2007: The Physical Science Basis. Contribution of Working Group I to the Fourth Assessment Report of the Intergovernmental Panel on Climate Change. Cambridge, UK and New York, NY, USA; Cambridge University Press. 385-431.

Brekke, L.D., Kiang, J.E., Olsen, J.R., Pulwarty, R.S., Raff, D.A., Turnipseed, D.P., Webb, R.S. and White, K.D. (2009). Climate Change and Water Resources Management: A Federal Perspective. US Geological Survey Circular, 1331, 65p. ⟨http://pubs.usgs.gov/circ/1331/ ⟩

Brooks, R. H. and Corey, A. H. (1988). Hydraulic properties of porous media. Hydrology Papers, Colorado State University, 3.

Bruhn , J.A., Fry, W.E. and Fick, G.W. (1980). Simulation of daily weather using theoretical probability distributions. Journal of Applied Meteorology, 19(9):1029-1036.

Burn D. H., Cunderlik J. M. and Pietroniro A. (2004). Hydrological trends and variability in the Liard River basin. Hydrological Sciences–Journal–des Sciences Hydrologiques, 49:53–67

Burn, D. H. and Hesch, N. M. (2007). Trends in evaporation for the Canadian Prairies, Journal of Hydrology, 336:61-73.

Burn, D.H. and Hag Elnur, M.A. (2002). Detection of hydrological trends and variability. Journal of Hydrology, 255:107-122.

Carter, T.R., Parry, M.L., Harasawa, H. and Nishioka, S. (1994). Inte-gevernmental panel on climate change technical guidelines for assessing climate change impacts and

adaptation. University College London and Center for Global Environmental Research, London.

Chattopadhyay, N. and Hulme, M. (1997). Evaporation and potential evapotranspiration in India under conditions of recent and future climate change. Agricultural and Forest Meteorology, 87:55-73.

Chaudhary A. and Abhyankar V. P. (1979). Does precipitation pattern foretell Gujarat climate becoming arid. Mausam, 30:85-90.

Chen, F. and Dudhia, J. (2001): Coupling an advanced land surface–hydrology model with the Penn State–NCAR MM5 Modeling System. Part I: Model implementation and sensitivity. Monthly Weather Review, 129:569-585.

Chiew, F. and McMahon, T. (2002). Global ENSO-streamflow tele-connection, streamflow forecasting and inter-annual variability. Hydrological Sciences-Journal-des Sciences Hydrologiques 47(3):505-522.

Cigizoglu, H.K., Bayazıt, M. and Önöz, B. (2005). Trends on the maximum, mean and low flows of Turkish rivers. Journal of Hydrometeorology 6:280-295.

Coulibaly, P., Dibike, Y.B. and Anctil F. (2005). Downscaling precipitation and temperature with temporal neural networks. Journal of Hydrom-eteorology 6 (4):483-496.

Cunderlik, J.M. and Burn, D.H. (2004). Linkages between Regional Trends in Monthly Maximum Flows and Selected Climatic Variables, ASCE Journal of Hydrologic Engineering, 9(4):246-256.

Cunderlik, M.J. (2003). Hydrologic model selection fort the CFCAS project: Assessment of water resources risk and vulnerability to changing climatic conditions, Project Report I. University of Western Ontario, Canada.

Dadhwal, V.K., Aggarwal, S.P. and Mishra, N. (2010). Hydrological Simulation Of Mahanadi River Basin and Impact of Land Use / Land Cover Change On Surface Runoff Using A Macro Scale Hydrological Model. In: Wagner W., Székely, B. (eds.): ISPRS TC VII

Symposium – 100 Years ISPRS, Vienna, Austria, July 5–7, 2010, IAPRS, Vol. XXXVIII, Part 7B, 165-170.

Dai, A., Del Genio, A. D. and Fung, I.Y. (1997). Clouds, precipitation and temperature range. Nature, 386:665-666.

Dash S. K., Jenamani R. K., Kalsi S. R. and Panda S. K. (2007). Some evidence of climate change in twentieth-century India. Climatic Change, 85:299-321.

Daubechies, I. (1992). Ten lectures on Wavelets. CSBM-NSF Series Application Mathematics, vol. 61. SIAM Publication, Philadelphia, PA (pp357).

De Luis, M., Raventós, J., González-Hidalgo, J.C., Sánchezand, J. R. and Cortina, J. (2000). Spatial analysis of rainfall trends in the region of Valencia (east Spain). International Journal of Climatology, 20 (12):1451-1469.

Dettinger, M.D. and Diaz, H.F. (2000). Global characteristics of stream flow seasonality and variability. Journal of Hydrometeorology 1: 289–310, DOI: 10.1175/1525-7541(2000)001<0289: GCOSFS>2.0.CO; 2

Dickinson, R. E., Henderson-Sellers, A., Kennedy, P. J. and Wilson, M. F. (1986). Biosphere-atmospherteransfer scheme (BATS) for the NCAR community climate model. NCAR Tech. Note TN-275 +STR.

Dolman, A. J., Hall, A. J., Kavvas, M. L., Oki, T. and Pomeroy, J. W. (Eds.), (2001). Soil-Vegetation-Atmosphere Transfer Schemes and Large-Scale Hydrological Models. IAHS Publ. No 270, pp 372.

Douglas, E. M., Vogel, R. M. and Kroll, C. N. (2000). Trends in floods and low flows in the United States: impact of spatial correlation. Journal of Hydrology, 240: 90-105.

Duband, D., Obled, Ch. and Rodriguez, J. Y. (1993). Unit-hydrograph revised - an alternate iterative approach to UH and effective precipitation identification. Journal of Hydrology, 150(1):115-149.

Dümenil, L. and Todini, E. (1992). A rainfall–runoff scheme for use in the Hamburg climate model. Advance Theoretical Hydrology, 9:129-157.

Easterling, D. R., Horton, B., Philip D. J., Peterson, T.C., Karl, T. R., Parker, D. E., Salinger, J. M., Razuvayev, V., Plummer, N., Jamason, P. and Folland, C. K. (1997). Maximum and minimum temperature trends for the globe. Science, 277:364-367.

Engeland, K., Gottschalk, L. and Tallaksen, L. (2001). Estimation of regional parameters in a macro scale hydrological model. Nordic Hydrology 32:161-180.

Fall, S.G, Watts, A., Nielsen-Gammon, J., Jones, E., Niyogi, D., Christy, J. and Pielke Sr., R. A. (2011). Analysis of the impacts of station exposure on the U.S. Historical Climatology Network temperatures and temperature trends. Journal of Geophysical Research, doi:10.1029/ 2010JD015146

Franchini, M. and Pacciani, M. (1991). Comparative-analysis of several conceptual rainfall runoff models. Journal of Hydrology, 122(1-4):161-219.

Frans, C., Istanbulluoglu, E., Mishra, V., Munoz-Arriola, F., and Lettenmaier, D.P. (2013). Are climatic or land cover changes the dominant cause of runoff trends in the Upper Mississippi River Basin?. Geophysical Research Letter, 1-7.

Frederick, K.D. and Gleick, P.H. (1999). Water and Global Climate Change: Potential Impacts on U.S. Water Resources. Pew Center on Global Climate Change, Arlington, VA.

Ghosh, S. and Mujumdar, P. P. (2009). Climate Change Impact Assessment- Uncertainty Modeling with Imprecise Probability. Journal of Geophysical Research - Atmospheres, 114, D18113, doi:10.1029/2008JD011648.

Ghosh, S. and Mujumdar, P.P. (2008). Statistical Downscaling of GCM Simulations to Streamflow using Relevance Vector Machine. Advances in Water Resources, 31(1):132-146.

Ghosh, S., Raje, D. and Mujumdar, P. P. (2010). Mahanadi Streamflow: Climate Change Impact Assessment and Adaptive Strategies. Current Science, 98(8):1084-1091.

Gleick, P. H. (1989). Climate change, hydrology, and water resources, Reviews of Geophysics, 27(3):329-344.

Graedel, T.E. and Crutzen, P.J. (1993). Atmospheric Change: An earth system perspective. W.H. Freeman and Company, New York, pp 446.

Graham, L. P. (2004). Climate change effects on river flow to the Baltic Sea. AMBIO, 33:235-241.

Haan, C.T. (1995). Statistical Methods in Hydrology. Iowa State University Press, pp 378.

Haigh, M.J. (2004). Sustainable management of headwater resources: the Nairobi headwater declaration (2002) and beyond. Asian Journal of Water, Environ. Pollution, 1 (1-2):17-28.

Hamed, K.H. and Rao. A.R. (1998). A Modified Mann-Kendall Trend Test for Auto correlated Data. *Journal of* Hydrology, 204:182-196.

Hamlet, A. F. and Lettenmaier, D. P. (1999). Effects of climate change on hydrology and water resources in the Columbia River basin. Journal of American Water Resources Association, 35:1597-1623.

Hartkamp, A.D. White, J.W. and Hoogenboom. G.(2003). Comparison of three weather generators for crop modeling: a case study for subtropical environments. Agricultural System, 76:539-560.

Hartmann, D.L., A.M.G. Klein Tank, M. Rusticucci, L.V. Alexander, S. Brönnimann, Y. Charabi, F.J. Dentener, E.J. Dlugokencky, D.R. Easterling, A. Kaplan, B.J. Soden, P.W. Thorne, M. Wild and P.M. Zhai, 2013: Observations: Atmosphere and Surface. In: Climate Change 2013: The Physical Science Basis. Contribution of Working Group I to the Fifth Assessment Report of the Intergovernmental Panel on Climate Change [Stocker, T.F., D. Qin, G.-K. Plattner, M. Tignor, S.K. Allen, J. Boschung, A. Nauels, Y. Xia, V. Bex and P.M. Midgley (eds.)]. Cambridge University Press, Cambridge, United Kingdom and New York, NY, USA

Helsel, D.R. and Hirsch, R.M. (2002). Statistical Methods in Water Resources. United States Geological Survey, 524

Hirsch, R. M., Slack, J. R. and Smith, R.A. (1982). Techniques of trend analysis for monthly water quality data. Water Resources Research, 18(1):107-121.

Houghton, J. T., Ding, Y., Griggs, D. J., Noguer, M., van der Linden, P. J., Dai, X., Maskell, K. and Johnson, C. A. (Eds.) (2001). Climate Change 2001: The Scientific Basis. Cambridge Univ. Press, New York.

Hulme, M., Mitchell, J.F.B., Ingram, W., Johns, T.C., Lowe, J.A., New, M.G. and Viner, D. (1999). Climate change scenarios for global impacts studie. Global Environmental Change, (9): S3-S19.

IPCC (2007a) Report of the 26th session of the IPCC. Bangkok. April 30–May 4 2007. Intergovernmental Panel on Climate Change, Geneva, Switzerland.

IPCC, (2001). Climate Change 2001: Impacts, Adaptation, and Vulnerability. Contribution of WG II to TAR of the Intergovernmental Panel on Climate Change [McCarthy, M.C., O.F. Canziani, N.A. Leary, D.J. Dokken and K.S. White (eds.)] Cambridge, pp 1031.

IPCC, (2001a). Climate Change 2001: The scientific basis. Contribution of Working Group I to the Third Assessment report of the Intergovernmental Panel on Climate Change [Houghton, J.T., Y. Ding, D.J. Griggs, M. Noguer, P.J. van der Linden, X. Dai, K. Maskell and C.A. Johnson (eds.)]. Cambridge University Press, Cambridge, pp 881.

IPCC, (2001b). Climate Change 2001: Synthesis Report. Contribution of Working Groups I, II, and III to the Third Assessment Report of the Intergovernmental Panel on Climate Change [Watson, R.T. and the Core Writing Team (eds.)]. Cambridge University Press, Cambridge, pp 398.

IPCC, (2007). Climate Change 2007: The Physical Science Basis. Contribution of Working Group I to the Fourth Assessment Report of the Intergovernmental Panel on Climate Change [Solomon, S., D. Qin, M. Manning, Z. Chen, M. Marquis, K.B. Averyt, M.Tignor and H.L. Miller (eds.)]. Cambridge University Press, Cambridge, United Kingdom and New York, NY, USA.

IPCC. (2001). Climate change (2001). Impacts, Adaptation and Vulnerability. Third assessment report: report of working group II. [McCarty, M.C., O.F. Canziani, N.A. Leary, D.J. Dokken and K.S. White (eds.)] Cambridge, UK, Cambridge University Press.

IPCC-TGICA. (2007). General Guidelines on the Use of Scenario Data for Climate Impact and Adaptation Assessment. Version 2. Prepared by T.R. Carter on behalf of the Intergovernmental Panel on Climate Change, Task Group on Data and Scenario Support for Impact and Climate Assessment.

Jagannathan, P. and Parthasarathy, B. (1973). Trends and periodicities of rainfall over India. Monthly Weather Review, 101:371-375.

Jain, S. K. and Kumar, V. (2012). Trend analysis of rainfall and temperature data for India. Current Science, 102(1):37-49.

Jin K., Speed T. P. and Thomson, G. (1995). Tests of Random Mating for a Highly Polymorphic Locus: Application to HLA Data. Biometrics, 51(3):1064-1076.

Kahya, E. and Kalayci, S. (2004). Trend analysis of streamflow in Turey. Journal of Hydrology, 289:28-144.

Kane, R. P. (1997). Relationship of El Niño Southern Oscillation and Pacific Sea Surface Temperature with rainfall in various Regions of the globe. Monthly Weather Review, 125:1792-1800.

Kane, R. P. (1999). Rainfall extremes in some selected parts of Central and South America: ENSO and other relationships reexamined. International Journal of Climatology, 19:423-455.

Kendall, M. G. (1955). Rank Correlation Methods. Griffin, London

Khattak, M. S., Babel, M. S. and Sharif, M. (2011). Hydro-meteorological Trends in Upper Indus River Basin in Pakistan. Climate Research, 46:103-119.

Kiladis, G. and Diaz, H. (1989). Global climatic anomalies associated with extremes in the Southern Oscillation. Journal of Climate, 2:1069-1090.

Kilsby, C.G., Jones, P. D., Burton, A., Ford, A.C., Fowler, H.J., Harpham, P., James, C, Smith A and Wilby R.L. (2007). A daily weather generator for use in climate change studies. Environmental M odelling and Software, 22:1705-1719.

Kite, G. (1998). Land surface parameterizations of GCMs and macro-scale hydrological models. Journal of American Water Resources Association, 34:1247-1254.

Kittel, T.G.F., Rosenbloom, N.A., Painter, T.H., Schimel D.S. and VEMAP Modeling Participants, (1995). The VEMAP integrated database for modeling United States ecosystem/vegetation sensitivity to climate change. Journal of Biogeography, (22):857-862.

Koteswaram P. and Alvi S. M. A. (1969). Secular trends and periodicities in rainfall at west coast stations in India. Current Science, 38:229-231.

Kothawale, D. R., Munot, A. A. and Krishna Kumar, K. (2010). Surface air temperature variability over India during 1901–2007, and its association with ENSO. Climate Research, 42:89-104.

Kothyari, U.C. and Singh, V. P. (1996). Rainfall and Temperature trends in India. Hydrological Processes, (10):357-372.

Krasovskaia, I. (1995). Quantification of the stability of river flow regimes. Hydrological Sciences Journal, 40:587-598.

Krishna Kumar, K., Rajagopalan, B., Hoerting M., Bates G., and Cane, M. A. (2006). Unraveling the mystery of Indian monsoon failure during El Niño. Science, 314:115-119.

Krishna Kumar, K., Rajagopalan, B. and Cane, M. A. (1999). On the weakening relationship between the Indian monsoon and ENSO. Science, 284:2156-2159.

Kuhl, S. C. and Miller, J. R. (1992). Seasonal river runoff calculated from a global atmospheric model. Water Resources Research, 28:2029-2039.

Kumar K R, Kumar K K and Pant G B 1994 Diurnal asymmetry of surface temperature trends over India; Geophysical Research. Letter, 21:677-680.

Kumar, P., Rupa Kumar, K., Rajeevan, M., and Sahai, A.K. (2007). On the recent strengthening of the relationship between ENSO and northeast monsoon rainfall over South Asia. Climate Dynamics, 28:649-660.

Kumar, V. and Jain ,S. K. (2010). Trends in seasonal and annual rainfall and rainy days in Kashmir valley in the last century. Quaternary International, 212:64-69.

Kumar, V. and Jain, S.K. (2011).Trends in rainfall amount and number of rainy days in river basins of India (1951 – 2004). Hydrological Research, 42(4):290-306.

Kumar, V., Jain, S. K. and Singh, Y. (2010). Analysis of long-term rainfall trends in India. Hydrological Sciences Journal, 55(4):484-496.

Kumar, V., Singh, P. and Jain, S. K. (2005). Rainfall trends over Himachal Pradesh, Western Himalaya, India. In: Development of Hydro Power Projects – A Prospective Challenge. Conference, Shimla, 20–22 April, 2005.

Lal, M. (2001). Climatic change – implications for India's water resources. Journal of Indian Water Resource Society, 21:101-119.

Latif M, Coauthors (2001). ENSIP: The El Niño Simulation Inter-comparison Project. Climate Dynamics, 18:255-276.

Leavesley, G.H. (1994). Modeling the effects of climate change on water resources- a review. Climatic Change, 28(1):159-177.

Legates, D. R. and McCabe, G. J. (1999). Evaluating the use of "goodness-of-fit" measures in hydrologic and hydroclimatic model validation. Water Resources Research, 35(1): 233-241.

Lettenmaier, D. P., Wood, E. F. and Wallis, J. R. (1994). Hydroclimatological trends in the continental United States, 1948-1988. Journal of Climate, 7:586-607.

Liang X., Lettenmaier, D. P. and Wood, E. F. (1996a). Surface soil moisture parameterization of the VIC-2L model: evaluation and modification. *Global Planet. Change* 13:195–206, DOI: 10.1016/0921-8181(95)00046-1.

Liang, X., Lattenmaier, D.P., Wood, E.F. and Burgess, S.J., (1994). A simple hydrologically based model of land surface, water, and energy flux for general circulation models. Journal of Geophysical Research, 99(D7):14,415-14,428.

Liang, X., Lettenmaier, D. P., Wood, E. F. and Burges, S. J. (1994), A simple hydrologically based model of land surface water and energy fluxes for general circulation models, Journal of Geophysical Research, 99(D7), 14415-14428, doi:10.1029/94JD00483.

Liang, X., Lettenmaier, D. P. and Wood, E. F. (1996). One-dimensional statistical dynamic representation of subgrid spatial variability of precipitation in the two-layer variable infiltration capacity model, Journal of Geophysical Research, 101(D16):21403-21422. doi:10.1029/96JD01448.

Lim, H.S., Boochabun, K. and Ziegler, A.D. (2012). Modifiers and Amplifiers of High and low Flows on the Ping River in Northern Thailand (1921– 2009): The Roles of Climatic Events and Anthropogenic Activity. Water Resource Management DOI 10.1007/s11269-012-0140-z.

Lin, E.D., Zhang, H.X. and Wang, J.H. (eds). (1997). Simulation of Impact of Global Climate Change on Chinese Agriculture (in Chinese). Chinese Agricultural and Scientific Publishing House, Beijing

Liston, G. E., Sud, Y. C. and Wood, E. F. (1994). Evaluating GCM land surface hydrology parameterizations by computing river discharges using a runoff routing model. Journal of Applied Meteorology, 33:394-405.

Lohmann, D., Nolte-Holube, R. and Raschke, E. (1996). A large scale horizontal routing model to be coupled to land surface parameterization schemes. Tellus, (48A):708-721

Lohmann, D.E., Raschke, Nijssen, B. and Lettenmaier, D.P. (1998). Regional scale hydrology: II. Application of the VIC-2L model to the Weser river, Germany. Hydrological Sciences, 43(1):143-158.

Mahmood, R. and Babel, M. S. (2012). Evaluation of SDSM Developed by Annual and Monthly Sub-models for Downscaling of Max Temperature, Min Temperature and

Precipitation in Jhelum River Basin, Pakistan. Theoretical and Applied Climatology, DOI 10.1007/s00704-012-0765-0. Published online 25 September 2012.

Mann, H.B. (1945). Non-parametric tests against trend. Econometrica, 13:245-259.

Martìnez-Meyer, E. (2005). Climate change and biodiversity: some consideration in forecasting shifts in species' potential distributions. Biodiversity Informatics, 2:42-55.

Mearns L. O., Schneider S.H., Thompson S.L., McDaniel L.R., (1990). Analysis of climate variability in general circulation models: comparison with observation and changes in variability in CO_2 experiments. Journal of Geophysical Research, 95:20469-20490.

Meehl, G. A., Covey, C., Delworth, T., Latif, M., McAvaney, B., Mitchell, J. B. F., Stouffer, R. J. and Taylor, K. E. (2007a). The WCRP CMIP3 multi-model dataset: a new era in climate change research. Bulletin of the American Meteorological Society, 88:1383-1394.

Meehl, G. A., et al. (2007b). Global climate projections. Pages 747–845 in S. Solomon, D. Qin, M. Manning, Z. Chen, M. Marquis, K. B. Averyt, M. Tignor, and H. L. Miller, editors. "Climate change 2007: the physical science basis. Contribution of Working Group I to the Fourth Assessment Report of the Intergovernmental Panel on Climate Change. Cambridge University Press, Cambridge, UK.

Meehl, G.A., T.F. Stocker, W.D. Collins, P. Friedlingstein, A.T. Gaye, J.M. Gregory, A. Kitoh, R. Knutti, J.M. Murphy, A. Noda, S.C.B. Raper, I.G. Watterson, A.J. Weaver and Z.C. Zhao, (2007). Global Climate Projections. In: Climate Change 2007: The Physical Science Basis. Contribution of Working Group I to the Fourth Assessment Report of the Intergovernmental Panel on Climate Change. [Solomon, S., D. Qin, M. Manning, Z. Chen, M. Marquis, K.B. Averyt, M. Tignor and H.L. Miller (eds.)]. Cambridge University Press, Cambridge, United Kingdom and New York, USA.

Meenu, R., Rehana, S. and Mujumdar, P. P. (2013). Assessment of hydrologic impacts of climate change in Tunga-Bhadra river basin, India with HEC-HMS and SDSM. Hydrological Processes, 27(11):1572-1589.

Miital, N., Mishra, A. and Singh, R. (2013). Combining climatological and participatory approaches for assessing changes in extreme climatic indices at regional scale. Climate Change, 119:603-615.

Miller, J. R., Russell, G. L. and Caliri, G. (1994). Continental-scale river flow in climate models. Journal of Climate, 7:914-928.

Mishra, A., Singh, R., Raghuwanshi, N. S., Chatterjee, C., and Froebrich (2013). Spatial variability of climate change impacts on yields of rice and wheat in the Indian Ganga basin. Journal of Science of Total Environment, 468-469:S132-S138.

Mishra, V. and Lettenmaier, D.P. (2011). Climatic trends in major US urban areas, 1950–2009. Geophysical Research Letter, 38.

Mishra, V., Cherkauer, K.A. and Bowling, L.C. (2010). Parameterization of lakes and wetlands for energy and water balance studies in the Great Lakes region. Journal of Hydrometeorology, 11:1057-1082.

Mishra, V., Cherkauer, K.A. and Bowling, L.C. (2011c). Changing thermal dynamics of lakes in the Great Lakes region: Role of ice cover feedbacks. Global Planetary Change, 75:155-172.

Mishra, V., Cherkauer, K.A. and Shukla, S. (2010b). Assessment of drought due to historic climate variability and projected future climate change in the midwestern United States. Journal of Hydrometeorology, 11: 46-68.

Mishra, V., Cherkauer, K.A., Niyogi, D., Lei, M., Pijanowski, B.C., Ray, D.K., Bowling, L.C. and Yang, G. (2010a). A regional scale assessment of land use/land cover and climatic changes on water and energy cycle in the upper Midwest United States. International Journal of Climatology, 30:2025-2044.

Mishra, V., Wallace, J.M. and Lettenmaier, D.P. (2012c). Relationship between hourly extreme precipitation and local air temperature in the United States. Geophysical Research Letter, 39.

Misir, V., Arya, D. S. and Murumkar, A.R, (2013). Impact of ENSO on River Flows in Guyana. Water Resource Management, 27:4611-4621. DOI: 10.1007/s11269-013-0430-0.

Mitchell, J.F.B., Karoly, D.J., Hegerl, G.C., Zwiers, F.W., Allen, M.R. and Marengo, J. (2001). Detection of Climate Change and Attribution of Causes. In: C.A. Johnson (Editor), Climate Change 2001: The Scientific Basis. Contribution of Working Group I to the Third Assessment Report of the Intergovernmental Panel on Climate Change. Cambridge University Press, Cambridge, UK, 695-738.

Mitchell, T.D. and Jones, P.D. (2005). An improved method of constructing a database of monthly climate observations and associated high-resolution grids. International Journal of Climatology, 25:693-712.

Mooley, D. A. and Parthasarthy, B. (1984). Fluctuations of all India summer monsoon rainfall during 1871–1978. Climatic Change, 6:287-301.

Moriasi, D. N., Arnold, J.G., Van Liew, M. W., Bingner, R. L., Harmel, R.D, and Veith, T. L. (2007). Model Evaluation guidelines for systematic quantification of Accuracy in Watershed Simulation. American Society of Agricultural and Biological Engineers, 50(3):885-900.

Moss, R.H., Edmonds, J. A., Hibbard, K.A., Manning, M.R., Rose, S.K., Detlef P. van Vuuren, Carter, T.R., Emori, S., Kainuma, M., Kram, T., Meehl, G. A., Mitchell, J. F. B., Nakicenovic, N., Riahi, K., Smith, S.J., Stouffer, R.J., Thomson, A. M., Weyant, J.P., Wilbanks, T.J., (2010). The next generation of scenarios for climate change research and assessment. Nature, 463: 747-756. doi:10.1038/nature08823.

Mujumdar, P. P. and Ghosh, S. (2008). Modeling GCM and scenario uncertainty using a possibilistic approach: Application to the Mahanadi River, India. Water Resources Research, 44, W06407, doi:10.1029/2007WR006137.

Murumkar, A., Arya, D.S. and Rahman, M.M. (2013). Seasonal and Annual Variations of Rainfall Pattern in the Jamuneswari Basin, Bangladesh. On a Sustainable Future of the Earth's Natural Resources (ed.), Springer Earth System Sciences, DOI 10.1007/978-3-642-32917-3_19, Springer-Verlag Berlin Heidelberg, 2013, pp. 349-362.

Nakicenovic, N., Alcamo, J., Davis, G., de Vries, H.J.M., Fenhann, J., Gaffin, S., Gregory, K., Grubler, A., Jung, T.Y., Kram, T., La Rovere, E.L., Michaelis, L., Mori, S., Morita, T., Papper, W., Pitcher, H., Price, L., Riahi, K., Roehrl, A., Rogner, H-H., Sankovski, A., Schlesinger, M., Shukla, P., Smith, S., Swart, R., van Rooijen, S., Victor, N. and Dadi. Z. and Swart, R. (Eds.), (2000). Special Report on Emissions Scenarios, IPCC, Cambridge University Press, Cambridge, UK, 2000. pp 570.

Narayanana P., Basistha, A., Sarkar, S. and Sachdevaa, K. (2013). Trends analysis and ARIMA modelling of pre-monsoon rainfall data for western India. Comptes Rendus Geoscience, 345:22-27.

Nash, J. E. and Sutcliffe, J. V. (1970). River flow forecasting through conceptual models part I -A discussion of principles. Journal of Hydrology, 10 (3): 282–290. DOI: 10.1016/0022-1694(70)90255-6.

Neena, D. (1998). Inter-state variation in cropping pattern in India. Indian Journal of Regional. Science, 30:57-69.

Nicks, A.D. and Harp, J.F. (1980). The stochastic generation of temperature and solar radiation data. Journal of Hydrology, 48:1-17.

Nijssen, B., Lettenmaier, D. P., Liang, X., Wetzel, S. W. and Wood, E. F. (1997). Streamflow simulation for continental-scale river basins. Water Resources Research, 33:711-724.

Oliver, J. E. and Hidore, J. J. (2003). Climatology: An Atmospheric Science. Pearson Education, New Delhi, pp 410.

Pant, G.B. and Rupa Kumar, K. (1997). Climates of South Asia. John Wiley & Sons, Chichester, pp 320.

Park, J. and Mann, M.E., (2000). Interannual temperature events and shifts in global temperature: a multiple wavelet correlation approach. Earth Interactions, 19:391-403.

Parry, M. L. (2007). Climate Change 2007: Impacts, adaptation and vulnerability: contribution of Working Group II to the fourth assessment report of the Intergovernmental Panel on Climate Change. UK: Cambridge University Press.

Partal T. and Kahya E. (2006). Trend analysis in Turish precipitation data. Hydrological Processes, 20:2011-2026.

Patra, J., Mishra, A., Singh, R. and Raghuwanshi, N. S. (2012). Detecting rainfall trends in twentieth century (1871-2006) over Orissa State, India. Climate Change, DOI 10.1007/s10584-0

Pattanaik, D.R. (2007). Analysis of deficient and excess rainfall over different homogeneous regions of India in relation to variability in westward movement frequency of monsoon depression. Natural Hazards, 40:635-646.

Penalba, O.C. and Vargas, W.M. (2004). Interdecadal and interannual variations of annual and extreme precipitation over central-northeastern Argentina. International Journal of Climatology, 24:1565-1580.

Pierce, D. W., Barnett, T.P., Santer, B.D. and Gleckler P.J., (2009). Selecting global climate models for regional climate change studies. – Proceeding National Academy Science, USA 106: 8441- 8446.

Pisoft, P., Kalvova, J. and Brazdil, R. (2004). Cycles and trends in the Czech temperatures series using wavelet transform. International Journal of Climatology, 24:1661-1670.

Polikar, R. (1999). In: Mastorakis, N. (Ed.), The story of wavelets, in physics and modern topics in mechanical and electrical engineering. World Scientific and Engineering Society Press, pp. 192-197.

Poveda German, and Mesa, and Oscar, J. (1997). Feedbacks between Hydrological Processes in Tropical South America and Large-Scale Ocean-Atmospheric Phenomena. Journal of Climate, 10:2690-2701.

Prentice, I.C., Farquhar, G.D., Fasham, M.J.R., Goulden, M.L., Heimann, M., Jaramillo, V.J., Kheshgi, H.S., Le Quéré, C., Scholes, R.J. and Wallace, D.W.R. (2001). The carbon cycle and atmospheric carbon dioxide. In: Climate Change 2001: The Scientific Basis. Contribution of Working Group I to the Third Assessment Report of the Intergovernmental Panel on Climate Change [J.T. Houghton, Y. Ding, D.J. Griggs, M.

Noguer, P.J. van der Linden, X. Dai, K. Maskell, and C.A. Johnson (eds.)]. Cambridge University Press, Cambridge, United Kingdom and New York, NY, USA, 183-237.

Racsko, P., Szeidl, L. and Semenov, M. (1991). A serial approach to local stochastic weather models. Ecological Modelling, 57:27-41.

Raghavendra, V. K. (1974). Trends and periodicities of rainfall in sub-divisions of Maharashtra state. Indian Journal of Meteorology and Geophysics, 25:197-210.

Raje, D. and Mujumdar, P. P. (2010). Hydrologic drought prediction under climate change: Uncertainty modeling with Dempster-Shafer and Bayesian approaches. Advances in Water Resources, doi: 10.1016 / j.advwatres.2010.08.001

Raje, D. and Mujumdar, P. P. (2010). Reservoir performance under uncertainty in hydrologic impacts of climate change. Advances in Water Resources, 33(3): 312-326. doi:10.1016 /j.advwatres.2009.12.008

Raje, D. and Mujumdar, P. P. (2010a). Constraining uncertainty in regional hydrologic impacts of climate change: nonstationarity in downscaling. Water Resources Research, 46, W07543, doi:10.1029/2009WR008425.

Raje, D. and Mujumdar, P. P. (2011). A comparison of three methods for downscaling daily precipitation in the Punjab region. Hydrological Processes, 25 (23):3575-3589.

Rajeevan, M., Bhate, J. and Jaswal A. K. (2008), Analysis of variability and trends of extreme rainfall events over India using 104 years of gridded daily rainfall data, Geophysical Research Letter, 35, L18707, doi:10.1029/2008GL035143.

Rajeevan, M., Bhate, J., Kale, J.D. and Lal, B. (2006). High resolution daily gridded rainfall data for the Indian region: Analysis of break and active monsoon spells. Current Science, 91(3):296-306.

Ramesh, K.V.and Goswami, P. (2007). Reduction in temporal and spatial extent of the Indian summer monsoon. Geophysical Research letter, 34, L23704, doi:10.1029/2007 GL031613.

Randall, D. A., Wood, R. A., Bony, S., Colman, R., Fichefet, T., Fyfe, J., Kattsov, V., Pitman, A., Shukla, J., Srinivasan, J., Stouffer, R. J., Sumi, A. and Taylor, K.E. (2007). Climate Models and Their Evaluation, in Climate Change 2007: The Physical Science Basis. Contribution of Working Group I to the Fourth Assessment Report of the Intergovernmental Panel on Climate Change", edited by S. [Solomon, D. Qin, M. Manning,Z. Chen, M. Marquis, K.B. Averyt, M.Tignor and H.L. Miller], pp. 589-662, Cambridge University Press, Cambridge.

Rao, A.R., Hamed, K.H. and Chen, H.L. (2003). Nonstationarities in Hydrologic and Environmental Time Series. Kluwer Academic Publishers, The Netherlands, pp 362.

Rasmusson, E.M., and Carpenter, T.H., (1983). The relationship between the eastern sea surface temperature and rainfall over India and Sri Lanka. Monthly Weather Review, 111:517-528.

Raucher, R.S., (2011). The Future of Research on Climate Change Impacts on Water: A Workshop Focused on Adaption Strategies and Information Needs. Water Research Foundation. ⟨http://www.waterrf.org/projectsreports/publicreportlibrary/4340.pdf ⟩.

Rehana, S. and Mujumdar, P.P. (2013). Regional impacts of climate change on irrigation water demands. Hydrological Processes, 27 (20):2918-2933.

Richardson, C.W. (1981). Stochastic Simulation of Daily Precipitation, Temperature, and Solar Radiation. Water Resources Research, 17:182-190.

Richardson, C.W. and Wright, D.A. (1984). WGEN: A model for generating daily weather variables. US Department of Agriculture, Agricultural Research Service, ARS-8, USDA, Washington, DC.

Riha, S.J., Wilks, D.S. and Simoens, P. (1996). Impact of temperature and precipitation variability on crop model predictions. Climactic Change, 32:293-311.

Risby, J.S. and Entekhabi, D. (1996). Observed Sacremento Basin streamflow response to precipitation and temperature changes and its relevance to climate impact studies. Journal of Hydrology, 184:209-223.

Robert Keirle and Colin Hayes, (2007). A Review of Climate Change and its Potential Impacts on Water Resources in the UK", Official Publication of the European Water Association (EWA), UK.

Robertson, D.E. and Wang, Q. J. (2013). Seasonal Forecasts of Unregulated Inflows into the Murray River, Australia. Water Resource Management DOI: 10.1007/s11269-013-0313-4.

Rogelj, J., Meinshausen, M. and Knutti, R. (2012). Global warming under old and new scenarios using IPCC climate sensitivity range estimates. Nature Climate Change, (2):248-253.

Ropelewski and Halpert (1987). Global and Regional Scale Precipitation Patterns Associated with the El Niño/Southern Oscillation. Monthly Weather Review, 115:1606-1626.

Roy, M., Jordan, T.H. and Pederson, J. (2009). Colorado Plateau magmatism and uplift by warming of heterogeneous lithosphere. Nature, 459:978-982.

Russell, G. L. and Miller, J. R. (1990). Global river runoff calculated from a global atmosphere general circulation model. Journal of Hydrology, 116:241-254.

Sausen, R., Schubert, S. and Dümenil, L. (1994). A model of river runoff for use in coupled atmosphere–ocean models. Journal of Hydrology, 155:337-352.

Schoof, H., Ernst, R, Nazarov, V, Pfeifer, L, Mewes, H.W. and Mayer, K.F. (2005). MIPS Arabidopsis thaliana Database (MATDB): an integrated biological knowledge resource for plant genomics. Nucleic Acids, 32:373-376

Semenov, M. A. (2006). Using weather generators in crop modeling. Acta Horticulturae, 707:93-100.

Semenov, M. A. (2009). Impacts of climate change on wheat in England and Wales. Royal Society Interface. 6:343-350.

Semenov, M. A. and Barrow, E. M. (1997). Use of a stochastic weather generator in the development of climate change scenarios. Climatic Change, 35:397-414.

Semenov, M. A. and Brooks, R.J. (1999). Spatial interpolation of the LARS-WG stochastic weather generator in Great Britain. Climate Research, 11:137-148.

Semenov, M. A., Brooks, R. J., Barrow, E. M. and Richardson, C.W (1998). Comparison of the WGEN and LARS-WG stochastic weather generators in diverse climates. Climate Research, 10:95-107.

Semenov, M.A. and Stratonovitch, P. (2010). Use of Multi-model ensembles from global climate models for assessment of climate change impacts. Climate Research 41:1-14.

Semenov, M.A., Brooks, R.J., Barrow, E.M. and Richardson, C.W. (1998). Comparison of the WGEN and LARS-WG stochastic weather generators in diverse climates. Climate Research, 10:95-107.

Sikka, D. R. (1980). Some aspects of the large-scale fluctuations of summer monsoon rainfall over India in relation to fluctuations in the planetary and regional scale circulation parameters. Proceeding of Indian Academy of Sciences (Earth & Planet. Sci.), 89:179-195.

Singh, V. P. and Frevert, D. (Eds.), (2002). Mathematical Models of Large Watershed Hydrology. Water Resources Publications LLC, Colorado, pp 891.

Singh, V.P. (1988). Hydrologic Systems. Rainfall-Runoff Modeling, Vol. I, Englewood Cliffs, Prentice Hall.

Singhrattna, N. and Babel, M. S. (2011). Changes in Summer Monsoon Rainfall in the Upper Chao Phraya River Basin, Thailand. Climate Research, 49:155-168.

Singhrattna, N., Babel, M. S. and Perret, S. R. (2012). Hydroclimate Variability and Long-Lead Forecasting of Rainfall over Thailand by Large-scale Atmospheric Variables. Hydrological Sciences Journal, 57(1):26-41.

Smith, L.C., Turcotte, D.L. and Isacks, B.L., (1998). Stream flow characterization and feature detection using a discrete wavelet transform. Hydrological Processes, 12:233-249.

Snedecor, G.W. and Cochran, W.G. (1994). Statistical Methods, 8e, Affiliated East-West Press, New Delhi, pp 503.

Solomon, S., Qin, D., Manning, M., Alley, R.B., Berntsen, T., Bindoff, N.L., Chen, Z., Chidthaisong, A., Gregory, J.M., Hegerl, G.C., Heimann, M., Hewitson, B., Hoskins, B.J., Joos, F., Jouzel, J., Kattsov, V., Lohmann, U., Matsuno, T., Molina, M., Nicholls, N., Overpeck, J., Raga, G., Ramaswamy, V., Ren, J., Rusticucci, M., Somerville, R., Stocker, T.F., Whetton, P., Wood R.A. and Wratt, D. (2007). Technical Summary. In: Climate Change 2007: The Physical Science Basis. Contribution of Working Group I to the Fourth Assessment Report of the Intergovernmental Panel on Climate Change [Solomon, S., D. Qin, M. Manning, Z. Chen, M. Marquis, K.B. Averyt, M. Tignor and H.L. Miller (eds.)]. Cambridge University Press, Cambridge, United Kingdom and New York, NY, USA.

Srivastava A. K., Rajeevan, M. and Kshirsagar, S. R. (2009). Development of a high resolution daily gridded temperature data set (1969-2005) for the Indian Region. Atmospheric Science Letter, (10):249-254.

Steele, T.D., Gilroy, E. J. and Hawkinson, R. O. (1974). Techniques for the assessment of areal and temporal variations in streamflow quality. Open File Report, US Geological Survey, Washington, DC.

Tabor, K. and Williams, J. W. (2010). Globally downscaled climate projections for assessing the conservation impacts of climate change. Ecological Applications, 20(2):554-565.

Taxak, A. K., Murumkar, A. R. and Arya, D.S. (2014). Long term Spatial and Temporal Rainfall Trends and Homogeneity Analysis in Wainganga Basin, Central India. Weather and Climate Extreme, http://dx.doi.org/10.1016/j.wace.2014. 04.005

Taylor, C. H. and Loftis, J. C. (1989). Testing for trend in ae and groundwater quality time series. Water Resource Bulletin, 25 (4):715-726.

Thapliyal, V. and Kulshrestha, S. M. (1991). Decadal changes and trends over India. Mausam, 42:333-338.

Thodsen, H. (2007). The influence of climate change on stream flow in Danish rivers. Journal of Hydrology, 333(2-4):226-238.

Thomas, A. (2000). Climatic changes in yield index and soil water deficit trends in China. Agricultural and Forest Meteorology, 102:71-81.

Torrence, C. and Compo, G. P. (1998). A Practical Guide to Wavelet Analysis. Bulletin of American Meteorological Society, 79:61-78.

Türkeş, M. (1996). Spatial and temporal analysis of annual rainfall variations in Turkey. International Journal of Climatology, 16:1057-1076.

Van Belle, G. and Hughes, J.P. (1984). Nonparametric tests for trend in water quality. Water Resources Research, 20:127-136.

Vojinovic, Z. (2010). Supporting Flood Disaster Management with Numerical Modelling and Spatial Mapping Tools, International Journal of Geoinformatics, 5(4): 33-40.

Vose, R.S., et al., (1992): The Global Historical Climatology Network: Long-Term Monthly Temperature, Precipitation, Sea Level Pressure, and Station Pressure Data. ORNL/CDIAC-53, NDP-041, Carbon Dioxide Information Analysis Center, Oak Ridge National Laboratory, Oak Ridge, TN, pp 325.

Wagesho, N., Goel, N. K. and Jain, M. K. (2012). Investigation of non-stationarity in hydro-climatic variables at Rift Valley lakes basin of Ethiopia. Journal of Hydrology, 444-445:113-133.

Wagesho, N., Goel, N.K. and Jain, M.K. (2013). Temporal and Spatial Variability of Annual and Seasonal Rainfall over Ethiopia. Hydrological Sciences Journal, 58 (2):1-20.

Wagesho, N., Jain, M.K. and Goel, N.K. (2013). Effect of Climate Change on Runoff Generation: An Application to Rift Valley Lakes Basin of Ethiopia. American Society of Civil Engineering (ASCE). Hydrologic Engineering Journal, 18:1048-1063.

Ward, P.J., Beets, W., Bouwer L.M., Aerts J.C.J.H. and Renssen, H. (2010). Sensitivity of river discharge to ENSO. Geophysical Research Letters, 37, L12402, DOI: 10.1029/2010GL043215.

Webster P.J. (1987). The elementary monsoon. Monsoons. J. S. Fein and P. L. Stephens, Eds., John Wiley and Sons, 399-464.

Webster, P. J, Magaña, V. O., Palmer, T.N., Shukla, J., Tomas, R. A., Yanai, M. and Yasunari, T. (1998). Monsoons: Processes, predictability and the prospects for prediction. Journal of Geophysical Research, 103:14451-14510.

Webster, P.J. and Palmer (1997). The past and future of El Niño. Nature, 390:562-564.

Webster, P.J. and Yang, S. (1992). Monsoon and ENSO: Selectively interactive systems. Quarterly Journal of the Royal Meteorological Society, 118:877-926.

Wigley, T.M.L., Jones, P.D., Briffa, K.R. and Smith, G. (1990). Obtaining sub-grid-scale information from coarse-resolution general circulation model output. Journal of Geophysical Research 95: doi: 10.1029/JD095iD02p01943. issn: 0148-0227.

Wilby, R. L. and Dawson C. W. (2004). Using SDSM Version 3.1 – A decision support tool for the assessment of regional climate change impacts. User manual. Sponsored by A Consortium for the Application of Climate Impact Assessments (ACACIA), Canadian Climate Impacts Scenarios (CCIS) Project and Environment Agency of England and Wales

Wilby, R.L. and Wigley, T.M.L. (1997). Downscaling general circulation model output: a review of methods and limitations. Progress in Physical Geography, 21:530-548.

Wilby,R.L., Dawson, C.W. and Barrow, E.M. (2002). SDSM — a decision support tool for the assessment of regional climate change impacts. Environmental Modelling & Software, 17:147-159.

Wilks, D.S. (1992). Adapting stochastic weather generation algorithms for climate changes studies. Climate Change, 22:67-84.

Wilks, D.S. and Wilby, R. L. (1999). The weather generation game: a review of stochastic weather models". Progress in Physical Geography, 23 (3):329-357.

Wolter, K. (1987). The Southern Oscillation in surface circulation and climate over the tropical Atlantic, Eastern Pacific, and Indian Oceans as captured by cluster analysis. Journal of Climate Applied Meteorology, 26:540-558.

Wolter, K. and Timlin, M.S. (1993). Monitoring ENSO in COADS with a seasonally adjusted principal component index. Proceedings of the 17th Climate Diagnostics Workshop, Norman, OK, NOAA/NMC/CAC, NSSL, Oklahoma Climate Survey, CIMMS and the School of Meteorology, Univiverity of Oklahoma, 52-57.

Wood, A.W., Lettenmaier, D.P. and Palmer, R.N. (1997). Assessing climate change implications for water resource planning. Climatic Change, 37:203-228.

Wood, E. F., Liang, X., Nijssen, B. and Wetzel, S. W. (1997). Hydro-logical modeling of continental-scale basins. Annual Review of Earth and Planetary Science, 25:279-300.

Wood, E. F., Lettenmaier, D. P., Liang, X., Nijssen, B. and Wetzel S. W. (1997). Hydrological Modelling of continental scale basins, Annual Review Earth Planetary Science, 25:279-300. DOI: 10.1146/annurev.earth.25.1.279.

Wood, E.F. (1998). Scale Analysis for Land-Surface Hydrology. In: G. Sposito (Editor), Scale Dependence and Scale Invariance in Hydrology Cambridge University Press, Cambridge, UK, pp. 1-29.

Xu, C.Y. (1999). Climate change and hydrologic models: A review of existing gaps and recent research developments. Water Resources Management, 13(5):369-382.

Yadav, R. K. (2009a). Changes in the large-scale features associated with the Indian summer monsoon in the recent decades. International Journal of Climatology, 29:117-133.

Yadav, R. K. (2009b). Role of equatorial central Pacific and northwest of North Atlantic 2-metre surface temperatures in modulating Indian summer monsoon variability. Climate Dynamics, 32:549-563.

Yadav, R.K., Yoo, J.H., Kucharski, F. and Abid, M.A. (2010). Why is ENSO influencing northwest India winter precipitation in recent decades? Journal of Climate, 23: 1979–1993. DOI: 10.1175/2009JCLI3202.1.

Yan, Z., Tsimplis, M.N. and Woolf, D. (2004). Analysis of the relationship between the North Atlantic oscillation and sea level changes in northeast Europe. International Journal of Climatology, 24:743-758.

Yanai, M. and Li, C. (1994). Mechanism of heating and the boundary layer over the Tibetan Plateau. Monsoon Weather Review, 122:305-323.

Yao and Hashino (2001). A completely-formed distributed rainfall-runoff model for the catchment scale, Soil-Vegetation-Atmosphere Transfer Schemes and Large-Scale Hydrological Models. (Edited by A. J. Dolman, A. J. Hall, M. L. Kavvas, T. Oki & J. W. Pomeroy), IAHS Publication, No.270:183-190.

Yao and Terakawa (1999). Distributed hydrological model for Fuji River basin. Journal of Hydrologic Engineering, ASCE, 4(2):108-116.

Yao, H. and Yoshida (1995). Prediction of future changes in climate and water cycle by using step-wise regression method. Journal of Japan Society of Hydrology and Water Resources, 8(6):574-582.

Yao, H. and Yuan (2005). Simulating effects of climate change on evapotranspiration of major crops in China, Regional Hydrological Impacts of Climatic Change – Impacts Assessment and Decision Making. (Proceedings of Symposium S6 held during the seventh IAHS Scientific Assembly at Foz do Iquacu, Brazil, April 2005), IAHS Publ. 295:189-197.

Yao, H., Terakawa and Suzuki (1998). Comparison of distributed and lumped hydrological models. Annual Journal of Hydraulic Engineering, JSCE, 42:163-168.

Yao, Scott, Guay and Dillon (2009). Hydrological impacts of climate change predicted for an inland lake catchment in Ontario by using monthly water balance analyses. Hydrological Processes, 23:2368-2382.

Yatagai, A., Kamiguchi, K., Arakawa, O., Hamada, A., Yasutomi, N. and Kitoh, A. (2012). APHRODITE: Constructing a Long-term Daily Gridded Precipitation Dataset for Asia based on a Dense Network of Rain Gauges. Bulletin of American Meteorological Society, doi:10.1175/BAMS-D-11-00122.1.

Yu, Y.S., Zou, S. and Whittemore, D. (1993). Nonparametric trend analysis of water quality data of rivers in Kansas. Journal of Hydrology, pp:61-80.

Yuan, F., Xie, Z., Liu Q., Yang, H., Su, F., Liang, X. and Ren, L. (2004). An application of the VIC-3L land surface model and remote sensing data in simulating streamflow for the Hanjiang River basin, Canadian Journal of Remote Sensing, 30(5):680-690.

Yue, S. and Hashino, M. (2003). Long Term Trends of Annual and Monthly Precipitation in Japan, Journal of the American Water Resources Association, 587-596.

Yue, S., Pilon, P. and Cavadias, G. (2002a). Power of the Mann-Kendall and Spearman's Rho Tests for Detecting Monotonic Trends in Hydrologic Series, Journal of Hydrology, 259 (1-4):254-271.

Yue, S., Pilon, P. and Phinney, B. (2003). Canadian streamflow trend detection: impacts of serial and cross-correlation. Hydrological Sciences Journal, 48:51-63.

Yue, S., Pilon, P., Phinney, B. and Cavadias, G. (2002b). The influence of Autocorrelation on the Ability to Detect Trend in Hydrological Series. Hydrological Processes, 16:1807-1829.

Zhang, X., Harvey, K.D., Hogg, W.D. and Yuzyk, T.R. (2001). Trends in Canadian Streamflow. Water Resources Research, 37 (4):987-998.

APPENDICES

Appendix I

A) AUTOCORRELATION TEST - r_1 TEST

Only autocorrelation coefficient at lag-1 i.e., r_1 is compared with the limits suggested by Anderson (Yue et al., 2003).

$$r_1 = \frac{\sum_{t=1}^{n-1}(x_t - \overline{x_t})(x_{t+1} - \overline{x_{t+1}})}{\left[\sum_{t=1}^{n-1}(x_t - \overline{x_t})^2 * \sum_{t=1}^{n-1}(x_{t+1} - \overline{x_{t+1}})^2\right]^{1/2}}$$

where, $\overline{x}_t$ and Var(x_t) are the sample mean and sample variance of the first (n-1) terms, and $\overline{x}_{t+k}$ and Var(x_{t+k}) are the sample mean and sample variance of the last (n-1) terms. The series is considered to be significantly auto-correlated at a level of significance if the Anderson's limits defined as

$$r_k(90\%) = \frac{-1 \pm 1.645\sqrt{n-2}}{n-1}$$ are crossed for the corresponding level.

B) STUDENT'S 't' TEST FOR AUTOCORRELATION

Student's t test can be used for determining significance of autocorrelation (Snecodor and Cochran, 1994; Cunderlik and Burn, 2004). Serial independence is tested using

$$t = \rho_1\sqrt{\frac{n-2}{1-\rho_1^2}}$$

where, the test statistic t has a Student's t-distribution with (n-2) degrees of freedom. If $|t| \geq t_{\alpha/2}$, the null hypothesis about serial independence is rejected at significance level α.

TEST FOR TREND DETECTION

    A) MANN KENDALL TEST (MK)

It is based on the test statistic S defined as (Yue et al., 2002a):

$$S = \sum_{i=1}^{n-1} \sum_{j=i+1}^{n} \text{sgn}(x_j - x_i)$$

where, x_j are the sequential data values, n is the length of the data set and

$$\text{sgn}(y) = \begin{cases} 1 \cdots if\,(y > 0) \\ 0 \cdots if\,(y = 0) \\ -1 \cdots if\,(y < 0) \end{cases}$$

It has been documented that when n ≥ 8, the statistic S is approximately normally distributed with the mean E(S) = 0

and variance as
$$V(S) = \frac{n(n-1)(2n+5) - \sum_{i=1}^{m} t_i(t_i - 1)(2t_i + 5)}{18}$$

where, m is the number of tied groups and t_i is the size of the ith tied group. The standardised test statistic Z is computed by

$$Z_{MK} = \begin{cases} \dfrac{S-1}{\sqrt{Var(S)}} \; when\, S > 0 \\ 0 \cdots when\, S = 0 \\ \dfrac{S+1}{\sqrt{Var(S)}} \; when\, S < 0 \end{cases}$$

The standardised Mann-Kendall statistic Z follows the standard normal distribution with mean of zero and variance one.

    B) MODIFIED MANN KENDALL TEST (MMK)

This was proposed by Hamed and Rao (1998), and has also been described by Rao et al., (2003). In this autocorrelation between ranks of the observations ρ_k are evaluated after subtracting a non-parametric trend estimate like Theil and Sen's Median slope from the data. Only significant values of ρ_k are used to calculate variance correction factor n/n_S^*, as the variance of S is underestimated when data are positively autocorrelated:

$$\frac{n}{n_S^*} = 1 + \frac{2}{n(n-1)(n-2)} \times \sum_{k=1}^{n-1}(n-k)(n-k-1)(n-k-2)\rho_k$$

where, n is actual number of observations, n_s^* is considered as an 'effective' number of observations to account for autocorrelation in data and ρ_k is the autocorrelation function of ranks of the observations. To account for significant autocorrelation in data only, number of lags can be limited to 3 (Rao et al., 2003). The corrected variance is then computed as

$$V^*(S) = V(S) \times \frac{n}{n_S^*}$$

where, $V(S) = \dfrac{n(n-1)(2n+5) - \sum_{i=1}^{m} t_i(t_i-1)(2t_i+5)}{18}$

The standardised test statistic Z (N (0,1)) is computed by

$$Z_{MK} = \begin{cases} \dfrac{S-1}{\sqrt{Var(S)}} \; when S > 0 \\ \quad\;\; 0 \cdots when S = 0 \\ \dfrac{S+1}{\sqrt{Var(S)}} \; when S < 0 \end{cases}$$

where, $S = \displaystyle\sum_{i=1}^{n-1} \sum_{j=i+1}^{n} \operatorname{sgn}(x_j - x_i)$

TREND SLOPE ESTIMATION

A) THEIL AND SEN'S MEDIAN SLOPE

If a linear trend is present, this simple non-parametric procedure can be used to estimate the true slope (change per unit time). The methodology is described by Yu et.al. (1993) and Kahya and Kalayci (2004). The procedure is not greatly affected by gross data errors or outliers and can be used for records with missing values. In this approach, the slope estimates of N pairs of data are first computed by

$$Q_i = (x_j - x_k)/(j - k) \quad \text{for} \quad i = 1, \ldots N$$

where, x_j and x_k are data values at times j and k, $(j > k)$ respectively. The median of these N values of Q_i is Sen's estimator of slope. If there is only one data in each time period, then

$$N = n(n-1)/2$$

where n is the number of time periods. The median of the N estimated slopes is obtained in the usual way, i.e., the N values of Q_i are ranked by $Q_1 \leq Q_2 \leq \ldots \leq Q_{N-1} \leq Q_N$ and

$$\text{Sen's estimator} = \begin{bmatrix} Q_{(N+1)/2} & \text{if } N \text{ is odd} \\ \dfrac{1}{2}\left(Q_{N/2} + Q_{(N+2)/2}\right) & \text{if } N \text{ is even} \end{bmatrix}$$

B) CHANGE MAGNITUDE AS PERCENTAGE OF MEAN

Change percentage has been computed by approximating it with a linear trend. That is change percentage equals median slope multiplied by the period length divided by the corresponding mean, expressed as percentage (Pc) followed by Yue and Hashino (2003).

$$Percentage\ Change\ (\%) = \frac{Sen's\ Slope * length\ of\ year}{mean} * 100$$

TEST FOR HOMOGENEITY

VAN BELLE AND HUGHES' HOMOGENEITY OF TREND TEST

Homogeneity test (van Belle and Hughes, 1984; Helsel and Hirsch, 2002) is used on data by combining data from several stations to obtain a single global trend. The method uses the Mann–Kendall-statistic for each station. To test for homogeneity of trend direction at multiple stations the homogeneity χ^2 statistic χ^2_{homog} is calculated as;

$$x^2_{\text{hom}og} = x^2_{trend} - x^2_{trend} = \sum_{j=1}^{p} Z_j^2 \ - pZ^2$$

where p is the total number of stations; Z_{Sj} is the test statistic Z_S for the jth station obtained as:

$$z \ = \frac{1}{p} \sum_{i=1}^{p} Z_{Sj}$$

213

Appendix V

ENSO years based on Southern Oscillations Index

El Niño = SOI ≤ -5.5

Neutral = -5.5 > SOI < +5.5

La Niña = SOI ≥ +5.5

La Niña	Neutral	El Niño
2008 - 2007	2005	2009
2000	2003	2006
1998	2001	2004
1996	1999	2002
1988	1995	1997
1975-1973	1990-1989	1994-1991
1971-1970	1986-1983	1987
1964	1985-1983	1982
1956-1955	1981-1978	1977
1950	1976	1972
1947	1968-1966	1969
1938	1962-1958	1965
1924	1954	1963
1921	1952	1957
1917-1916	1949-1948	1953
1910-1908	1945-1942	1951
1906	1939	1946
1893-1982	1937-1933	1941

La Niña	Neutral	El Niño
	1931-1927	1940
	1926	1932
	1922	1925
	1920	1923
	1915	1919-1918
	1912	1914-1913
	1907	1911
	1904-1903	1905
	1901-1897	1902
	1895-1994	1896
	1891-1890	

GCMs from IPCC AR4 incorporated into the LARS-WG version 5.0. Baseline 1960-1990; T1: 2011–2030; T2: 2046–2065; T3: 2081–2100

Research centre	Country	GCM	Model acronym	Grid resolution
Commonwealth Scientific and Industrial Research Organization	Australia	CSIRO-MK3.0	CSMK3	1.9°x 1.9°
Canadian Centre for Climate Modelling and Analysis	Canada	CGCM33.1 (T47)	CGMR	2.8°x 2.8°
Institute of Atmospheric Physics	China	FGOALS-g1.0	FGOALS	2.8°× 2.8°
Centre National de Recherches Meteorologiques	France	CNRM-CM3	CNCM3	1.9°× 1.9°
Institute Pierre Simon Laplace	France	IPSL-CM4	IPCM4	2.5°× 3.75°
Max-Planck Institute for Meteorology	Germany	ECHAM5-OM	MPEH5	1.9°× 1.9°
National Institute for Environmental Studies	Japan	MRI-CGCM2.3.2	MIHR	2.8°× 2.8°
Bjerknes Centre for Climate Research	Norway	BCM2.0	BCM2	1.9°× 1.9°
Institute for Numerical Mathematics	Russia	INM-CM3.0	INCM3	4° × 5°
UK Meteorological Office	UK	HadCM3	HADCM3	2.5° × 3.75°
		HadGEM1	HADGEM	1.3° × 1.9°
Geophysical Fluid Dynamics Lab	USA	GFDL-CM2.1	GFCM21	2.5 ° × 2.5° 2.0° × 2.5°
Goddard Institute for Space Studies	USA	GISS-AOM	GIAOM	3° × 4°
National Centre for Atmospheric	USA	PCM	NCPCM	2.8° × 2.8°

Appendix VII

Kolmogorov-Smirnov Test

This test tries to determine if two datasets differ significantly. The KS-test has the advantage of making no assumption about the distribution of data, i.e., it is non-parametric and distribution free. This test is given by

$$D = Max(F_N(x) - F_0(x))$$

(5.1)

Where the values of $F_N(x)$ are estimated as N_j/N, and N_j is the cumulative number of sample events at class limit j;

$F_0(x)$ is then $1/k$, $2/k$...etc., where k is the number of class interval. Class limits are obtained the same way as in chi- square test (Rao and Hameed, 2000). The critical value of KS test, d_α at 5% significance level is given by

$$d_\alpha = 1.36/\sqrt{N}$$

(5.2)

With N, the sample size. If $D < d_\alpha$, then the distribution is fitting (Hogg and Tannis, 1988).

t-test

The t-test can be used to test

i.   If a random sample ($x_i = 1, 2,....n$) of size n has been drawn from a normal population with a specified mean, say μ_0, or

ii.   If the sample mean differs significantly from the hypothetical value μ_0 of the population mean.

Under the null hypothesis, H_o

i.   The sample mean differs significantly from a hypothetical value μ_0 or

ii.   There is no significant differences between the sample mean $\bar{x}$ and the population mean μ_0,

The statistic

$$t = \frac{\bar{x} - \mu_0}{S / \sqrt[2]{n}}$$

(5.3)

Where $\bar{x} = \frac{1}{n} \sum_{i=1}^{n} x_i$ and $S^2 = \frac{1}{n-1} \sum_{i=1}^{n} (x_i - \bar{x})^2$ follows the student's t-distribution with (n-1) degrees of freedom. The calculated value of t with the tabulated value is compared at certain level of significance to decide the acceptance or rejection of the null hypothesis.

F-Test

F test refer to test

i. Whether two independent samples x_i, (i = 1, 2,....n_1) and y_i, (j = 1, 2,...,n_2) have been drawn from the normal populations with the same variance σ^2 (say), or

ii. Whether the two independent estimates of the population variance are homogenous or not.

Under the null hypothesis (H_o) that

i. $\sigma_{x^2} = \sigma_{y^2} = \sigma_{z^2}$ i.e., the population variances are equal, or

ii. Two independent estimates of the population variance are homogenous, the statistic F is given by

$$F = \frac{S_{X^2}}{S_{Y^2}}$$

(5.4)

Where $S_{X^2} = \frac{1}{n-1} \sum_{i=1}^{n_1} (x_i - \bar{x})^2$ and $S_{Y^2} = \frac{1}{n-1} \sum_{i=1}^{n_2} (y_i - \bar{y})^2$ are unbiased estimates of the common population variance σ^2 obtained from two independent samples.

220

LIST OF PUBLICATIONS

Papers Submitted and Published in International Journals/Conferences

1. Murumkar A. R. and Arya D. S. (2014), Trend and Periodicity Analysis in Rainfall Pattern of Nira Basin, Central India. *American Journal of Climate Change*, 3: 60-70.

2. Murumkar A. R. and Arya D.S. (2014), Rainfall Variability Analysis in the Nira River Basin Using Multi-Model GCM Ensemble. 11th International Conference on Hydro informatics HIC 2014, New York, USA.

3. Arya D. S., Murumkar A. R. and Gareeballa A. (2014), Impact of El Niño Southern Oscillation on Summer Monsoon Rainfall in Bhima Basin, Central India. 11th International Conference on Hydro informatics HIC 2014, New York, USA.